



Université  
de Toulouse

# THÈSE

En vue de l'obtention du

## DOCTORAT DE L'UNIVERSITÉ DE TOULOUSE

Délivré par :

Institut National Polytechnique de Toulouse (INP Toulouse)

Discipline ou spécialité :

Génie des Procédés et de l'Environnement

---

Présentée et soutenue par :

M. ALEX MAZUBERT

le jeudi 27 novembre 2014

Titre :

SELECTION, DEVELOPMENT AND DESIGN OF A CONTINUOUS AND  
INTENSIFIED REACTOR TECHNOLOGY TO TRANSFORM WASTE  
COOKING OIL IN BIODIESEL AND BIOSOURCED FORMULATIONS

---

Ecole doctorale :

Mécanique, Energétique, Génie civil, Procédés (MEGeP)

Unité de recherche :

Laboratoire de Génie Chimique (L.G.C.)

Directeur(s) de Thèse :

MME JOELLE AUBIN

MME MARTINE POUX

Rapporteurs :

M. ADAM P. HARVEY, UNIVERSITY OF NEWCASTLE GB

M. GEORGIOS STEFANIDIS, KATHOLIEKE UNIVERSITEIT LEUVEN

Membre(s) du jury :

M. CHRISTOPHE GOURDON, INP TOULOUSE, Président

M. CHRISTOPHE LEN, UNIVERSITE DE TECHNOLOGIE DE COMPIEGNE, Membre

M. MARK ROELANDS, TNO, Membre

Mme JOELLE AUBIN, INP TOULOUSE, Membre

Mme MARTINE POUX, INP TOULOUSE, Membre



# Remerciements

---

Les remerciements qui ont été fait en fin de soutenance orale sont retranscrits en version complète dans ces pages, à tête reposée, passée l'émotion d'avoir réalisé l'achèvement de ces travaux de thèse. Ce manuscrit clôt trois années riches et intenses, en interaction avec de nombreux acteurs, au sein d'un laboratoire convivial et enthousiaste. Je profite ainsi de ces pages pour remercier et citer (de façon non bibliographique) toutes les personnes ayant participé, directement ou indirectement à cette thèse. Un grand merci tout d'abord à mes deux directrices Martine Poux et Joelle Aubin. Vous avez toujours été présentes tout au long de la thèse, toujours de bon conseil, pour générer de nouvelles idées ou me permettre d'entrer en contacts avec les bonnes personnes. Je vous remercie de la confiance que vous m'avez témoignée, de votre intérêt et de votre investissement pour ce projet. Je remercie ensuite les piliers du laboratoire qui m'ont épaulé pour la partie expérimentale, Lucien Pollini et Franck Dunglas, père et fils spirituels, ainsi qu'Alec Manaury. Avec eux, nous avons mis en place les premiers essais et amélioré le réacteur micro-ondes. Merci au passage à Jean-François Blanco pour avoir mis à disposition la salle de travail.

Merci ensuite à la MEPI de m'avoir accueilli parmi ses rangs pour faire passer nos huiles dans leur réacteurs. Merci à Sébastien Elgue d'avoir rendu cela possible, à Annelise Conté pour sa précieuse aide, ainsi qu'à Sophie Cerdan et Laurène Despènes. Merci à mes anciens stagiaires qui ont participé à ces essais : Jean-Marc Peroulmanaïk, merci pour ta bonne humeur et tes remarques pertinentes, « thank you » Cameron Taylor, stagiaire écossais qui m'a lui aussi aidé, merci pour ton travail soigneux et rigoureux, ton adaptation, quel dommage cependant d'avoir fini avec un maillot du stade toulousain sur le dos.

Merci ensuite à la MEPI de m'avoir accueilli parmi ses rangs pour faire passer nos huiles dans leur réacteurs. Merci à Sébastien Elgue d'avoir rendu cela possible, à Annelise Conté pour sa précieuse aide, ainsi qu'à Sophie Cerdan et Laurène Despènes. Merci à mes anciens stagiaires qui ont participé à ces essais : Jean-Marc Peroulmanaïk, merci pour ta bonne humeur et tes remarques pertinentes, « thank you » Cameron Taylor, stagiaire écossais qui m'a lui aussi aidé, merci pour ton travail soigneux et rigoureux, ton adaptation, quel dommage cependant d'avoir fini avec un maillot du stade toulousain sur le dos.

De plus, j'ai pu séjourner aux Pays-Bas durant trois mois dans le cadre d'une collaboration avec TNO (acronyme de Toegepast Natuurwetenschappelijk Onderzoek), à Delft, la Venise des Pays-Bas. Ce séjour m'a permis de m'immerger dans la culture hollandaise, un pays où pour reprendre l'expression d'un autre sage « sun is shining between rain showers ». J'ai pu apprécier les charmes de ce pays : ses plages, ses paysages, les promenades à vélo, les peintures flamandes, le hareng cru du marché, le gouda à tous les parfums, les canaux et les moulins qui sillonnent le paysage et enfin les coupe du monde de hockey et football. J'ai intégré TNO dont le QG est situé au Leeghwaterstraat, 46, sur l'immense campus du TU Delft. Je remercie les personnes qui m'ont épaulé durant ces trois mois : Gerhard Reeling-Brouwer, qui a mis en place et coordonné cette collaboration côté TNO, Mark Roelands, pour son apport scientifique, son engouement pour le projet, Richard Van Someren pour la partie technique. Je remercie également Nirmal Patil, Hans van der Meer, Marc Crockatt et Leon Geers

pour leur apport au projet, ainsi que tout le personnel de TNO qui a toujours été intéressé et accueillant envers moi, visiteur français, à qui ils n'ont pas hésité à faire part de leur admiration pour leur équipe nationale et à m'encourager à me vêtir d'orange, la couleur locale.

Pour continuer, mes remerciements vont au consortium AGRIBTP, qui a toujours assuré un suivi régulier de l'avancée des différents travaux et de l'intérêt mutuel qui s'est créée pour les différentes branches pluridisciplinaires du projet. Merci en particulier à Patrick Barsi, Serge Da Silva, Rémi Lacroix et Erick Ringot pour leur aide, conseils et discussions, ainsi qu'au groupe de liaison, ciment de ce projet, qui réunissait les doctorants, stagiaires, apprentis et jeunes cadres du projet.

Je me tourne maintenant vers l'ensemble du département STPI du laboratoire qui a généré son lot de réunions toujours intéressantes, à tous les doctorants qui sont partis et arrivés durant mon séjour au LGC. Je citerais ainsi dans l'ordre chronologique de sortie : Céline, Emeline, Vincent Loisel, Maxime, Tristan, et dans l'ordre d'arrivée : Séda, Martial, Sara, Jennifer, Juan et Mylène, Léo, Benoit, Kévin, et Alexandre, qui partage mon bureau et mon prénom. Représentant avec force et honneur l'association de l'Alambic, la recherche a de beaux jours devant elle avec de si bons éléments.

Enfin, je remercie Claudine Lorenzon, dont l'aide a été précieuse pour la négociation de livraison des produits, et dont la bonne volonté et la gentillesse est un exemple pour nous tous. Merci également à Alain Philip, plaque tournante du laboratoire, la vague bleue. Merci pour ton investissement total, ta bienveillance et ton énergie.

Concernant l'extra-laboratoire, je remercie ma famille qui a bien accepté d'accueillir un docteur dans son clan, dans l'attente d'un autre en médecine. Je remercie enfin ma deuxième maison, mes colocataires-doctorants Maxime et Jean-Baptiste pour leur soutien sans faille. Puisque j'ai finalement cité tout le monde, je n'oublie pas mes amis qui m'ont soutenu. Enfin je remercie les Phoenix de l'INPT, cette équipe intergénérationnelle de l'ENSIACET.

J'espère que ma reconversion dans la recherche, non pas scientifique mais d'emploi, sera de courte durée et que de nouveaux défis passionnants m'attendent. Au plaisir, j'en suis certain, de recroiser l'un ou plusieurs d'entre vous très prochainement.

# Introduction

---

This thesis has been written thanks to collaboration between industrial and academic research, which has given birth to the AGRIBTP Project. AGRIBTP project (2011-2015) is a collaborative research project funded by the European Union, the French Government and the Région Midi-Pyrénées, whose finality is the creation of an industrial tool for the reuse of co-products from the agroindustry.

There are two main objectives of this project. The first is to develop formulations for building and public works that integrate brand new properties. Four products applied for building and public works are focused upon. Two formulations are for concrete: an anti-adherent for concrete formwork and a curing agent for concrete slabs. The former is used to reduce the adherence between concrete and formwork to facilitate the release, and the latter is to retain water in the concrete to prevent its desiccation. Two other formulations are aimed for the bitumen domain: an anti-adherent agent and an agro-regenerator. The former is used to protect the material and equipment from worn coated materials, the latter to remobilize the old bitumen in order to recycle it with new bitumen. This objective is challenging since it not only requires these brand new molecules with new functionalities to be created, but also requires the processes gravitating around these new reactions to be developed and the effect of these new products on concrete or bitumen samples to be characterized.

The second objective of the AGRIBTP project is to create an industrial sector that reuses co-products and products from agroindustry for use in the building and public works industry. In other terms, the objective is to substitute the currently used products composed of mineral oils or first generation vegetable oils (e.g. sunflower or rapeseed oil) with waste vegetable oils. Indeed, products manufactured from vegetable oils, as substitutes for mineral oil based products, have already been developed in the building and public works industry over the last decades because they are more sustainable, less toxic and more environmental friendly. However, such oils compete with food demands, are expensive and their properties of their formulations still do not offer all of the same properties as those produced with mineral oils. The novelty of this project is the reuse of waste cooking oils for the development of new products with equivalent properties to those mineral oil based products. In this way, co-products or waste from agro-industry are not only being reused, but also they do not compete with food demands and are a cheaper feedstock for the production of formulated products.

To carry out these objectives, a consortium of companies and laboratories has been constituted including the following partners.

Three SME (small or medium enterprises):

- **LRVision, Castanet-Tolosan, France**: start-up created in 2004, it brings novel solutions in the area of siding architectural concrete and chemistry for the building and public works;
- **Coreva Technologies, Auch, France**: created in 2007, their activity is the collection, the treatment and the regeneration of waste from food industry, particularly waste vegetal oil and animal fats in order to commercialize as feedstock for biodiesel production;
- **6TMIC, Toulouse, France**: created in 2004, it is specialized in the development of new industrial and sustainable processes.

Two subsidiaries of the European leader in building and public works, Spie Batignolles group:

- **Malet, Toulouse, France:** created in 1910, specialized in the road construction and public works;
- **Spie SCGPM, Arcueil, France:** specialized to manage building projects.

Three research laboratories:

- **LMDC** (Laboratoire Matériaux et Durabilité des Constructions, Université de Toulouse, France) brings its expertise in the domain of concrete characterization and modeling.
- **LCA** (Laboratoire de Chimie Agroindustrielle, Institut National Polytechnique, Université de Toulouse, France) is specialized in knowledge acquisition on properties and reactivities of agro-molecules.
- **LGC** (Laboratoire de Génie Chimique, Institut National Polytechnique, Université de Toulouse, France) is specialized in the design, optimization, scale-up and operation of new innovative processes for manufacturing products or materials.

The website of the AGRIBTP project is available at the address [www.agribtp.fr](http://www.agribtp.fr).

The project is divided into a number of different tasks:

- **Task n°0:** Project management. Control the project advancement, build a collaborative platform ([www.agribtp.fr](http://www.agribtp.fr)) and communicate on the project. This task is coordinated by **LRVision**.
- **Task n°1:** Synthesis of molecules of interest having suitable physico-chemical properties and susceptible to be candidates for building and public works formulations. This task is coordinated by **LCA**.
- **Task n°2:** Study of chemical processes to transform fatty compounds. Work carried out by **6TMIC** aims at improving the design of a pulverization reactor belonging to **Coreva** and characterizing its performance. In parallel, the **LGC** aims at developing a continuous reactor with new technology that is suitable for different reaction types and allows the reactions to be carried out faster and under milder conditions. This is the objective developed in the thesis. This task is coordinated by **Coreva**.
- **Task n°3:** Concrete applications. The objective is to characterize the effect of the new formulations (anti-adherent for concrete formwork and curing agent for concrete slabs). This task is coordinated by **LRVision**.
- **Task n°4:** Bitumen applications. The objective is to characterize the effect of the new formulations (anti-adherent agent and agro-regenerator). This task is coordinated by **Malet**.
- **Task n°5:** Economic and environmental study. This task is coordinated by **6TMIC**.
- **Liaison Group:** This small group, created in 2012, is composed of one member from each partner: PhD students from LGC, LCA and LMDC, Project Manager from Malet R &D, apprentices and interns from LRVision, 6TMIC and Coreva. It allows an overall vision of the project advancement to be obtained within in an informal atmosphere.

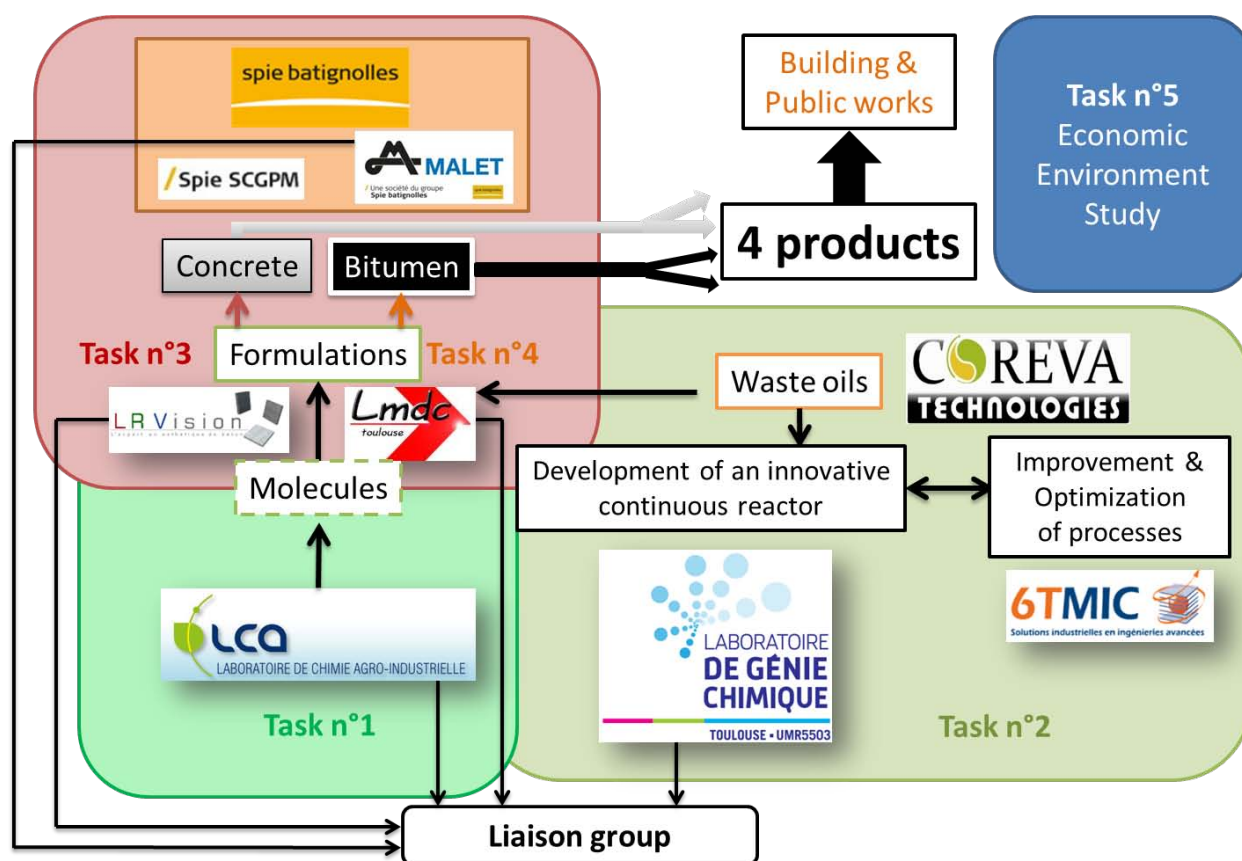


Fig. 1. Organization of the AGRIBTP project.

This manuscript describes the work done in the part of the Task n°2 relative to the development of a continuous reactor based on intensified technology. At the start of the project, specific molecules targeted for the final products were not yet identified. As a result, the work in Task n°2 focused on the development of chemical processes for the common transformation reactions of fatty compounds including four chemical families: methyl esters, glycerol, fatty acids and monoglycerides. These families are the base molecules used in the molecule design work undertaken by LCA. The raw material for the reactions is used vegetal oil or fat collected by Coreva from food industries and restaurants.

Used vegetable oils and fats present the advantage of being collected for free and can be reused to create higher value products after filtration and decantation steps. The first reaction studied is the transesterification reaction, which transforms triglycerides, major compounds of oil, into methyl esters (more commonly known as biodiesel) and glycerol. This reaction is accelerated in presence of alkaline compounds, which play the role of catalyst. This catalysis is only possible if the oil has a low level of fatty acids, or if the oil has a low acidity. This is the case for virgin oils but waste oils have significantly high levels of fatty acids, being between 3% and 45% in mass. The fatty acids are formed during cooking processes when oils have been exposed to high temperatures. Consequently, a pre-treatment step is needed to decrease the fatty acids level, in order to regenerate the waste oils. This is possible with three more reactions. The esterification reaction transforms fatty acids into methyl esters if it reacts with methanol, or tri-, di- and monoglycerides (with a majority of monoglycerides) if it reacts with glycerol. If however fatty acids are the chemical family of interest, a hydrolysis reaction enables fatty acid production from glycerides with water.

The objective of this three year PhD project is to design a continuous and flexible reactor to perform transesterification, esterification and hydrolysis reactions using waste cooking oil and derivatives with a production capacity around 100 kg/h. This project offers a strong opportunity for the LGC and its STPI (Science et Technologie des Procédés Intensifiés) department to show and to increase its expertise in the field of Process Intensification. Process intensification involves the use of novel equipment (and often dramatic reduction in equipment size) and new methods that leading to higher productions, better purities, less waste, cheaper operation and more sustainable processes.

Taking into account the relatively short period to design such a reactor, a pragmatic approach has been undertaken and comprises four parts. Firstly, the significantly rich literature has been reviewed in order to select the most promising intensified technologies for the transformation of fatty compounds. Secondly, a new experimental screening of three intensified technologies, namely a microstructured reactor, a microwave reactor and a continuous oscillatory baffled reactor for the different waste cooking oil transformation reactions has been carried out. The performance of these reactors has been compared with a batch reactor. Thirdly, the study has focused on the improvement of the oscillatory baffled reactor technology. Finally, a design for a continuous process has been proposed.



## Nomenclature

### Latin letters

$\overline{v}_x$	Phase averaged axial velocity (m/s)
a	Interfacial area
A	Amplitude of OBR oscillations (mm)
Ac	Acid value of the oil (%)
$A_i$	Surface area of i (m <sup>2</sup> )
c	Conversion (%)
C	Concentration (mol/L)
c/n	Conversion after n cycles (%)
$C_0$	Orifice coefficient
$C_{\text{KOH}}$	Concentration of the KOH-ethanol solution
D	Diameter of the tube (mm)
$D_0$	Orifice diameter (mm)
$D_{\text{ax}}$	Axial dispersion coefficient (m <sup>2</sup> .s <sup>-1</sup> )
$d_m$	Droplet mean diameter (μm)
e	Baffle thickness (m)
E(t)	Residence time distribution function
f	Frequency (of OBR oscillations or of a microwave reactor) (Hz)
F	Mass flow rate (kg/h)
$F_{\text{net}}$	Net flow rate (L/h)
$f_s$	Frequency of vortex shedding
h	Heat transfer coefficient
h	Convective heat transfer coefficient (W.m <sup>-2</sup> .K <sup>-2</sup> )
k	Thermal conductivity (W.m <sup>-1</sup> .K <sup>-1</sup> )
L	Characteristic length (m)
M	Molecular weight (g/mol)
m	Molar fraction of the catalyst (%)
$M_{\text{C18}}$	Molar mass of oleic acid (g/mol)
$m_{\text{oil}}$	Mass of oil of the titrated sample (g)
n	Total number of baffles
$n_i$	Amount of substance of i (mol)
Nu	Nusselt number (-)
P	Pressure (bar)
P	Power (W)
p	Pitch of the baffle (m)
Pe	Peclet number (-)
PSR	Particle shear strain rate (s <sup>-1</sup> )
$\text{PSR}_m$	Particle-averaged and time-averaged particle shear strain rate (s <sup>-1</sup> )
$\text{PSR}_{m,\text{max}}$	Particle-averaged of the maximum particle shear strain rate (s <sup>-1</sup> )
r	Radial position on the XY plane (m)
R	Molar ratio of reactants (methanol to oil for transesterification reaction, methanol to fatty acids for esterification with methanol, glycerol to fatty acids for esterification reaction with glycerol and water to oil for hydrolysis reaction) (-)
$\text{Re}_{\text{net}}$	Net Reynolds number (-)
$\text{Re}_o$	Oscillatory Reynolds number
S	Opening section of a baffle (m <sup>2</sup> )

$S_{DG/FFA}$	Selectivity of triglycerides related to free fatty acids (%)
$S_{ij}$	Viscous strain rate ( $s^{-1}$ )
$S_{j/i}$	Selectivity of the product j related to the consumption of the reactant i (%)
$S_{MG/FFA}$	Selectivity of monoglycerides related to free fatty acids (%)
SSR	Shear strain rate
Str	Strouhal number (-)
t	Residence time (s, min or h)
T	Temperature ( $^{\circ}C$ )
$t_m$	Mean residence time (s)
v	Velocity (m/s)
V	Volume (mL or L)
$V_{eq}$	Volume at the equivalence point (mL)
$v_{x,RMS}$	Root-mean-square axial velocity (m/s)
w	Mass fraction of catalyst related to oil (-)
x	Molar fraction of catalyst to fatty acids (-)
X	Conversion (%)
$X_0$	X where particles are released
$X_{detection}$	X where particles are recorded
y	Yield (%)

#### Greek letters

$\psi$	Velocity ratio (-)
$\mu$	Dynamic viscosity (cP or Pa.s)
$\rho$	Density ( $kg/m^3$ )
$\phi$	Reactor dimension (mm)
$\Delta P$	Pressure drop (bar)
$\Delta R$	Difference of position of initially adjacent particles on R
$\Delta X$	Difference of position of initially adjacent particles on X
$\alpha$	Ratio of diameters ( $D/D_0$ )
$\varepsilon_{xx}$	Axial shear strain rate ( $s^{-1}$ )
$\phi$	Pore size ( $\mu m$ )
$\tau_{ij}$	Viscous stress ( $s^{-1}$ )

#### Acronyms

CFD	Computational Fluid Dynamics	H	Horizontal
COBR	Continuous Oscillatory Baffled Reactor	MG	Monoglyceride (monoacylglycerol ester)
DBSA	Dodecylbenzenesulfonic acid	OBR	Oscillatory Baffled Reactor
DG	Diglyceride (diacylglycerol ester)	PIV	Particle Image Velocimetry
FAME	Fatty Acids Methyl Esters	TG	Triglyceride (triacylglycerol ester)
FFA	Free Fatty Acids	V	Vertical
GL	Glycerol		

## Table of contents

<b>Remerciements</b> .....	<b>3</b>
<b>Introduction</b> .....	<b>5</b>
<b>Nomenclature</b> .....	<b>9</b>
<b>Table of contents</b> .....	<b>11</b>
<b>Part I : Review of intensified technologies applied to the transformation of fatty compounds</b> ....	<b>13</b>
Introduction .....	15
General summary.....	15
References .....	17
Intensified processes for FAME production from waste cooking oil: a technological review.....	19
<b>Part II : Screening of intensified technologies</b> .....	<b>43</b>
Chapter 1: Transesterification and esterification reactions in the microwave reactor.....	47
Key role of temperature monitoring in interpretation of microwave effect on transesterification and esterification reactions for biodiesel production.....	51
Determination of operating conditions for esterification with methanol reaction .....	61
Complementary tests with heterogeneous catalysts .....	63
Conclusion .....	63
References .....	64
Chapter 2: Transesterification and esterification reactions in microstructured and oscillatory baffled reactors .....	65
Intensification of waste cooking oil transformation by transesterification and esterification reactions in oscillatory baffled and microstructured reactors for biodiesel production .....	69
Conclusion .....	81
Chapter 3: Esterification with glycerol in microstructured, oscillatory baffled and microwave reactors .....	83
Introduction .....	85
1. Material and methods .....	86
2. Results and discussion .....	88
Conclusion .....	95

References .....	96
Conclusions of Part II .....	98
<b>Part III: Characterization and improvement of oscillatory baffled reactor technology .....</b>	<b>101</b>
Introduction .....	103
Chapter 1: Improvement of the robustness of oscillatory baffled reactor applied to viscous reactants .....	105
Preamble.....	107
Performance comparison of a continuous oscillatory baffled reactor and a Helix reactor for the esterification of fatty acids using waste cooking oil and glycerol.....	109
1. Introduction .....	109
2. Material and methods .....	110
3. Results and discussion .....	113
4. Conclusions .....	118
References .....	120
Chapter 2: Characterization of oscillatory baffled reactors.....	121
Contents .....	122
1. Introduction .....	124
2. State of the art .....	124
3. Experimental measure of velocity by PIV .....	137
4. Numerical simulations using Computational Fluid Dynamics (CFD) .....	152
5. Sizing of an industrial scale OBR .....	176
6. Conclusions .....	179
References .....	180
Conclusions of Part III .....	185
<b>Conclusion.....</b>	<b>187</b>

# Part I

Review of intensified technologies  
applied to the transformation  
of fatty compounds

---



## Introduction

Biodiesel production reactions, i.e. transesterification and esterification reactions have been vastly studied in the literature and this chapter aims at collecting, organizing and reviewing the available data. This review, which is inserted hereafter, has been published Chemical Engineering Journal and has been available online since July 2013 [1].

## General Summary

Even if the final products targeted by the AGRIBTP project are for applications in the building and public works sector, a large number of publications concern biodiesel production in general, representing about 5800 publications between 2010 and 2014 and as many as 741 in 2014. This alternative source of energy has increasingly been investigated as it offers low CO<sub>2</sub> emission and is produced from a renewable source. Biodiesel production has increased by a factor 10 in the last decade (2000-2010) [2]. The annual worldwide production of biodiesel in 2011 is given in **Fig. 1**. In Europe, 7% of biodiesel is used as fuel for vehicles (EN590) [3]. This is part of the consistent effort of research to bring renewable solutions with efficient transformation of biomass into energy, not only with transesterification reaction of triglycerides but also via the transformation of cellulose, starch, sugar-based or cellulosic feedstocks [4]. The interest of biodiesel produced from waste cooking oil has only been investigated more recently (162 publications between 2010 and 2014 and 26 publications in 2014). This feedstock is of great interest since it does not compete with food demands and CO<sub>2</sub> emissions (10 g CO<sub>2</sub> eq./MJ) are even lower than that associated with biodiesel made from rapeseed (46 g CO<sub>2</sub> eq./MJ) [3].

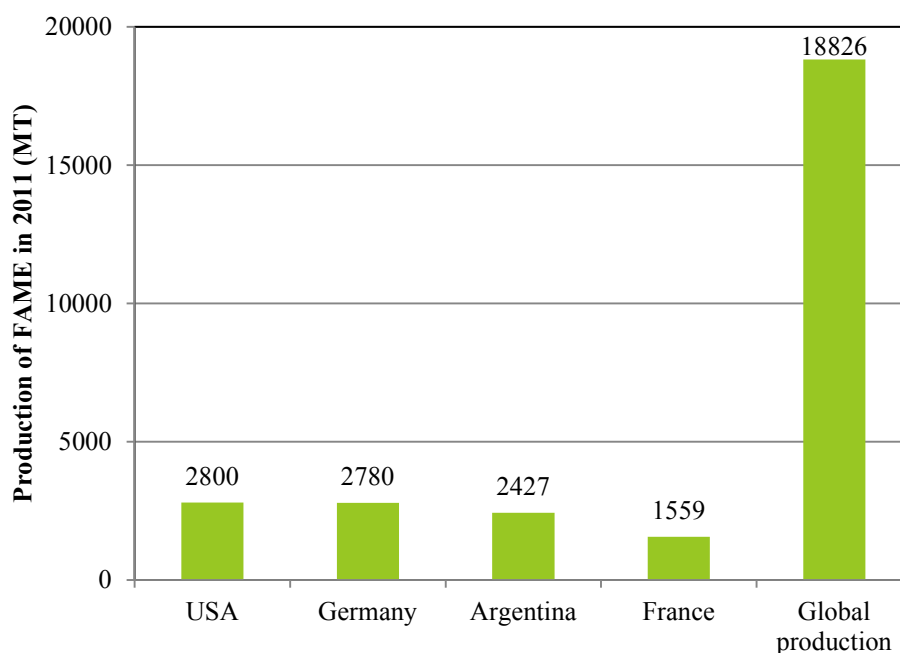


**Fig. 1.** Production of FAME in 2011 in megatons in USA, Germany, Argentina, France and in the world [2], [3].

In addition to the literature review presented in Part I, several reviews and works have now been published. Recently reviews [5]–[9] have been published on the different ways to catalyze the transesterification reaction, in addition to those mentioned in Section 1.1. (ref. 21 to 26), and particularly with solid carbohydrate catalysts [10].

Concerning new studies in the field of microreactors, Table 4 can be completed with new data from the work of Aghel et al. [11]. They obtain a conversion of 99% at 60°C with a molar ratio of methanol to oil of 9 and a mass fraction of catalyst of 1.2 wt.% in 3 min using a stainless steel 0.9 mm diameter microtube containing a wire coil, which plays the role of a “micro” static mixer. The flow-pattern is an emulsion and the flow rate corresponding to 3 min is 1 mL/min. Recent results obtained in microwave reactors are discussed in Part II, chapter 1. Work using a membrane reactor [12] coupled with a fixed catalyst (p-toluenesulfonic acid on MCM-41) has also been recently published. The ceramic membrane retains oil, then the FAME, methanol and glycerol are sent to a product vessel. The yield obtained is 84.1% at 80°C with a flow rate of 4.15 mL/min, but the membrane separation gives a high ester content (99%).

Indeed, the global conclusion made in our published review is not affected by this more recent work. It highlights the interest of using process technology that is able to decrease droplet size of emulsions of the oleic and polar phase and as well as a separation unit as a decanter. A list of intensified technologies, which are particularly adapted to the transformation of waste cooking oil, is provided:

- Microreactors. These allow a decrease in reaction times by decreasing the size of droplets of immiscible reactants through the small characteristic size of the reactor. However microreactors also imply relatively low flow rates.
- Cavitational reactors. These enable reaction times to be decreased even at mild operating conditions. However, such devices are still difficult to operate in terms of the flow rate range required to generate cavitation, the lack of global understanding of the phenomena and the process.
- Microwave reactors. These reduce residence times and enhance the decantation of emulsions, which can lead to good reaction conversion when heterogeneous catalysts are used. However, they still require significant investigation for the scale-up to a continuous process with higher flow rates.
- Oscillatory baffled reactors. These offer good flexibility since mixing is independent of flow rate, they are compatible with heterogeneous catalysts and they allow a reduction in residence times.
- Static mixers. These enable residence times to be reduced and they provide interesting solutions for reaction performance if coupled with a separation module, such as a decanter.
- Membrane reactors. These allow separation of triglycerides for higher purity biodiesel, but this can lead to high costs of materials. They also lack resistance when strong bases or acids are used.
- Reactive distillation. This combines the reactive step and the separation of products, however it requires very high amounts of energy.

This chapter compiles and summarizes many research efforts dedicated to the development of innovative processes in the field of biodiesel production. The list of potential technologies identified is the basis of the work developed in the next part, where innovative process technologies for transforming waste cooking oil are selected and experimentally tested.



## References

- [1] A. Mazubert, M. Poux, and J. Aubin, "Intensified processes for FAME production from waste cooking oil: A technological review," *Chem. Eng. J.*, vol. 233, pp. 201–223, Nov. 2013.
- [2] "European Biodiesel Board website." [Online]. Available: <http://www.ebb-eu.org>.
- [3] "European Biofuels Technology Platform website." [Online]. Available: <http://www.biofuelstp.eu>.
- [4] G. W. Huber and A. Corma, "Synergies between Bio- and Oil Refineries for the Production of Fuels from Biomass," *Angew. Chem. Int. Ed.*, vol. 46, no. 38, pp. 7184–7201, Sep. 2007.
- [5] T. Issariyakul and A. K. Dalai, "Biodiesel from vegetable oils," *Renew. Sustain. Energy Rev.*, vol. 31, pp. 446–471, Mar. 2014.
- [6] Y. M. Sani, W. M. A. W. Daud, and A. R. Abdul Aziz, "Activity of solid acid catalysts for biodiesel production: A critical review," *Appl. Catal. Gen.*, vol. 470, pp. 140–161, Jan. 2014.
- [7] L. P. Christopher, Hemanathan Kumar, and V. P. Zambare, "Enzymatic biodiesel: Challenges and opportunities," *Appl. Energy*, vol. 119, pp. 497–520, Apr. 2014.
- [8] V. B. Veljković, O. S. Stamenković, and M. B. Tasić, "The wastewater treatment in the biodiesel production with an alkali-catalyzed transesterification," *Renew. Sustain. Energy Rev.*, vol. 32, pp. 40–60, Apr. 2014.
- [9] E. F. Aransiola, T. V. Ojumu, O. O. Oyekola, T. F. Madzimbamuto, and D. I. O. Ikhu-Omoregbe, "A review of current technology for biodiesel production: State of the art," *Biomass Bioenergy*, vol. 61, pp. 276–297, Feb. 2014.
- [10] I. M. Lokman, U. Rashid, R. Yunus, and Y. H. Taufiq-Yap, "Carbohydrate-derived Solid Acid Catalysts for Biodiesel Production from Low-Cost Feedstocks: A Review," *Catal. Rev.*, vol. 56, no. 2, pp. 187–219, Apr. 2014.
- [11] B. Aghel, M. Rahimi, A. Sepahvand, M. Alitabar, and H. R. Ghasempour, "Using a wire coil insert for biodiesel production enhancement in a microreactor," *Energy Convers. Manag.*, vol. 84, pp. 541–549, Aug. 2014.
- [12] W. Xu, L. Gao, S. Wang, and G. Xiao, "Biodiesel production in a membrane reactor using MCM-41 supported solid acid catalyst," *Bioresour. Technol.*, vol. 159, pp. 286–291, May 2014.





## Review

# Intensified processes for FAME production from waste cooking oil: A technological review



Alex Mazubert, Martine Poux, Joëlle Aubin \*

Université de Toulouse, INP, LGC (Laboratoire de Génie Chimique), 4 Allée Emile Monso, BP-84234, F-31030 Toulouse, France  
CNRS, LGC, F-31030 Toulouse, France

## HIGHLIGHTS

- Intensified technologies are reviewed to transform waste cooking oil in fatty acid methyl esters.
- Intensified technologies are compared on mass-transfer limited reactions.
- The possible catalysts and the anticipation of the downstream separation steps are discussed.
- A summary table is proposed to compare the different technologies.

## ARTICLE INFO

### Article history:

Received 14 January 2013  
Received in revised form 8 July 2013  
Accepted 18 July 2013  
Available online 26 July 2013

### Keywords:

Process intensification  
Biodiesel  
Waste cooking oil  
Transesterification  
Esterification  
Hydrolysis

## ABSTRACT

This article reviews the intensification of fatty acid methyl esters (FAME) production from waste cooking oil (WCO) using innovative process equipment. In particular, it addresses the intensification of WCO feedstock transformation by transesterification, esterification and hydrolysis reactions. It also discusses catalyst choice and product separation. FAME production can be intensified via the use of a number of process equipment types, including as cavitation reactors, oscillatory baffled reactors, microwave reactors, reactive distillation, static mixers and microstructured reactors. Furthermore, continuous flow equipment that integrate both reaction and separation steps appear to be the best means for intensifying FAME production. Heterogeneous catalysts have also shown to provide attractive results in terms of reaction performance in certain equipment, such as microwave reactors and reactive distillation.

© 2013 Elsevier B.V. All rights reserved.

## Contents

1. Introduction	202
1.1. Context and objectives	202
1.2. Reactions and catalysis	202
1.3. Regeneration of waste cooking oil	203
1.4. Conventional processes	204
2. Process equipment for the intensification of FAME production	205
2.1. Microreactors	205
2.2. Cavitation reactors	207
2.3. Microwave reactor	209
2.4. Oscillatory baffled reactors	210
2.5. Static mixers and other motionless inline device	212
2.6. Membrane reactors	214
2.7. Reactive distillation	214
3. Recommendations for the choice of process technologies for FAME production	216
3.1. Catalyst type	216

\* Corresponding author at: Université de Toulouse, INP, LGC (Laboratoire de Génie Chimique), 4 Allée Emile Monso, BP-84234, F-31030 Toulouse, France. Tel.: +33 534323714.

E-mail address: [joelle.aubincano@ensiacet.fr](mailto:joelle.aubincano@ensiacet.fr) (J. Aubin).

3.2.	Product separation .....	217
3.3.	Equipment choice .....	219
3.3.1.	Transesterification .....	219
3.3.2.	Esterification with methanol .....	219
3.3.3.	Esterification with glycerol .....	220
3.3.4.	Hydrolysis .....	220
4.	Conclusion .....	220
	Acknowledgments .....	220
	References .....	220

## 1. Introduction

### 1.1. Context and objectives

Biological resources are currently the best alternative to fossil fuels or petrochemical solvents for renewable energy and green chemistry applications. The production of biodiesel, composed of fatty acid methyl esters (FAME), has received much attention in research over the last 15 years as it is an organic, biodegradable and non-toxic fuel source that is made from renewable resources such as vegetable oils and animal fats. Although virgin and food-grade oils have proven to be suitable feedstocks for biodiesel production, the use of edible vegetable oils evokes the ‘food versus fuel’ debate on the use of widespread farmland areas for biofuel production in detriment of food supply [1]. Furthermore, in addition to increasing food demands the increasing demand for oil for biofuel production could ultimately lead to deforestation and desertification [2]. The use of non-edible crops, such as jatropha or castor oil, avoids the direct competition for food oils but does not resolve the problem of requiring large plantation land areas [3]. This competition explains the high price of edible oils, representing about 60–90% of the process cost [4]. Waste cooking oil (WCO) as a potential renewable feedstock appears to be an economically and environmentally viable solution for FAME production and presents a number of advantages: e.g. WCO are two to three times cheaper than virgin oils [5], the recycling of WCO reduces waste treatment costs [6], and the quality of the FAME is the same as that produced with virgin oils [7]. In France, the release of waste oils in sewage is prohibited and governmental legislations require waste cooking oils from restaurants and food industries to be collected for recycling and disposal (France, article R. 1331-2, public health code [8]). In the UK, the collect of waste cooking oil is strongly supported for reducing costs of waste disposal and for the production of renewable energy (Food standards Agency [9]). In the USA, several companies and communities (e.g. Restaurant Technologies Inc. [10], Shakopee Mdewakanton Dakota Community [11]) provide solutions for waste oil management and recycling.

Although the main use of FAME is biodiesel, many other industrial applications exist [12]. Indeed, FAME possess good solvent properties with low volatility, as well as being biodegradable and non-toxic. As a result, FAME have been used to wash metal pieces [13], printing material, graffiti [14], automobiles and plane parts [15], as well as for cleaning up oil spills [16]. FAME are also used as binders in inks [17], as well as thinning agents for building and civil engineering work [18]. Other applications include the production of pesticides [19] and phytosanitary products [20].

Numerous publications on FAME production are available in the current literature and most of these studies focus on various aspects of the transesterification reaction. Amongst these, a number of reviews have concentrated on the different ways to catalyze the transesterification reaction [21–26] and particularly with calcium oxide [27] or heterogeneous catalysis [28–31]. Some papers have also focused on the different means for pre-treating WCO before

transesterification [6,7,21,23]. Qiu et al. [32] reviewed process intensification technologies for biodiesel production via homogeneous base-catalyzed transesterification. Talebian-Kiakalaieh et al. [33] and Maddikeri et al. [34] reviewed novel biodiesel processes using WCO feedstocks. Emerging processes for biodiesel production are also reviewed by Oh et al. [35]. A number of authors also discuss acoustic cavitation, microwaves [22,24,26,36], membrane reactors and reactive distillation [37] as means to intensify the transesterification reaction for FAME production. Finally, the methods for separation and purification of biodiesel at the outlet of the reactor have been discussed by Leung et al. [21], Enweremadu and Mbarawa [23], and Atadashi et al. [38].

The objective of this article is to critically review the different intensified process equipment available and adapted to the global FAME production process and to evaluate their use for the transesterification reaction, as well as the pretreatment reactions (i.e. esterification and hydrolysis) in the case where WCO is used as feedstock. In particular, reaction performance, mass transfer enhancement, ease of separation, possible catalyst types (acid or base, homogeneous or heterogeneous) and energy efficiency of the equipment are discussed. Finally, recommendations on the choice of intensified process equipment for FAME production are given.

In this review the discussion and evaluation of the capacities of various intensified process equipment for FAME production (Sections 2 and 3) is preceded with technical information on the related reactions, catalysis, WCO regeneration, and conventional industrial processes (Sections 1.2–1.4) as introductory material.

### 1.2. Reactions and catalysis

In the biodiesel industry, vegetable oil is usually transformed into FAME by transesterification. In this reaction, triglyceride reacts with alcohol to give FAME and glycerol, as shown in Fig. 1. Typically, methanol is preferred as the alcohol because of its higher reactivity and low price [21].

This reaction is catalyzed using either homogeneous or heterogeneous, acid or basic catalysts, or enzymes. Various catalysts exist and have been well described in a number of recent reviews [21–26,36]. Table 1 summarizes the strengths and weaknesses of the

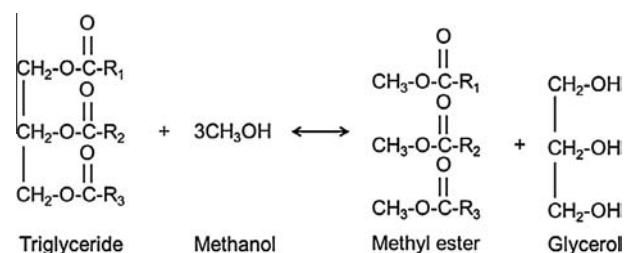


Fig. 1. Transesterification reaction scheme.

**Table 1**  
Comparison of the different types of catalysis of the transesterification reaction [22].

Type of catalyst	Advantages	Disadvantages
Homogenous base	<ul style="list-style-type: none"> <li>– Very fast reaction rate</li> <li>– Mild reaction conditions</li> </ul>	<ul style="list-style-type: none"> <li>– Sensitive to FFA content</li> <li>– Soap formation (causing yield to decrease and increase difficulty for product and catalyst separation)</li> </ul>
Heterogeneous base	<ul style="list-style-type: none"> <li>– Inexpensive</li> <li>– Faster than acid-catalyzed reaction</li> <li>– Mild reaction conditions</li> <li>– Easy separation of catalyst</li> <li>– Easy reuse and regeneration of catalyst</li> </ul>	<ul style="list-style-type: none"> <li>– Poisoned at ambient air</li> <li>– Sensitive to FFA content</li> <li>– Soap formation</li> <li>– Leaching of catalyst causing contamination of product</li> <li>– Energy intensive</li> </ul>
Homogeneous acid	<ul style="list-style-type: none"> <li>– Insensitive to FFA and water content</li> <li>– Simultaneous esterification and transesterification possible</li> <li>– Mild reaction conditions</li> </ul>	<ul style="list-style-type: none"> <li>– Very slow reaction rate</li> <li>– Corrosive catalysts (e.g. H<sub>2</sub>SO<sub>4</sub>)</li> </ul>
Heterogeneous acid	<ul style="list-style-type: none"> <li>– Insensitive to FFA and water content</li> <li>– Simultaneous esterification and transesterification</li> <li>– Easy separation of catalyst</li> <li>– Easy reuse and regeneration of catalyst</li> </ul>	<ul style="list-style-type: none"> <li>– Separation of catalyst is difficult</li> <li>– Complicated reaction synthesis leading to higher processing costs</li> <li>– High reaction temperature, high alcohol to oil molar ratio, long reaction times</li> <li>– Energy intensive</li> <li>– Leaching of catalyst causing contamination of product</li> </ul>
Enzyme	<ul style="list-style-type: none"> <li>– Low reaction temperature (lower than for homogenous base catalysts)</li> <li>– Only one purification step necessary</li> </ul>	<ul style="list-style-type: none"> <li>– Very slow reaction rate</li> <li>– High costs</li> <li>– Sensitive to alcohol (typically methanol, causing deactivation)</li> </ul>

different catalyst types. In industrial FAME processes, homogeneous alkali catalysts (e.g. KOH, NaOH) are the most often used. These inexpensive catalysts lead to short reaction times and are easy to handle in terms of transportation and storage [36]. However, base-catalyzed transesterification is very sensitive to the presence of free fatty acids (FFA) in the oil, which leads to undesired soap formation. Soap formation decreases the reaction yield and facilitates the formation of emulsions, thereby causing difficulties in the downstream separation process [3,39]. Consequently, it is generally recommended that the acidity of the oil must be less than 1 mg KOH/g oil [6,23]. Alkali catalysis is also sensitive to presence of water, forming inactive alkaline soaps [40]. Water content is therefore limited to 0.05 vol.% (ASTM D6751 standard) [21]. It is important to point out that the FFA content is very different in unused vegetable oils compared with WCO. Cooking processes and the presence of water cause the hydrolysis of triglycerides, which increases the FFA content in the oil [3,41]. The absence of oxygen at high temperatures causes thermolytic reactions whereas oxidative reactions occur if air is dissolved [22], thereby changing the composition of the oil. Polymerization and saponification can also occur [7]. Furthermore, the viscosity, surface tension and color of virgin oils change after the cooking processes [42]. Unlike base-catalyzed transesterification, acid-catalyzed transesterification is insensitive to FFA content. However, it is associated with a number of disadvantages, for example the need of higher reaction temperatures and alcohol to oil molar ratios, the difficulty of catalyst separation, as well as serious environmental and corrosion issues [22]. Most importantly, the reaction rate of acid-catalyzed transesterification has been reported to be 4000 times slower than that using alkalis [43]. This has been proven in a number of studies: e.g. a base-catalyzed transesterification carried out at 65 °C, a methanol to oil molar ratio of 6:1, and 1% w/w of KOH has shown to give a 96.15% yield in 1 h [44] whereas an acid-catalyzed transesterification carried out at 65 °C, a methanol to oil molar ratio of 30:1 and 1% w/w of sulfuric acid has shown to give 90% yield in 69 h [45].

As summarized in Table 1, heterogeneous catalysis offers a number of advantages over homogenous catalysis and in particular, the ease of catalyst separation and the possibility to reuse and regenerate it. However, in industrial practice, heterogeneous catalysts are less widely used due to the high temperatures required, the problems related to catalyst leaching, and their sensi-

tivity to FFA and water content [46]. Nevertheless, recently studies show that a novel heterogeneous catalyst, strontium oxide (SrO), gives faster reaction rates than the usual homogenous catalyst types, such as potassium hydroxide [46,47]. The yield is greater than 95% at 65 °C in 30 min of reaction time in presence of 3 wt.% of SrO and the activity is retained for 10 cycles [47]. A SrO/SiO<sub>2</sub> catalyst leads to a 95% conversion in 10 min and even with about 3 wt.% of FFA and water, the conversion is still greater than 90% in 20 min [46]. One of the main advantages of this novel alkali heterogeneous catalyst is that it allows WCO treatment with less strict requirements: indeed, SrO can catalyze the transesterification of WCO even if the FFA and water content are greater than the limits required for conventional homogeneous base-catalysts (3 wt.%).

### 1.3. Regeneration of waste cooking oil

Since the interest in WCO for biofuel production has increased in recent years, there is an increased need for the reduction of FFA in WCO. Indeed, if the FFA content of WCO is too high (superior to 1 mg KOH/g oil), the transesterification conversion rate is insufficient and too much soap is produced, hindering the separation of glycerol and ester. In such cases, a pretreatment step is required to regenerate the WCO, thereby improving its quality in terms of FFA and water content in detriment of increased processing costs [23]. As described in a recent review [36], many physical methods for reducing FFA, moisture and solids content in WCO exist. Moisture can be removed by drying (with MgSO<sub>4</sub>, calcium chloride, ion exchange resins), by filtration (under vacuum, through a chromatography column, silica gel or cellulose fiber, under microwave irradiation), with steam injection and sedimentation treatment, as well as by distillation. FFA content can be reduced by the neutralization and the separation of soaps in a decanter, membrane filtration [48], and solvent extraction (particularly with anhydrous methanol or ethanol) [49]. Filtration is typically used for the removal of suspended solids and water washing is employed for the separation of soluble salts from the WCO [6].

Chemical pretreatment methods are another way to reduce FFA content. Three alternatives exist for FAME production. The first is acid-catalyzed esterification shown in Fig. 2. The esterification of

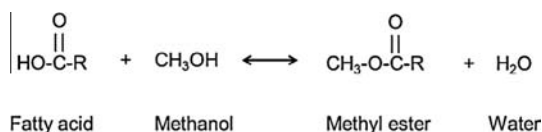


Fig. 2. Reaction scheme for the esterification of fatty acids with methanol to methyl esters and water.

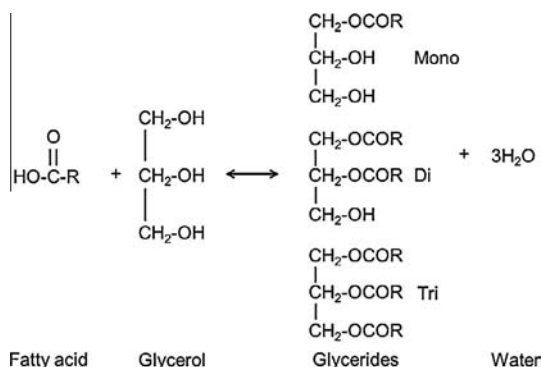


Fig. 3. Reaction scheme of the esterification of fatty acids with glycerol to glycerides and water.

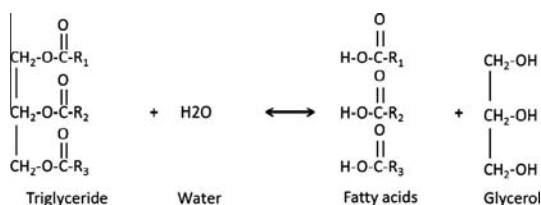


Fig. 4. Reaction scheme of the hydrolysis of triglycerides to fatty acids and glycerol.

FFA in WCO is a solution to reduce the level of FFA in the oil before performing the transesterification.

Esterification typically uses methanol (or ethanol) but glycerol may also be employed [50] as shown by the reaction scheme, given in Fig. 3. This direct esterification of fatty acids with glycerol is of particular interest since the WCO is not only regenerated but the FFA levels are also reduced using glycerol, which is the side-product of the biodiesel reaction. Another industrial application of this reaction is production of monoglycerides [51]. A number of recent studies have focused on the development of various heterogeneous catalysts for this reaction including zinc [50], Fe–Zn double-metal cyanide catalyst [52], and solid superacid  $\text{SO}_4^{2-}/\text{ZrO}_2 - \text{Al}_2\text{O}_3$  [53] leading to acceptable conversion at 200 °C and under atmospheric pressure after 3–4 h reaction time. Enzymatic catalysis has also been explored and has shown to give about 90% conversion in about 80 h with immobilized lipase (*Rhizomucor miehei*) [54] and a 96.5% yield is obtained in 72 h with Novozym 435 [55].

Another chemical route for the regeneration of WCO and the production of FAME is hydroesterification. In this reaction the, FFA are first concentrated via hydrolysis as shown in Fig. 4, and then transformed to FAME via esterification. Continuous hydrolysis processes have existed in industry for many years (e.g. Colgate-Emery, Foster-Wheeler). They are typically conducted at high temperature (260 °C) due to the absence of catalyst and at high pressures (50 bar) to maintain the reactants in a liquid state, enabling thus 98% conversion [56,57]. More recently, Satyarthi et al. [58] obtained 80% of FFA at 190 °C with a solid catalyst (Fe–Zn) in 12 h. Hydroesterification thus combines the well-known hydrolysis process with fatty acid esterification. It is currently used in commercial biodiesel plants in Brazil [59].

It is interesting to point out that all three reactions related to FAME production (i.e. transesterification, esterification and hydrolysis) involve a reaction between two immiscible reactants and are mass-transfer limited. Further, a numbers of similarities can be found between these three reaction types. A comparison of performance of these different reactions in conventional processes is given in the next section.

#### 1.4. Conventional processes

Before entering the discussion on the various intensified process equipment for FAME production, it is important to highlight the characteristics of existing FAME production or related processes using conventional equipment, such as stirred tank reactors, packed beds and columns.

Table 2 gives typical examples of process characteristics of transesterification and esterification reactions performed in laboratory-scale stirred tank reactors. The most important features of these reactions are the immiscibility (or partial miscibility) of the reactants and products, and the reaction time for acceptable conversion, which is of the order of a couple of hours in these small scale reactors.

At the level of industrial production, the French Institute of Petroleum (IFP) has developed both a discontinuous and a continuous process for transesterification using a homogenous alkali catalyst [62]. The discontinuous reactor operates at temperatures between 45 and 85 °C with a maximum pressure of 2.5 bar and produces 80,000 tons of FAME per year. The time required to reach thermodynamic equilibrium is on the scale of 1 h and the yield is between 98.5% and 99.4%. The continuous process leads to similar yields and the production capacity is superior to 100,000 tons per year. A continuous heterogeneous base-catalyzed transesterification process named ESTERFIP-H™ has also been developed by IFP [62]. The catalyst is a zinc aluminate spinel ( $\text{Zn Al}_2 \text{O}_4$ ), the operating temperature and pressure ranges between 180–220 °C and 40–60 bar, respectively. The yields achieved are greater than 98%. In Brazil, there are a significant number of biodiesel plants in operation. One example is the biodiesel plant in Belém-PA-Brazil that started up in April 2005. This plant produces 12,000 ton/year using a heterogeneous catalytic esterification of fatty acids in a fixed bed reactor and involves several steps of chemical reaction and product separation [59].

Examination of the literature data on the performance of laboratory and industrial processes highlights that transesterification, esterification and hydrolysis are all limited by mass transfer. In the case of transesterification, the mass transfer limitation [63] results in reaction times of the order of a couple of hours for desired conversion (up to 96.5%) [60,64]. Indeed, the reaction rate is limited by the immiscibility of triglycerides and methanol at the beginning of the reaction and then because the glycerol phase separates out taking most of the catalyst with it as the reaction proceeds [66]. This latter point is confirmed by kinetics, which show that the reaction rate is sigmoidal, i.e. slow at both the beginning and end of the reaction but fast at an intermediate stage [67]. Indeed, the initial immiscibility between reactants rapidly disappears because of the formation of diglycerides and monoglycerides, which play the role of emulsifier [68]. As the mono and diglycerides appear, the size of the dispersed phase droplets decreases and then increases as glycerol is formed [67]. The size of droplets (and consequently the interfacial area) therefore directly influences the reaction rate [69]. Esterification with both methanol and glycerol is limited by mass transfer due to the low solubility between the reactants [70,71]. Partial miscibility is observed with short-chain fatty acids and equilibrium can be shifted with an excess of reactant or the removal of the product. In hydrolysis, high temperatures allow higher oil solubility in

**Table 2**  
Comparison of the characteristics of the different reactions in conventional processes [50,60,61].

Reaction	Catalyst	Reactor	Miscibility			Operation conditions		Reaction time and conversion		Reference
			Reactants	During the reaction	Products	T (°C)	P (atm)	t (h)	c (%)	
Transesterification	Base/ Homogenous	1.5 L glass cylindrical reactor	No	Yes	No	60	1	1	88	[60]
Esterification (with Methanol)	Acid/ Homogenous	0.5 L three neck round bottom flask	Low	Low	Low	60	1	1.5	96.6	[61]
Esterification (with Glycerol)	Acid/ Heterogeneous	Lab scale stirred reactor	No	Partial (increased with high temperatures)	No	200	1	3	90	[50]

water and a better electrolytic dissociation of water, both of which improve mass transfer. Equilibrium can also be shifted using an excess in water [56] or by removing product.

The use of process intensification equipment for FAME production provides a means to reduce the mass transfer limitations related to transesterification, esterification and hydrolysis with less energy consumption, as well as under safer and cleaner conditions. A step towards integrating process intensification in biofuel plants is illustrated by the Biobrax plant (Bahia, Brazil), which produces 60,000 tons of biodiesel per year by hydroesterification [72]. The process is based on a combination of a counter current splitting column and reactive distillation with a heterogeneous catalyst operated at 260 °C. Although distillation is an energy demanding operation, the reactive distillation step has the advantage of combining the reaction and separation steps of the esterification, providing thus a more efficient and cleaner process. Indeed, it has been shown under batch conditions, where the reaction and separation steps are carried out consecutively, that the time required to separate the ester product from the glycerol is sixteen times greater than the time required reach 95% conversion [44].

## 2. Process equipment for the intensification of FAME production

A number of means to intensify processes exist and these involve a range of equipment types and methods, including microreaction technology, multifunctional reactors and novel activation techniques like microwaves and ultrasounds [73,74]. In this section, the use of process intensification techniques that are adapted to liquid–liquid mass transfer limited reactions, such as transesterification, esterification and hydrolysis are reviewed and assessed. In the following sections, yield is defined by the relation:

$$y = n_{\text{FAME}}/3n_{\text{TG}} \quad (1)$$

$y$  is the yield,  $n_{\text{FAME}}$  is the number of moles of FAME and  $n_{\text{TG}}$  is the initial number of moles of triglycerides.

Conversion is defined by the relation:

$$c = (n_{\text{TG initial}} - n_{\text{TG final}})/n_{\text{TG initial}} \quad (2)$$

$c$  is the conversion (%),  $n_{\text{TG initial}}$  is the initial number of moles of triglycerides and  $n_{\text{TG final}}$  is the final number of moles of triglycerides.

### 2.1. Microreactors

Microreaction technology for chemical and biological applications has undergone major technical and scientific development since the mid-1990s and these miniaturized reaction systems have now proven, through both research and industrial practice, to provide innovative and sustainable solutions for the chemical and process industries [75,76]. Due to the small characteristic dimensions and the extremely high surface to volume ratio of these reactors, heat and mass transfer are remarkably intensified

and the temperature within can be tightly controlled. These features make microreactors particularly adapted to mixing limited, highly exo/endermotic and/or mass transfer limited reactions.

Microreactors are of particular interest for performing immiscible liquid–liquid reactions because they potentially offer very high interfacial area between phases, thereby improving the rate of mass transfer [77]. Indeed, mass transfer enhancement is highly dependent on the liquid–liquid flow regime and droplet size, which depend not only on the physical properties of the fluids (viscosity, density, interfacial tension...) but also the operating conditions, the reactor geometry, as well as the properties of the construction material (e.g. wettability, roughness) [76]. In liquid–liquid flow, two types of flow regimes typically occur, namely slug-flow and parallel flow as depicted in Fig. 5 [77,78]. The slug-flow pattern is characterized by drops of uniform size, separated by uniform lengths of the continuous phase. Two mechanisms contribute to the mass transfer process: convection within the dispersed drops and the continuous phase slugs due to the creation of recirculation flow patterns [77,79] and diffusion between adjacent slugs of dispersed and continuous phases. Mass transfer can be enhanced by increasing the interfacial area and the intensity of recirculation in the slugs, which depend on operating conditions. Parallel flow consists of two continuous streams of the dispersed and continuous phases flowing parallel to one another, without convective mixing. Here, the rate of mass transfer is governed by the diffusive mechanism and depends directly on the characteristic size of the fluid streams and therefore the microreactor geometry. The fact that no droplets are formed means that phase separation at the reactor outlet is relatively easy [80]. It is worthwhile point out that the interfacial area and intensity of internal recirculation in slug flow can be modified by changing the flow rate in a given microreactor, whereas in parallel flow the interfacial area is determined by the characteristic dimension of the microreactor geometry or microchannel.

For the transesterification reaction, a microreactor may be a viable choice because the reaction is limited by mass transfer and the

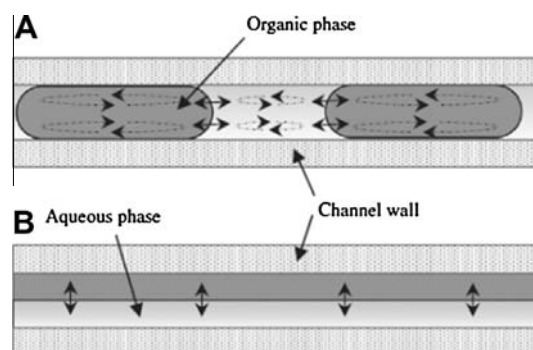


**Fig. 5.** Types of liquid–liquid flow patterns in microreactors: (A) slug flow; and (B) parallel flow [78].

small characteristic size of microreactors allows high interfacial areas between phases to be obtained. In transesterification, the reactants (e.g. methanol and glycerides) are immiscible at the beginning of the reaction, an emulsion of fine droplets (or pseudo-homogenous phase) is obtained during the reaction, and then at the end of the reaction the products (esters and glycerol) form two distinct and immiscible phases again [69]. The emulsion of fine droplets formed during the course of the reaction (depicted in Fig. 6) is specific to transesterification and due to the formation of mono and diglycerides [68]. Table 3 shows a typical advantage of microreactors over batch reactors in the fact that a smaller emulsion droplet size is achieved in a shorter processing time [81], which means that higher conversion in a shorter time can be achieved in microreactors.

A number of studies in the literature have demonstrated the feasibility of using microreactors for improving the performance of transesterification reactions. Table 4 compares the different data available for a homogeneous base-catalysed transesterification reaction in terms of reaction and flow conditions, microreactor characteristics and reaction performance.

From the ensemble of these data, it can be seen that it is very difficult to correlate reaction conditions, flow conditions and microreactor characteristics. However, a general observation for all results can be made being that very high yields and conversions can be obtained for the transesterification within just a few minutes in the microreactor, compared with a reaction time of the order of an hour in conventional batch conditions [81]. This can be attributed to the small droplet size and large interfacial area obtained almost immediately in the microreactor.

Although it is not directly clear from the results in Table 4, the characteristic dimension of the microreactor (typically the diameter of the microchannel) has an important effect on the reaction

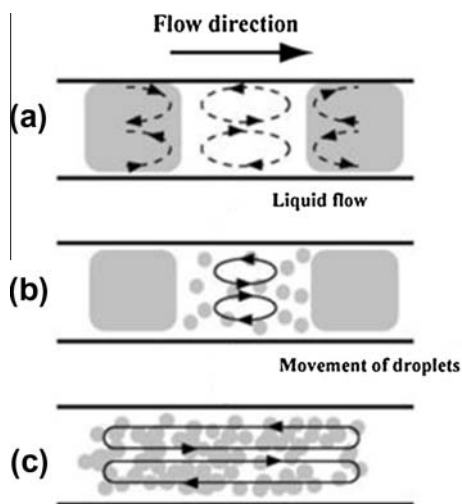


**Fig. 6.** Evolution of liquid–liquid flow patterns over the course of a transesterification reaction in a microreactor. (a) Slug flow whereby the reactants form two distinct phases; (b) Beginning of emulsion formation in the continuous phase due to the production of mono- and di-glycerides; and (c) Emulsion during the course of the reaction, before phase separation of products. [82].

**Table 3**  
Influence of the type of reactor on the droplets mean diameter (dm) for the transesterification reaction [94,81].

Type of reactor	Operating time (min)	dm ( $\mu\text{m}$ )
Batch (250 mL)	3	12.9
(two flat-blade paddle agitator)	60	5.1
Microreactor ( $d = 140 \mu\text{m}$ )	0.5	1.9

performance as it directly influences drop size and interfacial area. This effect of miniaturisation is clearly illustrated in Table 5. As the microreactor diameter decreases from 2 mm to 250  $\mu\text{m}$ , the interfacial area increases 8-fold. Further, the yield increases whilst the residence time remains fixed, which shows that the increased reaction performance is directly due to the effects of miniaturisation.

Although reaction performance improves with decreasing drop size, the downside is that phase separation at the outlet of the reactor becomes more difficult if an emulsion is formed. Indeed, smaller drop size typically signifies a more stable dispersion [86]. Nevertheless, it has been shown that the separation of transesterification products is almost instantaneous for slug and parallel flow [83,84] in continuous microreactors due to the relatively large size of the slugs/streams compared with droplets in an emulsion formed in batch tanks.

In addition to transesterification reactions, microreactors have also shown to be effective for use in the pretreatment step of WCO via acid-catalyzed esterification for the reduction of FFA. Table 6 [87] summarizes the reaction performance of an esterification and a transesterification both carried out with an acid catalyst in a microreactor. The novelty of this work is that the same acid catalyst is employed for both the esterification and the transesterification, which means that the final catalyst neutralization and separation steps are not required. The results show that in the first step of acid-catalyzed esterification, the FFA present in the oil is esterified in 7 min. The second step is the acid-catalyzed transesterification, which has very slow reaction rate in conventional systems (e.g. 90% conversion in 69 h with 1%w sulfuric acid), but demonstrates a dramatic decrease in reaction time in the miniaturized system, with a 99.9% yield obtained in only 5 min [87].

There are no studies on the esterification of fatty acids with glycerol in microreactors reported in the literature. Indeed, operating temperatures above 200  $^{\circ}\text{C}$  are conventionally employed to increase solubility between the reactants. Microreaction technology may therefore be an attractive alternative to current processes since the high interfacial area and the excellent heat transfer characteristics of microreactors could provide mass transfer enhancement with reduced energy consumption. The hydrolysis of triglycerides has however been demonstrated in a microreactor (0.65 mm diameter) using immobilized enzymes at 25  $^{\circ}\text{C}$ . Although the reaction yield is particularly low at this temperature – only 16.8% – it is ten times greater than that obtained in a batch reactor [88]. It can therefore be inferred from these results that the improved reaction performance in the microreactor is due to the miniaturization effects and increased interfacial area between phases.

Table 7 presents the advantages and drawbacks of microreactors for the different reactions involved in FAME production. In summary, the literature data show that the miniaturization of reactors clearly has a positive effect on mass transfer limited reactions principally due to an increase in the interfacial area between phases. For the best performance of these reactors, it appears important that process parameters be controlled such that an emulsion (i.e. small drop sizes) is formed during the reaction for the enhancement of reaction rates and that slug or parallel flow patterns are formed before the reactor outlet to facilitate the separation of products. The combination of parallel flow and the continuous extraction of one of the products (e.g. glycerol or water, depending on the reaction) also appears as an attractive means to shift reaction equilibrium, as shown by Jachuck et al. [84] for base-catalyzed transesterification. The effects of miniaturization have also shown to provide new ways to perform the reactions, e.g. the use of a common catalyst and reactor for the both the pretreatment of high FFA content feedstock via esterification and FAME production via an acid-catalyzed transesterification, which takes only 5 min compared with tens of hours in conventional



**Table 4**

Results obtained for homogeneous base-catalyzed transesterification in microreactors. *y*: yield (%), *c*: conversion (%), *R*: molar ratio methanol:oil, *t*: residence time (min), *w*: weight fraction of catalyst (%), *T*: temperature (°C),  $\phi$ : reactor dimension (mm), *F*: flow-rate (mL/h). I: beginning of the reaction, II: during the reaction, III: end of the reaction, s-f: slug-flow, e: emulsion, p: parallel flow [81–85].

Oil	Catalyst	Performance		Reaction conditions				Type of reactor	Flow-pattern			Material	$\phi$	<i>F</i>	Reference
		<i>y</i>	<i>c</i>	<i>R</i>	<i>t</i>	<i>w</i>	<i>T</i>		I	II	III				
Cottonseed (0.8% FFA)	KOH	99.4	–	6	6	1	60	Micromixer + Tube	s-f	–	s-f	Quartz	0.25	14.7	[83]
Soybean	NaOH	99.5	–	9	0.47	1.2	56	Zigzag microchannel	e	e	e	Stainless steel	0.24	8.1	[81]
Canola	NaOH	–	99.8	6	3	1	60	T-mixer + Tube	–	s-f	p	Teflon	1.5	231	[84]
Sunflower	KOH	–	100	23.9	1	4.5	60	T-joint + tube	s-f	e	e	FEP	0.8	8.2	[82]
		–	59.3	4.6	3.7	4.5	60	T-joint + tube	s-f	e	s-f	FEP	0.8	8.2	[82]
		–	100	23.9	1.6	4.5	40	T-joint + tube	s-f	e	s-f	FEP	0.8	8.2	[82]
		–	97	11.3	0.83	4.5	60	T-joint + tube	–	–	–	FEP	0.8	8.2	[82]
Soybean	KOH	–	100	6	1.5	3.32	60	T-joint + Slit-channel	s-f	s-f	s-f	Nylon	2 × 152.4 × 1	12.2	[85]

**Table 5**

Influence of the characteristic dimension of the microreactor on interfacial area, *a*, and on reaction yield.  $\phi$ : reactor dimension (mm), *F*: flow-rate (mL/h), *a*: interfacial area, *y*: yield (%) [83].

$\phi$ (mm)	<i>F</i> (mL/h)	<i>t</i> (min)	<i>a</i> (m <sup>2</sup> /m <sup>2</sup> )	<i>y</i> (%)	Reference
2	706.7	8	2000	78.6	[83]
0.53	48.4	8.2	7547	96.7	
0.25	14.7	6	16,000	98.8	

equipment. The use of microreactors for mass transfer enhancement in hydrolysis reactions has also been demonstrated and is certainly a means for improving the performance of the esterification of glycerol.

The drawback of the use of microchannels and capillary tubes is the low flow rate capacity, which typically ranges from about 10–200 mL/h. However, commercial microreaction technology equipment exist (e.g. reactors by Corning Inc. [89], Chart<sup>®</sup> [90], Ehrfeld<sup>®</sup> [91], IMM<sup>®</sup> [92]) and allow high flow rate capacities up to 10 L/h, which may be more suitable to FAME production at an industrial scale. Indeed, the performance of these reactors for FAME production has rarely been studied and the enhancement of reaction rates and mass transfer due to miniaturization, as well as the ease of product separation are still yet to be demonstrated.

## 2.2. Cavitation reactors

Cavitation is the generation, growth and collapse of gaseous cavities, which causes the release of large levels of energy in very small volumes, thereby resulting in very high energy densities. The phenomena can occur at millions of locations in the reactor simultaneously, thereby generating conditions of very high local temperature and pressures at overall ambient conditions. The generation of cavities is caused by pressure variations and occurs when the local pressure is less than the saturation pressure. Four techniques exist for the generation of cavitation: acoustic, hydrodynamic, optical and particle. Acoustic and hydrodynamic cavitation are the most commonly employed techniques since the intensity of optic and particle cavitation is insufficient for FAME production. In acoustic cavitation, ultrasounds produce pressure variations in the liquid. Hydrodynamic cavitation, on the other hand, is generated by creating a sudden variation in velocity due

to a change in the geometry of the system (e.g. an orifice or venturi). For detailed general information on cavitation and existing technologies, the reader is referred to reviews by Gogate et al. [93–95].

When using cavitation to activate liquid phase reactions, two mechanistic steps can be identified. Firstly, the cavity, which contains vapor from the liquid phase or dissolved volatile gases, collapses. The collapsing of the cavity induces extreme temperatures and pressures causing molecules to fragment and generate highly reactive radical species. These species react either within the collapsing bubble or in the bulk liquid. Secondly, the sudden collapse results in an inrush of the liquid, which fills the void and produces shear forces in the surrounding bulk liquid that are capable of breaking the chemical bounds of any molecules. For liquid–liquid reactions, such as transesterification, the cavitation collapse near the liquid–liquid interface causes the rupture of the interface and enhances mixing. This results in very fine emulsions that are typically more stable than those obtained in conventional reactors [93]. Indeed, the creation of such fine emulsions, and therefore high interfacial area between reacting phases, enables mass-transfer limited reactions such as transesterification, esterification or hydrolysis to be greatly enhanced.

Tables 8, 9 and 10 present the performance of esterification, transesterification and hydrolysis reactions activated via acoustic and hydrodynamic cavitation, respectively. Indeed, acoustic cavitation has been more widely studied than hydrodynamic cavitation and a detailed reviews of acoustic cavitation as a means for intensifying FAME production have been given in Gole and Gogate [94], Veljkovic et al. [96] and Badday et al. [97]. Ultrasonic cavitation using heterogeneous catalysts have also been reviewed by Ramachandran et al. [98] (see Tables 10 and 13).

In Table 8 it can be seen that the residence time of base-catalyzed transesterification reactions in the presence of ultrasounds is around 15–20 min for most of the cases and only a few minutes or seconds for others. This is significantly shorter than reactions times achieved in conventional reactors that are on the order of one hour. Another interesting point is that short reaction times and high yields can be achieved even at ambient temperature. On the other hand, the reaction time of acid-catalyzed esterification at overall ambient temperatures and pressures is not improved with acoustic cavitation. The heterogeneous superacid clay catalyst used gives

**Table 6**

Results obtained for acid-catalyzed esterification in microreactors. *y*: yield (%), *c*: conversion (%), *R*: molar ratio methanol:oil, *t*: residence time (min), *w*: weight fraction of catalyst (%), *T*: temperature (°C),  $\phi$ : tube diameter (mm), *F*: flow-rate (mL/h) [87].

Reaction	Oil	Catalyst	Performance		Reaction conditions				Type of reactor	Materiau	$\phi$	<i>F</i>	Reference
			<i>y</i>	<i>c</i>	<i>R</i>	<i>t</i>	<i>w</i>	<i>T</i>					
Esterification	Cottonseed (54% FFA)	H <sub>2</sub> SO <sub>4</sub>	99.1	–	30	7	3	100	Micro-mixer + Tube	Stainless steel	1.2	12	[87]
Transesterification	Cottonseed (0,8% FFA)	H <sub>2</sub> SO <sub>4</sub>	–	99.9	20	5	3	120	Micro-mixer + Tube	Stainlesssteel	1.2	12	

**Table 7**

Advantages and drawbacks of microreactors for transesterification, esterification with methanol and glycerol, as well as hydrolysis reactions.

Microreactors	Advantages	Drawbacks
Transesterification	– short reaction times – control of the flow pattern to increase mixing during the reaction and to facilitate the separation at the outlet of the reactor	– Low flow rates (10–200 mL/)
Esterification (with methanol)	– short reaction times – possibility to keep the same catalyst to transform the remaining glycerides after a pretreatment step	
Esterification (with glycerol)	<i>No studied</i>	
Hydrolysis	– Positive effect	– Yield still low with enzymatic catalysis

long reaction times of about 7 h for a conversion of 97%. Furthermore, the conversion was found to be only 41% when the catalyst is regenerated and reused a second time for a new reaction under the same conditions [110]. The feasibility of glycerol esterification of fatty acids with a homogenous acid catalyst in an ultrasonic reactor has also been demonstrated [111]. Although 98.5% conversion is obtained after a reaction time of 6 h and a temperature of 90 °C, these conditions are better than those required in conventional batch reactors (Gomes and Vergueiro [50] obtain a 90% conversion in 3 h with a molar ratio of fatty acid to glycerol of 3 at 220 °C, and Robles Medina et al. [55] obtain a 96.5% yield in 72 h with an enzymatic catalyst). Indeed, glycerol esterification typically requires high temperature conditions and good mass transfer, and cavitation (via the generation of localized hot spots) appears to be a promising way for enhancing the reaction. The generation of local-

ized hot spots at overall ambient operating temperatures is also the principal interest in performing hydrolysis reactions in cavitation reactors [112]. This reaction type typically requires high temperatures around 200 °C and the limit is set at 250 °C [115] in conventional processes. Cavitation reactors typically allow milder and safer operating conditions, do not require catalysts and enable the reaction time to be reduced (e.g. 10 h to obtain 80% of FFA compared with 12 h to obtain the same quantity of FFA with a solid catalyst in batch conditions [58]).

The most important issue concerning acoustic cavitation is related to reactor scale-up so that large fluid volumes can be processed. The ultrasound probe generates the cavitation phenomena in the vicinity of the probe tip and the major difficulty is then obtaining a homogeneous ultrasonic field throughout the entire reactor volume. Therefore, as the reactor volume increases, an increased amount of ultrasound power must be dissipated to the reaction mixture. A complex design with several powerful probes is required in order to obtain a homogenous acoustic field in larger reactors [96]. Continuous reactors may also be preferred to batch reactors as they enable processing with smaller volumes for the same production capacity. The results obtained by Thanh et al. [108] demonstrate the interest in employing acoustic cavitation in a continuous reactor. Their results show that high yield can be attained in less than a minute at room temperature conditions and a throughput capacity that is potentially of interest for industrial applications. Moreover, Thanh et al. [107] noticed that product separation is facilitated with the decrease of operating temperature and molar ratio of methanol to oil.

Hydrodynamic cavitation is more energy efficient than acoustic cavitation ( $1 \times 10^{-4}$ – $1 \times 10^{-3}$  g/J for hydrodynamic cavitation,  $5 \times 10^{-6}$ – $2 \times 10^{-5}$  g/J for acoustic cavitation [110,114]) although academic examples of its use for FAME production are relatively rare. Industrial examples of hydrodynamic cavitation reactors are given by Arisdyne Syst. Inc. [116] and Hydro Dynamics Inc. [117], who commercialize the Controlled Flow Cavitation (CFC)

**Table 8**

Results obtained for transesterification, esterification (with methanol and glycerol) and hydrolysis in acoustic cavitation reactors. *y*: yield (%), *c*: conversion (%), *R*: molar ratio methanol:(acid or oil), *t*: residence time (min), *w*: weight fraction of catalyst (%), *T*: temperature (°C), *P*: power (W), *f*: frequency (kHz), *V*: volume (L), *F*: flow rate (L/h) [99–112].

Oil/acid	Catalyst	Performance		Reaction conditions								Reference
		<i>y</i>	<i>c</i>	<i>R</i>	<i>t</i>	<i>w</i>	<i>T</i>	<i>P</i>	<i>f</i>	<i>V</i>	<i>F</i>	
<i>Acoustic cavitation</i>												
<i>Transesterification (batch)</i>												
Neat vegetable oil	NaOH	98	–	6	20	0.5	25	400	40	–	–	[99]
Vegetable oil	NaOH	98	–	6	20	0.5	36	720 (60%)	40	0.1	–	[100]
Crude cottonseed oil	NaOH	98	–	6.2	8	1	25	–	40	–	–	[101]
Soybean	KOH	99.4	–	6	15	1	40	14.5	20	0.25	–	[102]
Soybean	KOH	99	–	6	5	1	89	400	24	0.125	–	[103]
Soybean	NaOH	95	–	5	1.5	1	40	2200	20	0.75	–	[104]
Soybean	NaOH	98	–	23.9	15	0.5	–	–	–	8	–	[95]
Triolein	KOH	99	–	6	30	1	ambient	1200	40	–	–	[105]
Beef tallow	KOH	–	92	6	1.17	0.5	60	400	24	2	–	[106]
<i>Continuous transesterification</i>												
Canola	KOH	>99	–	5	50	0.7	25	–	20	0.8	480	[107]
WCO	KOH	1st Reactor: 81	–	2.5	0.53	0.7	ambient	1000	20	0.8	90	[108]
		2nd Reactor: 97.5	–	1.5	0.4	0.3	ambient	–	–	–	120	
		Global: 93.8	–	–	0.93	–	–	–	–	–	–	
Commercial oil	KOH	–	95	6	20	–	40	600	45	2.62	7.8	[109]
		–	~85	6	20	–	40	–	–	6.35	19	
<i>Esterification (batch)</i>												
Caprylic (C8)	H <sub>2</sub> SO <sub>4</sub>	–	99	10	75	2	40	120	20	3.5	–	[110]
Capric (C10)	H <sub>2</sub> SO <sub>4</sub>	–	98	10	75	2	40	–	–	–	–	[110]
Fatty acid	Superacid clay	–	97	10	420	2	40	–	–	–	–	[110]
<i>Esterification with glycerol (batch)</i>												
FFA (C8–C10)	H <sub>2</sub> SO <sub>4</sub>	–	98.5	3	360	5	90	–	–	–	–	[111]
<i>Hydrolysis</i>												
Kerdi oil	None	80	–	10	600	0	40	–	–	–	–	[112]

**Table 9**

Results obtained for transesterification in continuous hydrodynamic cavitational reactors. *c*: conversion (%), *R*: molar ratio methanol:oil, *t*: residence time (min), *m*: molar fraction of catalyst (%), *T*: temperature (°C),  $\Delta P$ : pressure drop (bar), (1): first reactor, (2): second reactor [113,114].

Oil	Catalyst	Performance <i>c</i>	Reaction conditions				Configuration	$\Delta P$		Reference
			<i>R</i>	<i>t</i>	<i>m</i>	<i>T</i>		(1)	(2)	
<i>Hydrodynamic cavitation</i>										
<i>Transesterification</i>										
Soybean	NaOH	98.7	6	0.12	3	100	1 Cavitational reactor	17.2	–	[113]
							2 Cavitational reactors in series	17.2	8.3	
Soybean	NaOH	99	6	0.71	3	60	4 Cavitational reactors in series	37.9 (total)		[114]
		99.9	6	0.71	3	100	4 Cavitational reactors in series	37.9 (total)		
Used Frying Oil	KOH	95	–	10	–	60	A plate with 1, 25, 16 or 20 holes	From 1 to 3		

**Table 10**

Results obtained for esterification with methanol in hydrodynamic cavitational reactors. *c*: conversion (%), *R*: molar ratio methanol:oil, glycerol: fatty acid and water: oil, *t*: residence time (min), *w*: weight fraction of catalyst (%), *T*: temperature (°C) [110].

Reactant	Catalyst	Performance <i>c</i>	Reaction conditions				Reference
			<i>R</i>	<i>t</i>	<i>w</i>	<i>T</i>	
<i>Hydrodynamic cavitation</i>							
<i>Esterification with methanol</i>							
FFA	H <sub>2</sub> SO <sub>4</sub>	92	10	90	1	30	[110]

and the Shockwave Power Reactor (SPR), respectively. These reactors allow flexible industrial scale flow conditions with capacities ranging from hundreds to tens of hundreds of liters per hour. An example of results obtained for the transesterification of soybean oil using one cavitational reactor or several in series are given in Table 9. Clearly, the main advantage of these reactors is the possibility to obtain almost 100% conversion in only few microseconds. Moreover, an important consequence of such short reaction times is also the reduction of soap formation and emulsification [118], which in turn facilitates the decantation and separation of the products.

The advantages and drawbacks of acoustic and hydrodynamic cavitation for FAME production are summarized in Table 11. From the literature data it can be concluded that transesterification is clearly intensified by cavitation phenomena, which provides short reaction times especially in industrial hydrodynamic cavitational reactors. For the esterification of methanol, however, cavitation does not allow a reduction in reaction times, although it does enable the reaction to be carried out at ambient conditions. Esterification of glycerol is conventionally performed at high temperatures and the use of cavitation allows the operating temperature to be decreased and, at the same time, provides shorter reaction times. Finally, the use of cavitation in hydrolysis of oils has proved to enable milder operating conditions than the usual high temperature and pressure requirements, however, the reaction times still remain long. In terms of flow rate or processing volumes, hydrodynamic cavitation appears to be more adapted to high capacity demands compared with acoustic cavitation devices since obtaining a uniform acoustic field in large volumes is difficult. Indeed, hydrodynamic cavitation has proved to be industrially interesting for the intensification of transesterification reactions; however too few data for the other types of reactions in such reactors are available making it difficult to definitely conclude on the potential of this technique for the intensification of FAME production. Esterification with methanol has been performed in an hydrodynamic cavitational reactor, see Table 10. The performance is similar to esterification in acoustic cavitational reactor.

### 2.3. Microwave reactor

The development of microwave technology for the process industries is rather recent and relatively slow because of the lack

of control and reproducibility of results, the poor understanding of the dielectric phenomenon occurring, several safety issues and the difficulty to scale-up microwave processes for industrial production. The two major mechanisms involved in microwave technology are dipolar polarization and ionic conduction. Dipolar polarization occurs when dipoles are forced to align with the direction imposed by the electric field, which is caused by the microwave irradiation. The electric field, however, rapidly oscillates and the dipole therefore tries to realign itself with this electric field as fast as possible by rotation. The frequency of microwaves is sufficiently high to cause a phase difference between the field and the dipole orientation and the resulting frictional and collision forces between the molecules thus generate heat. Ionic conduction occurs as the charged dissolved particles oscillate under the influence of the microwave field. When the direction of the electric field is changing, the ions slow down and change direction thereby dissipating kinetic energy as heat. This dissipation is caused by friction [119,120]. A more detailed description of microwaves applied in chemistry can be found in [121,122]. In addition, two recent reviews focus on biodiesel production assisted by microwaves [123,124].

Microwaves are a technology of interest for transesterification, esterification or hydrolysis reactions since they allow increased heating of the reaction medium, which leads to an increase in reaction rate. In early studies on the effects of microwaves in organic synthesis, Lidström et al. [120] observed that for a reaction rate  $K = A \cdot \exp(-\Delta G/RT)$ , the constant *A*, which describes the molecular mobility, is increased under microwave irradiation due to the increased vibration frequency of the molecules. Terigar et al. [125] also observed that transesterification reaction rates are significantly increased under microwave irradiation and that transesterification with methanol is more sensitive to microwaves than that with ethanol due to the lower gyration radius and molecular inertia of methanol. The efficiency of the transesterification reactions is explained by the dielectric properties of the ionic mixtures and the polar compounds present in the vegetal oil, alcohol and catalyst. Asamuka et al. [126] further attributed the positive effect of microwaves on transesterification to factors other than heating efficiency. Firstly, the conformational isomer of the triglyceride has a lower dipolar moment under microwave irradiation and consequently a lower activation energy. Secondly, the vibration around the C=O bond is stronger under microwave irradiation, thereby

**Table 11**  
Advantages and drawbacks of acoustic and hydrodynamic cavitation for transesterification, esterification with methanol and glycerol, and hydrolysis reactions.

Cavitation	Advantages		Drawbacks	
	Acoustic	Hydrodynamic	Acoustic	Hydrodynamic
Transesterification	<ul style="list-style-type: none"> <li>– Shorter reaction times than conventional reactors</li> <li>– Ambient temperatures and pressures conditions</li> </ul>	<ul style="list-style-type: none"> <li>– Reaction times of only a few microseconds</li> <li>– Ambient temperature and pressure conditions</li> <li>– Less saponification and emulsion</li> <li>– Less energy consumption than acoustic cavitation</li> </ul>	<ul style="list-style-type: none"> <li>– Processing of high volumes is difficult due to non-uniform acoustic fields</li> </ul>	<ul style="list-style-type: none"> <li>– A minimum flow rate is required in order to generate the cavitation phenomenon</li> </ul>
Esterification (with methanol) Esterification (with glycerol)	<ul style="list-style-type: none"> <li>– Ambient temperature conditions</li> <li>– Milder temperatures than in conventional processes</li> <li>– Shorter reaction times than conventional reactors</li> </ul>	<ul style="list-style-type: none"> <li><i>No data available</i></li> </ul>	<ul style="list-style-type: none"> <li>– No particular improvement on reaction rates</li> <li>– Reaction times remain long</li> </ul>	<ul style="list-style-type: none"> <li><i>No data available</i></li> </ul>
Hydrolysis	<ul style="list-style-type: none"> <li>– Milder operating conditions than in conventional processes</li> </ul>	<ul style="list-style-type: none"> <li>– Milder operating conditions than in conventional processes</li> </ul>	<ul style="list-style-type: none"> <li>– Long reaction times</li> </ul>	

facilitating the reaction. Finally, the conformational isomer has a planar structure, which is more easily accessible for the nucleophile attack.

A comparison of the literature data for homogeneous and heterogeneous base-catalyzed transesterification and for heterogeneous acid-catalyzed esterification is given in Tables 12 and 14, respectively. From this information, it can be clearly seen that the effect of microwaves on both the transesterification and esterification reactions is a drastic reduction in reaction time (down to several minutes, and even less than a minute in some cases) when compared with conventional processes and without excessive operating temperatures. Indeed, in conventional processes, heterogeneous catalysts for transesterification and esterification are usually associated with low reaction rates and high working temperatures, even though heterogeneous catalysts can facilitate product separation downstream since the solid catalyst is more easily recovered without a neutralization step thereby allowing high purity glycerol as a side product [59]. The literature data also show that under microwave irradiation the performance of heterogeneous catalyzed transesterification reactions – in terms of yield and conversion – are comparable to or better than that when a homogeneous catalyst is used. Indeed, strontium oxide as a solid catalyst gives excellent performance – high conversions for very short residence times – compared with the conventional homogeneous potassium hydroxide catalyst [138], see Table 13. In the case of heterogeneous catalyzed esterification, however, the conversions are typically lower than those obtained with a homogeneous catalyst. Indeed, it does appear that the catalyst type has a strong effect since a 100% yield was obtained with scandium triflate, which continues to provide high conversion even after 5 cycles [136], even though process volumes are very low. Further work in the area of catalyst choice is therefore necessary before solid conclusions on the performance of esterification under microwaves can be made. It may also be interesting to test the scandium triflate catalyst in a larger reactor and then develop a continuous process similar to the experimental setup presented by Barnard et al. [135] in order to investigate the industrial potential of this catalyst.

Although glycerol esterification and hydrolysis reactions under microwaves have been rarely studied, the available data suggests that reaction times are typically reduced and less harsh operating conditions are required under microwave irradiation. For example, Luque et al. [144] obtained 99% conversion in 30 min at 130 °C for

glycerol esterification of acetic acid using a heterogeneous catalyst (Starbon<sup>®</sup>-400-SO<sub>3</sub>H) under microwave irradiation, but only 85% conversion with a sulfuric acid catalyst under the same conditions. Marcel et al. [145] showed that it takes only 5 min to obtain a 100% yield of free fatty acid via the hydrolysis of castor oil triglycerides (in the presence of KOH and ethanol) using microwave irradiation. Another example is given by Saxena et al. [146]: they demonstrated that the complete hydrolysis of triolein with an enzymatic catalyst can be performed in just 75 s at a high power level (800 W, 90 °C), whereas the reaction time needed without at 37 °C and atmospheric conditions is 24 h.

In summary, as presented in Table 15, the current literature shows that microwave irradiation enables a noteworthy reduction of reaction times for transesterification, esterification and hydrolysis and it offers the possibility to operate under milder conditions compared with conventional processes. In addition, the use of microwaves provides a means to obtain good reaction performance with heterogeneous catalysts, which facilitate product separation and higher purity products. Moreover, microwave irradiation is known to break emulsions between a polar and an oil phase [147] thereby facilitating separation further. However, the use of microwave batch reactors for industrial production (i.e. high volumes) is limited for a number of reasons. Firstly, specific security measures have to be taken if microwaves are used at high intensities (power up to 5000 W) that typically require sophisticated cooling systems, thereby increasing the complexity, cost and size of the reactor. Secondly, the penetration depth of microwaves is only few centimeters, which means that a homogeneous field of microwave intensity is extremely difficult to achieve in large volume reactors. For these reasons, most batch experiments in the literature are limited to low volume processing. Indeed, if industrial scale FAME production processes are to be intensified using microwaves then continuous processing will be required and the feasibility of such processes (432 L/h and 98.9% conversion) has already been demonstrated [135]. Furthermore, the combination of microwave-assisted heterogeneous catalysis and continuous processing may have strong industrial potential for FAME production.

#### 2.4. Oscillatory baffled reactors

An oscillatory baffled reactor (OBR) is composed of a tube containing equally spaced orifice plate baffles, as shown in Fig. 7a. It

**Table 12**

Results obtained for homogeneous and heterogenous base-catalyzed transesterification in microwave reactors. *y*: yield(%), *c*: conversion (%), *c/n*: conversion after *n* cycles, *R*: molar ratio methanol:oil, *t*: residence time (min), *w*: weight fraction of catalyst (%), *T*: temperature (°C), *P*: Power (W), *V*: Volume (mL), *F*: flow rate (L/h) [127–139].

Oil	Catalyst	Performance			Reaction conditions						Reference	
		<i>y</i>	<i>c</i>	<i>c/n</i>	<i>R</i>	<i>t</i>	<i>w</i>	<i>T</i>	<i>P</i>	<i>V</i>		<i>F</i>
<i>Homogenous base-catalyzed transesterification</i>												
Vegetal	NaOH	>97	–	–	–	<2	–	–	750	250	–	[127]
Triolein	KOH or NaOH	–	98	–	6	1	5	50	25	–	–	[128]
WCO	KOH	100	–	–	6	2	1	65	500	500	–	[129]
Rapeseed	KOH	–	93.7	–	6	1	1	40	1200 (67%)	–	–	[130]
Yellow horn	KOH	>96	–	–	6	6	1	60	500	50	–	[131]
Soybean	NaOH	–	98.64	–	5	20	0.15–0.18	80	1600	270	–	[132]
Rice	NaOH	–	98.82	–	5	20	0.15–0.18	80	1600	270	–	
Safflower	NaOH	98.4	–	–	10	6	1	60	300	500	–	[133]
Frying palm oil (waste)	NaOH	–	>97	–	12	0.5	3	–	800	16	4.5	[134]
Vegetal	KOH	–	98.9	–	6	0.56	1	50	1600	4000	432	[135]
<i>Heterogeneous base-catalyzed transesterification</i>												
Palmitate	Sc(Otf) <sub>3</sub>	99	–	97/5	48	2.5	10	20	–	0.2–2	–	[136]
Yellow horn	Cs <sub>2.5</sub> H <sub>0.5</sub> PW <sub>12</sub> O <sub>40</sub>	96.2	–	96/9	12	0.17	1	60	1000	50	–	[137]
Cooking oil (without FFA)	SrO	–	99	–	6	0.66	1.84	60	900	50	–	[138]
Soybean	SrO	–	–	96/4	6	2	1.84	–	–	–	–	[138]
Cooking oil (without FFA)	SrO	–	99.8	–	–	0.17	1.84	–	1100	–	–	[138]
Palm	Eggshell waste (CaO 99.2 wt%)	96.7	–	–	18	4	15	122	900	43	–	[139]

**Table 13**

Results obtained for transesterification in microwave reactors. *R*: molar ratio methanol:oil, *t*: residence time (s), *P*: Power (W), *V*: Volume (mL) [138].

Oil	Conversion (%)		Reaction conditions				Reference
	With SrO	With KOH	<i>R</i>	<i>t</i> (s)	<i>P</i> (W)	<i>V</i> (mL)	
Cooking oil (without FFA)	99	83	6	40	900 (70%)	50	[138]
Soybean	96	87	6	120	–	–	

**Table 14**

Results obtained for heterogeneous acid-catalyzed esterification in microwave reactors. *y*: yield(%), *c*: conversion (%), *c/n*: conversion after *n* cycles, *R*: molar ratio methanol:oil, *t*: residence time (min), *w*: weight fraction of catalyst (%), *T*: temperature (°C), *P*: power (W), *V*: volume (mL) [136,140–144].

Acid	Catalyst	Performance			Reaction conditions						Reference	
		<i>y</i>	<i>c</i>	<i>c/n</i>	<i>R</i>	<i>t</i>	<i>w</i>	<i>T</i>	<i>P</i>	<i>V</i>		
<i>Heterogeneous acid-catalyzed esterification with methanol</i>												
Oleic	Sc(Otf) <sub>3</sub>	100	–	97/5	48	1	1	150	–	0.2–2	–	[136]
Oleic	NbO <sub>2</sub> and ZrO <sub>2</sub>	–	68	68/3 and 58/3	5	20	10.5	200	1400	80	–	[140]
Oleic	None	–	60	–	5	60	0	200	1400	80	–	[141]
Oleic	Dry Amberlyst15	–	39.9	–	20	15	10	60	1600 (100%)	1000	–	[142]
		–	66.1	–	20	15	10	60	1600 (pulsed 10%)	1000	–	[142]
Oleic	S–ZrO <sub>2</sub>	–	>90	–	20	20	5	60	1600	2000	–	[143]
<i>Heterogeneous acid-catalyzed esterification with glycerol</i>												
Acetic	Starbon-400-SO <sub>3</sub> H	–	>99	–	1	30	1.8	130	300	<100	–	[144]

operates with an oscillatory or pulsed flow rate, which creates recirculation flow patterns in the vicinity of the baffles as illustrated in Fig. 7b, thereby enhancing mixing and mass and heat transfer. Due to this recirculating flow, OBRs can thereby provide flexible and long residence times, which are comparable to those achieved in batch reactors [148], without having a high length-to-diameter ratio tube. Smaller reactors called mesoscale oscillatory baffled reactor (MOBR) designs with sharp periodic baffles and sharp-edged helical baffles also exist, as presented in Fig. 8.

The OBR technology is particularly adapted to liquid–liquid reactions, such as transesterification, because it allows good inter-phase contacting, enhanced mixing and sufficiently long residence times for reaction. Table 16 compares FAME production data obtained in OBRs; note that the literature studies have been limited to transesterification only. The results show that in an OBR, 99% conversion can be reached in only 10 min at 60 °C, which is half the time required to carry out the reaction in conventional reactors [148]. Furthermore, the same study shows that the meth-

anol stream can be recycled in the continuous OBR technology, thereby allowing a very low methanol to oil ratio to be used. Meso-scale OBRs, which are particularly adapted to feasibility studies and screening tests due to their lower capacity, have also been shown to provide high conversions and yields in short times compared with what can be achieved in conventional batch tanks [149,150].

In addition to the advantages of OBRs for reaction performance, which are summarized in Table 17, this type of equipment is particularly suited to industrial scale production where a certain flow capacity may be required. Indeed, commercial equipment exists – such as that developed by NiTech Solutions®, which has demonstrated successful biodiesel production [151]. OBRs have also been shown to provide good solids handling, whether it is solids suspension or crystallization applications [148,151], which is interesting if heterogeneous catalysis is to be used. Although only transesterification reactions in OBRs have been demonstrated in the literature, the results of these studies and the characteristics

**Table 15**

Advantages and drawbacks of microwave reactors for transesterification, esterification with methanol and glycerol and hydrolysis reactions.

Microwaves	Advantages	Drawbacks
Transesterification	<ul style="list-style-type: none"> <li>– Reaction times reduced</li> <li>– High flow rates for continuous processes</li> <li>– Excellent results with heterogeneous catalysis</li> <li>– Separation of emulsions</li> </ul>	<ul style="list-style-type: none"> <li>– Scale-up difficult in batch conditions</li> </ul>
Esterification (with methanol)	<ul style="list-style-type: none"> <li>– Reaction times reduced</li> <li>– Good results with heterogeneous catalysis (scandium triflate)</li> </ul>	<ul style="list-style-type: none"> <li>– Studies done with low volumes</li> </ul>
Esterification (with glycerol)	<ul style="list-style-type: none"> <li>– Milder temperatures</li> <li>– Good results with heterogeneous catalysis (Starbon-400-SO<sub>3</sub>H)</li> </ul>	<ul style="list-style-type: none"> <li>– Study done with low volumes</li> </ul>
Hydrolysis	<ul style="list-style-type: none"> <li>– Short reaction times</li> <li>– Effective enzymatic catalysis</li> </ul>	<ul style="list-style-type: none"> <li>– Literature data found with enzymatic catalysis only</li> </ul>

of this continuous process equipment suggest that they could also provide significant advantages for esterification and hydrolysis reactions.

### 2.5. Static mixers and other motionless inline device

Static mixers are motionless elements that are inserted in a tube or pipe and enable fluid mixing by creating transverse flows. They are typically used in continuous processes but can also be employed in a closed loop system or for premixing before feeding to a batch tank. Static mixers are well adapted to variety of applications, including simple blending and multiphase mixing problems, in both the laminar and turbulent flow regimes [152]. The advantages of static mixers over conventional batch stirred tanks are their smaller size, a lower energy consumption, a very good control of the residence time with a plug flow reactor behavior, and finally very good mixing with low shear rates [153]. A large number of more or less intricate static mixer designs exist – about 2000 US patents have been granted and more than 30 models are commercially available, e.g. Kenics, HEV, KMS and KMX mixers by Chemineer Inc., Dayton, OH (see Fig. 9) and the SMX and SMX plus mixers by Sulzer Chemtech, Switzerland. However, other inline devices, such as randomly packed beds of spherical particles

and metallic foams, can also be used to ensure mixing in tubes and pipes with relatively low pressure drop [154,155].

Amongst the different applications, static mixers are well adapted to liquid–liquid dispersion processes, including extraction, reaction and emulsification, providing a means to disperse immiscible phases with typically less energy requirements than other technologies. This has been demonstrated by Frascari et al. [157] who have shown that in the case of a transesterification reaction, the energy consumption for a static mixer is less than that required by mechanical stirring. In particular, they show that if the reactants are premixed using a static mixer and fed to a batch reactor with two 4-bladed disk turbines rotating at 100 rpm, the conversion is the same as that achieved in the batch reactor alone with an impeller speed of 700 rpm. Further, they show that the droplet size created by the static mixer is comparable to that generated with mechanical agitation at 700 rpm, which explains the similar reaction performance.

The studies reported in the literature concerning the transesterification of vegetable oil mostly employ static or inline mixing devices in a continuous mode. The transesterification reaction performance obtained in different static mixer and inline mixing configurations are summarized in Table 18. Thompson and He [158] developed a static mixer closed-loop system, which allows the residence time to be easily varied. With this system, the production of total free glycerol (ASTM D6584 specification, 0.24%w max.) was achieved in a residence time of 15 min. Boucher et al. [159] designed a system with a static mixer and an integrated decanter as shown in Fig. 10. The immiscible reactants are contacted in the static mixer and the products are released into a glass column. Where the glycerol settles to the bottom and is continuously removed, whilst the esters are continuously removed from the top of the column. The same group then improved the transesterification process performance by inclining the reactor as presented in Fig. 11 [160]. By inclining the reactor, larger glycerol droplets are formed, thereby facilitating the separation of the esters and glycerol, although the conversion is slightly affected with a decrease from 99% to 95% probably due to the increased drop size. In both reactor designs, the phase contacting via the static mixer and the continual removal of glycerol enhance the reaction and high conversion is obtained in less than 30 min, which is significantly faster than in conventional equipment. Metallic foams and other inserts, such as steel spheres and various types of fibers, have also shown to enhance transesterification reactions [155,161–163]. These devices create tortuous interstices with micron-sized dimensions that promote fluid contacting and mixing, and consequently the chemical reaction. The data show that these mixing devices allow high conversion rates in short residence times, which are of the order of several minutes. Furthermore, some authors also observed

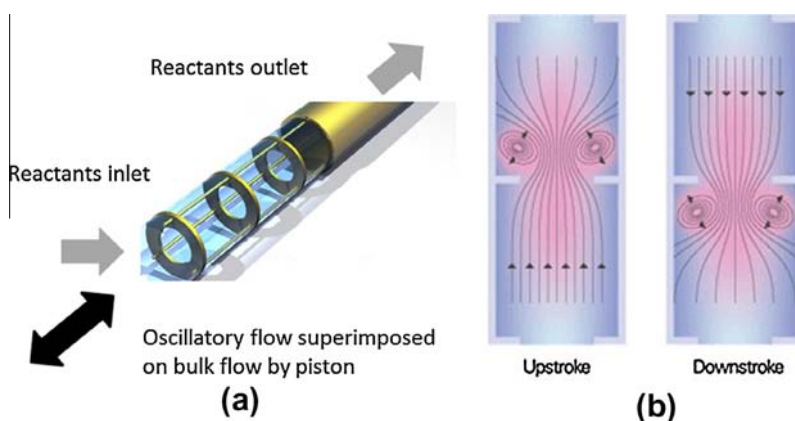


Fig. 7. The oscillatory baffled reactor (a) and the flow-pattern corresponding to a upstroke or downstroke current (b) [150].

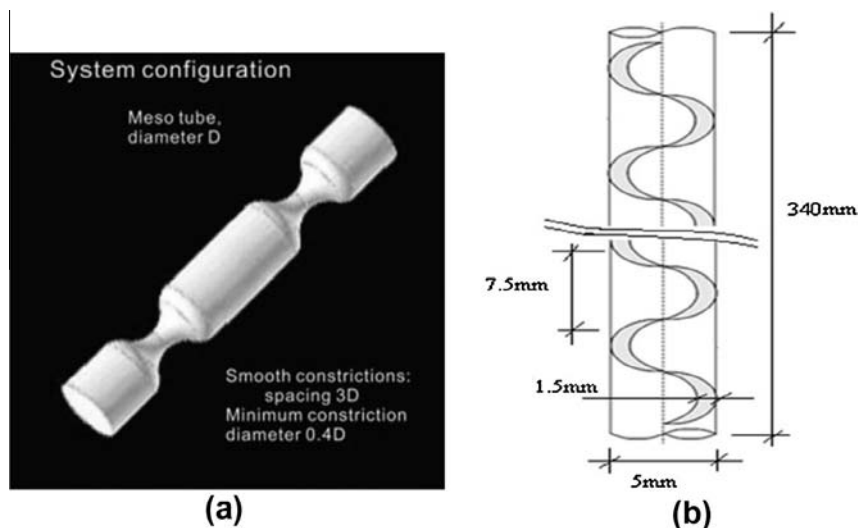


Fig. 8. Mesoscale oscillatory baffled reactors with (a) sharp periodic baffles (SPB) [150] or (b) sharp-edged helical baffles (SEHB) [149].

Table 16

Results obtained for transesterification in oscillatory baffled reactors.  $y$ : yield(%),  $c$ : conversion (%),  $R$ : molar ratio methanol:oil,  $t$ : residence time (min),  $T$ : temperature ( $^{\circ}\text{C}$ ),  $V$ : volume (mL),  $F$ : flow rate (L/h) [148–150].

Oil	Catalyst	Performance		Reaction conditions					Type of reactor	Reference
		$y$	$c$	$R$	$t$	$T$	$V$	$F$		
Rapeseed	NaOH	–	99	1.5	30	50	1.56	3.12	OBR	[148]
Refined vegetable oil	NaOMe	–	99	6	40	60	0.005	0.126	SPB-MOBR	[150]
Rapeseed	KOH	90	–	9	20–25	50	0.04	0.12	SEHB-MOBR	[149]

Table 17

Advantages and drawbacks of OBRs for transesterification reaction.

OBR	Advantages	Drawbacks
Transesterification	<ul style="list-style-type: none"> <li>– Reaction times significantly reduced compared with batch processing</li> <li>– Compatible with heterogeneous catalysis</li> <li>– Molar ratio methanol to oil reduced</li> <li>– Large flexibility in residence times</li> </ul>	<ul style="list-style-type: none"> <li>– No integrated separation unit for end products</li> </ul>

good product separation at the reactor outlet, despite the formation of liquid–liquid emulsions [163].

A summary of the advantages and drawbacks of static mixers and inline devices is given in Table 19. In general, this type of

equipment allows high reaction conversions to be reached in relatively short times and requires less energy input compared with conventional batch processing. A novel attribute of these devices is the possibility to couple the mixing/reaction and separation steps that are required for the transesterification process. Continual separation and removal of products during the reaction shifts the equilibrium and means that the sequential product separation steps that are required in conventional processes can be avoided. Indeed, the other reactions related to FAME production, i.e. esterification with various alcohols and hydrolysis, could potentially benefit from the integration of the reaction and separation steps in one device, although no studies have yet been dedicated to this. Also, heterogeneous catalysis has not yet been tested with static mixing and inline technologies; indeed solids handling in some of these devices may be difficult (e.g. due to clogging), however catalytic coatings on foams or fibers may be a means to resolve such problems.

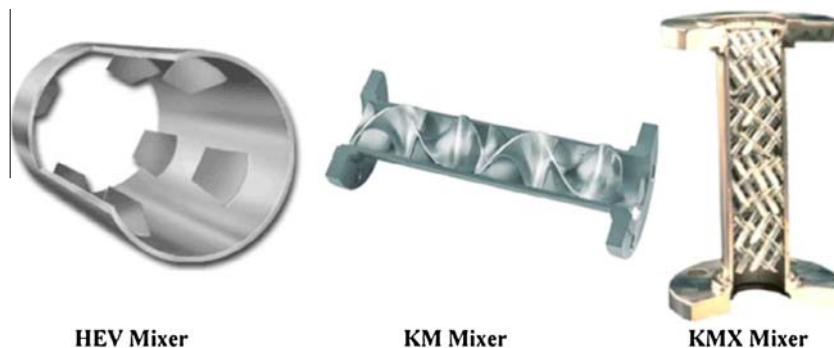


Fig. 9. Geometries of commercially available mixers [156].

**Table 18**

Results obtained for transesterification in static mixer reactors. *y*: yield(%), *c*: conversion (%), *g*: glycerol treatment, *R*: molar ratio methanol:oil, *t*: residence time (min), *w*: weight fraction of catalyst (%), *T*: temperature (°C), *F*: flow rate (L/h) [158–163].

Oil	Catalyst	Performance			Reaction conditions					Type of reactor	Reference
		<i>y</i>	<i>c</i>	<i>g</i>	<i>R</i>	<i>t</i>	<i>w</i>	<i>T</i>	<i>F</i>		
Canola	NaOH	–	–	–	6	30	1.5	60	0.104	Closed-loop system	[158]
Waste canola (pretreated)	KOH	99	70–99% removal	–	6	19	1.3	40–50	72	Reactor-separator	[159]
Waste oil	KOH	96	36–95% separation	–	6	17.5	1–1.3	40–50	72	Reactor-separator	[160]
Soybean	NaOH	95.2	–	–	10	2.16	1	55	0.918	Metal foam	[155]
Soybean	KOH	98.2	–	–	6	0.99	2	60	0.366	Tube filled with stainless steel spheres (2.5 and 1.0 mm)	[161]
Soybean	KOH	97.05	–	–	6	3	1	60	0.279	Packed bed reactor with 2.5 mm spheres	[162]
Soybean	NaOMe	–	99	–	–	5.8	2	60	1.44	216,000 Fibers 8 μm	[163]

## 2.6. Membrane reactors

Microporous inorganic membranes enable product separation by a molecular sieving effect. They can be made of ceramic, zeolites, silica, carbon or polymers. Carbon membranes are most commonly used due to their easy production and low cost [164]. Membrane reactors are also employed for pervaporation processes that enable the separation of a liquid retentate from a vapor permeate [165]. A detailed review of membrane technology as an alternative means for biodiesel production has been given by Shuit et al. [166].

In the case of transesterification, the principal objective of the membrane reactor is to retain the triglycerides [167–172]; this then facilitates the downstream purification steps [167]. The retention of mono- di-, and triglycerides is also possible [168], thus allowing the separation of FAME and glycerol at room temperature and avoiding onerous downstream processing. Furthermore, the separation of glycerol reduces waste water generated by washing steps [171]. The retention of soaps and glycerol is also possible by adding a little amount of water as depicted in Fig. 12 [172]. Membrane separation also allows product specifications to be met (i.e. glycerol < 0.2%w in FAME), as well as the treatment of waste cooking oils with high FFA content (5%) [173]. As it is summarized by Sdrula [170], others advantages of membrane reactors for transesterification are the high purification of glycerol, the absence of chemical additives and the low process cost.

Numerous studies have shown that membranes reactors can improve conversion and facilitate the product purification step of transesterification reactions, compared with conventional processes [172]. A summary of the performance of transesterification reactions carried out in membrane reactors is given in Table 20. It can be seen that in most cases good conversion and acceptable flow rates can be achieved, however the time required for the reaction is on the order of 1–2 h, which is similar to conventional batch processing.

Esterification has been demonstrated in membrane reactors via a pervaporation process where water is removed in a vapor stream allowing a shift in the reaction equilibrium, thereby leading to higher conversion rates. The results obtain by Sarkar et al. [174], which are given in Table 21, show that almost 100% conversion of the fatty acid is achieved in 6 h.

The advantages and drawbacks of membrane reactors for FAME production processes are summarized Table 22. The major advantage of this technology is that separation is integrated in the reaction step. This in turn allows high reaction conversion to be achieved, however there is no reduction in reaction time compared with conventional processing. Although no studies have yet focused on the hydrolysis of triglycerides or esterification using glycerol, membrane reactors could potentially provide benefits by shifting the reaction equilibrium, thereby promoting product formation and facilitating the product separation. Heterogeneous catalysts can be incorporated in and mobilized on the membranes,

leading to conversions superior to 90% without washing steps [175–177]. The use of membrane reactors with an immobilized enzymatic catalyst for hydrolysis has also been demonstrated [178].

## 2.7. Reactive distillation

Reactive distillation combines reaction and distillation in a multifunctional reactor and is suited to heterogeneous, homogeneous and non-catalyzed reactions [179]. The principle is based on the removal of one reaction product in order to shift the reaction equilibrium, thereby leading to high and even total conversions. A more complex configuration is the reactive divided-wall column, which enables three high-purity streams to be obtained at the outlet of a single distillation tower as depicted in Fig. 13 [180]. In conventional distillation, two distillation columns are required to separate three products.

Reactive distillation has shown to be particularly adapted to transesterification and esterification reactions since these are equilibrium reactions that benefit from equilibrium shifts. The literature data on the performance of transesterification and esterification reactions are presented in Tables 23 and 24, respectively.

In the case of reactive distillation for transesterification reactions, the reaction of methanol and triglycerides and the separation of any excess or unreacted methanol are achieved simultaneously [181,184]. Unreacted methanol is recovered at the top of the column and is recycled to the feedstock, whilst the glycerol and esters are recovered at the bottom of the column and sent to a decanter. This processing method enables the use of a lower methanol to oil molar ratio and provides short residence times.

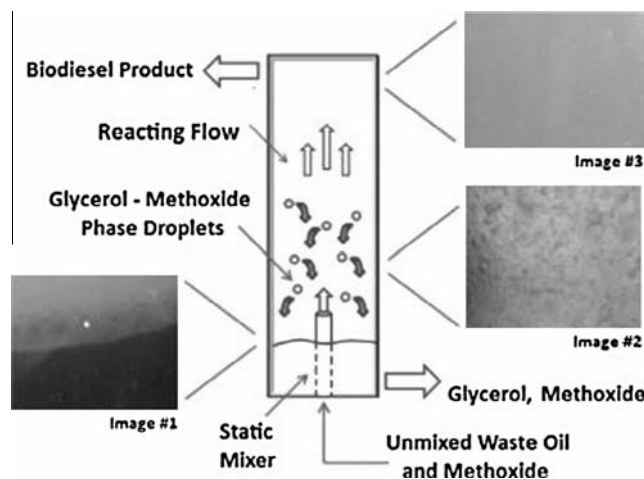


**Fig. 10.** Schematic diagram of the static mixer reactor/separator and corresponding images of the flow at different positions within the reactor [159].



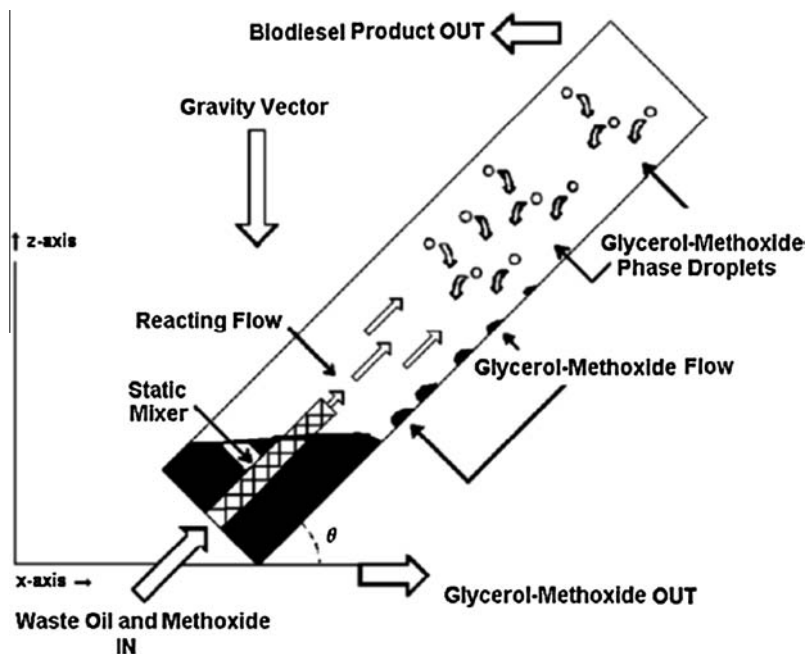


Fig. 11. Schematic diagram of the inclined static mixer reactor/separator and operating concept [160].

Table 19

Advantages and drawbacks of static mixers for the reaction of transesterification.

Static mixers	Advantages	Drawbacks
Transesterification	<ul style="list-style-type: none"> <li>– Reaction times reduced (<math>\times 2</math>–<math>10</math>)</li> <li>– Low energy-consumption</li> <li>– Relatively simple devices</li> <li>– Separation step implemented in the reactive part for the reactor-decanter</li> </ul>	<ul style="list-style-type: none"> <li>– May not be adapted to heterogeneous catalysis</li> </ul>

Esterification has also been successfully carried out by reactive distillation. It provides the opportunity to use a heterogeneous catalyst, thereby avoiding the neutralization, washing, separation and waste recovery steps [185]. It also enables the removal of water throughout the reaction at the top of the column, which shifts the reaction equilibrium and promotes product formation. Steini-geweg and Gmehling [182] used Amberlyst 15, an ion exchange resin that is fixed on the packing, to esterify decanoic acid and obtained 100% conversion at a pilot scale with a flow rate of 34 mol/h. Kiss et al. [185] investigated the choice of the heterogeneous catalyst. They found that zeolites have too small pores, which limit the diffusion of large molecules like fatty acids or esters. Ion exchange resins, such as Nafion or Amberlyst, have strong acid activity but a low thermal stability. Tungstophosphoric acid is very active but is also soluble in water and therefore cannot be reused. The authors concluded that sulfated zirconia is a good candidate as catalyst for esterification because it is active, stable and selective. Dimian et al. [186] investigated the possibility of using a co-solvent – 2-ethylhexanol – to increase the immiscibility between water and fatty acids so that the water can be more easily separated.

Fig. 14 shows the concept of reactive absorption using a heterogeneous catalyst as proposed by Kiss and Bildea [187]. Fatty acids

and methanol are fed at the top and bottom of the column, respectively, and water with some acid exits at the top of the column, whilst the bottom outlet stream contains FAME with some methanol.

The reactive distillation process can be further improved by using a divided wall column (DWC), which is particularly useful for reactive systems that have more than two products or that operate with an excess of reagent. This technology, which is analogous to the assembly of two distillation columns in one unit, allows the separation of multicomponents [188] and solves the problem encountered in reactive absorption, which is the necessity to use methanol in an exact stoichiometric ratio since it has to be completely converted. Indeed, this ratio is difficult to obtain especially because the amount of fatty acids in the feed is often unknown. Reactive distillation using a DWC allows the use of an excess of methanol, which is then recovered as the top distillate; water is then recovered as a side stream and FAME as the bottom product, as depicted in Fig. 15 [183].

Although there have been no demonstrative studies on the use of reactive distillation for the esterification with glycerol presented in the literature, this technology may be of interest for the reaction due to the high boiling points of glycerol and fatty acids, thereby allowing the removal of methanol and water. The use of reactive distillation for hydroesterification (i.e. combination of hydrolysis and esterification) is also of potential interest. Indeed, hydrolysis can be firstly performed with reactive distillation to concentrate the FFA content of oils that already have a high level of FFA before carrying out the esterification. This has been demonstrated numerically in a two-section reactive distillation process using WCO and Jatropa oil [189].

The advantages and drawbacks of reactive distillation for FAME production are summarized in Table 25. The main advantage of reactive distillation for FAME reactions is the fact that reaction and separation can be combined in the same device, thereby enabling the reaction equilibrium to be shifted and enhancing product formation. The principal disadvantage of this type of process is the high energy requirement, which is also an issue in conventional distillation processes.

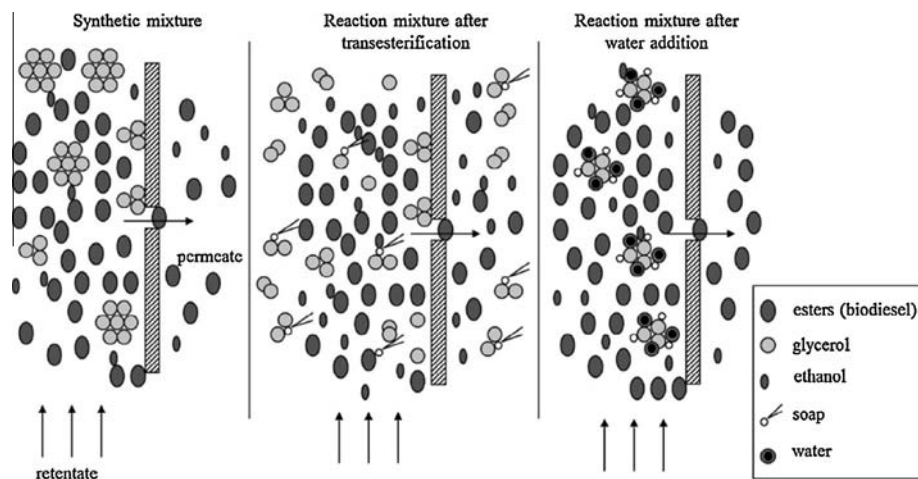


Fig. 12. Mechanism of separation of glycerol by microfiltration with a ceramic membrane [172].

Table 20

Results obtained for transesterification in membrane reactors. *y*: yield(%), *c*: conversion (%), *g*: glycerol content in permeate (%), *R*: molar ratio methanol:oil, *t*: residence time (min), *w*: weight fraction of catalyst (%), *T*: temperature (°C), *F*: flow rate.  $\phi$ : pore size ( $\mu\text{m}$ ), *V*: volume of the reactor (L) [167–169,171–173].

Oil	Catalyst	Performance			Reaction conditions					Reactor			Reference
		<i>y</i>	<i>c</i>	<i>g</i>	<i>R</i>	<i>t</i>	<i>w</i>	<i>T</i>	<i>F</i>	Membrane	$\phi$	<i>V</i>	
Canola	H <sub>2</sub> SO <sub>4</sub>	64	–	–	–	49	6	70	16.6 L/m <sup>2</sup> /h	Carbon	0.05	0.3	[167]
	NaOH	96	–	–	–	49	1	70	16.6 L/m <sup>2</sup> /h	Carbon	0.05	0.3	
Canola	NaOH	98.7	–	0	16	210	0.5	–	9 L/m <sup>2</sup> /h	Carbon	0.2	0.32	[168]
Canola	NaOH	98	–	–	24	5	0.5	65	120 kg/h	Filtanium ceramic	–	6	[169]
Canola	NaOH	–	–	<0.02	6	180	1	25	40–180 L/m <sup>2</sup> /h	Polyacrylonitrile membrane	–	–	[171]
Soybean (Ethanol)	NaOH	–	98.7	<0.02	9	80	1	30	10.3 kg/m <sup>2</sup> /h	Ceramic	0.2	0.25	[172]
WCO (FFA = 5%)	Base	>99	–	<0.02	23.9	35–105	0.5–1.4	65	30–40 L/m <sup>2</sup> /h	Titanium oxide	0.03	0.48–0.63–0.74	[173]

Table 21

Results obtained for esterification in membrane reactors. *y*: yield(%), *c*: conversion (%), *g*: glycerol content in permeate (%), *R*: molar ratio methanol:oil, *t*: residence time (min), *w*: weight fraction of catalyst (%), *T*: temperature (°C), *t*: residence time (h) [174].

Acid	Catalyst	Performance			Reaction conditions				Reactor			Reference
		<i>y</i>	<i>c</i>	<i>g</i>	<i>R</i>	<i>w</i>	<i>T</i>	<i>t</i>	Membrane	$\phi$ ( $\mu\text{m}$ )	<i>V</i> (L)	
Oleic	H <sub>2</sub> SO <sub>4</sub>	–	99.9	–	27	0.3	65	6	Polyvinylalcohol on polyether sulfone	–	0.073	[174]

Table 22

Advantages and drawbacks of membrane reactors for the reaction of transesterification.

Membrane reactors	Advantages	Drawbacks
Transesterification	<ul style="list-style-type: none"> <li>Retains Triglycerides (unreacted glycerides stay in the reactor), economy of downstream process costs</li> <li>Retains Di and Monoglycerides, allowing phase separation at room temperature</li> <li>Better separation of glycerol means less washing and less waste water</li> <li>Retains Glycerol, separation step during the reaction</li> <li>Low cost</li> </ul>	<ul style="list-style-type: none"> <li>No increase of reaction rates</li> </ul>
Esterification	<ul style="list-style-type: none"> <li>Separation of water during the reaction: shift of the equilibrium</li> </ul>	<ul style="list-style-type: none"> <li>No heterogeneous catalysts used</li> </ul>

### 3. Recommendations for the choice of process technologies for FAME production

Mass-transfer is the main limitation of the WCO transformation reactions, however, two additional parameters are also important when considering the choice of process technology. Firstly, the choice of the catalyst directly impacts the process performance. Secondly, the possibility to combine the reaction and separation steps to shift reaction equilibriums and easily separate products is important for process efficiency. The objective of this section is to give recommendations, following the review of literature data, on the choice of equipment taking into account the catalyst type and the separation aspects for the intensification of the different transesterification, esterification and hydrolysis reactions.

#### 3.1. Catalyst type

Table 26 summarizes the different types of catalysts that have been used for FAME production in various types of innovative process equipment. It can be seen that majority of studies have employed homogenous catalysts for transesterification and

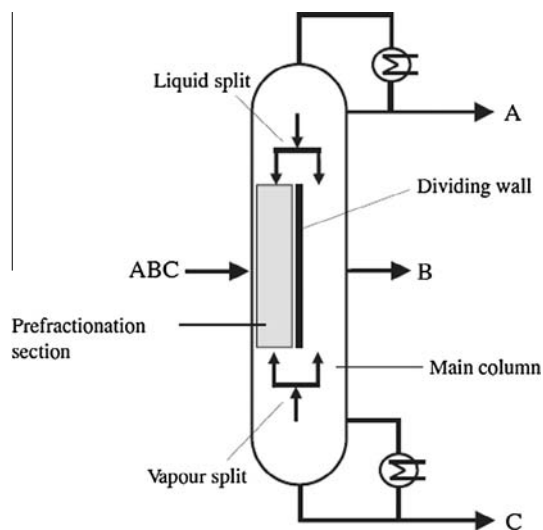


Fig. 13. Dividing wall column [180].

Table 23

Results obtained for transesterification in a reactive distillation column. *y*: yield(%), *c*: conversion (%), *R*: molar ratio methanol:oil, *t*: residence time (min), *w*: weight fraction of catalyst (%), *T*: temperature (°C), *F*: flow rate (L/h) [181].

Oil	Catalyst	Reaction conditions						Reference
		<i>y</i>	<i>c</i>	<i>R</i>	<i>t</i>	<i>w</i>	<i>F</i>	
Canola	KOH	94.4	95	4	3	1	4.9 L/h	[181]

esterification reactions because they are inexpensive and easy to use. On the other hand, heterogeneous catalysts have been less widely used due to traditionally higher operating temperatures and long reaction times. However, new catalysts, such as strontium oxide, scandium triflate or sulfated zirconia, have been developed and give similar performance to homogenous catalysts. For sustainable FAME production processes, the ensemble of the literature studies suggest that heterogeneous catalysts may be preferred over the conventional homogeneous catalysts because they can be easily reused and regenerated, and also allow easy product separation and elimination of the neutralization step. Moreover, heterogeneous catalysts coupled with intensified processes, such as microwaves and reactive distillation, have been shown to significantly enhance FAME production [136,183]. It is expected that heterogeneous catalysts may also provide improved reaction performance in other types of innovative continuous flow equipment, e.g. microstructured reactors, cavitation reactors, OBRs and static mixers, which have been proven successful for other applications in solids handling (suspensions or catalytic reactions) [110,190–192]. Indeed, further exploratory work on the use of heterogeneous catalysts in innovative process equipment for transesterification or other FAME production reactions is still required.

Table 24

Results obtained for esterification in a reactive distillation column. *y*: yield(%), *c*: conversion (%), *R*: molar ratio methanol:oil, *t*: residence time (min), *T*: temperature (°C), *P*: pressure (bar), *F*: flow rate [182,183].

Acid	Catalyst	Reaction conditions								Reference
		<i>y</i>	<i>c</i>	<i>R</i>	<i>t</i>	<i>T</i>	<i>P</i>	<i>F</i> (mol/h)		
Decanoic	Amberlyst 15		100	2	–	50	3	34 mol/h	[182]	
Dodecanoic			>99.99	1				1250 kg/h	[183]	

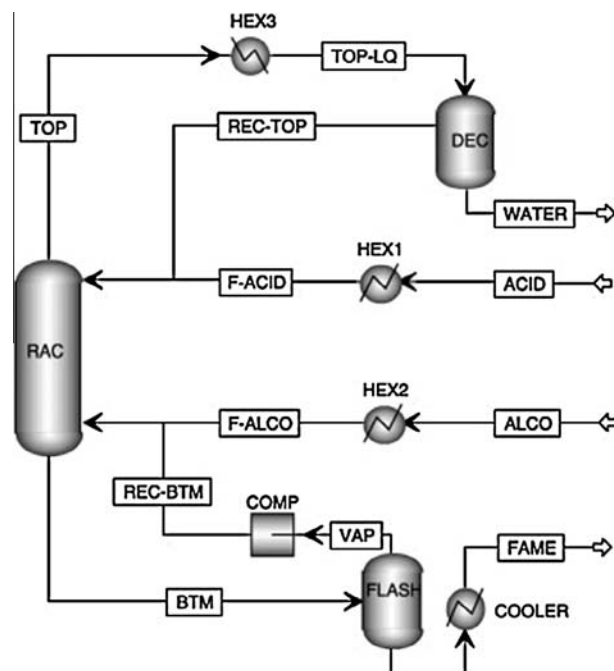


Fig. 14. Diagram of the reactive absorption. Water is recovered at the top of the column, FAME is recovered at the bottom of the column [187].

### 3.2. Product separation

Product separation is an important point to be considered in the design of sustainable processes since separation steps can be highly costly in terms of energy and time [38]. Separation steps can be combined with mixing and reaction operations in innovative equipment thereby shifting reaction equilibrium and enhancing process performance. Product separation and purification can also be facilitated by the use of heterogeneous catalysis and by inducing specific physical or chemical phenomena in the different process equipment.

Table 26 indicates how easy it is to separate products for the four reactions with different types of catalysts in various process equipment. Results from the literature show that microstructured reactors accelerate decantation due to the formation of parallel flow patterns or of bigger droplets with slug-flow. In cavitation reactors, the reaction is very fast, thereby hindering the formation of di and monoglycerides, which have surfactant properties. As a result, the emulsion is unstable and the phases are easy to separate. Microwave irradiation has also shown to accelerate the decantation process by enhancing drop coalescence. Membrane reactors have been shown to retain glycerides and soaps in transesterification, leading to highly pure products. Pervaporation membrane is also used to remove continuously water during esterification. It is expected that this type of technology may also be of interest for the other reactions. Reactive distillation has of course proven to be adapted to product separation for transesterification and esterification. However, it may not be of interest for

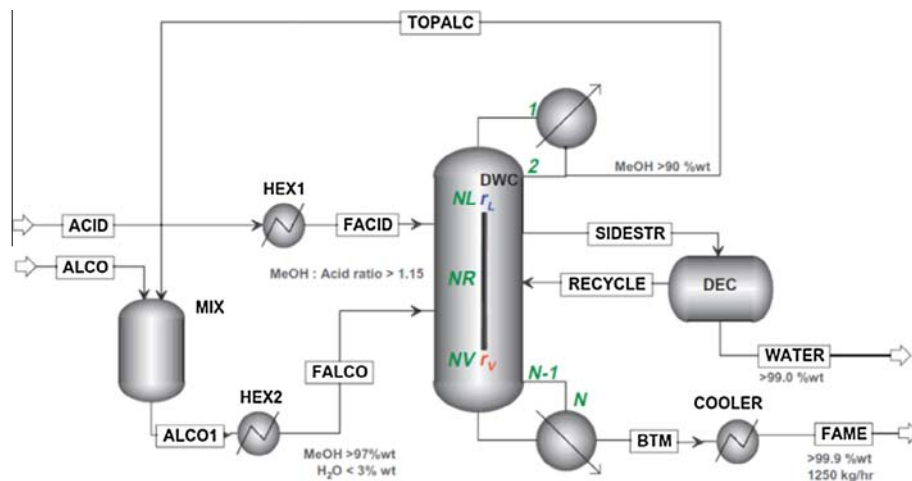


Fig. 15. Reactive dividing-wall column configuration [183]. Excess of methanol is recycled at the top, water is removed at the side and FAME is recovered at the bottom.

Table 25

Advantages and drawbacks of reactive distillation columns for the reaction of transesterification, esterification and hydrolysis.

Reactive Distillation	Advantages	Drawbacks
Transesterification	– Reaction and separation of the methanol in one single step	– Energy requirements
Esterification (with methanol)	– Reaction and separation in one single step – Possibility to have 3 streams, methanol (top), water (middle) and FAME (bottom) with R-DWC – Compatible with a heterogeneous catalyst	– Energy requirements ( $10^{-3} \text{ g}_{\text{FAME}}/\text{J}_{\text{reboiler}}$ ) (136 kW at the reboiler for a production of 1250 kg/h, data of Table 3 from Ref. [187])
Esterification (with glycerol)	– Remove of water (with methanol)	– No results found
Hydrolysis		– Products with high boiling points

Table 26

Summary of the type of catalyst used and the ease of separation in different process technologies for the four reactions. + indicates a positive effect of the technology; – indicates a negative effect; 0 indicates no effect. The data without brackets has been proven in literature studies whereas data between brackets is deduced from the results in the literature.

Reactor	Catalysis			Hydrolysis	Separation facilitation			
	Trans-esterification	Esterification			Trans-esterification	Esterification		Hydrolysis
		Methanol	Glycerol			Methanol	Glycerol	
Microreactor	Homogenous base Homogenous acid	Homogenous acid	Enzymes	Enzymes	++	(++)	(++)	(++)
Cavitation	Homogenous base	Homogenous acid Heterogeneous acid	Homogenous acid	None	+	(0)	(0)	(0)
Microwave	Homogenous base	Homogenous acid	Enzymes	Homogenous base	++	++	++	++
	Heterogeneous base	Heterogeneous acid	Heterogeneous acid	Enzymes				
Oscillatory Baffled Static mixers	Homogenous base	Homogenous acid	/	/	0	(0)	(0)	(0)
	Homogenous base	Homogenous acid	/	/	0	(0)	(0)	(0)
Membrane reactor	Homogenous base	Homogenous acid	/	/	+++	+++	(+++)	(+++)
Reactive distillation	Homogenous base	Homogenous acid	Homogenous acid	None	+++	+++	(+++)	(– – –)
		Heterogeneous acid						

the hydrolysis of triglycerides because it would remove water, which is in this case a reactant, and would shift equilibrium in the wrong direction. Oscillatory baffled reactors and static mixers do not integrate any specific separation operation. As a result, they

most often followed by a decanter for phase separation. However, novel devices such as static mixer with integrated decanter have shown to shift the transesterification reaction equilibrium by withdrawing the glycerol product [159,160].

**Table 27**

Summary of heterogeneous catalyzed reactions with forces of the different technologies. Technologies highlighted in bold are technologies of interest on an energy consumption criterion. *c*: conversion (%), *t*: residence time (min).

Catalysis		Process Equipment					
		Reactor performance		Recommended equipment for mass transfer	Selection criteria	Recommended equipment for product separation	Energy requirements (g/J)
<i>c</i> (%)	<i>t</i> (min)						
Transesterification	Heterogeneous (SrO/SiO <sub>2</sub> ) FFA and water tolerance increase to 3%	96–99	2–30	Static mixers	Less energy consuming Reaction time reduced	Decanter: glycerol removal	10 <sup>1</sup>
		97–100	1–6	Millireactors		Flow-pattern: accelerated decantation	10 <sup>-2</sup>
		95–99	<1 μs	Cavitation reactors	No DG/MG formation	10 <sup>-4</sup>	
		96–99.8	1–6	Microwave	Break emulsion between a polar and an oil phase Membrane: Keep unreacted glycerides (higher purity)	10 <sup>1</sup>	
		96–99	5–210	Membrane		Integrated separation unit	/
Esterification (Methanol)	Heterogeneous (Sulfated zirconia, Scandium trisulfate)	100	/	Reactive distillation	Shifted equilibrium due to product removal	Separation of water, methanol and esters	10 <sup>-6</sup>
		/	/	Static mixers		Decanter (water removal)	10 <sup>1</sup>
		99.9	/	Membrane		Membrane: Removal of water	/
Esterification (Glycerol)	Heterogeneous (Sulfated zirconia, Scandium trisulfate)	/	/	Cavitation Millireactors	Mixing intensification (reduce T, P) Reaction time reduced	Compatibility with an integrated decanter	10 <sup>-4</sup> 10 <sup>-2</sup>
		/	/	OBR		Recovery of unreacted glycerol	–
		99	30	Microwave	Shifted equilibrium due to product removal	Break emulsion between a polar and an oil phase	10 <sup>1</sup>
		/	/	Reactive distillation		Removal of water	>10 <sup>-6</sup>
		/	/				
Hydrolysis	Heterogeneous (SrO/SiO <sub>2</sub> ) (FFA and water tolerance increase to 3%)	/	/	Cavitation Millireactors	Mixing intensification (reduce T, P)	Compatibility with an integrated decanter	10 <sup>-4</sup> >10 <sup>-6</sup>
		/	/			Recovery of unreacted glycerol	
		100	5	Microwave	Integrated separation unit	Distillation (under vacuum)	10 <sup>-2</sup>
/	/	Membrane	Membrane: Keep unreacted glycerides (higher purity)retains soaps	/			

### 3.3. Equipment choice

Table 27 presents recommended choices of catalyst type and process equipment, for both reaction and separation, for the four different reactions related to FAME production and provides characteristic information on reaction conversion, time and the process energy requirements.

#### 3.3.1. Transesterification

Transesterification is the most common reaction used for obtaining FAME. In terms of catalysts, strontium oxide with silica is a very good candidate for transesterification reactions because its tolerance to FFA and water is high compared with other catalysts. Indeed, conversion of more than 90% can be achieved with FFA and water contents greater than 3 wt.%. Under these conditions, this means that WCO pretreatment steps may be not always be essential.

In transesterification reactions, the mixing process is important at the beginning of the operation where the objective is to increase the interfacial area between the triglycerides and the alcohol so that the reaction can take place. However, once the reaction starts, the generation of interfacial area by mixing is less difficult due to the formation of di- and monoglycerides, which facilitate liquid–liquid contacting and dispersion, leading to a pseudo-homogenous phase. Therefore, sophisticated mixing technology is not particularly required, which is why a low energy consumption reactor with static mixers may often be preferred. However, if the process objective is to reduce processing times, other intensified reactors

such cavitation, microstructured, microwave or oscillatory baffled reactors are recommended. In such equipment, the separation step of the transesterification process is facilitated naturally by inherent characteristics of the process and flow conditions or by combining it with a specific device for separation. For example: micro/microstructured reactors enable the generation of liquid–liquid flow patterns that ease product separation at the outlet; the formation of di- and monoglycerides and consequent pseudo-homogenous phase is avoided in cavitation reactors, thereby leading to a less stable emulsion and facilitating phase separation; microwaves promote the drop coalescence process, thereby speeding up the separation process. These different equipment types can also be used in combination with a decanter for product separation or with a membrane, which retains any unreacted glycerides and allows high purity esters to be obtained at 90% conversion.

#### 3.3.2. Esterification with methanol

In FAME production processes, esterification with methanol is often performed to reduce FFA levels in feedstock before performing base-catalyzed transesterification. Heterogeneous catalysts are preferred for the same reasons than previously. Good catalyst candidates are sulfated zirconia or scandium trisulfate, which have demonstrated high performance in reactive distillation and microwave reactors, respectively.

In esterification reactions, the mixing process has a more or less important role depending on the miscibility of the reactants, which is related to the length of the carbon chains. For immiscible reactants, mixing must be able to generate sufficient interfacial area

between the phases and flow circulation to promote the reaction. In the case of partially miscible reactants, drop break-up is less important but the mixing of reactants is still vital for reaction performance. Amongst the different innovative process equipment, both reactive distillation and static mixer systems with an integrated decanter appear to give best results for esterification. Indeed, in these systems the products are continuously separated from the reactive media, thereby shifting the reaction equilibrium and enhancing product formation. The use of membranes could also be considered in order to retain unreacted glycerides and produce high purity esters.

### 3.3.3. Esterification with glycerol

Esterification using glycerol, which is a side-product of transesterification, is an interesting way to decrease the FFA levels in high FFA content WCO. Heterogeneous acid catalysis using sulfated zirconia or scandium triflate appears to be the most appropriate means to catalyse the reaction.

In esterification reactions using glycerol, mixing is an important step of the process due to the very low solubility of reactants (i.e. fatty acids and glycerol). Indeed, the mixing operation determines interfacial area available for mass transfer and the fluid circulation, both of which are important for the progress of the reaction. Conventionally, high temperatures are used to increase reactant solubility and to facilitate fluid contacting with the disadvantage of high operating costs. Cavitation, microwave, oscillatory baffled and microstructured reactors provide a means to intensify mixing and fluid contacting at ambient operating conditions, thereby being more energy efficient. Reactive distillation under vacuum conditions can also be used to shift the reaction equilibrium and separate products, but with the disadvantage of requiring higher energy input. A static mixer reactor-decanter that shifts the reaction equilibrium may also be a recommended choice if reaction yield is the principal process objective.

### 3.3.4. Hydrolysis

The primary interest of the hydrolysis of triglycerides is to concentrate fatty acids in the feedstock. Strontium oxide is possibly a good candidate for heterogeneous catalysis. Like for the esterification reaction with glycerol, the mixing process is very important due to low solubility of reactants. As a result, conventional processing often requires high temperatures and pressures to ensure sufficient yield and acceptable reaction times. Intensified process technologies such as cavitation, microwave, oscillatory baffled or microstructure reactors can be used to intensify mixing and allow good reaction performance with milder operating conditions. Reactive distillation is not recommended since it would result in the removal of water and would not promote the formation of products. The separation of products – fatty acids and glycerol – can be carried out with a distillation column under vacuum conditions or in microstructured reactors by generating slug-flow or parallel flow, which accelerate the decanting process. Since glycerol and fatty acids are miscible if the reactive medium is basic [193], the combined reactor-decanter is a means to facilitate product separation and limit the formation of soap. Contactors combined with membranes, which retain unreacted glycerides, are also a recommended means for obtaining high purity products.

## 4. Conclusion

A review of the different process equipment that can be used to intensify FAME production has been presented. Continuous process technologies that intensify mixing and fluid contacted are recommended because the four reactions related to FAME production involved immiscible liquid–liquid reactants. The product separation

step has been taken into account in the discussion and equipment that combine the reaction and separation steps are particularly recommended. The implementation of heterogeneous catalysis in these innovative process intensification technologies has also been discussed. Finally, specific process equipment has been recommended for the intensification of FAME based on different selection criteria.

It can be seen from this review that various types of innovative process equipment, such as cavitation reactors, oscillatory baffled reactors, microwave reactors, reactive distillation, static mixers and microstructured reactors enable significant mass transfer enhancement and improved performance of FAME production compared with conventional batch tank processes. Furthermore, the integration of continuous reaction and separation units appears to provide the best means for intensifying FAME production, leaving thus a vast number of configurations to be explored or invented. Amongst the different reactor types mentioned in this review, several are poorly understood in terms of physical phenomena and operating characteristics in liquid–liquid reaction applications. In particular, much fundamental knowledge on the operation of cavitation reactors, oscillatory baffled reactors and microwave reactors is still required. Further to this, the development of microwave reactors that are adapted to industrial FAME demands still requires significant work and considering this, continuous microwave reactors may be particularly interesting to explore. It should also be pointed out that heterogeneous catalysts have shown provide attractive results in terms of reaction performance in certain equipment (e.g. microwave reactors, reactive distillation) and therefore deserve to be explored further in other innovative process equipment, such as oscillatory baffled reactors and cavitation reactors.

Indeed, the choice of one process technology over another for FAME production is not that straightforward and it clearly depends on the global process objectives. Of course, some equipment (e.g. static mixers and microwave reactors) may be attractive due to their low energy consumption; others, such as reactive distillation, may be preferred due to effective product separation despite high energy requirements. However, although the number of studies on the feasibility of different process technologies for FAME production is significant, detailed economical and energy efficiency analyses of the various technologies and processes are still needed. These, in addition to studies on reaction performance, will of course be vital for the development of sustainable and green FAME production processes and therefore should be considered in the future studies.

## Acknowledgments

This study is part of the AGRIBTP Project on bioproducts for building and public work that is funded by the European Union, the French Government and the Région Midi-Pyrénées.

## References

- [1] J. Kansedo, K.T. Lee, S. Bhatia, Cerbera odollam (sea mango) oil as a promising non-edible feedstock for biodiesel production, *Fuel* 88 (2009) 1148–1150.
- [2] J.O. Metzger, Fats and oils as renewable feedstock for chemistry, *European Journal of Lipid Science and Technology* 111 (2009) 865–876.
- [3] M.M. Gui, K.T. Lee, S. Bhatia, Feasibility of edible oil vs. non-edible oil vs. waste edible oil as biodiesel feedstock, *Energy* 33 (2008) 1646–1653.
- [4] H. Taher, S. Al-Zuhair, A.H. Al-Marzouqi, Y. Haik, M.M. Farid, A review of enzymatic transesterification of microalgal oil-based biodiesel using supercritical technology, *Enzyme Research* 2011 (2011) 1–25.
- [5] Y. Zhang, M.A. Dube, D.D. McLean, M. Kates, Biodiesel production from waste cooking oil: 2. Economic assessment and sensitivity analysis, *Bioresource Technology* 90 (2003) 229–240.
- [6] A. Banerjee, R. Chakraborty, Parametric sensitivity in transesterification of waste cooking oil for biodiesel production—a review, *Resources, Conservation and Recycling* 53 (2009) 490–497.

- [7] M.G. Kulkarni, A.K. Dalai, Waste cooking oil an economical source for biodiesel: a review, *Industrial & Engineering Chemistry Research* 45 (2006) 2901–2913.
- [8] Article R1331–2, n.d.
- [9] Food Standards Agency website, (n.d.).
- [10] Restaurant Technologies Inc. <<http://www.rti-inc.com>>.
- [11] Shakopee Mdewakanton Dakota Community. <<http://www.shakopeedakota.org>>.
- [12] D. Bégin, M. Gérin, I. de recherche en santé et en sécurité du travail du Québec, U. de M.D. de médecine du travail et d'hygiène du milieu, in: *La substitution des solvants par la N-méthyl-2-pyrrolidone*, Institut de recherche en santé et en sécurité du travail du Québec, 1999.
- [13] Kooperationsstelle Hamburg, Layman Report – Reduction of VOC emissions by using fatty acid esters for metal cleaning processes, n.d.
- [14] A.J. Hutchinson, V.G. Gomes, L.J. Hyde, Engineering an anti-graffiti system: a study in industrial product design, *Chemical Engineering & Technology* 27 (2004) 874–879.
- [15] NDCEE, NDCEE Determines Lactate Esters Are Effective Nontoxic Cleaning Materials, 2003.
- [16] R. von Wedel, Cytosol-cleaning oiled shorelines with a vegetable oil biosolvent, *Spill Science & Technology Bulletin* 6 (2000) 357–359.
- [17] P.A. Noirot, Green ink for all colors, *Ink Maker* 82 (2004) 29–31.
- [18] P. Van Broekhuizen, Technical and non-technical aspects in the substitution of mineral oil based products by vegetable alternatives, *Agro Food Industry Hi-tech* 12 (2001) 39–43.
- [19] R. Höfer, J. Bigorra, Green chemistry – a sustainable solution for industrial specialties applications, *Green Chemistry* 9 (2007) 203.
- [20] D. Charlemagne, The contribution of lipochemistry to the plant protection industry, *OCL-Oléagineux, Corps Gras, Lipides* 6 (1999) 401–404.
- [21] D.Y.C. Leung, X. Wu, M.K.H. Leung, A review on biodiesel production using catalyzed transesterification, *Applied Energy* 87 (2010) 1083–1095.
- [22] M.K. Lam, K.T. Lee, A.R. Mohamed, Homogeneous, heterogeneous and enzymatic catalysis for transesterification of high free fatty acid oil (waste cooking oil) to biodiesel: a review, *Biotechnology Advances* 28 (2010) 500–518.
- [23] C.C. Enweremadu, M.M. Mbarawa, Technical aspects of production and analysis of biodiesel from used cooking oil—a review, *Renewable and Sustainable Energy Reviews* 13 (2009) 2205–2224.
- [24] A.P. Vyas, J.L. Verma, N. Subrahmanyam, A review on FAME production processes, *Fuel* 89 (2010) 1–9.
- [25] Z. Helwani, M.R. Othman, N. Aziz, W.J.N. Fernando, J. Kim, Technologies for production of biodiesel focusing on green catalytic techniques: a review, *Fuel Processing Technology* 90 (2009) 1502–1514.
- [26] E.M. Shahid, Y. Jamal, Production of biodiesel: a technical review, *Renewable and Sustainable Energy Reviews* (2011).
- [27] P.-L. Boey, G.P. Maniam, S.A. Hamid, Performance of calcium oxide as a heterogeneous catalyst in biodiesel production: a review, *Chemical Engineering Journal* 168 (2011) 15–22.
- [28] Y.C. Sharma, B. Singh, J. Korstad, Latest developments on application of heterogeneous basic catalysts for an efficient and eco friendly synthesis of biodiesel: a review, *Fuel* 90 (2011) 1309–1324.
- [29] A.P. Chouhan, A.K. Sarma, Modern heterogeneous catalysts for biodiesel production: a comprehensive review, *Renewable and Sustainable Energy Reviews* 15 (2011) 4378–4399.
- [30] S. Semwal, A.K. Arora, R.P. Badoni, D.K. Tuli, Biodiesel production using heterogeneous catalysts, *Bioresource Technology* 102 (2011) 2151–2161.
- [31] I.M. Atadashi, M.K. Aroua, A.R. Abdul Aziz, N.M.N. Sulaiman, The effects of catalysts in biodiesel production: a review, *Journal of Industrial and Engineering Chemistry* 19 (2013) 14–26.
- [32] Z. Qiu, L. Zhao, L. Weatherley, Process intensification technologies in continuous biodiesel production, *Chemical Engineering and Processing: Process Intensification* 49 (2010) 323–330.
- [33] A. Talebian-Kiakalaieh, N.A.S. Amin, H. Mazaheri, A review on novel processes of biodiesel production from waste cooking oil, *Applied Energy* 104 (2013) 683–710.
- [34] G.L. Maddikeri, A.B. Pandit, P.R. Gogate, Intensification approaches for biodiesel synthesis from waste cooking oil: a review, *Industrial & Engineering Chemistry Research* 51 (2012) 14610–14628.
- [35] P.P. Oh, H.L.N. Lau, J. Chen, M.F. Chong, Y.M. Choo, A review on conventional technologies and emerging process intensification (PI) methods for biodiesel production, *Renewable and Sustainable Energy Reviews* 16 (2012) 5131–5145.
- [36] A.A. Refaat, Different techniques for the production of biodiesel from waste vegetable oil, *International Journal of Environmental Science and Technology* 7 (2010) 183–213.
- [37] A.A. Kiss, C.S. Bildea, A review of biodiesel production by integrated reactive separation technologies, *Journal of Chemical Technology & Biotechnology* 87 (2012) 861–879.
- [38] I.M. Atadashi, M.K. Aroua, A.A. Aziz, Biodiesel separation and purification: a review, *Renewable Energy* 36 (2011) 437–443.
- [39] M. Canakci, J. Van Gerpen, Biodiesel production from oils and fats with high free fatty acids, *Transactions-American Society of Agricultural Engineers* 44 (2001) 1429–1436.
- [40] V. Makareviciene, E. Sendzikiene, P. Janulis, Solubility of multi-component biodiesel fuel systems, *Bioresource Technology* 96 (2005) 611–616.
- [41] J.M. Encinar, J.F. González, A. Rodríguez-Reinos, Biodiesel from used frying oil. Variables affecting the yields and characteristics of the biodiesel, *Industrial & Engineering Chemistry Research* 44 (2005) 5491–5499.
- [42] J. Cvengroš, Z. Cvengrošová, Used frying oils and fats and their utilization in the production of methyl esters of higher fatty acids, *Biomass and Bioenergy* 27 (2004) 173–181.
- [43] H. Fukuda, A. Kondo, H. Noda, Biodiesel fuel production by transesterification of oils, *Journal of Bioscience and Bioengineering* 92 (2001) 405–416.
- [44] A.A. Refaat, N.K. Attia, H.A. Sibak, S.T. El Sheltawy, G.I. El Diwani, et al., Production optimization and quality assessment of biodiesel from waste vegetable oil, *International Journal of Environmental Science and Technology* 5 (2008) 75–82.
- [45] B. Freedman, E.H. Pryde, T.L. Mounts, Variables affecting the yields of fatty esters from transesterified vegetable oils, *Journal of the American Oil Chemists' Society* 61 (1984) 1638–1643.
- [46] C.L. Chen, C.C. Huang, D.T. Tran, J.S. Chang, Biodiesel synthesis via heterogeneous catalysis using modified strontium oxides as the catalysts, *Bioresource Technology* 113 (2012) 8–13.
- [47] X. Liu, H. He, Y. Wang, S. Zhu, Transesterification of soybean oil to biodiesel using SrO as a solid base catalyst, *Catalysis Communications* 8 (2007) 1107–1111.
- [48] E. Tur, B. Onal-Ulusoy, E. Akdogan, M. Mutlu, Surface modification of polyethersulfone membrane to improve its hydrophobic characteristics for waste frying oil filtration: radio frequency plasma treatment, *Journal of Applied Polymer Science* 123 (2012) 3402–3411.
- [49] C.E.C. Rodrigues, C.B. Gonçalves, E. Batista, A.J.A. Meirelles, Deacidification of vegetable oils by solvent extraction, *Recent Patents on Engineering* 1 (2007) 95–102.
- [50] J.F. Gomes, D. Vergueiro, Study on the glycerolysis reaction of high free fatty acid oils for use as biodiesel feedstock, *Fuel Processing Technology* 92 (2011) 1225–1229.
- [51] D.A. Echeverri, F. Cardeño, L.A. Rios, Glycerolysis of soybean oil with crude glycerol containing residual alkaline catalysts from biodiesel production, *Journal of the American Oil Chemists' Society* 88 (2010) 551–557.
- [52] M. Kotwal, S.S. Deshpande, D. Srinivas, Esterification of fatty acids with glycerol over Fe–Zn double-metal cyanide catalyst, *Catalysis Communications* 12 (2011) 1302–1306.
- [53] Y. Wang, R.H. Natelson, L.F. Stikeleather, W.L. Roberts, Solid superacid catalyzed glycerol esterification of free fatty acids in waste cooking oil for biodiesel production, *European Journal of Lipid Science and Technology* (2012).
- [54] S.M. Kim, J.S. Rhee, Production of medium-chain glycerides by immobilized lipase in a solvent-free system, *Journal of the American Oil Chemists' Society* 68 (1991) 499–501.
- [55] A. Robles Medina, L. Esteban Cerdán, A. Giménez Giménez, B. Camacho Páez, M.J. Ibáñez González, E. Molina Grima, Lipase-catalyzed esterification of glycerol and polyunsaturated fatty acids from fish and microalgae oils, *Progress in Industrial Microbiology* 35 (1999) 379–391.
- [56] W.-C. Wang, R.H. Natelson, L.F. Stikeleather, W.L. Roberts, CFD simulation of transient stage of continuous countercurrent hydrolysis of canola oil, *Computers & Chemical Engineering* 43 (2012) 108–119.
- [57] H.L. Barnebey, A.C. Brown, Continuous fat splitting plants using the Colgate-Emery process, *Journal of the American Oil Chemists' Society* (1948) 95–99.
- [58] J.K. Satyarthi, D. Srinivas, P. Ratnasamy, Hydrolysis of vegetable oils and fats to fatty acids over solid acid catalysts, *Applied Catalysis A: General* 391 (2011) 427–435.
- [59] G.D. Machado, D.A.G. Aranda, M. Castier, V.F. Cabral, L. Cardozo-Filho, Computer simulations of fatty acid esterification in reactive distillation columns, *Industrial & Engineering Chemistry Research* 50 (2011) 10176–10184.
- [60] H. Noureddini, D. Zhu, Kinetics of transesterification of soybean oil, *Journal of the American Oil Chemists' Society* 74 (1997) 1457–1463.
- [61] H.A. Farag, A. El-Maghraby, N.A. Taha, Optimization of factors affecting esterification of mixed oil with high percentage of free fatty acid, *Fuel Processing Technology* 92 (2011) 507–510.
- [62] D. Ballerini, T. Chapus, G. Hillion, X. Montagne, Les esters d'huile végétale, in: *Les Biocarburants*, 2011: p. 129.
- [63] D. Frascari, M. Zuccaro, A. Paglianti, D. Pinelli, Optimization of mechanical agitation and evaluation of the mass-transfer resistance in the oil transesterification reaction for biodiesel production, *Industrial & Engineering Chemistry Research* 48 (2009) 7540–7549.
- [64] Y. Zhang, M.A. Dube, D.D. McLean, M. Kates, Biodiesel production from waste cooking oil: 1. Process design and technological assessment, *Bioresource Technology* 89 (2003) 1–16.
- [65] P. Cintas, S. Mantegna, E.C. Gaudino, G. Cravotto, A new pilot flow reactor for high-intensity ultrasound irradiation, Application to the Synthesis of Biodiesel, *Ultrasonics Sonochemistry* 17 (2010) 985–989.
- [66] M. Slinn, K. Kendall, Developing the reaction kinetics for a biodiesel reactor, *Bioresource Technology* 100 (2009) 2324–2327.
- [67] G. Guan, M. Teshima, C. Sato, S. Mo Son, M. Faisal Irfan, K. Kusakabe, et al., Two-phase flow behavior in microtube reactors during biodiesel production from waste cooking oil, *AIChE Journal* 56 (2009) 1383–1390.
- [68] O.S. Stamenkovic, Z.B. Todorovic, M.L. Lazic, V.B. Veljkovic, D.U. Skala, Kinetics of sunflower oil methanolysis at low temperatures, *Bioresource Technology* 99 (2008) 1131–1140.
- [69] R. Heryanto, M. Hasan, E.C. Abdullaha, A.C. Kumoro, Solubility of stearic acid in various organic solvents and its prediction using non-ideal solution models 33 (2007) 469–472.

- [71] L. Marrone, L. Pasco, D. Moscatelli, S. Gelosa, Liquid-liquid phase equilibrium in glycerol-methanol-fatty acids systems, *Chemical Engineering* 11 (2007).
- [72] D.A. Aranda, C. da Silva, C. Detoni, Current processes in Brazilian biodiesel production, *International Review of Chemical Engineering* 1 (2009) 603–608.
- [73] D. Reay, C. Ramshaw, A. Harvey, *Process Intensification: Engineering for Efficiency, Sustainability and Flexibility*, first ed., Butterworth-Heinemann, 2008.
- [74] M. Poux, P. Cognet, C. Gourdon, *Génie des procédés durables: Du concept à la concrétisation industrielle*, Paris, 2010.
- [75] W. Ehrfeld, V. Hessel, H. Löwe, *Microreactors: New Technology for Modern Chemistry*, Wiley-VCH, Weinheim, 2000.
- [76] N. Kockmann, *Micro Process Engineering: Fundamentals, Devices, Fabrication and Applications*, Wiley-VCH, Weinheim, 2006.
- [77] M.N. Kashid, L. Kiwi-Minsker, Microstructured reactors for multiphase reactions: state of the art, *Industrial & Engineering Chemistry Research* 48 (2009) 6465–6485.
- [78] A.L. Dessimoz, L. Cavin, A. Renken, L. Kiwi-Minsker, Liquid-liquid two-phase flow patterns and mass transfer characteristics in rectangular glass microreactors, *Chemical Engineering Science* 63 (2008) 4035–4044.
- [79] J. Jovanovic, E. Rebrov, T.A. Nijhuis, M.T. Kreutzer, V. Hessel, J.C. Schouten, Liquid-liquid flow in long capillaries: hydrodynamic flow patterns and extraction performance, *Industrial & Engineering Chemistry Research* 51 (2011) 1015–1026.
- [80] A. Pohar, M. Lakner, I. Plazl, Parallel flow of immiscible liquids in a microreactor: modeling and experimental study, *Microfluidics and Nanofluidics* 12 (2011) 307–316.
- [81] Z. Wen, X. Yu, S.-T. Tu, J. Yan, E. Dahlquist, Intensification of biodiesel synthesis using zigzag micro-channel reactors, *Bioresource Technology* 100 (2009) 3054–3060.
- [82] G. Guan, K. Kusakabe, K. Moriyama, N. Sakurai, Transesterification of sunflower oil with methanol in a microtube reactor, *Industrial & Engineering Chemistry Research* 48 (2009) 1357–1363.
- [83] J. Sun, J. Ju, L. Ji, L. Zhang, N. Xu, Synthesis of biodiesel in capillary microreactors, *Industrial & Engineering Chemistry Research* 47 (2008) 1398–1403.
- [84] R. Jachuck, G. Pherwani, S.M. Gorton, Green engineering: continuous production of biodiesel using an alkaline catalyst in an intensified narrow channel reactor, *Journal of Environmental Monitoring* 11 (2009) 642.
- [85] E.E. Kalu, K.S. Chen, T. Gedris, Continuous-flow biodiesel production using slit-channel reactors, *Bioresource Technology* 102 (2011) 4456–4461.
- [86] D.E. Leng, R.V. Calabrese, E.L. Paul, V.A. Atiemo-Obeng, S.M. Kresta, *Immiscible Liquid-Liquid Systems in Handbook of Industrial Mixing: Science & Practice*, John Wiley & Sons Inc., Hoboken NJ, 2004.
- [87] P. Sun, J. Sun, J. Yao, L. Zhang, N. Xu, Continuous production of biodiesel from high acid value oils in microstructured reactor by acid-catalyzed reactions, *Chemical Engineering Journal* 162 (2010) 364–370.
- [88] S. Matsuura, R. Ishii, T. Itoh, S. Hamakawa, T. Tsunoda, T. Hanaoka, et al., Immobilization of enzyme-encapsulated nanoporous material in a microreactor and reaction analysis, *Chemical Engineering Journal* 167 (2011) 744–749.
- [89] Corning Microreactor technology brings new market to Corning, (n.d.).
- [90] Chart: Compact Heat Exchange Reactors, (n.d.).
- [91] Ehrfeld website, (n.d.).
- [92] IMM Website: Liquid/Liquid Microreactor, (n.d.).
- [93] P.R. Gogate, Cavitation reactors for process intensification of chemical processing applications: a critical review, *Chemical Engineering and Processing: Process Intensification* 47 (2008) 515–527.
- [94] V.L. Gole, P.R. Gogate, A review on intensification of synthesis of biodiesel from sustainable feed stock using sonochemical reactors, *Chemical Engineering and Processing: Process Intensification* 53 (2012) 1–9.
- [95] P.R. Gogate, R.K. Tayal, A.B. Pandit, Cavitation: a technology on the horizon, *Current Science* 91 (2006) 35–46.
- [96] V.B. Veljkovic, J.M. Avramovic, O.S. Stamenkovic, Biodiesel production by ultrasound-assisted transesterification: state of the art and the perspectives, *Renewable and Sustainable Energy Reviews* 16 (2012) 1193–1209.
- [97] A.S. Badday, A.Z. Abdullah, K.T. Lee, M.S. Khayoon, Intensification of biodiesel production via ultrasonic-assisted process: a critical review on fundamentals and recent development, *Renewable and Sustainable Energy Reviews* 16 (2012) 4574–4587.
- [98] K. Ramachandran, T. Suganya, N. Nagendra Gandhi, S. Renganathan, Recent developments for biodiesel production by ultrasonic assist transesterification using different heterogeneous catalyst: a review, *Renewable and Sustainable Energy Reviews* 22 (2013) 410–418.
- [99] C. Stavarache, M. Vinatoru, R. Nishimura, Y. Maeda, Conversion of vegetable oil to biodiesel using ultrasonic irradiation, *Cheminfor* 34 (2003).
- [100] C. Stavarache, M. Vinatoru, R. Nishimura, Y. Maeda, Fatty acids methyl esters from vegetable oil by means of ultrasonic energy, *Ultrasonics Sonochemistry* 12 (2005) 367–372.
- [101] X. Fan, F. Chen, X. Wang, Ultrasound-assisted synthesis of biodiesel from crude cottonseed oil using response surface methodology, *Journal of Oleo Science* 59 (2010) 235–241.
- [102] J.A. Colucci, E.E. Borrero, F. Alape, Biodiesel from an alkaline transesterification reaction of soybean oil using ultrasonic mixing, *Journal of the American Oil Chemists' Society* 82 (2005) 525–530.
- [103] A.K. Singh, S.D. Fernando, R. Hernandez, Base-catalyzed fast transesterification of soybean oil using ultrasonication, *Energy & Fuels* 21 (2007) 1161–1164.
- [104] P. Chand, V.R. Chintareddy, J.G. Verkade, D. Grewell, Enhancing biodiesel production from soybean oil using ultrasonics, *Energy & Fuels* 24 (2010) 2010–2015.
- [105] H.D. Hanh, N. The Dong, C. Stavarache, K. Okitsu, Y. Maeda, R. Nishimura, Methanolysis of triolein by low frequency ultrasonic irradiation, *Energy Conversion and Management* 49 (2008) 276–280.
- [106] L.S. Teixeira, J.C. Assis, D.R. Mendonça, I.T. Santos, P.R. Guimaraes, L.A. Pontes, et al., Comparison between conventional and ultrasonic preparation of beef tallow biodiesel, *Fuel Processing Technology* 90 (2009) 1164–1166.
- [107] L.T. Thanh, K. Okitsu, Y. Sadanaga, N. Takenaka, Y. Maeda, H. Bandow, Ultrasound-assisted production of biodiesel fuel from vegetable oils in a small scale circulation process, *Bioresource Technology* 101 (2010) 639–645.
- [108] L.T. Thanh, K. Okitsu, Y. Sadanaga, N. Takenaka, Y. Maeda, H. Bandow, A two-step continuous ultrasound assisted production of biodiesel fuel from waste cooking oils: a practical and economical approach to produce high quality biodiesel fuel, *Bioresource Technology* 101 (2010) 5394–5401.
- [109] C. Stavarache, M. Vinatoru, Y. Maeda, H. Bandow, Ultrasonically driven continuous process for vegetable oil transesterification, *Ultrasonics Sonochemistry* 14 (2007) 413–417.
- [110] M.A. Kelkar, P.R. Gogate, A.B. Pandit, Intensification of esterification of acids for synthesis of biodiesel using acoustic and hydrodynamic cavitation, *Ultrasonics Sonochemistry* 15 (2008) 188–194.
- [111] V.G. Deshmane, P.R. Gogate, A.B. Pandit, Process intensification of synthesis process for medium chain glycerides using cavitation, *Chemical Engineering Journal* 145 (2008) 351–354.
- [112] A.B. Pandit, J.B. Joshi, Hydrolysis of fatty oils: effect of cavitation, *Chemical Engineering Science* 48 (1993) 3440–3442.
- [113] O.V. Kozyuk, Apparatus and Method for Producing Biodiesel from Fatty Acid Feedstock, US Patent 7754905, 2010.
- [114] D. Ghayal, A.B. Pandit, V.K. Rathod, Optimization of biodiesel production in a hydrodynamic cavitation reactor using used frying oil, *Ultrasonics Sonochemistry* 20 (2013) 322–328.
- [115] P.R. Muniyappa, S.C. Brammer, H. Nouredini, Improved conversion of plant oils and animal fats into biodiesel and co-product, *Chemical and Biomolecular Engineering Research and Publications* (1996).
- [116] Arisdyn website, (n.d.).
- [117] Hydro Dynamics, Inc. website, (n.d.).
- [118] D.G. Mancosky, D.A. Armstead, T. McGurk, G. Hopkins, K. Hudson, *The Use of a Controlled Cavitation Reactor for Bio-Diesel Production*, 2007.
- [119] D.M.P. Mingos, D.R. Baghurst, Tilden lecture. Applications of microwave dielectric heating effects to synthetic problems in chemistry, *Chemical Society Reviews* 20 (1991) 1.
- [120] P. Lidström, J. Tierney, B. Wathey, J. Westman, Microwave assisted organic synthesis—a review, *Tetrahedron* 57 (2001) 9225–9283.
- [121] A. Loupy, *Microwave en Organic Synthesis*, Wiley-VCH, Weinheim, 2006.
- [122] C.O. Kappe, D. Dallinger, S.S. Murphree, *Practical Microwave Synthesis for Organic Chemists: Strategies, Instruments and Protocols*, Wiley-VCH, Weinheim, 2009.
- [123] F. Motasemi, F.N. Ani, A review on microwave-assisted production of biodiesel, *Renewable and Sustainable Energy Reviews* 16 (2012) 4719–4733.
- [124] V.G. Gude, P. Patil, E. Martinez-Guerra, S. Deng, N. Nirmalakhandan, Microwave energy potential for biodiesel production, *Microwave Energy Potential for Biodiesel Production* 1 (2013) 1–31.
- [125] B.G. Terigar, S. Balasubramanian, M. Lima, D. Boldor, Transesterification of soybean and rice bran oil with ethanol in a continuous-flow microwave-assisted system: yields, Quality, and Reaction Kinetics, *Energy & Fuels* 24 (2010) 6609–6615.
- [126] Y. Asamuka, Y. Ogawa, K. Maeda, K. Fukui, H. Kuramochi, Effects of microwave irradiation on triglyceride transesterification: experimental and theoretical studies, *Biochemical Engineering Journal* 58–59 (2011) 20–24.
- [127] A. Breccia, B. Esposito, G. Breccia Fratadocchi, A. Fini, Reaction between methanol and commercial seed oils under microwave irradiation, *International Microwave Power Institute* 34 (1999) 1–8.
- [128] N.E. Leadbeater, L.M. Stencel, Fast, easy preparation of biodiesel using microwave heating, *Energy & Fuels* 20 (2006) 2281–2283.
- [129] A.A. Refaat, S.T. El Sheltawy, K.U. Sadek, et al., Optimum reaction time, performance and exhaust emissions of biodiesel produced by microwave irradiation, *International Journal of Environmental Science and Technology* 5 (2008) 315–322.
- [130] N. Azcan, A. Danisman, Microwave assisted transesterification of rapeseed oil, *Fuel* 87 (2008) 1781–1788.
- [131] Y. Zu, S. Zhang, Y. Fu, W. Liu, Z. Liu, M. Luo, et al., Rapid microwave-assisted transesterification for the preparation of fatty acid methyl esters from the oil of yellow horn (*Xanthoceras sorbifolia* Bunge.), *European Food Research and Technology* 229 (2009) 43–49.
- [132] A. Kanitkar, S. Balasubramanian, M. Lima, D. Boldor, A critical comparison of methyl and ethyl esters production from soybean and rice bran oil in the presence of microwaves, *Bioresource Technology* 102 (2011) 7896–7902.
- [133] M.Z. Duz, A. Saydut, G. Ozturk, Alkali catalyzed transesterification of safflower seed oil assisted by microwave irradiation, *Fuel Processing Technology* 92 (2011) 308–313.
- [134] V. Lertsathapornasuk, R. Pairintra, K. Aryusuk, K. Krisnangkura, Microwave assisted in continuous biodiesel production from waste frying palm oil and its performance in a 100 kW diesel generator, *Fuel Processing Technology* 89 (2008) 1330–1336.



- [135] T.M. Barnard, N.E. Leadbeater, M.B. Boucher, L.M. Stencel, B.A. Wilhite, Continuous-flow preparation of biodiesel using microwave heating, *Energy & Fuels* 21 (2007) 1777–1781.
- [136] A.M. Socha, J.K. Sello, Efficient conversion of triacylglycerols and fatty acids to biodiesel in a microwave reactor using metal triflate catalysts, *Organic & Biomolecular Chemistry* 8 (2010) 4753.
- [137] S. Zhang, Y.G. Zu, Y.J. Fu, M. Luo, D.Y. Zhang, T. Efferth, Rapid microwave-assisted transesterification of yellow horn oil to biodiesel using a heteropolyacid solid catalyst, *Bioresource Technology* 101 (2010) 931–936.
- [138] M. Koberg, R. Abu-Much, A. Gedanken, Optimization of bio-diesel production from soybean and wastes of cooked oil: combining dielectric microwave irradiation and a SrO catalyst, *Bioresource Technology* 102 (2011) 1073–1078.
- [139] P. Khemthong, C. Luadthong, W. Nualpaeng, P. Changsuwan, P. Tongprem, N. Viriya-empikul, et al., Industrial eggshell wastes as the heterogeneous catalysts for microwave-assisted biodiesel production, *Catalysis Today* 190 (2012) 112–116.
- [140] C.A.R. Melo Júnior, C.E.R. Albuquerque, J.S.A. Carneiro, C. Dariva, M. Fortuny, A.F. Santos, et al., Solid-acid-catalyzed esterification of oleic acid assisted by microwave heating, *Industrial & Engineering Chemistry Research* 49 (2010) 12135–12139.
- [141] C.A.R. Melo-Júnior, C.E.R. Albuquerque, M. Fortuny, C. Dariva, S. Egues, A.F. Santos, et al., Use of microwave irradiation in the noncatalytic esterification of C18 fatty acids, *Energy & Fuels* 23 (2009) 580–585.
- [142] D. Kim, J. Choi, G.J. Kim, S.K. Seol, S. Jung, Accelerated esterification of free fatty acid using pulsed microwaves, *Bioresource Technology* 102 (2011) 7229–7231.
- [143] D. Kim, J. Choi, G.J. Kim, S.K. Seol, Y.C. Ha, M. Vijayan, et al., Microwave-accelerated energy-efficient esterification of free fatty acid with a heterogeneous catalyst, *Bioresource Technology* 102 (2011) 3639–3641.
- [144] R. Luque, J. Budarin, J.H. Clark, D.J. Macquarrie, Glycerol transformations on polysaccharide derived mesoporous materials, *Applied Catalysis B: Environmental* 82 (2008) 157–162.
- [145] S.F. Marcel, K.J. Lie, Y.-K. Cheung, The use of a microwave oven in the chemical transformation of long chain fatty acid esters, *Lipids* (1988) 367–369.
- [146] R.K. Saxena, J. Isar, S. Saran, R. Kaushik, W.S. Davidson, Efficient microwave-assisted hydrolysis of triolein and synthesis of bioester, bio-surfactant and triglycerides using *Aspergillus carneus* lipase, *Current Science* 89 (2005) 1000–1003.
- [147] C.S. Fang, P.M.C. Lai, Microwave heating and separation of water-in-oil emulsions, *Journal of Microwave Power and Electromagnetic Energy* 30 (1995) 46–57.
- [148] A.P. Harvey, M.R. Mackley, T. Seliger, Process intensification of biodiesel production using a continuous oscillatory flow reactor, *Journal of Chemical Technology & Biotechnology* 78 (2003) 338–341.
- [149] A.N. Phan, A.P. Harvey, M. Rawcliffe, Continuous screening of base-catalysed biodiesel production using new designs of mesoscale oscillatory baffled reactors, *Fuel Processing Technology* 92 (2011) 1560–1567.
- [150] M. Zheng, R.L. Skelton, M.R. Mackley, Biodiesel reaction screening using oscillatory flow meso reactors, *Process Safety and Environmental Protection* 85 (2007) 365–371.
- [151] <http://www.nitechsolutions.co.uk/market-sectors/clean-technology/>, (n.d.).
- [152] A.W. Etchells III, C.F. Meyer, Chapter 7: mixing in pipelines, in: *Handbook of Industrial Mixing: Science and Practice*, John Wiley & Sons, 2004.
- [153] C. Xuereb, M. Poux, J. Bertrand, *Mélangeurs statiques*, in: *Agitation et Mélange*, Dunod, 2006.
- [154] A. Baumann, S.A.K. Jeelani, B. Holenstein, P. Stössel, E.J. Windhab, Flow regimes and drop break-up in SMX and packed bed static mixers, *Chemical Engineering Science* 73 (2012) 354–365.
- [155] X. Yu, Z. Wen, Y. Lin, S.T. Tu, Z. Wang, J. Yan, Intensification of biodiesel synthesis using metal foam reactors, *Fuel* 89 (2010) 3450–3456.
- [156] M. Al-Atabi, Design and assessment of a novel static mixer, *The Canadian Journal of Chemical Engineering* 89 (2011) 550–554.
- [157] D. Frascari, M. Zuccaro, D. Pinelli, A. Paglianti, A pilot-scale study of alkali-catalyzed sunflower oil transesterification with static mixing and with mechanical agitation, *Energy & Fuels* 22 (2008) 1493–1501.
- [158] J.C. Thompson, B.B. He, Biodiesel production using static mixers, *Transactions of the ASABE* 50 (2007) 161–165.
- [159] M.B. Boucher, C. Weed, N.E. Leadbeater, B.A. Wilhite, J.D. Stuart, R.S. Parnas, Pilot scale two-phase continuous flow biodiesel production via novel laminar flow reactor–separator, *Energy & Fuels* 23 (2009) 2750–2756.
- [160] S.A. Unker, M.B. Boucher, K.R. Hawley, A.A. Midgette, J.D. Stuart, R.S. Parnas, Investigation into the relationship between the gravity vector and the flow vector to improve performance in two-phase continuous flow biodiesel reactor, *Bioresource Technology* 101 (2010) 7389–7396.
- [161] E. Santacesaria, M. Di Serio, R. Tesser, M. Tortorelli, R. Turco, V. Russo, A simple device to test biodiesel process intensification, *Chemical Engineering and Processing: Process Intensification* 50 (2011) 1085–1094.
- [162] E. Santacesaria, M. Di Serio, R. Tesser, R. Turco, M. Tortorelli, V. Russo, Biodiesel process intensification in a very simple microchannel device, *Chemical Engineering and Processing: Process Intensification* 52 (2012) 47–54.
- [163] J.L. Massingill, P.N. Patel, M. Guntupalli, C. Garret, C. Ji, High efficiency nondispersive reactor for two-phase reactions, *Organic Process Research & Development* 12 (2008) 771–777.
- [164] M. Yoshimune, K. Haraya, Microporous carbon membranes, in: *Membranes for Membrane Reactors: Preparation, Optimization and Selection*, Wiley, 2011.
- [165] X. Feng, R.Y.M. Huang, Liquid separation by membrane pervaporation: a review, *Industrial & Engineering Chemistry Research* 36 (1997) 1048–1066.
- [166] S.H. Shuit, Y.T. Ong, K.T. Lee, B. Subhash, S.H. Tan, Membrane technology as a promising alternative in biodiesel production: a review, *Biotechnology Advances* 30 (2012) 1364–1380.
- [167] M.A. Dube, A.Y. Tremblay, J. Liu, Biodiesel production using a membrane reactor, *Bioresource Technology* 98 (2007) 639–647.
- [168] P. Cao, A.Y. Tremblay, M.A. Dubé, K. Morse, Effect of membrane pore size on the performance of a membrane reactor for biodiesel production, *Industrial & Engineering Chemistry Research* 46 (2007) 52–58.
- [169] P. Cao, A.Y. Tremblay, M.A. Dubé, Kinetics of canola oil transesterification in a membrane reactor, *Industrial & Engineering Chemistry Research* 48 (2009) 2533–2541.
- [170] N. Sdrula, A study using classical or membrane separation in the biodiesel process, *Desalination* 250 (2010) 1070–1072.
- [171] J. Saleh, M.A. Dubé, A.Y. Tremblay, Separation of glycerol from FAME using ceramic membranes, *Fuel Processing Technology* 92 (2011) 1305–1310.
- [172] M.C.S. Gomes, P.A. Arroyo, N.C. Pereira, Biodiesel production from degummed soybean oil and glycerol removal using ceramic membrane, *Journal of Membrane Science* 378 (2011) 453–461.
- [173] H. Falahati, A.Y. Tremblay, The effect of flux and residence time in the production of biodiesel from various feedstocks using a membrane reactor, *Fuel* 91 (2012) 126–133.
- [174] B. Sarkar, S. Sridhar, K. Saravanan, V. Kale, Preparation of fatty acid methyl ester through temperature gradient driven pervaporation process, *Chemical Engineering Journal* 162 (2010) 609–615.
- [175] W. Shi, B. He, J. Ding, J. Li, F. Yan, X. Liang, Preparation and characterization of the organic-inorganic hybrid membrane for biodiesel production, *Bioresource Technology* 101 (2010) 1501–1505.
- [176] M. Zhu, B. He, W. Shi, Y. Feng, J. Ding, J. Li, et al., Preparation and characterization of PSSA/PVA catalytic membrane for biodiesel production, *Fuel* 89 (2010) 2299–2304.
- [177] L. Guerreiro, J.E. Castanheiro, I.M. Fonseca, R.M. Martin-Aranda, A.M. Ramos, J. Vital, Transesterification of soybean oil over sulfonic acid functionalised polymeric membranes, *Catalysis Today* 118 (2006) 166–171.
- [178] V.R. Murty, J. Bhat, P.K.A. Muniswaran, Hydrolysis of oils by using immobilized lipase enzyme: a review, *Biotechnology and Bioengineering* 7 (2002) 57–66.
- [179] G.J. Harmsen, Reactive distillation: the front-runner of industrial process intensification: a full review of commercial applications, research, scale-up, design and operation, *Chemical Engineering and Processing* 46 (2007) 774–780.
- [180] Ö. Yildirim, A.A. Kiss, E.Y. Kenig, Dividing wall columns in chemical process industry: a review on current activities, *Separation and Purification Technology* 80 (2011) 403–417.
- [181] B.B. He, A.P. Singh, J.C. Thompson, A novel continuous-flow reactor using reactive distillation for biodiesel production, *Transactions of the ASAE* 49 (2006) 107–112.
- [182] S. Steinigeweg, J. Gmehling, Esterification of a fatty acid by reactive distillation, *Industrial & Engineering Chemistry Research* 42 (2003) 3612–3619.
- [183] A.A. Kiss, J.G. Segovia-Hernández, C.S. Bildea, E.Y. Miranda-Galindo, S. Hernández, Reactive DWC leading the way to FAME and fortune, *Fuel* (2012) 352–359.
- [184] A.P. Singh, J.C. Thompson, B.B. He, A continuous-flow reactive distillation reactor for biodiesel preparation from seed oils, in: *Canada*, 2004.
- [185] A.A. Kiss, F. Omota, A.C. Dimian, G. Rothenberg, The heterogeneous advantage: biodiesel by catalytic reactive distillation, *Topics in Catalysis* 40 (2006) 141–150.
- [186] A.C. Dimian, C.S. Bildea, F. Omota, A.A. Kiss, Innovative process for fatty acid esters by dual reactive distillation, *Computers & Chemical Engineering* 33 (2009) 743–750.
- [187] A.A. Kiss, C.S. Bildea, Integrated reactive absorption process for synthesis of fatty esters, *Bioresource Technology* 102 (2011) 490–498.
- [188] N. Asprion, G. Kaibel, Dividing wall columns: fundamentals and recent advances, *Chemical Engineering and Processing: Process Intensification* 49 (2010) 139–146.
- [189] S. Phuentuang, P. Siricharnsakunchai, L. Simasatitkul, W. Paengjuntuek, A. Arpornwichanop, in: *Optimization of Biodiesel Production from Jatropha Oil Using Reactive Distillation*, 2011.
- [190] N.G. Patil, A.I.G. Hermans, F. Benaskar, J. Meuldijk, L.A. Hulshof, V. Hessel, et al., Energy efficient and controlled flow processing under microwave heating by using a millireactor-heat exchanger, *AIChE Journal* (2011).
- [191] M.E. Fabyi, R.L. Skelton, Photocatalytic mineralisation of methylene blue using buoyant TiO<sub>2</sub>-coated polystyrene beads, *Journal of Photochemistry and Photobiology A: Chemistry* 132 (2000) 121–128.
- [192] J.G. Khinast, A. Bauer, D. Bolz, A. Panarello, Mass-transfer enhancement by static mixers in a wall-coated catalytic reactor, *Chemical Engineering Science* 58 (2003) 1063–1070.
- [193] R.B.R. Choudhury, The preparation and purification of monoglycerides. II. Direct esterification of fatty acids with glycerol, *Journal of the American Oil Chemists' Society* 39 (1962) 345–347.



# Part II

## Screening of intensified technologies

---



Part I of this thesis has identified potential process technologies from literature data about intensified processes applied to FAME reactions for the choice and design of the final reactor. Three technologies have been selected in this list: microwave reactor, available in the laboratory, and microstructured and oscillatory baffled reactors, available in the Maison Européenne des Procédés Innovants (MEPI). The MEPI ([www.mepi.fr](http://www.mepi.fr)) is a non-profit organization that promotes alternative chemistry, often using novel process equipment. It holds a variety of intensified technologies that can be tested on different reactions to prove the feasibility and the potential implementation of intensified technology and new chemistry in industry. These reactor types are commercially available for industrial applications. They are preferred to other technologies for the following reasons:

- Reactive distillation, which requires a high amount of energy;
- Hydrodynamic cavitation reactors, which are still difficult to handle (range of flow rate to generate cavitation, design of the orifices...);
- Membrane reactors, which can lead to high costs of materials, lack of resistance due to the use of strong base or acid.

In Part II of this thesis, the objective is to compare the performance of the three selected technologies to test and identify the most suitable technology for the four reactions that transform fatty compounds: transesterification, esterification (with methanol or with glycerol) and hydrolysis. The three reactor technologies studied in Part I are compared to a reference reactor, which is a conventionally heated and mechanically stirred batch reactor. This experimental screening of process technologies should enable the most promising and suitable technology to be identified rapidly, thereby respecting the short time constraints of the AGRIBTP project.

Part II is composed of three chapters. The first details the use of microwave technology applied to these two reactions and the potential non-thermal enhancement of reactions under microwave irradiation is discussed. The second chapter focuses on the transesterification and esterification reactions in microstructured and oscillatory baffled reactors. Finally, the third chapter details the performance of the three process technologies for the esterification reaction of fatty acids with glycerol its opposite reaction, the hydrolysis reaction.



# Chapter 1

## **Transesterification and esterification reactions in the microwave reactor**

---





The literature review, presented in Part I, allowed the identification of three process technologies (microreactor, continuous oscillatory baffled reactor and microwave reactor) that could potentially enhance FAME reactions. This chapter focuses on transesterification and esterification reactions performed in a microwave reactor. This chapter is based on the article 'Key role of temperature monitoring in the determination of non-thermal microwave effects on transesterification and esterification reactions', published in *Bioresource Technology* in March 2014 [1]. Two additional parts have been added after the publication: the determination of molar ratio between reactants and amount of catalyst for the two reactions which has been kept for the rest of Part II, and complementary tests carried out with heterogeneous catalysts.





# Key role of temperature monitoring in interpretation of microwave effect on transesterification and esterification reactions for biodiesel production



Alex Mazubert<sup>a</sup>, Cameron Taylor<sup>b</sup>, Joelle Aubin<sup>a</sup>, Martine Poux<sup>a,\*</sup>

<sup>a</sup>Laboratoire de Génie Chimique CNRS/INPT/UPS, University of Toulouse, 4 Allée Emile Monso, BP-84234, 31030 Toulouse Cedex, France

<sup>b</sup>Department of Chemical & Process Engineering, University of Strathclyde, 16 Richmond Street, Glasgow, Lanarkshire, Scotland G1 1XQ, United Kingdom

## HIGHLIGHTS

- Temperature monitoring is more accurate using an optical fiber than an infrared sensor.
- Transesterification is not accelerated under microwave irradiation.
- Esterification with methanol is not accelerated under microwave irradiation.
- Main cause of “the microwave effect” is temperature underestimation.
- Temperature underestimation may be associated with superheating of methanol.

## ARTICLE INFO

### Article history:

Received 20 December 2013

Received in revised form 25 February 2014

Accepted 4 March 2014

Available online 20 March 2014

### Keywords:

Transesterification

Esterification

Waste cooking oil

Microwave

Biodiesel

## ABSTRACT

Microwave effects have been quantified, comparing activation energies and pre-exponential factors to those obtained in a conventionally-heated reactor for biodiesel production from waste cooking oils via transesterification and esterification reactions. Several publications report an enhancement of biodiesel production using microwaves, however recent reviews highlight poor temperature measurements in microwave reactors give misleading reaction performances. Operating conditions have therefore been carefully chosen to investigate non-thermal microwave effects alone. Temperature is monitored by an optical fiber sensor, which is more accurate than infrared sensors. For the transesterification reaction, the activation energy is 37.1 kJ/mol (20.1–54.2 kJ/mol) in the microwave-heated reactor compared with 31.6 kJ/mol (14.6–48.7 kJ/mol) in the conventionally-heated reactor. For the esterification reaction, the activation energy is 45.4 kJ/mol (31.8–58.9 kJ/mol) for the microwave-heated reactor compared with 56.1 kJ/mol (55.7–56.4 kJ/mol) for conventionally-heated reactor. The results confirm the absence of non-thermal microwave effects for homogenous-catalyzed reactions.

© 2014 Elsevier Ltd. All rights reserved.

## 1. Introduction

### 1.1. Context

In recent years, bio-sourced raw material has been investigated as a substitute for fossil fuels or as solvents for renewable energy and green chemistry applications. Virgin and food-grade oils were initially studied to produce the first generation of biofuels, constituted of Fatty Acids Methyl Esters (FAME). Waste Cooking Oils (WCO) are of particular interest for biodiesel production for two

reasons. Firstly, WCO are two to three times cheaper than virgin oils (Zhang et al., 2003). Secondly, by re-using and transforming of WCO, instead of discarding it into sewers, water treatment costs are significantly decreased (Banerjee and Chakraborty, 2009). This double effect propels WCO as a very good environment-friendly feedstock.

The use of waste cooking oil, however, brings additional challenges. During the cooking process oils are subjected to high temperatures, and in the presence of water (released by foods) fatty acids are formed by a hydrolysis reaction (Gui et al., 2008). Normally transesterification is base-catalyzed since the reaction is 4000 times faster than that with acid catalysis (Fukuda et al., 2001). However, with a basic catalyst the high acidity of the oil leads to undesired soap formation, which decreases the reaction yield and acts as a surfactant between the two final immiscible

\* Corresponding author. Tel.: +33 5 34 32 36 84; fax: +33 5 34 32 36 97.

E-mail addresses: [alex.mazubert@gmail.com](mailto:alex.mazubert@gmail.com) (A. Mazubert), [cameron.taylor@strath.ac.uk](mailto:cameron.taylor@strath.ac.uk) (C. Taylor), [joelle.aubin@ensiacet.fr](mailto:joelle.aubin@ensiacet.fr) (J. Aubin), [martine.poux@ensiacet.fr](mailto:martine.poux@ensiacet.fr) (M. Poux).

products, making downstream separation more difficult. The limit of acceptable acidity is not clearly defined; the advised limit is 1 mg KOH/g<sub>oil</sub> (fatty acid mass fraction of 0.5%) (Banerjee and Chakraborty, 2009), however reactions have been successfully performed at 3 mg KOH/g<sub>oil</sub> (fatty acid mass fraction of 1.5%) (Banerjee and Chakraborty, 2009; Enweremadu and Mbarawa, 2009). The water content is limited to 0.05% vol/vol (ASTM D6751 standard) because it forms inactive alkaline soaps (Leung et al., 2010). Due to these undesirable outcomes, WCO needs to be pre-treated before reactions are performed.

### 1.2. FAME production from waste cooking oils

The first pre-treatment step required is to reduce the acidity of the oil. Both physical (such as drying, filtration, or distillation (Tur et al., 2012)) and chemical pre-treatment can be used. Chemical treatment is carried out with an acid-catalyzed esterification reaction. The fatty acids in the oil react with methanol producing methyl esters and water. This is an immiscible liquid–liquid reaction, which is mass-transfer limited (Santacesaria et al., 2007). After the esterification reaction the oil mainly contains tri, di and mono glycerides and the mass fraction of fatty acids is generally below 1.5%.

Following the esterification reaction and after a water removal step, the pretreated oil is then transformed using a base-catalyzed transesterification. Like the esterification reaction, the transesterification reaction is mass-transfer limited at the beginning due to the immiscibility of triglycerides and methanol, as well as at the end of the reaction because most of the catalyst is in the glycerol phase (Cintas et al., 2010).

A number of types of reactors can be used to carry out the esterification and transesterification of WCO transformations and these have been reviewed in our previous paper (Mazubert et al., 2013). In comparison to conventional batch reactors, a number of intensified equipment types (such as microstructured reactors, cavitation reactors, microwave reactors, oscillatory flow reactors, membrane reactors, as well as static mixers and reactive distillation) have shown to enhance FAME production. Microwave reactors show particularly promising results in terms of residence times, which are significantly reduced compared with other technologies. The next section presents the basic principle of microwave heating and some background on their use for biodiesel production.

### 1.3. Microwave background

#### 1.3.1. Principle

The two major mechanisms involved in microwave technology are dipolar polarization and ionic conduction. Dipolar polarization occurs when dipoles are forced to align with the direction of the electric field that is imposed by the microwave. The electric field rapidly oscillates, as does the dipole, which tries to realign itself with the field as fast as possible by rotation. The frequency of the microwaves is sufficiently high to cause a phase difference between the field and the dipole orientation. The frictional and collision forces between the molecules thus generate heat. The second mechanism is ionic conduction. It occurs as the charged dissolved particles oscillate under the influence of the microwave field. When the direction of the electric field changes, the ions slow down and change direction, dissipating their kinetic energy as heat. This dissipation is caused by friction (Lidström et al., 2001; Míngos and Baghurst, 1991).

The absorption of microwaves by a dielectric compound can be characterized by the complex permittivity  $\epsilon^*$ , which depends on the dielectric constant  $\epsilon'$  that represents the ability of the compound to store energy, and the dielectric loss  $\epsilon''$  that represents

the ability of the compound to convert the absorbed energy into heat.

$$\epsilon^* = \epsilon' - j\epsilon'' \quad (1.1)$$

One limitation of the use of microwaves on a larger scale is the small penetration depth of the microwaves in the reactive media. This penetration depth,  $d_p$ , is a function of the dielectric properties and the frequency of the microwaves. A limited penetration depth will make uniform heating difficult at higher volumes.

As it is expressed in literature (Metaxas and Meredith, 1983), the general expression for the penetration depth approximates to:

$$d_p = \frac{\lambda_0 \sqrt{\epsilon'}}{2\pi\epsilon''} \quad \text{where the free space wavelength is} \quad \lambda_0 = \frac{c_0}{f} \quad (1.2)$$

As an example, at 2.45 GHz the penetration depth of microwaves in methanol at 20 °C is 0.76 cm and at 60 °C, it is 1.4 cm (calculated from work of Grant and Halstead (1998)). This small penetration depth is the reason why mechanical stirring is required to homogenize temperature.

#### 1.3.2. Microwave effects

It is generally believed that reaction enhancement and other observed effects in microwave-assisted processes are due to thermal phenomena caused by the microwave dielectric heating mechanisms. Amongst the different thermal effects caused by microwaves some examples are (Kappe et al., 2012):

- The superheating of solvents due to extremely fast heating to temperatures above the solvent boiling point; in such cases solvents boil at temperatures that are higher than the usual boiling point due to absence of nucleation points.
- The heating of selected phases or reagents of the reaction medium, e.g. microwave-absorbing solid catalysts.
- The generation of inverted temperature gradients between the wall and the bulk of the reactor, and the subsequent elimination of wall effects.

Despite some controversy, claims that non-thermal microwave effects on reactions still exist (Perreux et al., 2013). The reduction of reaction times exclusively due to microwave irradiation is referred to as non-thermal microwave effects when the comparison of reaction performance with and without microwave irradiation is made at the same temperatures and operating conditions (e.g. agitation intensity, mixing quality). It has been postulated that these effects are due to the interaction of the electromagnetic field with the molecules in the reaction medium. It is believed for some reactions that the electromagnetic field modifies the orientation of the molecules and could change the pre-exponential factor  $A$  in the Arrhenius equation:

$$K = A.e^{\left(\frac{-\Delta G}{RT}\right)} \quad (1.3)$$

where  $\Delta G$  is the activation energy or entropy term. The pre-exponential factor, which describes the probability of molecular impacts, depends on the vibration frequency of the atoms at the reaction interface. It is thought that this vibration frequency could be affected under microwave irradiation and leads to an increase of the pre-exponential factor. The decrease in activation energy under microwaves is attributed to the increase of the entropy term.

#### 1.3.3. Transesterification and esterification reactions under microwaves

The use of microwaves for enhancing chemical reactions has been a topic of significant interest in past years (Baig and Varma, 2012) and the investigations of transesterification and esterification

reactions under microwave irradiation has been numerous as identified by Mazubert et al. (2013). For these reactions in particular, microwave efficiency is increased by the high polarity and high dielectric loss of methanol. Indeed, the dielectric constant of methanol at 25 °C and 2.45 GHz is 32.7 (Albright and Gosting, 1946) compared with that of water at 78.5, which is high, and that of oil is only between 3 and 4. The dielectric loss for methanol at 25 °C is around 11.8, which is close to that of water, around 13.

In general, the literature studies show that for homogenous base-catalyzed transesterification reactions under microwave irradiation in batch conditions, high conversions or yields are attained at very short reaction times in comparison with conventionally heated systems. For example:

- A 98% conversion of triolein is obtained in 1 min at 50 °C using an initial power of 25 W in a 100 mL round-flask reactor (Leadbeater and Stencel, 2006).
- A 93.7% conversion of rapeseed oil is obtained in 1 min at 40 °C using a power of 1200 W (Azcan and Danisman, 2008).
- A yield greater than 96% is obtained in 6 min with a KOH catalyst, at 60 °C using a maximum power of 500 W in a 50 mL reactor (Zu et al., 2009).
- A 97.2% conversion of rice oil is obtained in 5 min at 60 °C, using a maximum power of 1600 W in a 270 mL reactor (Kanitkar et al., 2011).
- A 98.4% conversion of safflower oil is obtained in 6 min at 60 °C using a maximal power of 300 W in a 500 mL reactor (Duz et al., 2011).

Similar results have also been found in continuous reactors. For example, using a 9 mm diameter coiled tube in a household microwave and a flow rate of 19.8 L/h Lertsathapornsuk et al. (2008) obtained a 97% conversion in 30 s using ethanol, at an average outlet temperature of 78 °C with a maximal power of 800 W. In a 4 L non-agitated continuous tank with a flow rate of 432 L/h, a 98.9% conversion was obtained in 30 s at 50 °C using a maximum power of 1600 W in a large multimode microwave cavity (Barnard et al., 2007).

Few studies on the esterification of fatty acids with a homogenous catalyst have been carried out; indeed most investigations on esterification reactions with microwaves have used heterogeneous catalysts. The use of microwaves for decreasing the fatty acid content with a homogenous catalyst has only recently been shown: the acidity of *Jatropha* oil was decreased from 14% to 1% using a sulfuric acid catalyst at a power of 110 W in a 500 mL reactor in 35 min (Jaliliannosrati et al., 2013).

In summary, the literature results globally show that the use of microwaves for FAME reactions allows high yields or conversions to be attained in very short times compared with conventionally heated reactors. However, it should be pointed out that very few of these studies provide details on how the temperature in the microwave reactor is measured. This is an extremely important point, which has been highlighted recently by Kappe and co-workers (Herrero et al., 2008; Kappe, 2013; Kappe et al., 2013). These authors report that erroneous temperature measurements and poor mixing of the reaction mixture are often responsible for the observation of reaction enhancement due to non-thermal microwave effects. Infrared (IR) temperature sensors are typically used for temperature measurement in commercial microwave systems. However, it is known that the use of IR sensors that measure the temperature at the outer bottom surface of the reactor do not provide correct information on the internal reaction temperature. *In situ* fiber-optic temperature probes provide much more accurate temperature measurements and therefore are highly recommended. As a result, it is clearly understood that poor temperature measurements in microwave reactors give misleading results in

terms of reaction performance. Indeed, in the current literature on the use of microwave heating for enhancing FAME reactions, infrared sensors are very often used and one may question the real gain in using this novel heating method compared with conventional techniques.

#### 1.4. Present work

This work investigates the effects of microwaves on the performance of transesterification and esterification reactions using WCO as feedstock. To do this, the reactions performed in a conventionally heated reactor and a microwave reactor have been compared under the same operating conditions (temperature and stirring conditions). The microwave reactor operates in single mode and is equipped with a mechanical rotating impeller to ensure good mixing quality and homogenous temperature in the reactor. The temperatures are measured directly in the reaction medium by a fiber optic probe to ensure the accuracy of the temperature measurements. To quantify a potential enhancement of the reaction by the microwave irradiation, the influence of microwave irradiation on the Arrhenius equation is presented for both reactions.

## 2. Methods

### 2.1. Products

WCO was collected in restaurants and supplied by the company Coreva Technologies (Auch, France). Two different WCOs are studied: one with low fatty acid content (2.1%) and the other with a higher level of fatty acids (39%). Both oils contain no water or solid wastes. The profiles of the carbon chains are as follows:

- Oil with 2.1% of FFA: palmitic C16:0 (15.2%), palmitoleic C16:1 (3.5%), stearic C18:0 (4.6%), oleic C18:1 (36.5%), linoleic C18:2 (36.1%) and alpha-linoleic C18:3 (3.5%).
- Oil with 39% of FFA: palmitic C16:0 (13.1%), stearic C18:0 (3.7%), oleic C18:1 (54.3%), linoleic C18:2 (24.6%), arachidic C20:0 (4.3%).

Methanol (99% HPLC grade), sodium hydroxide pellets, sulfuric acid (96%), cyclohexane (analytical grade) and ethanol (absolute, 99.9%) were supplied by VWR, France. Phenolphthalein and KOH-ethanol solution (1 M or 0.1 M) were supplied by Sigma-Aldrich, France. Methyl imidazole (MI) was supplied by Alfa Aesar. N-méthyl-N-triméthylsilyl-heptafluorobutyramide (MSHFBA) was supplied by Marcherey-Nagel.

### 2.2. Experimental apparatus

The conventionally heated reactor, as shown in Fig. 1(a), consists of a 1L-jacketed vessel equipped with a 3-bladed paddle, a cooling system to avoid the vaporization of methanol and a mercury thermometer. The agitation speed is fixed at 300 rpm for both reactions. The transesterification is carried out at four temperatures (25 °C, 40 °C, 50 °C and 60 °C) using the 2.1% FFA oil. The methanol to oil molar ratio is 6:1 and the mass fraction of KOH catalyst (with respect to the mass of oil) is 1%. An initial mass of 600 g of oil is preheated in the reactor before adding the methanol and catalyst solution.

The esterification is also carried out at four temperatures (30 °C, 40 °C, 50 °C and 60 °C) using the 39% FFA oil in the conventionally heated reactor. The methanol to oil ratio is 36:1 and the mass fraction of the sulfuric acid catalyst (with respect to the mass of oil) is 7%. The methanol and sulfuric acid are preheated in the reactor,

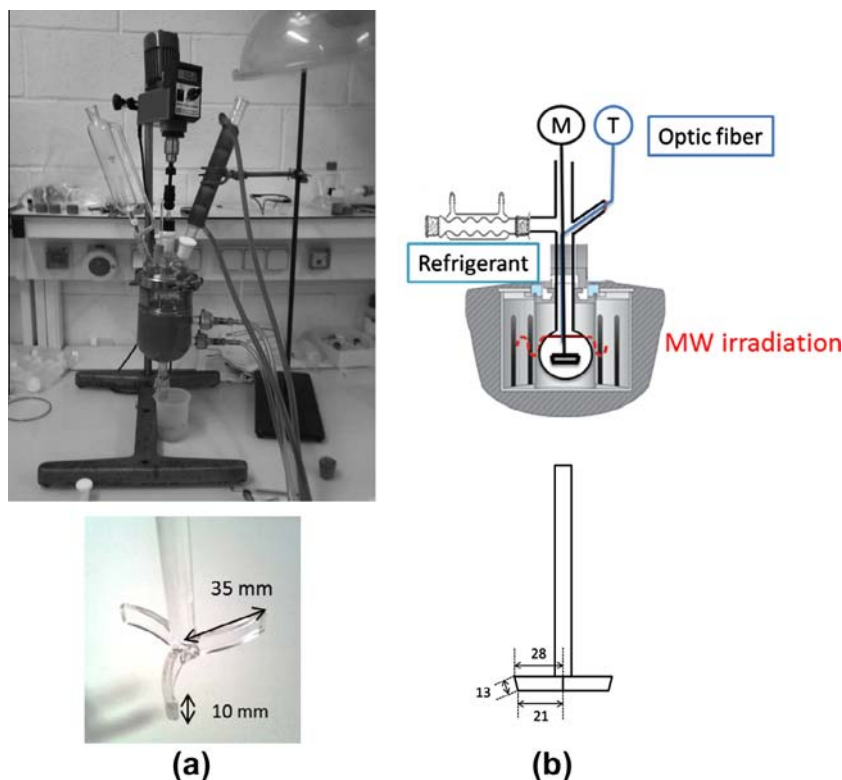


**Fig. 1.** Two experimental systems: (a) the conventionally heated reactor and its agitator and (b) the microwave heated reactor with its mechanical agitator (M) and temperature monitored by optical fiber (T). Dimensions are given in mm.

whilst the oil is preheated in a thermal bath. The total volume is fixed at 1 L.

The microwave reactor is a CEM<sup>®</sup> Discover SP ( $f = 2.45$  GHz) operates at atmospheric pressure and is equipped with a 100 mL round-flask and a 2-bladed paddle impeller made of PTFE, as shown in Fig. 1(b). The maximum power is 300 W. The power is automatically adjusted to the measured temperature via an optical fiber. The agitation speed is fixed at 300 rpm. The 2-bladed paddle impeller has been used instead of the conventional magnetic stirrer in order to homogenize the temperatures in the microwave cavity and to ensure good mixing of the reactants. Indeed, the default magnetic stirrer provided in the microwave reactor was unable to rotate in the viscous oils and therefore provided insufficient mixing. The temperature homogeneity was also assisted by the use of a single mode microwave reactor, instead of a multi-mode reactor type that has often been used in previous studies (Barnard et al., 2007; Lertsathapornsuk et al., 2008). The total reaction volume is 80 mL. The transesterification and the esterification are carried out at the four different temperatures as in the conventionally heated reactor. As stirring and microwave irradiation start simultaneously, the initial time is set to when the agitation starts even if the desired temperature is not reached yet. The times required to reach each of the set temperatures are given in Table 1.

### 2.3. Characterization of reaction performance

The composition of FAME produced from the transesterification and esterification reactions was characterized by gas chromatography (GC) using a Perkin Elmer Instrument based on the EN-14103 method. The chromatograph is equipped with a flame ionization detector (FID). The column used was Restek (CP-Sil 8 Rtx-5: 5% diphenyl, 95% dimethylpolysiloxane)  $15\text{ m} \times 0.32\text{ mm} \times 0.25\text{ }\mu\text{m}$ .

**Table 1**

Comparison of temperature measurements using an optical fiber probe (OF) and infrared sensor (IR) for the esterification reaction. The reactor volume is 80 mL and the stirring speed using an mechanical agitator is 300 rpm.

Experimental tests				
Setpoint $T$ ( $^{\circ}\text{C}$ )	30	40	50	60
Time needed by OF to reach setpoint $T$ (s)	20	26	34	45
$T$ (OF) ( $^{\circ}\text{C}$ )	30	40	50	60
$T$ (IR) ( $^{\circ}\text{C}$ )	23	33	39	33

The injection is “on-column” because the di- and triglycerides are not vaporized in the injector and are injected as liquids in the column. One internal standard (heptadecane) and six reference materials (triolein, monoolein, diolein, triolein, oleic acid, methyl oleate) supplied by Sigma–Aldrich were used for the GC calibration. The samples are diluted in cyclohexane (Analytical grade) supplied by VWR, France. The operating conditions used for the oven were  $55\text{ }^{\circ}\text{C}$  for 30 s,  $45\text{ }^{\circ}\text{C}/\text{min}$  to  $80\text{ }^{\circ}\text{C}$ ,  $10\text{ }^{\circ}\text{C}/\text{min}$  to  $360\text{ }^{\circ}\text{C}$  and hold for 11 min. The carrier gas was helium at a constant pressure at the top of the column of 15 psi. The hydrogen flow was kept at  $45\text{ mL}/\text{min}$  and the air flow was kept at  $450\text{ mL}/\text{min}$ . The hydroxylated compounds (fatty acids, mono, di- and triglycerides) are silylated by a mixture of *N*-methyl-*N*-trimethylsilyl-heptafluorobutyramide (MSHFBA) and methylimidazole (MI). This reaction increases the volatility and the stability of injected hydroxylated compounds to enhance their detection.

The fatty acid level is determined by titration with a 0.1 N KOH-ethanol solution using a Mettler Toledo DL50 titrator based on the ISO 660 norm. The sample (about 1 mL) is diluted in ethanol (about 30 mL). The titrator gives the exact volume added at the equivalence point, which is determined by a pH sensor. Phenolphthalein is used as the colored indicator to detect the equivalence point. The percentage of acidity  $A_c$  is given by the relationship:

$Ac = (V_{eq} \cdot M_{C18} \cdot C_{KOH}) / \text{mass of oil}$ , where  $V_{eq}$  is the volume at the equivalence point,  $M_{C18}$  the molar mass of fatty acids and  $C_{KOH}$  the concentration of the KOH-ethanol solution. The percent conversion is given by the relationship:  $X = (Ac_{initial} - Ac_{final}) / Ac_{initial}$  where  $Ac_{initial} = 39\%$ .

## 2.4. Operating conditions requirements

### 2.4.1. Reproducibility

In order to ensure the reproducibility of results, the microwave-assisted transesterification reaction has been performed five times for a duration of 8 min. The standard deviation, the interval of confidence at 95% and the average values of the compounds present following the reaction are given in Table 2. The quantity of esters is 91.3% ( $\pm 1\%$ ). The uncertainties of the other compounds are relatively larger in comparison to the small measured quantities. The control of the temperature and the reproducibility are therefore regarded as satisfactory considering the small changes in ester production for a fixed duration of reaction time.

### 2.4.2. Effect of hydrodynamics

As described above, the vessels used with conventional heating and with microwave heating have different sizes (1 L and 100 mL, respectively) and different agitators. To ensure that any potential enhancement of the reactions is not caused by differences in the mixing quality and hydrodynamics of the liquid-liquid reactive medium the reactions were also performed in the 100 mL vessel with conventional heating, using a thermal bath with a temperature of 60 °C. After 5 min, the concentration of esters in the 1 L conventionally heated reactor is 2.25 mol/L (2.23–2.28 mol/L) whereas for the 100 mL vessel heated with the thermal bath, the concentration of esters is 2.24 mol/L (2.26–2.21 mol/L). These concentrations obtained in both vessels are very close, thereby showing that the vessel size and the different agitators have no effect on the reaction performance. Consequently, it is supposed the difference of shape or size of the two different reactors has a small impact on reaction rates, and thereby makes it possible to directly compare the reaction performance in the reactor.

### 2.4.3. Importance of temperature monitoring

In order to quantify the difference in temperature measurements using different types of probes two experiments have been conducted. The first compares the temperature measured within the reaction medium during an esterification reaction using and optic fiber probe (OF) and the temperature measured by an infrared sensor (IR) at the bottom wall of the vessel. Table 1 shows that the temperatures measured by OF are equal to the set point temperature and are approximately 10–20 °C greater than those measured by IR. The second experiment aims at assessing the response time of the OF and IR probes when heating water in the microwave reactor; the results are given in Table 2. In the first step of this experiment, the power is fixed at 100 W for 90 s and the water temperature from 18 °C to 45 °C according to OF measurement and to 41 °C according to IR measurement; the difference in measurements is 4 °C. When the water is heated again for 30 s at a power of 300 W, the temperature increases from 37 °C to 64 °C

according to OF measurement but still reads as 37 °C with the IR sensor. At least half a minute is necessary for the IR sensor to detect the increase and temperature and the IR sensor finally measures 57 °C. After 30 more seconds of microwave irradiation, the temperature increases from 61 °C to 82 °C according to OF measurement but still reads as 60 °C with the IR sensor. The response time of the IR sensor is therefore somewhere between 30 and 60 s. Indeed, this time is incompatible with the very fast heating rates provided by microwaves (see Table 1). Finally, temperature measurements in the reactor using the optical fiber and the IR sensor are compared to the value given by a mercury thermometer inserted in the reactor without microwave irradiation. The results show that the IR always measures lower temperatures than OF and mercury thermometers. This confirms that the OF provides correct temperature measurements.

The reason for this difference is due to nature of the measurement. Indeed, the IR sensor measures the external surface temperature of the reaction vessel that is made of borosilicate glass, which has a low thermal conductivity ( $1.2 \text{ W m}^{-1} \text{ K}^{-1}$ ). This thermal inertia has been already been described in the literature in a study on the influence of reactor material on the synthesis of ionic liquids using microwaves (Obermayer and Kappe, 2010). Other authors show that the temperatures measured with OF probes are higher than those measured with the IR sensor (Herrero et al., 2008). The difference between the two types of measurements is also recognized by the microwave reactor manufacturer CEM who recommends the use of OF probes.

In some recent works focused on transesterification and esterification reactions under microwave irradiation, the temperature is controlled with an infrared sensor (Azcan and Danisman, 2008; Leadbeater and Stencel, 2006; Zu et al., 2009) or at the outlet of the reactor with a mercury thermometer (Lertsathapornsuk et al., 2008); only one study has used an OF probe (Barnard et al., 2007). The rest of the cited studies do not however specify how the temperature was measured. As a result, it is highly probable that many of the temperatures indicated in these literature studies were lower than the real temperature in the reaction medium. A consequence of inaccurate temperature measurement is the non-detection of superheating of the reaction media, which is purely thermal phenomena, not a non-thermal microwave effect. In order to ensure the accuracy of temperature measurement and the absence of superheating in the current experiments, temperature is monitored with an OF probe.

## 3. Results and discussion

### 3.1. Transesterification: conventional versus microwave reactor

In a previous study, it was found that the kinetics of sunflower transesterification at low temperatures is governed by three regimes: a mass-transfer limited regime, an irreversible pseudo-homogenous regime and a reversible pseudo-homogenous regime (Stamenkovic et al., 2008). In the current study, the regime is assumed to be a reversible pseudo-homogenous regime since the temperatures are higher and the agitation is strong, and thereby takes into account the reaction in both directions.

**Table 2**  
Repeatability study for transesterification reaction performed at  $T = 60 \text{ °C}$  for 8 min: statistics of the mass fraction of methyl esters (EM), fatty acids (FA), monoglycerides (MG), diglycerides (DG) and triglycerides (TG).

						Standard deviation (%)	Interval of confidence (%)	Average (%)
%EM	91.8	91.8	90.1	90.9	92.1	0.84	1.0	91.3
%FA	2.1	2.4	3.4	2.3	2.6	0.50	0.6	2.6
%MG	2.4	2.4	2.4	2.7	2.3	0.17	0.2	2.4
%DG	2.1	1.9	1.9	2.1	1.5	0.25	0.3	1.9
%TG	1.6	1.6	2.3	2.0	1.5	0.31	0.4	1.8

The global equation is:



During the reaction, the reaction rate is written as:

$$r = -\frac{d[TG]}{dt} = [TG]_0(1 - X) - k_2[TG]_0 3X \quad (3.2)$$

$$\frac{dX}{dt} = k_1(1 - X) - k_2(3X) \quad (3.3)$$

$$\frac{dX}{dt} + (k_1 + 3k_2)X - k_1 = 0 \quad (3.4)$$

The solution of this differential equation is:

$$X = Ke^{-(k_1+3k_2)t} + \frac{k_1}{k_1 + 3k_2} \quad (3.5)$$

At the initial time  $t = 0$ ,  $X$  is equal to 0, therefore:

$$K = \left( -\frac{k_1}{k_1 + 3k_2} \right) \quad (3.6)$$

The expression of  $X$  is then:

$$X = \frac{k_1}{k_1 + 3k_2} (1 - e^{-(k_1+3k_2)t}) \quad (3.7)$$

Gas chromatography gives access to the molar fraction  $x$  of methyl esters in the media. The quantity of methyl esters in moles  $E$  is therefore assumed to be:

$$E = 3[TG]_0 x \quad (3.8)$$

The experimental data is fitted with the equation:

$$E = a(1 - e^{bt}) \quad (3.9)$$

The coefficients are determined by identification:

$$\begin{aligned} -k_1 &= \left( \frac{ab}{3[TG]_0} \right) \\ -k_2 &= \frac{b}{3} - \frac{ab}{9[TG]_0} \end{aligned} \quad (3.10)$$

The experimental data and the corresponding models are presented in Fig. 2. Model and experimental data show good agreement. Mass fractions of esters increase with higher temperatures.

The kinetic constants, the pre-exponential factor and the activation energy have been determined from the data and are presented in Table 3. The minimum and maximum values given for coefficients  $b$  and  $c$  have been estimated with the Curve Fitting Tool in Matlab (R2011b). This tool uses a nonlinear least-squares method (*lsqcurvefit* function) which consists in minimizing the square of the difference between  $E = a(1 - e^{bt})$  and  $E$  obtained in experiments. Interval of confidence  $C$  is then calculated by *confint* function, given by:

$$C = b \pm t\sqrt{S} \quad (3.11)$$

where  $b$  contains the coefficients of the fit,  $t$  is the critical  $t$  value of the Student  $t$ -distribution with a confidence level of 95% at a degree of freedom equals to  $n - p$  (where  $n$  is the number of experiments and  $p$  is the number of coefficients).  $S$  is a vector of diagonal elements of covariance matrix equal to  $(X^T X)^{-1} s^2$ , where  $X$  is the Jacobian of the fitted values and  $s^2$  the mean squared error. The minimum and maximum values of kinetic constants have then been deduced from these values respecting error propagation rules:

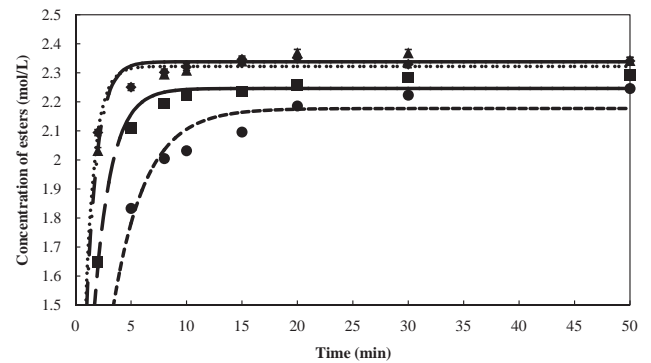
$$s(k_1)^2 = \left( \frac{1}{3[TG]_0} \right)^2 s(ab)^2 \quad (3.12)$$

$$s(ab)^2 = (ab)^2 \left[ \left( \frac{s(a)}{a} \right)^2 + \left( \frac{s(b)}{b} \right)^2 + 2\text{cov}(a, b) \right] \quad (3.13)$$

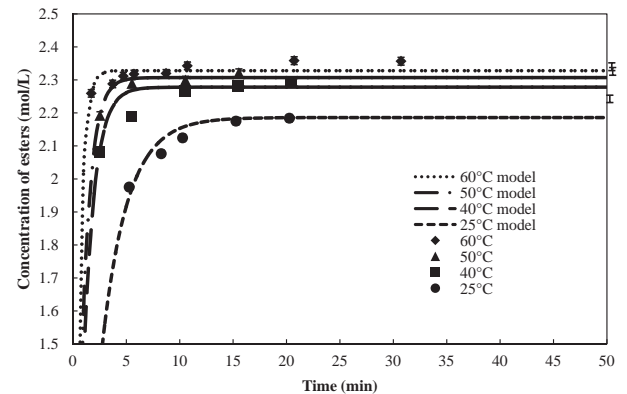
**Table 3**

Difference of temperature measured by IR or OF for 80 g of water in the 100 mL vessel heated at fixed power for 90 and 30 s. Magnetic agitation speed is 600 rpm. Temperatures are measured simultaneously by IR, OF and by a mercury thermometer ( $T_{Hg}$ ).

$P = 100 \text{ W}, t = 90 \text{ s}, T_0 (\text{°C}) = 18$		
$T_{IR} (\text{°C})$	$T_{OF} (\text{°C})$	$\Delta T (\text{°C})$
41	45	4
$P = 300 \text{ W}, t = 30 \text{ s}, T_0 (\text{°C}) = 37$		
$T_{IR} (\text{°C})$	$T_{OF} (\text{°C})$	$\Delta T (\text{°C})$
37	64	10
After 30 s without irradiation		
$T_{IR} (\text{°C})$	$T_{OF} (\text{°C})$	$\Delta T (\text{°C})$
57	61	4
$P = 300 \text{ W}, t = 30 \text{ s}, T_0 (\text{°C}) = 58$		
$T_{IR} (\text{°C})$	$T_{OF} (\text{°C})$	$\Delta T (\text{°C})$
60	82	22
After cooling at the open air		
$T_{IR} (\text{°C})$	$T_{OF} (\text{°C})$	$T_{Hg} (\text{°C})$
67	79	77
60	66	64
58	63	62
56	60	60
22	18	18



(a)



(b)

**Fig. 2.** Quantity of esters produced in the transesterification reaction as a function of time at different temperatures in the (a) conventionally heated and (b) microwave reactor.

$$\begin{aligned} s(k_2)^2 &= 2 \left( -\frac{b}{9[TG]_0} \left( \frac{1}{3} - \frac{a}{9[TG]_0} \right) \right)^2 \text{cov}(a, b) \\ &+ \left( -\frac{b}{9[TG]_0} \right)^2 s(a)^2 + \left( \frac{1}{3} - \frac{a}{9[TG]_0} \right)^2 s(b)^2 \end{aligned} \quad (3.14)$$



The covariance  $\text{cov}(a,b)$  is the value of non-diagonal elements of the covariance matrix. The interval of confidence,  $I$ , of the kinetic constants is then given by the relation:

$$I = k \pm t s(k) \quad (3.15)$$

The method for the determination of interval of confidence of regression coefficients has been used for the calculation of activation energy with the relation  $\ln k = A - E_a/RT$ , where  $A$  and  $E_a/R$  the coefficients of the fit between  $\ln k$  and  $1/T$  values, keeping the same method as for determination of intervals of confidence of the kinetic constants.

Models and experimental data are compared in Fig. 2. Corresponding parameters are given in Table 4. The differences in the kinetics obtained in the microwave reactor and the conventionally heated reactor are shown in Fig. 3. From these results, the following observations are made:

- Considering the intervals of confidence, the activation energies are close in both reactor types, with mean values of  $E_{a1}$  equal to 37.1 kJ/mol in microwave reactor compared with 31.6 kJ/mol in the conventionally heated reactor, and 17.9 kJ/mol in microwave reactor compared with 9.7 kJ/mol for  $E_{a2}$ . The confidence level of 95% of  $E_{a2}$  gives negative values. To respect physical considerations by obtaining only positive values,  $t$  value has been reduced, corresponding to a confidence level between 80% and 90%.
- The pre-exponential factors are in the same range for both systems with values in the range  $10^2$ – $10^8$  L/mol/min for  $A_1$  and in the range  $10^{-4}$ – $10^2$  L/mol/min for  $A_2$ .
- The average values of the kinetic constants are slightly higher in the microwave reactor, however the intervals of confidence of these constants shown in Fig. 3 suggest that there is little difference between the two reactor types.

These results can be compared with those found in the literature in conventionally heated reactors in the same temperatures conditions as present with a molar ratio of methanol to oil of 6 and a mass fraction of KOH of 1%. Darnoko and Cheryan (2000) calculated an activation energy of 61.4 kJ/mol with palm oil and a constant speed provided by a magnetic stirrer and Stamenkovic et al. (2008) found a value of 53.5 kJ/mol with sunflower oil at a constant speed of 200 rpm.

### 3.2. Esterification: conventional versus microwave reactor

The model used is a pseudo-homogeneous second-order model.

$$\frac{dE}{dt} = k \cdot \text{FFA}^2 \quad (3.16)$$

$$\frac{dE}{dt} = \text{FFA}_0 \cdot \frac{dX}{dt} = k \cdot (\text{FFA}_0 \cdot (1 - X)^2) \quad (3.17)$$

$$\frac{dX}{(1 - X)^2} = k \cdot \text{FFA}_0 \cdot dt \quad (3.18)$$

The integration between 0 and  $X$  and 0 and  $t$  gives:

$$\frac{1}{1 - X} = k \cdot \text{FFA}_0 \cdot t + 1 \quad (3.19)$$

The experimental data and the corresponding models are presented in Fig. 4. Model and experimental data show good agreements. Conversion increases with higher temperatures.

The kinetic constants, the pre-exponential factor and the activation energy have been determined and presented in Table 5. The intervals of confidence have been determined with a method

**Table 4**  
Comparisons of model coefficients, kinetic constants, activation energies and pre-exponential factors obtained at different temperatures in the microwave and conventionally heated reactor for the transesterification reaction. These values are given in bold and are associated with an interval of confidence that is given in italics.

Microwave heating	25	40	50	60
$T$ (°C)				
$b$ (L/mol/min)	-0.422	-0.979	-1.183	-2.038
Min value/max value	-0.507/-0.337	-1.235/-0.724	-1.320/-1.046	-2.534/-1.542
$a$ (mol/L)	2.186	2.278	2.307	2.328
Min value/max value	2.136/2.235	2.224/2.333	2.291/2.324	2.307/2.350
$R^2$	0.9983	0.9977	0.9998	0.9992
<b><math>k_1</math> (L/mol/min)</b>	<b>0.376</b>	<b>0.909</b>	<b>1.112</b>	<b>1.933</b>
Min value/max value	0.291/0.460	0.650/1.168	0.975/1.249	1.444/2.421
<b><math>k_2</math> (L/mol/min)</b>	<b>0.015</b>	<b>0.024</b>	<b>0.024</b>	<b>0.035</b>
Min value/max value	0.011/0.020	0.014/0.033	0.020/0.028	0.025/0.046
Conventional heating				
$T$ (°C)	25	40	50	60
$b$ (L/mol/min)	-0.3415	-0.646	-1.017	-1.149
Min value/max value	-0.416/-0.267	-0.713/-0.579	-1.134/-0.900	-1.312/-0.987
$a$ (mol/L)	2.177	2.246	2.338	2.322
Min value/max value	2.107/2.247	2.213/2.278	2.310/2.365	2.295/2.349
$R^2$	0.9948	0.9982	0.999	0.9987
<b><math>k_1</math> (L/mol/min)</b>	<b>0.302</b>	<b>0.590</b>	<b>0.969</b>	<b>1.087</b>
Min value/max value	0.237/0.368	0.529/0.652	0.852/1.085	0.928/1.245
<b><math>k_2</math> (L/mol/min)</b>	<b>0.013</b>	<b>0.018</b>	<b>0.016</b>	<b>0.021</b>
Min value/max value	0.009/0.017	0.015/0.022	0.012/0.020	0.016/0.026
	Microwave heating		Conventional heating	
<b><math>E_{a1}</math> (kJ/mol)</b>	<b>37.1</b>	$R^2$	<b>31.6</b>	$R^2$
Min value/max value	20.1/54.2	0.978	14.6/48.7	0.970
<b><math>A_1</math> (L/mol/min)</b>	<b><math>1.3 \times 10^6</math></b>		<b><math>1.1 \times 10^5</math></b>	
Min value/max value	$1.9 \times 10^3/8.2 \times 10^8$		$1.7 \times 10^2/7.2 \times 10^7$	
<b><math>E_{a2}</math> (kJ/mol)</b>	<b>17.9</b>	0.886	<b>9.7</b>	0.748
Min value/max value	2.2/33.5		0/19.4	
<b><math>A_2</math> (L/mol/min)</b>	<b><math>2.1 \times 10^1</math></b>		<b><math>6.7 \times 10^{-1}</math></b>	
Min value/max value	$5.5 \times 10^{-2}/7.9 \times 10^3$		$9.8 \times 10^{-4}/4.6 \times 10^2$	

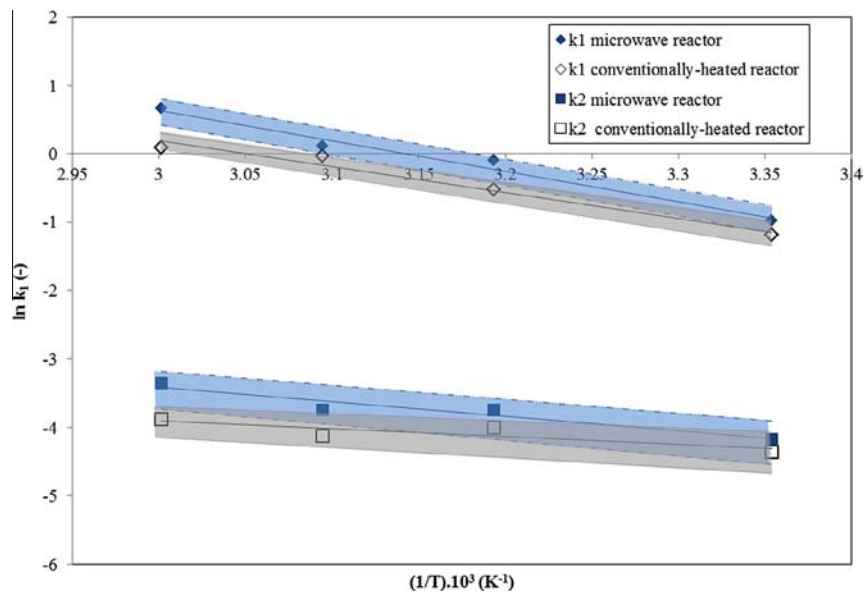


**Fig. 3.** Comparison of  $\ln k$  as a function of the inverse of temperature in conventionally heated and microwave reactors for the transesterification reaction with the limits of intervals of confidence denoted by (---) for the microwave reactor and (---) for the conventionally heated reactor. Corresponding zones are represented with a blue surface for results obtained in microwave, and in grey for results obtained in batch reactor. The intersection of the zones is darker. (For interpretation of the references to colour in this figure legend, the reader is referred to the web version of this article.)

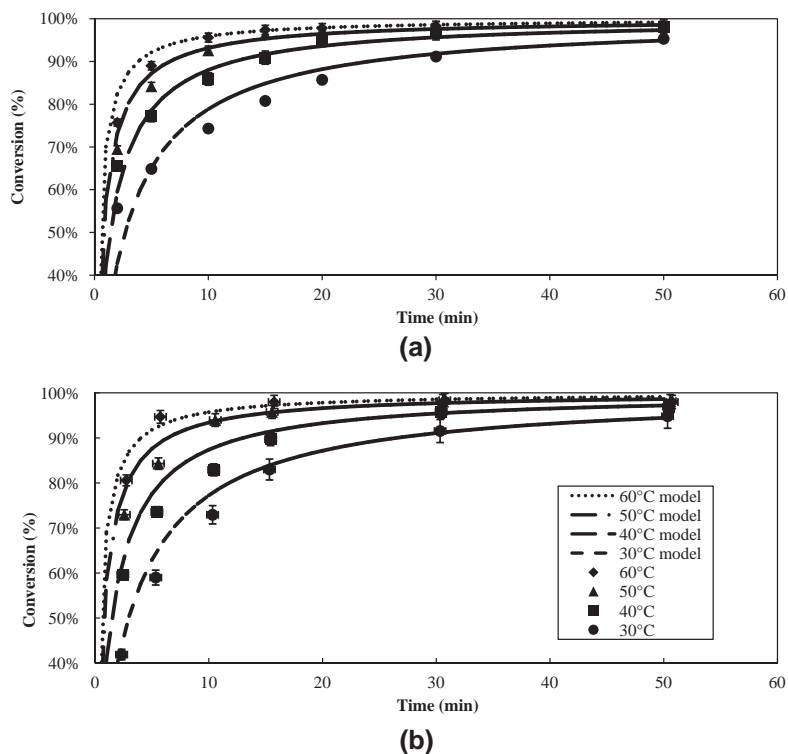


**Fig. 4.** Conversion as a function of time at different temperatures in the conventionally heated (a) and microwave reactor (b).

analogous to that used in the previous part, with the following regression function:

$$\frac{1}{1-X} = a \cdot t + 1 \quad \text{with } a = k \cdot \text{FFA}_0. \quad (3.20)$$

The differences in the kinetics between the microwave reactor and the conventionally heated reactor are shown in the Fig. 5.

The remarks pertaining to the results presented in Table 5 are very similar to those made for the transesterification reaction.

- The activation energies are approximately the same considering the intervals of confidence with an average value of 45.4 kJ/mol in the microwave reactor compared with 56.1 kJ/mol in the conventionally heated reactor.

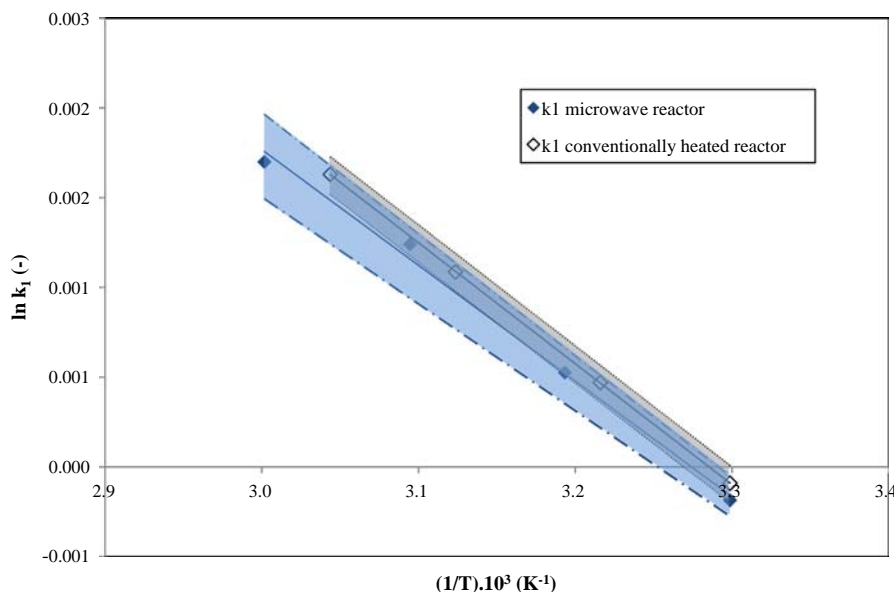


**Fig. 5.** Comparison of  $\ln(k)$  as a function of the inverse of temperature in the conventionally heated and microwave reactors for the esterification reaction with the intervals of confidence denoted by (---) for the microwave reactor and (---) for the conventionally heated reactor. Results relative to microwave are represented in blue. Corresponding zones are represented with a blue surface for results obtained in microwave, and in grey for results obtained in batch reactor. The intersection of the zones is darker. (For interpretation of the references to colour in this figure legend, the reader is referred to the web version of this article.)

**Table 5**  
Comparisons of model coefficients, kinetic constants, activation energies and pre-exponential factors obtained at different temperatures in the microwave and conventionally heated reactor for the esterification reaction. These values are given in bold and are associated with an interval of confidence that is given in italics.

<i>Microwave heating</i>				
<i>T</i> (°C)	30	40	50	60
<i>a</i> (L/mol/min)	0.339	0.691	1.413	2.236
<i>Min value/max value</i>	<i>0.305/0.374</i>	<i>0.571/0.812</i>	<i>1.216/1.610</i>	<i>1.603/2.868</i>
<i>R</i> <sup>2</sup>	0.985	0.960	0.978	0.914
<b><i>k</i><sub>1</sub> (L/mol/min)</b>	<b>0.830</b>	<b>1.691</b>	<b>3.457</b>	<b>5.471</b>
<i>Min value/max value</i>	<i>0.739/0.921</i>	<i>1.374/2.009</i>	<i>3.011/3.903</i>	<i>4.038/6.904</i>
<i>Conventional heating</i>				
<i>T</i> (°C)	30	37.8	47	55.4
<i>a</i> (L/mol/min)	0.373	0.654	1.212	1.872
<i>Min value/max value</i>	<i>0.332/0.414</i>	<i>0.5966/0.711</i>	<i>1.076/1.348</i>	<i>2.086/2.299</i>
<i>R</i> <sup>2</sup>	0.972	0.990	0.992	0.975
<b><i>k</i><sub>1</sub> (L/mol/min)</b>	<b>0.913</b>	<b>1.600</b>	<b>2.966</b>	<b>5.104</b>
<i>Min value/max value</i>	<i>0.813/1.013</i>	<i>1.459/1.741</i>	<i>2.632/3.299</i>	<i>4.582/5.626</i>
<b><i>E</i><sub>a1</sub> (kJ/mol)</b>	<b>45.4</b>	<b>R</b> <sup>2</sup>	<b>56.1</b>	<b>R</b> <sup>2</sup>
<i>Min value/max value</i>	<i>31.8/58.9</i>	0.991	<i>55.7/56.4</i>	1
<b><i>A</i><sub>1</sub> (L/mol/min)</b>	<b>7.0 × 10<sup>7</sup></b>		<b>4.2 × 10<sup>9</sup></b>	
<i>Min value/max value</i>	<i>4.1 × 10<sup>5</sup>/1.2 × 10<sup>10</sup></i>		<i>3.7 × 10<sup>9</sup>/4.8 × 10<sup>9</sup></i>	

- Considering the intervals of confidence, the pre-exponential factors are also approximately the same for both reactors, with a mean value of  $7.0 \times 10^7$  L/mol/min in the microwave reactor compared with  $4.2 \times 10^9$  L/mol/min in the conventionally heated reactor.

Fig. 5 shows that considering the intervals of confidence, the kinetic constants are more or less the same under microwave irradiation or in the conventionally heated reactor.

#### 4. Conclusions

In similar operating conditions, with accurate temperature monitoring, kinetics of transesterification and esterification reactions have been compared with conventional or microwave-heating. Similar results support the belief that non-thermal microwave

effects do not exist as claimed in previous reports. It also suggests the enhancement of transesterification and esterification reactions observed in previous studies may be an artifact of poor temperature measurements, underestimated using infrared sensors, and therefore results in higher reaction conversions since the real temperature is higher and possibly superior to boiling points due to the superheating of reactive media. Nevertheless, microwave thermal effects reduce heating and therefore process times.

#### Acknowledgements

This study is part of the AGRIBTP project on bioproducts for building and public works that is funded by the European Union, the French Government and the Région Midi-Pyrénées. The experimental facility was supported by the FNADT, Grand Toulouse, Prefecture Midi-Pyrenees and FEDER fundings.

## References

- Albright, P.S., Gosting, L.J., 1946. Dielectric constants of the methanol–water system from 5 to 55°. *J. Am. Chem. Soc.* 68, 1061–1063.
- Azcan, N., Danisman, A., 2008. Microwave assisted transesterification of rapeseed oil. *Fuel* 87, 1781–1788.
- Baig, R.B.N., Varma, R.S., 2012. Alternative energy input: mechanochemical, microwave and ultrasound-assisted organic synthesis. *Chem. Soc. Rev.* 41, 1559.
- Banerjee, A., Chakraborty, R., 2009. Parametric sensitivity in transesterification of waste cooking oil for biodiesel production – a review. *Resour. Conserv. Recycl.* 53, 490–497.
- Barnard, T.M., Leadbeater, N.E., Boucher, M.B., Stencel, L.M., Wilhite, B.A., 2007. Continuous-flow preparation of biodiesel using microwave heating. *Energy Fuels* 21, 1777–1781.
- Cintas, P., Mantegna, S., Gaudino, E.C., Cravotto, G., 2010. A new pilot flow reactor for high-intensity ultrasound irradiation. Application to the synthesis of biodiesel. *Ultrason. Sonochem.* 17, 985–989.
- Darnoko, D., Cheryan, M., 2000. Kinetics of palm oil transesterification in a batch reactor. *J. Am. Oil Chem. Soc.* 77, 1263–1267.
- Duz, M.Z., Saydut, A., Ozturk, G., 2011. Alkali catalyzed transesterification of safflower seed oil assisted by microwave irradiation. *Fuel Process. Technol.* 92, 308–313.
- Enweremadu, C.C., Mbarawa, M.M., 2009. Technical aspects of production and analysis of biodiesel from used cooking oil – a review. *Renew. Sustainable Energy Rev.* 13, 2205–2224.
- Fukuda, H., Kondo, A., Noda, H., 2001. Biodiesel fuel production by transesterification of oils. *J. Biosci. Bioeng.* 92, 405–416.
- Grant, E., Halstead, B.J., 1998. Dielectric parameters relevant to microwave dielectric heating. *Chem. Soc. Rev.* 27, 213–224.
- Gui, M.M., Lee, K.T., Bhatia, S., 2008. Feasibility of edible oil vs. non-edible oil vs. waste edible oil as biodiesel feedstock. *Energy* 33, 1646–1653.
- Herrero, M.A., Kremsner, J.M., Kappe, C.O., 2008. Nonthermal microwave effects revisited: on the importance of internal temperature monitoring and agitation in microwave chemistry. *J. Org. Chem.* 73, 36–47.
- Jaliliannosrati, H., Amin, N.A.S., Talebian-Kiakalaieh, A., Noshadi, I., 2013. Microwave assisted biodiesel production from *Jatropha curcas* L. seed by two-step in situ process: optimization using response surface methodology. *Bioresour. Technol.* 136, 565–573.
- Kanitkar, A., Balasubramanian, S., Lima, M., Boldor, D., 2011. A critical comparison of methyl and ethyl esters production from soybean and rice bran oil in the presence of microwaves. *Bioresour. Technol.* 102, 7896–7902.
- Kappe, C.O., 2013. How to measure reaction temperature in microwave-heated transformations. *Chem. Soc. Rev.* 42, 4977.
- Kappe, C.O., Pieber, B., Dallinger, D., 2013. Microwave effects in organic synthesis: myth or reality? *Angew. Chem. Int. Ed.* 52, 1088–1094.
- Kappe, C.O., Stadler, A., Dallinger, D., 2012. Microwave theory. In: *Microwaves in Organic and Medicinal Chemistry*, third ed. Wiley-VCH, Weinheim, pp. 9–39.
- Leadbeater, N.E., Stencel, L.M., 2006. Fast, easy preparation of biodiesel using microwave heating. *Energy Fuels* 20, 2281–2283.
- Lertsathapornasuk, V., Pairintra, R., Aryusuk, K., Krisnangkura, K., 2008. Microwave assisted in continuous biodiesel production from waste frying palm oil and its performance in a 100 kW diesel generator. *Fuel Process. Technol.* 89, 1330–1336.
- Leung, D.Y.C., Wu, X., Leung, M.K.H., 2010. A review on biodiesel production using catalyzed transesterification. *Appl. Energy* 87, 1083–1095.
- Lidström, P., Tierney, J., Wathey, B., Westman, J., 2001. Microwave assisted organic synthesis – a review. *Tetrahedron* 57, 9225–9283.
- Mazubert, A., Poux, M., Aubin, J., 2013. Intensified processes for FAME production from waste cooking oil: a technological review. *Chem. Eng. J.* 233, 201–223.
- Metaxas, A.C., Meredith, R.J., 1983. *Industrial Microwave Heating*. IET.
- Mingos, D.M.P., Baghurst, D.R., 1991. Tilden lecture. Applications of microwave dielectric heating effects to synthetic problems in chemistry. *Chem. Soc. Rev.* 20, 1.
- Obermayer, D., Kappe, C.O., 2010. On the importance of simultaneous infrared/fiber-optic temperature monitoring in the microwave-assisted synthesis of ionic liquids. *Org. Biomol. Chem.* 8, 114.
- Perreux, L., Loupy, A., Petit, A., 2013. Nonthermal effects of microwaves in organic synthesis. In: *Microwaves in Organic Synthesis*, third ed. Wiley-VCH, Weinheim, pp. 127–208.
- Santacesaria, E., Tesser, R., Di Serio, M., Guida, M., Gaetano, D., Garcia Agreda, A., 2007. Kinetics and mass transfer of free fatty acids esterification with methanol in a tubular packed bed reactor: a key pretreatment in biodiesel production. *Ind. Eng. Chem. Res.* 46, 5113–5121.
- Stamenkovic, O.S., Todorovic, Z.B., Lazic, M.L., Veljkovic, V.B., Skala, D.U., 2008. Kinetics of sunflower oil methanolysis at low temperatures. *Bioresour. Technol.* 99, 1131–1140.
- Tur, E., Onal-Ulusoy, B., Akdogan, E., Mutlu, M., 2012. Surface modification of polyethersulfone membrane to improve its hydrophobic characteristics for waste frying oil filtration: radio frequency plasma treatment. *J. Appl. Polym. Sci.* 123, 3402–3411.
- Zhang, Y., Dube, M.A., McLean, D.D., Kates, M., 2003. Biodiesel production from waste cooking oil: 2. Economic assessment and sensitivity analysis. *Bioresour. Technol.* 90, 229–240.
- Zu, Y., Zhang, S., Fu, Y., Liu, W., Liu, Z., Luo, M., Efferth, T., 2009. Rapid microwave-assisted transesterification for the preparation of fatty acid methyl esters from the oil of yellow horn (*Xanthoceras sorbifolia* Bunge). *Eur. Food Res. Technol.* 229, 43–49.

### Determination of operating conditions for esterification with methanol reaction

Transesterification reaction has been vastly investigated in the literature (see Part I). A large number of publications have determined the optimum of operating conditions to be a molar ratio of methanol to oil of 6 and a mass fraction of catalyst related to oil of 1% [1]–[12].

Concerning esterification reaction with methanol, the best operating conditions identified in the literature (see Part I) are esterification reaction is performed with a molar ratio of methanol to oil which is between 10:1 and 48:1 and a mass fraction of catalyst related to oil between 0.3 and 10% of mass related to the mass of oil [13]–[16] (Tables of Part I).

To determine the best operating conditions for esterification reaction, the reactor allowing the production of experimental data with the minimum amount of time and product is the microwave reactor with a volume of 100 mL. The objective is to have significant conversions and keep this set of conditions for the other technologies. The three variables are the molar ratio of methanol to fatty acids  $R$ , the molar ratio of catalyst to fatty acids  $x$  and the residence time  $t$  which are used to optimize the conversion  $X$ .

The results are given in **Table 1** and the cubic model is represented in 3D in **Fig. 1**. An optimum is found at  $R = 15.4$  and  $x = 0.18$  and this set of parameters is kept constant for the rest of the studies for all the types of reactors, corresponding to batch, microstructured and oscillatory baffled reactor for this Chapter 1. The optimum that has been found is tested experimentally. A 94.4% conversion has been obtained using a ratio of 15.4, a molar ratio of catalyst to fatty acid of 0.18 and a residence time of 35 minutes. In comparison, in the batch reactor at 60°C (see Part II, Chapter 2), conversion at 30 min is 94.3% with these conditions.

**Table 1.** Box-Behnken design. R varies between 6 and 50, t varies between 1 and 60 minutes, w varies between 0.5 and 10%. X is the conversion.

R	t (min)	x (-)	X (%)
21.4	60	0.14	95.8
12.0	60	0.26	94.6
21.4	30.5	0.26	93.7
12.0	30.5	0.14	89.1
2.6	60	0.14	56.2
21.4	1	0.14	41.6
21.4	30.5	0.01	41.3
12.0	1	0.26	34.6
12.0	60	0.01	13.0
2.6	30.5	0.26	6.0
2.6	30.5	0.01	3.0
12.0	1	0.01	2.1
2.6	1	0.14	0.0

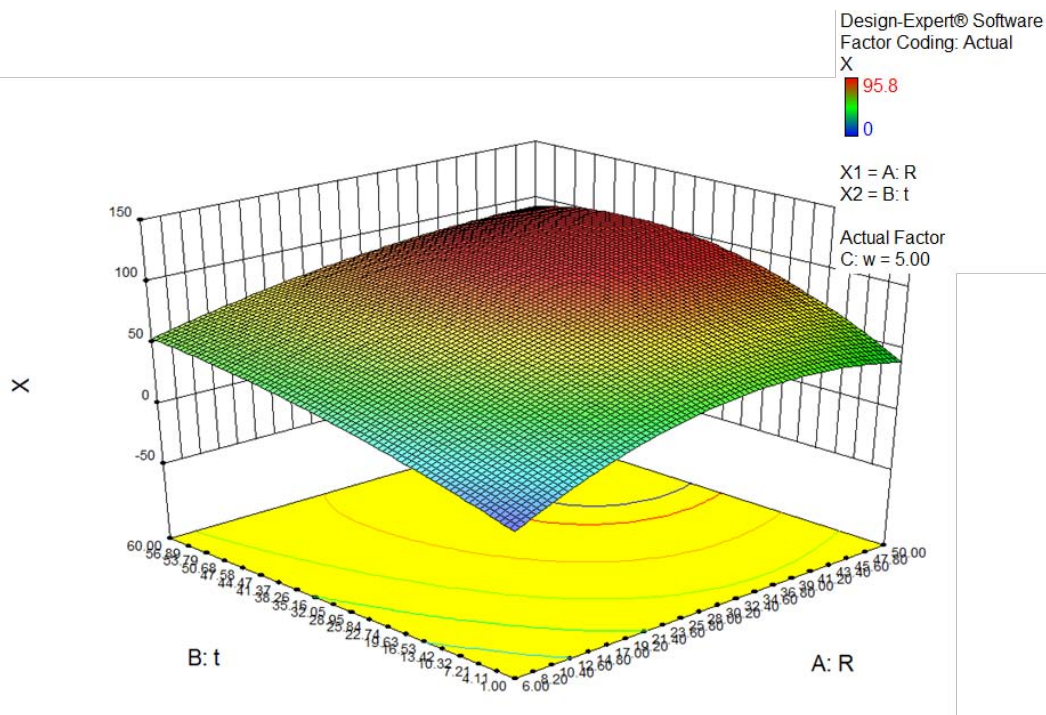


**Fig. 1.** Cubic model of the Box-Behnken design. X is the conversion, t the time in minutes, R the molar ratio of methanol to oil. The fraction of catalyst w is fixed at 5% on this representation.

## Complementary tests with heterogeneous catalysts

To complete this publication realized under homogenous catalysis, some results obtained with heterogeneous catalysts are given. The catalysts have been chosen on the basis of the work of Koberg et al. [2] and Socha et al. [3] promoting strontium oxide (SrO) and Scandium triflate (ScTf<sub>3</sub>) respectively for transesterification and esterification reactions.

SrO (99.5%) has been supplied by Alfa Aesar and ScTf<sub>3</sub> by Sigma Aldrich. **Table 1** shows the transesterification reaction performance using SrO as a catalyst (with molar ratio of methanol to oil fixed at 6 and mass fraction of catalyst to oil fixed at 1%). It can be seen that only low mass fractions of methyl esters have been obtained with this catalyst and microwave irradiation, even after 15 min of reaction time. This contradicts the work of Koberg et al. [2] who obtained 96% of conversion in 2 min with the same catalyst in the same reactive conditions as this work but with a mass fraction of catalyst to oil of 1.8%, and 93% of conversion with a mass fraction of catalyst of 0.92%. In their work, high conversions (93%) are attained even without stirring. Such a difference could be explained by the uncertainty of temperature measurement, which is the main issue according to this Chapter. In their work, microwave irradiation occurs by cycle, 21 s on and 9 s off, and the temperature is measured at the end of the reaction with a digital thermometer, which is not the exact temperature of the reaction. Consequently, the temperature might be underestimated. **Table 2** shows the conversions obtained with ScTf<sub>3</sub> catalyst for the esterification reaction. These are significantly higher than those of the transesterification reaction but after 50 min of reaction time the conversion is still lower than what is obtained with the homogeneous H<sub>2</sub>SO<sub>4</sub> catalyst.

**Table 1.** Mass fraction of methyl esters (ME) obtained in the microwave reactor (V = 100 mL) at 60°C for transesterification reaction catalyzed by SrO.

<b>time (min)</b>	2.5	8	15
<b>ME (wt. %)</b>	3.7	3.9	5.0

**Table 2.** Conversions obtained in the microwave reactor (V = 100 mL) at 60°C for esterification reaction catalyzed by ScTf<sub>3</sub> and H<sub>2</sub>SO<sub>4</sub>.

<b>time (min)</b>	15	50
<b>X(ScTf<sub>3</sub>) (%)</b>	82.4	84.0
<b>X (H<sub>2</sub>SO<sub>4</sub>) (%)</b>	82.0	97.7

## Conclusion

It has been previously claimed in the literature data as described in Part I and in this Chapter that homogeneously-catalyzed transesterification and esterification reactions are enhanced under microwave irradiation. In this work, a thorough experimental method and analysis of results has shown that the accuracy of temperature measurement in microwave reactors has a significant effect on estimation of the positive effect of microwaves. Supplementary tests with heterogeneous catalysts have also been studied. The transesterification reaction catalyzed with strontium oxide provides a mass fraction of methyl esters less than 5%, which is lower than that expected based on literature data. On the other hand, the esterification reaction catalyzed by scandium triflate has shown satisfactory results, with 84% conversion in 50 min. In conclusion, our results show that neither reaction is significantly

enhanced under microwave irradiation, as claimed in the literature. However, our results clearly show that heating rates provided by microwaves are much faster than those attained with conventional heating.

### References

- [1] A. Mazubert, C. Taylor, J. Aubin, and M. Poux, "Key role of temperature monitoring in interpretation of microwave effect on transesterification and esterification reactions for biodiesel production," *Bioresour. Technol.*, vol. 161, pp. 270–279, Jun. 2014.
- [2] M. Koberg, R. Abu-Much, and A. Gedanken, "Optimization of bio-diesel production from soybean and wastes of cooked oil: Combining dielectric microwave irradiation and a SrO catalyst," *Bioresour. Technol.*, vol. 102, no. 2, pp. 1073–1078, Jan. 2011.
- [3] A. M. Socha and J. K. Sello, "Efficient conversion of triacylglycerols and fatty acids to biodiesel in a microwave reactor using metal triflate catalysts," *Org. Biomol. Chem.*, vol. 8, no. 20, p. 4753, 2010.



# **Chapter 2**

## **Transesterification and esterification reactions in microstructured and oscillatory baffled reactors**

---



This chapter focuses on biodiesel production reactions – transesterification and esterification with methanol – in two intensified technologies: microstructured and oscillatory baffled reactors. This chapter is presented the form of a publication, which has been published in a special issue of Green Processing and Synthesis in July 2014, following the Congress on Green Process Engineering in Sevilla in 2014.

This publication is completed by a study of the parameters used for the esterification reaction: molar ratio of methanol to oil and mass fraction of catalyst.



Alex Mazubert, Joelle Aubin\*, Sébastien Elgue and Martine Poux

# Intensification of waste cooking oil transformation by transesterification and esterification reactions in oscillatory baffled and microstructured reactors for biodiesel production

**Abstract:** The transformation of waste cooking oils for fatty acid methyl ester production is investigated in two intensified technologies: microstructured Corning® and oscillatory baffled NiTech® reactors, compared to a reference batch reactor to quantify the process intensification provided by each technology. Both reactors achieve high conversions in shorter times. For transesterification, 96 wt.% of esters are obtained in 1.4 min at 97°C in the Corning® reactor and 92.1 wt.% of esters in 6 min at 44°C in the NiTech® reactor, compared with 94.8 wt.% of esters in 10 min at 60°C in the batch reactor. For esterification, 92% conversion is obtained in 2.5 min in the Corning® reactor at 75°C compared with 20–30 min in the batch reactor at 60°C, and at 40°C, 96.8% conversion is achieved in 13.3 min in the NiTech® reactor, compared with 30 min in the batch reactor. The advantage of the Corning® reactor is that it can operate at higher pressures (1–20 bar) and temperatures (100°C), thereby providing faster kinetics than the NiTech® reactor. However, oils with a high free fatty acid level (73%) cause the Corning® reactor channels to be blocked. A wider range of operating conditions could be obtained in NiTech® with a pressure-resistant material.

**Keywords:** biodiesel; microstructured reactor; oscillatory baffled reactor; process intensification; waste cooking oil.

DOI 10.1515/gps-2014-0057

Received July 27, 2014; accepted September 5, 2014

\*Corresponding author: Joelle Aubin, INP, LGC (Laboratoire de Génie Chimique), Université de Toulouse, 4 Allée Emile Monso, BP-84234, F-31030 Toulouse, France, e-mail: joelle.aubin@ensiacet.fr; and CNRS, LGC, F-31030 Toulouse, France

Alex Mazubert, Sébastien Elgue and Martine Poux: INP, LGC (Laboratoire de Génie Chimique), Université de Toulouse, 4 Allée Emile Monso, BP-84234, F-31030 Toulouse, France; and CNRS, LGC, F-31030 Toulouse, France

## Nomenclature

FAME	Fatty acid methyl esters
FFA	Free fatty acids
COBR	Continuous oscillatory baffled reactor
$Re_o$	Oscillatory Reynolds number (-)
$Str$	Strouhal number (-)
$R$	Molar ratio of methanol to oil for transesterification reaction (-)
$A$	Amplitude of oscillations (mm)
$f$	Frequency of oscillations (Hz)
%ME	Mass fraction of methyl esters (%)
$F_{total}$	Total flow rate in the reactor (kg/h)
$F_{esters}$	Flow rate of esters in the reactor (kg/h)

## 1 Introduction

### 1.1 Context

In recent years, bio-sourced raw material has been investigated as a substitute for fossil fuels or as solvent for renewable energy and green chemistry applications. In the past, virgin and food-grade oils were used to produce the first generation of biofuels, constituted of fatty acid methyl esters (FAME). However, the use of these oils for biodiesel production generates competition with food supply and implies that an increased production capacity is required to satisfy a higher global demand, with negative long-term consequences, including deforestation and desertification [1]. Due to such demands, the price of edible oils is therefore high, representing between 70% and 90% of the biodiesel process cost [2]. The use of non-edible oils, such as jatropha or castor oil, does not compete directly with food-grade oils; however, they still require large plantation areas [3]. Waste cooking oils (WCOs) are of particular interest for biodiesel production for two reasons. First, WCOs are two to three times cheaper than virgin oils [4]. Secondly, by re-using and transforming of WCOs, instead

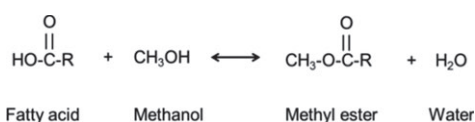
of discarding it into sewers, water treatment costs are significantly decreased [5]. This double effect propels WCOs as a very good environmentally friendly feedstock. The collection of WCOs is made in restaurants and food industries by specialized companies. Private household productions are not collected but can be collected in municipal waste disposals.

The use of WCOs for biodiesel production does however bring on additional processing challenges. During the cooking process and in the presence of water, oils are subjected to high temperatures, leading to formation of fatty acids by hydrolysis reactions [3]. In general, transesterification is base-catalyzed as the reaction is 4000 times faster than with acid catalysis [6]. However, the high acidity of the oil leads to undesired soap formation, which decreases the reaction yield and acts as a surfactant between the two final immiscible products, making downstream separation more difficult. The upper limit of fatty acid levels has never been clearly defined. An advised limit is 1 mg KOH/g<sub>oil</sub> (fatty acid mass fraction of 0.5%) [5]; however, reactions have been performed at 3 mg KOH/g<sub>oil</sub> (fatty acid mass fraction of 1.5%) [5, 7]. Water content is limited to 0.05%vol. (ASTM D6751 standard), because it forms inactive alkaline soaps [8].

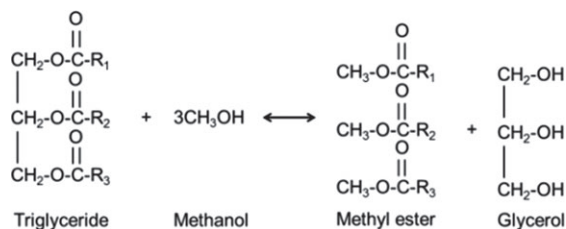
## 1.2 FAME production from WCOs

When producing biodiesel from WCOs, the first required step is to reduce the acidity of the oil. For this, both physical (drying, filtration or distillation [9]) and chemical pretreatments can be used. Chemical pretreatment with the acid-catalyzed esterification reaction will be the focus in this paper. In this reaction, which is a mass-transfer-limited reaction due to the immiscibility between the two reactants [10], the fatty acids in the oil are transformed into methyl esters and water, as presented in Scheme 1.

At this stage after the esterification pretreatment step, the oil contains mainly tri-, di- and mono-glycerides and its acidity is generally below 1.5%. After a subsequent water removal step, the pretreated oil is then transformed with base-catalyzed transesterification, where the products are FAME and glycerol, as given in Scheme 2. The transesterification



**Scheme 1** Reaction scheme for the esterification of fatty acids with methanol to methyl esters and water.



**Scheme 2** Transesterification reaction scheme.

reaction is mass-transfer-limited at the beginning because of the immiscibility between triglycerides and methanol and also at the end of the reaction because most of the catalyst is in the glycerol phase [11]. After treatment of the product: recovery of the oil phase, removal of methanol, neutralization of the catalyst, FAME meet requirements to be used as a biodiesel if European norm EN 14214 is respected, i.e., the mass fraction of esters is >96.5%, the mass fraction of methanol <0.2%, water and sediments <0.05% (vol.), free glycerin <0.02% (wt.), mono-glyceride <0.8% (wt.), and di- and triglycerides <0.2% (wt.). Several types of reactors have been used to carry out WCO transformations and these have been reviewed in our previous work [12]. Technologies include microstructured, cavitation, microwave oscillatory flow and membrane reactors, as well as static mixers and reactive distillation. Microstructured and oscillatory baffled reactors show promising results since the reaction times are significantly reduced. The objective of this work is to experimentally study the feasibility and intensification of transesterification and esterification reactions in microstructured and oscillatory baffle reactors, and compare the results obtained in a conventionally heated and mechanically stirred reactor.

## 2 Materials and methods

### 2.1 Products

WCO was collected, filtrated at 400 μm and supplied by Coreva Technologies (Auch, France). Four WCOs are studied: two oils with a low fatty acid content (0.4% and 2%) and two oils with a higher fatty acid content (39% and 73%). These four different oils have 0% water and 0% solid wastes, and the profiles of the carbon chains are characterized as follows.

- Oil with 0.4% FFA: myristic C14:0 (0.2%), palmitic C16:0 (6.2%), stearic C18:0 (4.0%), oleic C18:1 (31.3%), linoleic C18:2 (56.3%), alpha-linoleic C18:3 (0.57%), arachidic C20:0 (0.35%), behenic C22:0 (0.78%) and lignoceric C24:0 (0.3%);
- Oil with 2% FFA: palmitic C16:0 (6.7%), palmitoleic C16:1 (1.6%), stearic C18:0 (1.3%), oleic C18:1 (47.7%), linoleic C18:2 (29.7%), arachidic C20:0 (7.4%) and behenic C22:0 (5.6%);

- Oil with 39% FFA: palmitic C16:0 (13.1%), stearic C18:0 (3.7%), oleic C18:1 (54.3%), linoleic C18:2 (24.6%) and arachidic C20:0 (4.3%);
  - Oil with 73% FFA: caprylic C8:0 (7.3%), capric C10:0 (4.6%), lauric C12:0 (2.7%), myristic C14:0 (1.4%), palmitic C16:0 (19.4%), palmitoleic C16:1 (3.3%), stearic C18:0 (3.9%), oleic C18:1 (40.3%), linoleic C18:2 (11.3%) and alpha-linolenic C18:3 (0.53%).
- Methanol (99% HPLC grade), sodium hydroxide pellets, sulfuric acid (96%), cyclohexane (analytical grade) and ethanol (absolute, 99.9%) were supplied by VWR (Fontenay-sous-Bois, Val-de-Marne, France). Phenolphthalein and KOH-ethanol solution (1 M or 0.1 M) were supplied by Sigma-Aldrich (Saint-Quentin Fallavier, Isère, France). Methylimidazole (MI) was supplied by Alfa Aesar (Schiltigheim, Bas-Rhin, France). *N*-Methyl-*N*-trimethylsilyl-heptafluorobutyramide (MSHFBA) was supplied by Marcherey-Nagel (Hoerdt, Bas-Rhin, France).

## 2.2 Experimental systems

Reaction performance in three different experimental systems – namely a batch reactor, a microstructured reactor and a continuous oscillatory baffled reactor – has been compared.

The batch reactor, described in Figure 1, is a 1 l jacketed vessel, equipped with a cooling system to avoid methanol vaporization, a mercury thermometer and a mechanical agitator. The agitator is a curved bladed paddle 35 mm in diameter rotating at 300 rpm. Experiments using a Rushton turbine (40 mm diameter, 700 rpm) with baffles have also been used to study the effect of the agitation on the reaction performance. The transesterification and esterification reactions are carried out at 40°C and 60°C, respectively. For the transesterification reaction, the methanol-to-oil ratio is 6:1 and the mass fraction of catalyst (with respect to the mass of oil) is 1%. An initial mass of 600 g of oil (2% FFA) is preheated in the reactor before adding the solution containing methanol and catalyst, potassium hydroxide. For the esterification reaction, the methanol-to-oil ratio is respectively 15.4:1 and 29.4:1 for oil with 73% and 39% of FFA and the molar ratio of catalyst to fatty acid is respectively 0.179 and 0.512 for oil with 73% and 39% of FFA. Methanol and the catalyst, sulfuric acid, are preheated in the reactor. The oil is also preheated in a thermal bath.

The microstructured reactor is the Corning® Advanced Flow™ glass reactor. Two types of Corning® plates were used in series. In the first type, the immiscible fluids mix in a heart-shaped channel, as shown in Figure 2B. The second plate type, shown in Figure 2C, has a simpler design and consists of a meandering channel, which

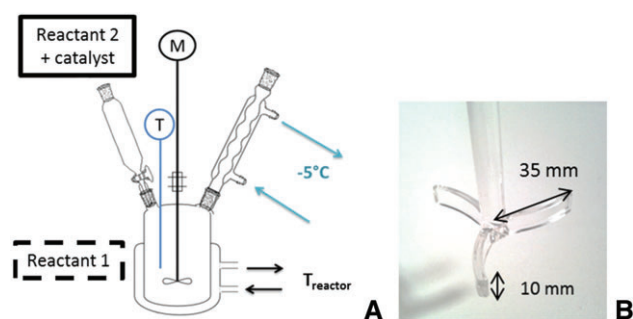


**Figure 1** Schematic diagram of (A) the batch reactor that is used as the reference technology and (B) the curved bladed paddle impeller.

allows longer residence times. The hydraulic diameter of the channel is 2 mm. The plates are composed of three layers: the process fluid flows in the middle layer, whilst the upper and lower plates allow circulation of the utility fluid, which is thermal oil and enables the temperature in the reactor to be regulated. The entire experimental setup, which is composed of eight plates, is depicted in Figure 2A. All the plates are mixing plates with hearts (first type) except for plate 3 (second type), which is a serpentine channel. The total reactor volume is 120 ml. The maximum allowed pressure drop is 15 bars. Temperature is monitored at three points by thermocouples, which are placed after the first, fourth and last plates. The reactants are injected in the first plate. The mobile Zeton® unit allows operation of the reactor. The rig is composed of two lines; one is fed with oil and the other is fed with the solution of catalyst in methanol. Each line is constituted by one solenoid valve, three more valves, an online densimeter, a flow meter, a pressure transducer and two pumps before entering the first Corning® plate. At the reactor outlet, a three-way valve allows sample collection. The possibility to work at pressures up to 15 bars theoretically enables higher operating temperatures than those at atmospheric pressure since the boiling point of methanol is increased. Flow rates vary from 3.2 to 7.1 kg/h for the transesterification reaction and from 2.2 to 5.2 kg/h for the esterification reaction.

The continuous oscillatory baffled reactor (COBR) is a device developed by NiTech® technologies. It is a tube equipped with orifice baffles along its length; instead of feeding the tube with a fixed flow rate, an oscillatory flow rate is applied, creating complex flow. Figure 3 shows a schematic diagram of the reactor; three baffled tubes are used for the transesterification reaction, whereas six baffled tubes are used for the esterification reaction to increase the residence time. Each tube is composed of four 70 cm long elements and comprises 25 cells. A cell is the space between two baffles, which is 26 mm long. The open area or orifice of the baffle is 8 mm in diameter for an inner tube diameter of 15 mm. The tubes are connected by elbows, which comprise six cells. Oscillations are generated by a piston with amplitude varying from 1.5 to 25 mm and frequency from 0.4 to 1.4 Hz. It corresponds to oscillatory flow rates varying from 21 to 69 kg/h for the transesterification reaction and from 79.4 to 104.9 kg/h for the esterification reaction.

Net flow rates vary from 4.9 to 8.1 kg/h for the transesterification reaction and from 2.1 to 8.4 kg/h for the esterification reaction. Temperature is measured at four points (T1 to T4) and samples are taken at three points along the reactor. Unlike the Corning® reactor, the maximum temperature is limited in the COBR used here. Indeed, the flow oscillations generate low-pressure zones due to fluid acceleration around the baffles and thereby decrease the boiling points of the compounds, especially methanol. Vaporization of fluids is not recommended in this type of reactor since the gas absorbs the flow oscillations and decreases the performance of the reactor. Considering the thermal losses and fluid vaporization, the maximum attainable temperatures in the COBR are 44°C and 38°C for the transesterification and esterification reactions, respectively.

## 2.3 Characterization

The composition of FAME produced from the transesterification and esterification reactions was characterized by gas chromatography (GC) using a Perkin Elmer instrument based on the EN-14103 method. The chromatograph is equipped with a flame ionization detector. The column used was Restek (CP-Sil 8 Rtx-5: 5% diphenyl,

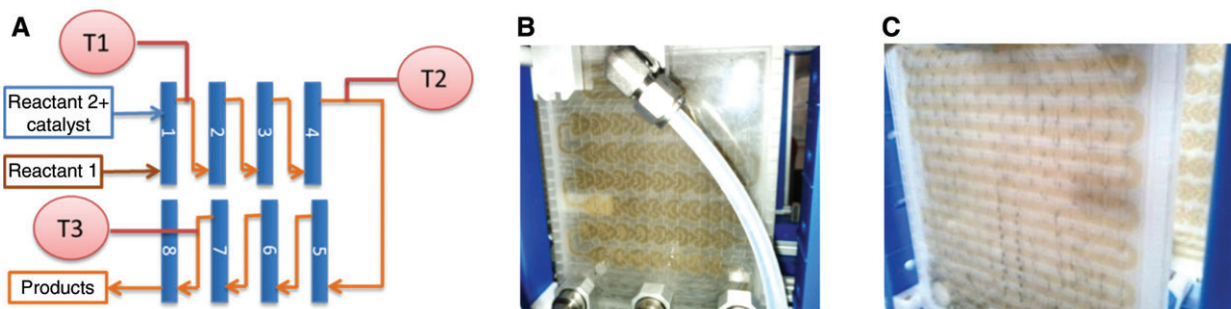


**Figure 2** (A) Schematic diagram of the Corning module composed of eight plates. The sensors T1 to T3 are thermocouples. The reactants are introduced in the first plate and flow in series through the eight plates that are all mixing plates (B) except for plate 3, which is a serpentine channel (C).

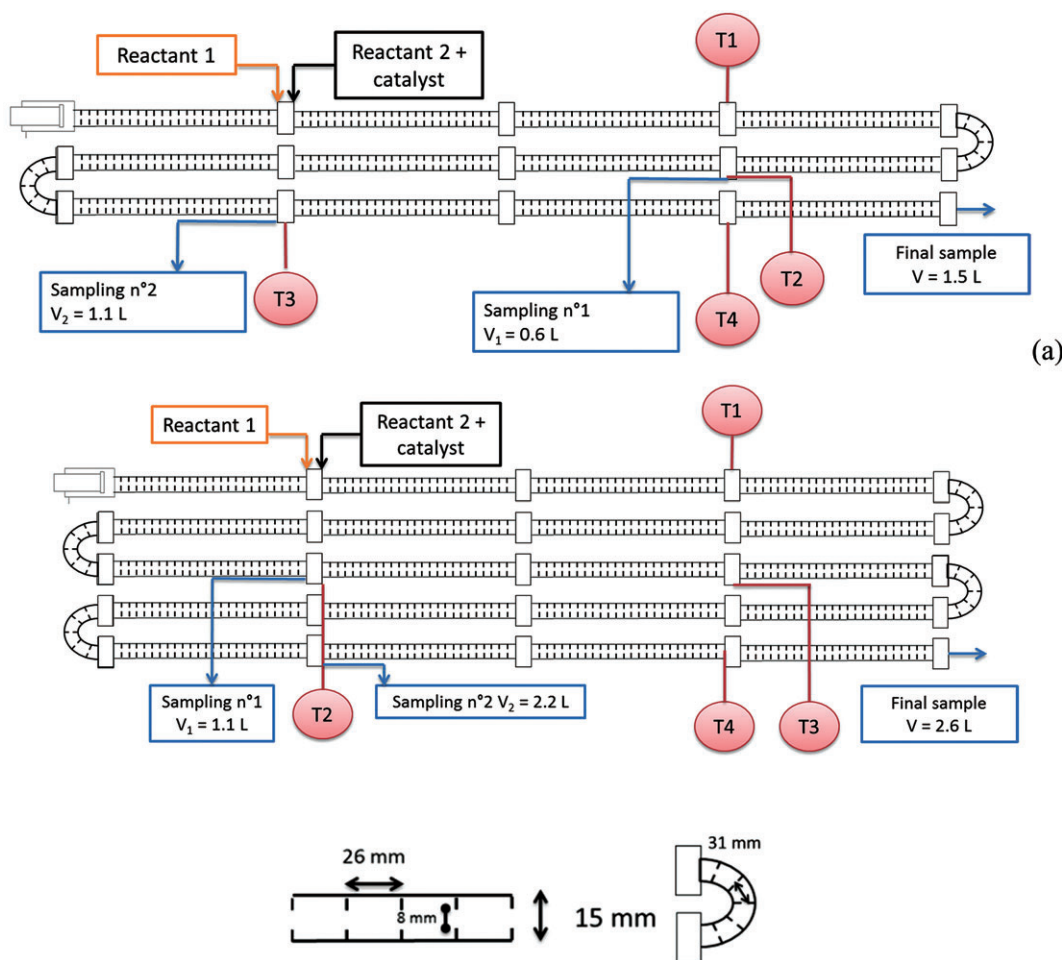


**Figure 3** Experimental set-up of the COBR for (A) three tubes for the transesterification reaction, (B) six tubes for esterification reaction and (C) with the corresponding dimensions.

95% dimethylpolysiloxane)  $15 \text{ m} \times 0.32 \text{ mm} \times 0.25 \text{ }\mu\text{m}$ . The injection is “on-column” because the di- and triglycerides are not vaporized in the injector and are injected as liquids in the column. One internal standard (heptadecane) and six reference materials (triolein, monoolein, diolein, triolein, oleic acid, methyl oleate) supplied by Sigma-Aldrich were used for the GC calibration. The samples are diluted in

cyclohexane (analytical grade) supplied by VWR (France). The operating conditions used for the oven were  $55^\circ\text{C}$  for 30 s,  $45^\circ\text{C}/\text{min}$  to  $80^\circ\text{C}$ ,  $10^\circ\text{C}/\text{min}$  to  $360^\circ\text{C}$  and hold for 11 min. The carrier gas was helium at a constant pressure at the top of the column of 15 psi. The hydrogen flow was kept at  $45 \text{ ml}/\text{min}$  and the air flow was kept at  $450 \text{ ml}/\text{min}$ . The hydroxyl compounds (fatty acids, mono-, di- and triglycerides)



are silylated by a mixture of MSHFBA and MI. This reaction increases the volatility and the stability of injected hydroxyl compounds to enhance their detection. Composition of samples is determined with the internal standard method; mass fractions of methyl esters in the samples are also determined, related to fatty acids, mono-, di- and triglycerides. Intervals of confidence were calculated based on a repeatability study involving five replicates.

The fatty acid level is determined by titration with a 0.1 N KOH-ethanol solution using a Mettler Toledo DL50 titrator based on the ISO 660 norm. The sample (about 1 ml) is diluted in ethanol (about 30 ml). The titrator gives the exact volume added at the equivalence point, which is determined by a pH sensor. Phenolphthalein is used as the colored indicator to detect the equivalence point. The percentage of acidity,  $Ac$ , is given by the relationship  $Ac = (V_{eq} M_{C_{18}} C_{KOH}) / \text{mass of oil}$ , where  $V_{eq}$  is the volume at the equivalence point,  $M_{C_{18}}$  the molar mass of fatty acids and  $C_{KOH}$  the concentration of the KOH-ethanol solution. The percent conversion is given by the relationship  $X = (Ac_{initial} - Ac_{final}) / Ac_{initial}$ , where  $Ac_{initial} = 39\%$  or  $73\%$ . Intervals of confidence were calculated based on two titrations.

## 3 Results and discussion

### 3.1 Transesterification

#### 3.1.1 Corning® reactor

Figure 4A shows the effect of flow rate on the amount of methyl ester produced at  $55^\circ\text{C}$ . Note that an increase in flow rate increases the Reynolds number but decreases the residence time in the reactor. Clearly, the influence of flow rate on the reaction is not significant for the range of Reynolds numbers ( $Re = 30\text{--}70$ ) and residence times (0.9–2 min) studied. On the other hand, the influence of temperature

on the course of the reaction is more important, as shown in Figure 4B. For a fixed flow rate of 4.8 kg/h (residence time equal to 1.4 min), the mass fraction of methyl ester increases rapidly with temperature (because the kinetics are increased) until about 95%, after which any increase in temperature has little effect (because the thermodynamic equilibrium has been reached). It can be noted that the increase in the Reynolds number, due to the decrease in viscosity with rising temperature, has no effect on the reaction. The reaction is controlled principally by kinetics, and the hydrodynamics of the two-phase flow have little effect in this reactor design.

#### 3.1.2 NiTech® reactor

Preliminary experiments were first carried out to determine the optimum conditions of oscillations; these experiments were performed at low temperature ( $27^\circ\text{C}$ ) such that the reaction was limited by the kinetics. Figure 5 presents the mass fraction of esters obtained as a function of the oscillatory Reynolds number  $Re_o$  and Strouhal number  $Str$ , which are defined by Eqs. (1) and (2), respectively. It appears that the reaction is not directly influenced by  $Re_o$ , whereas it is strongly correlated with  $Str$ .

$$Re_o = \frac{2\pi f A \rho D}{\mu} \quad (1)$$

$$Str = \frac{D}{4\pi A} \quad (2)$$

The results associated with Figure 5 are given in Table 1. In Figure 5A, it can be seen that after 9.8 min, the

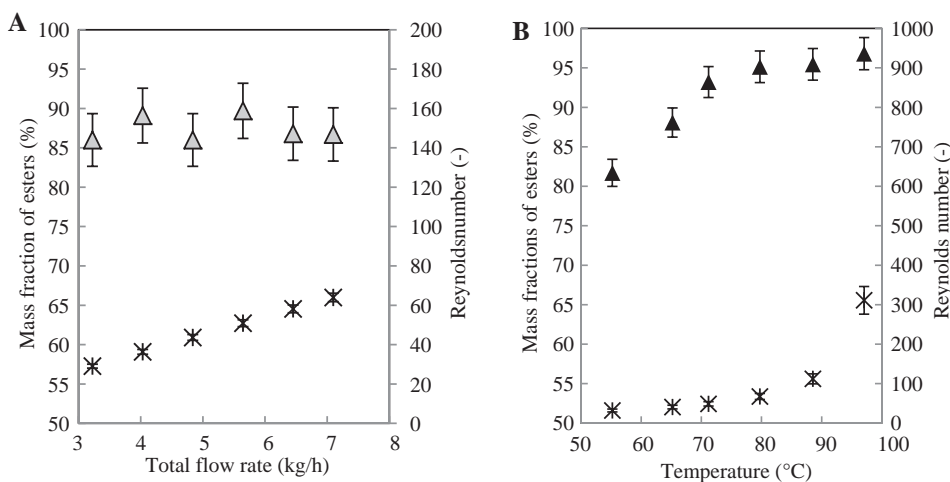


**Figure 4** Influence of (A) flow rate at  $55^\circ\text{C}$  and (B) temperature at a fixed flow rate of 4.8 kg/h on the mass fraction of methyl ester. Mass fractions of esters (left y-axis) are represented with triangles and Reynolds numbers (right y-axis) with stars.

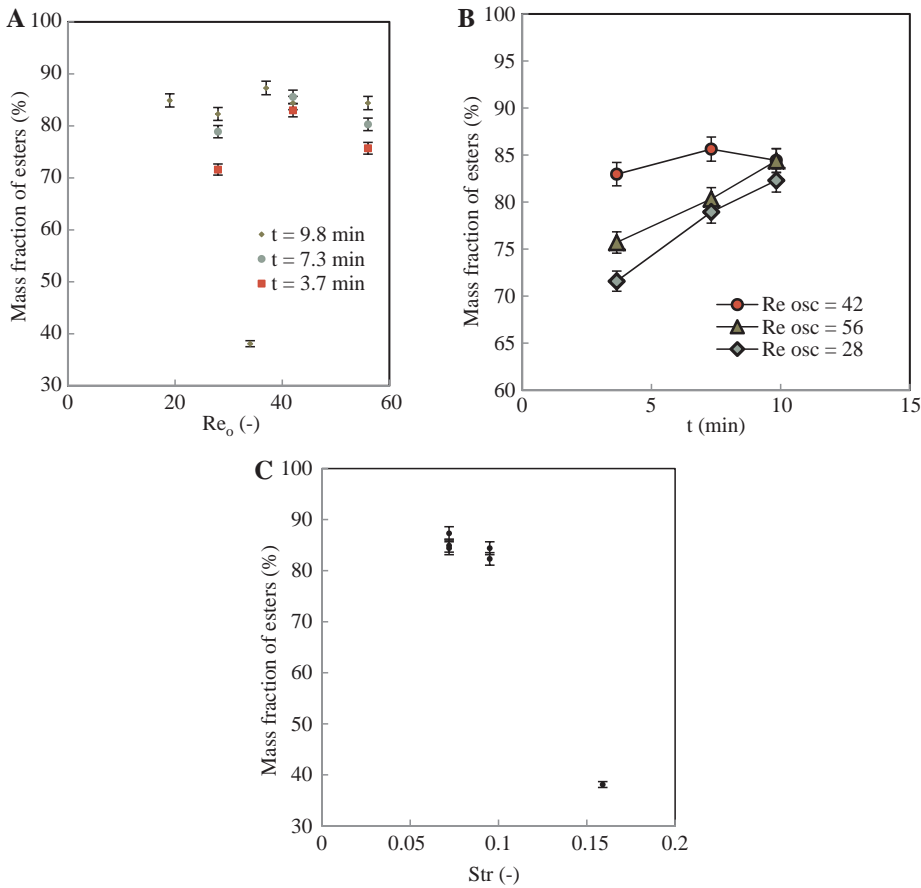


**Figure 5** (A, B) Influence of the oscillatory Reynolds number and (C) Strouhal number on the mass fraction of esters at  $T=27^{\circ}\text{C}$ .

mass fraction of esters is between 82.3% and 87.3% for all oscillation conditions, except for the experiment with low amplitude ( $A=7.5$  mm) and high frequency ( $f=1.4$  Hz). In Figure 5A and B, it can be seen that this mass fraction is reached most quickly at  $Re_{osc}=42$  with  $A=12.5$  mm and  $f=1.05$  Hz. At low amplitude ( $A=7.5$  mm) however, the mass fraction of esters is only 38.1%, which is low compared with other experiments at similar  $Af$  values. No other similar experimental data have been collected to confirm this result. Hamzah et al. [13] report an increase of eddy lengths with the increase of the Strouhal number,

**Table 1** Different amplitudes and frequency tested at  $27^{\circ}\text{C}$  for three different residence times (3.7, 7.3 and 9.8 min).

A (mm)	f (mHz)	%ME	Af (m/s)	Re (-)	Str (-)
7.5	1400	–	–	34	0.159
12.5	700	71.6%	78.9%	82.3%	8.8E-03
	1050	83.0%	85.6%	84.4%	1.3E-02
16.5	350	–	–	84.9%	5.8E-03
	700	–	–	87.3%	1.2E-02
	1050	75.7%	80.3%	84.4%	1.7E-02

Oscillatory Reynolds and Strouhal numbers are given.  $Re_{net}=7$ .

but the increase of the Strouhal number (Figure 5C) seems to decrease the mass fraction of esters in this case. The low value should be explained by poor liquid-liquid dispersion, visible to the naked eye, due to the decrease of the probability for the reactive mixture to meet baffles, spaced with 26 mm, with too low amplitude.

Figure 6 presents the mass fraction of esters obtained at the maximum operating temperature,  $44^{\circ}\text{C}$ , as a

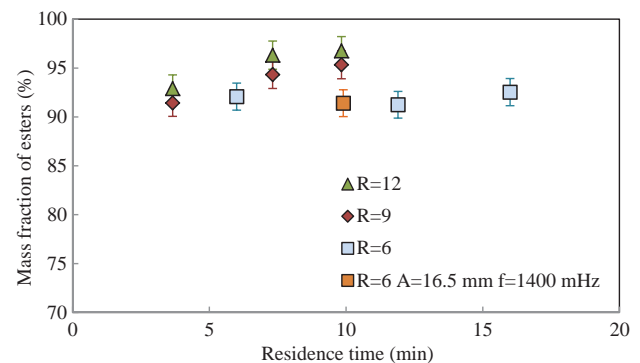


**Figure 6** Variation of the methanol-to-oil molar ratio at  $44^{\circ}\text{C}$ ,  $A=16.5$  mm and  $f=1050$  mHz. An experiment was also carried out at  $A=16.5$  mm and  $f=1400$  mHz.

function of the residence time. The oscillation conditions are fixed at  $A=16.5$  mm and  $f=1.05$  Hz. For the methanol-to-oil molar ratio of 6, the mass fraction of esters is consistently  $<94$  wt.%, regardless of the residence time or oscillation conditions, and this value does not meet the ASTM standard of 96.5 wt.%. To verify whether the mass fraction of esters obtained is limited by thermodynamics rather than chemical kinetics, the molar ratio of methanol to oil has been modified to shift the reaction equilibrium. It can be seen that as the molar ratio is increased from 6 to 9 and 12, higher reaction conversions are obtained. Indeed, increasing the methanol-to-oil ratio from 9 to 12 does not significantly increase the mass fraction of esters, but it allows values that reach the ASTM standard to be obtained. Although temperatures are low, it is possible to obtain satisfactory methyl esters' mass fractions and reach the thermodynamic equilibrium. A comparison of reaction performance obtained at different oscillation frequencies shows once again that conversion is independent of this parameter in the studied range.

### 3.1.3 Comparison with the batch reactor

Figure 7 compares the mass fraction of esters obtained with the microstructured reactor, the COBR and the batch reactor at various operating temperatures. The results clearly show that the reaction is accelerated in the microstructured reactor and the COBR. The thermodynamic equilibrium of the transesterification reaction is at a mass fraction of methyl esters between 90% and 95%. At 40°C, equilibrium is reached in 30 min in the batch reactor with the glass agitator. At 60°C, the equilibrium value is reached in 15 min in the batch reactor with the glass agitator and in 10 min in the batch reactor stirred with the Rushton turbine. This is due to the higher shear rates generated by the Rushton turbine and consequently smaller mean drop size, which promotes mass transfer.

Due to the limited residence time in the Corning® reactor, it was not possible to follow the reaction performance as a function of time or to reach equilibrium for some conditions. Nevertheless, the results show that the microstructured reactor enables conversions similar to those obtained in the batch reactor with the Rushton turbine but in much shorter times. Indeed, at higher temperatures ( $>80^\circ\text{C}$ ) where the ester mass fraction is  $>95\%$ , it is expected that equilibrium is almost reached after just 2 min. In comparison, equilibrium is reached in the NiTech® reactor in about 6 min at 40°C, which is five times faster than that in the batch reactor. Even if the temperature is limited, it is still possible to reach high conversions

in short times because of the good mixing generated by oscillations. The mentioned values are reported in Table 2. The total and ester flow rates are given and are in the same range.

Table 3 shows the time required to obtain a fixed amount of methyl esters in the Corning® and batch reactors at similar temperature and ester mass fraction. Even though thermodynamic equilibrium is not reached, it can be seen that the process is at least three times faster in the Corning® reactor compared with the batch reactor.

## 3.2 Esterification with methanol

Before comparing reactor performance for the esterification reaction, a preliminary study on the effect of net flow rate in the COBR has been carried out with oscillation conditions set at  $A=21.7$  mm and  $f=1.4$  Hz. Figure 8 shows the conversions obtained for different net flow rates but equal residence times. The main advantage of the COBR is illustrated here: the net flow rate value has no effect on the conversions. Mixing is promoted by the oscillations, not flow rate, and this provides great flexibility in the operation of the reactor and choice of the residence time.

Figure 9A and B and Table 4 compare reaction conversion in the different reactor types for oils with initial fatty acid levels of 73% and 39%, respectively. The thermodynamic equilibrium of the reaction is around 98% of conversion for both oils regardless of the fatty acid content. In the batch reactor, equilibrium is reached in 50 min at 60°C with the oil with 73% of FFA. However, when using the oil with 39% of FFA, equilibrium is reached in 50 min at 40°C and in just 15 min at 60°C. This shows that the initial oil composition has a non-negligible effect on reaction time.

In the Corning® reactor, using oil with 73% of FFA at 60°C, equivalent conversion is reached much faster than in the batch reactor: 63% conversion is reached in 1.7 min compared with 8 min in the batch reactor. An increase in temperature brings the reaction closer to equilibrium in short times: 92% conversion in 2.5 min. It is noted that after an hour of processing time, the high-level FFA oil blocked the channels in the Corning reactor and no further investigations were possible. However, no clogging problems were experienced when using the oil with 39% of FFA. Like in the previous results, at most temperatures, equilibrium was not reached in the limited residence time provided by the Corning. Nevertheless, a fixed level of conversion is obtained much more quickly in the Corning® reactor compared with the batch reactor. In the NiTech® reactor, equilibrium is reached in just 13.3 min at 38°C compared with 50 min at 40°C in the batch reactor.

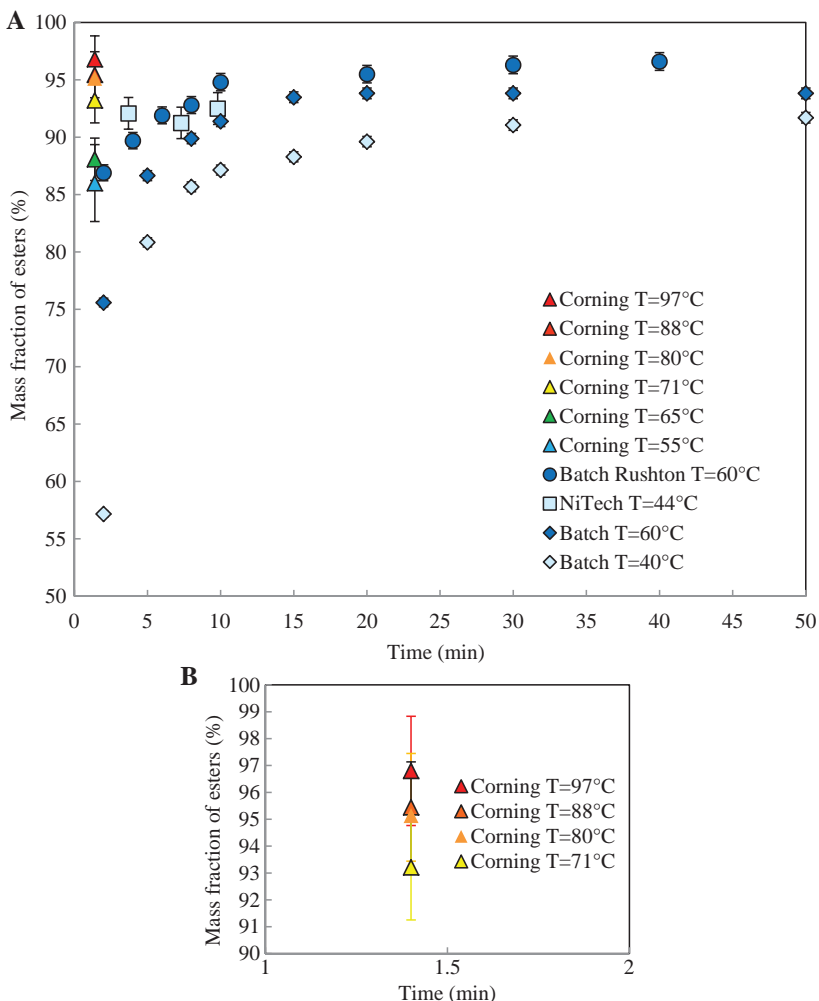


**Figure 7** (A) Comparison of the time evolution of methyl ester mass fraction in the batch, Corning and NiTech reactors. (B) A zoom has been made for Corning results at high temperatures.

## 4 Conclusions

A microstructured reactor and a continuous oscillatory baffled reactor have been tested with the aim of demonstrating the feasibility and the intensification of transesterification and esterification reactions in the continuous mode. Globally, the results of this study show that both

**Table 3** Comparison of time required to obtain a certain mass fraction of esters in the Corning® and batch reactors.

	%ME	$t$ (min)	$F_{\text{total}}$ (kg/h)	$F_{\text{esters}}$ (kg/h)	$T$ (°C)
Batch (glass agitator)	89.9	8	–	–	60
Batch (Rushton)	89.7	4	–	–	60
Corning	89.7	1.2	5.6	4.0	55

**Table 2** Comparison of methyl ester mass fractions obtained in the three reactors for the transesterification reaction.

	%ME (max)	$t$ (min)	$F_{\text{total}}$ (kg/h)	$F_{\text{esters}}$ (kg/h)	$T$ (°C)
Batch (glass agitator)	93.5	15	–	–	60
Batch (Rushton)	94.8	10	–	–	60
Corning	89.7	1.2	5.6	4.0	55
Corning	96.8	1.4	4.0	3.0	97
NiTech	92.1	6.0	5.0	3.7	44

reactors achieve significant reaction conversion in much shorter time than in a batch reactor:

- For the transesterification reaction, 96 wt.% of esters are obtained in 1.4 min at 97°C in the Corning® reactor and 92.1 wt.% of esters are obtained in 6 min at 44°C in the NiTech® reactor (96.3 wt.% with a higher molar ratio in 7.3 min), compared with 94.8 wt.% obtained in 10 min at 60°C in the batch reactor with the Rushton turbine.

- For the esterification reaction, 92% conversion is obtained in 2.5 min in the Corning® reactor at 75°C compared with 20–30 min in the batch reactor at 60°C; 96.8% of conversion is reached in 13.3 min in the NiTech® reactor compared with 30 min in the batch reactor at 40°C.

The Corning® reactor has the advantage of being able to operate at higher pressures, and therefore a wider range of temperatures can be reached. This allows high conversion to be obtained in relatively short times compared with the batch reactor. Indeed, in the current experimental set-up,

the Corning® reactor has limited residence time, but this can be increased by the addition of more reactor plates. However, with oils with high fatty acid levels, the Corning reactor was clogged, thereby has shown some lack of robustness.

Although the glass NiTech® reactor used in this work cannot operate under pressure due to limited mechanical resistance, it has been demonstrated that reaction equilibrium can be rapidly reached even at low temperatures (<40°C) and globally shows better performance than the batch reactor. Moreover, this reactor type shows high flexibility in the choice of the residence times, since mixing is dependent on the oscillation conditions and not the net flow

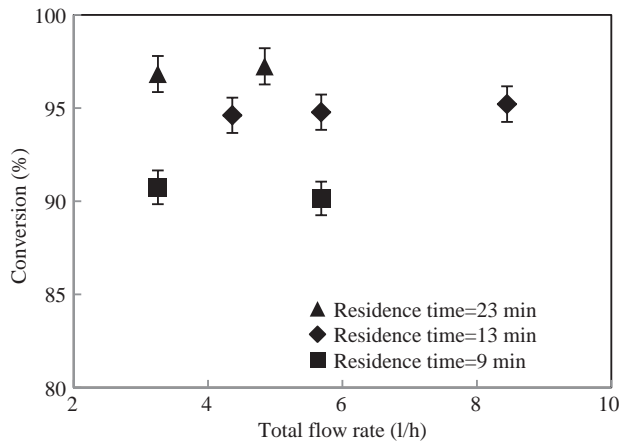


Figure 8 Reaction conversion in the COBR for different net flow rates but constant residence time.

Table 4 Comparison of esterification reaction performance obtained in the Corning®, NiTech® and batch reactors at fixed temperatures and conversions.

	Conversion (%)	t (min)	F <sub>total</sub> (kg/h)	F <sub>esters</sub> (kg/h)	T (°C)
73% FFA					
Batch	63.3	8	-	-	60
Corning	62.1	1.7	2.9	0.514	60
39% FFA					
Batch	94.3	30	-	-	60
Corning	92.0	2.5	2.9	0.86	75
73% FFA					
Batch	89.0	5	-	-	60
Corning	89.3	2.5	2.9	0.84	60
Batch	98.1	50	-	-	40
NiTech	96.8	13.3	3.3	0.70	38

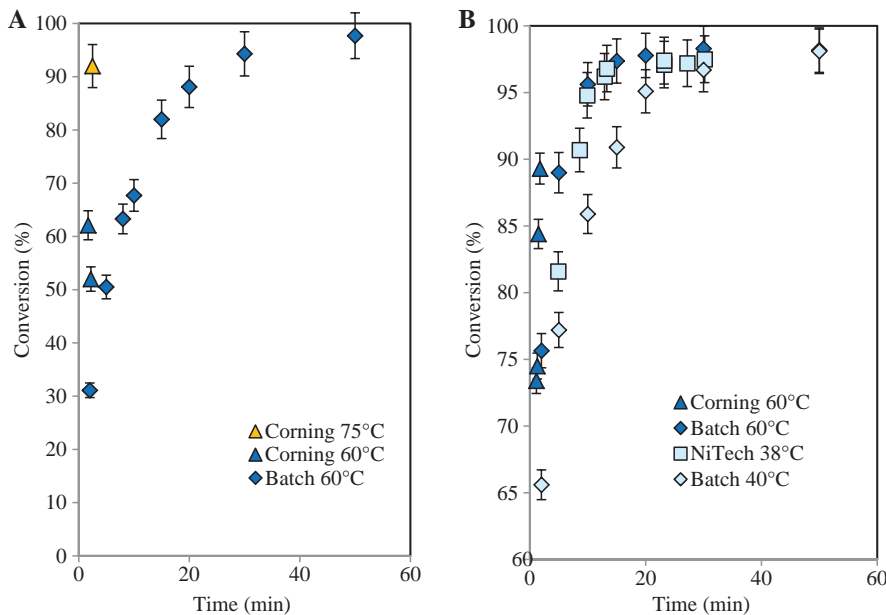


Figure 9 Comparison of esterification performance for the conversion of fatty acids using an oil with initial level of fatty acid of (A) 73% and (B) 39%.

rate. Indeed, it is expected that if the COBR were made from more resistant materials, such as stainless steel or other alloys, higher operating pressures and temperatures could be achieved, resulting in improved reaction performance.

**Acknowledgments:** This study is part of the AGRIBTP project on bioproducts for building and public works that is funded by the European Union, the French Government and the Région Midi-Pyrénées. The experimental facilities were supported by the FNADT, Grand Toulouse, Prefecture Midi-Pyrenees and FEDER fundings and were used in the Maison Européenne des Procédés Innovants (MEPI, Toulouse).

## References

- [1] Metzger JO. *Eur. J. Lipid Sci. Technol.* 2009, 11, 865–876.
- [2] Gerpen JV. *Fuel Process. Technol.* 2005, 86, 1097–1107.
- [3] Gui MM, Lee KT, Bhatia S. *Energy* 2008, 33, 1646–1653.
- [4] Zhang Y, Dube MA, McLean DD, Kates M. *Bioresour. Technol.* 2003, 90, 229–240.
- [5] Banerjee A, Chakraborty R. *Resour. Conserv. Recycl.* 2009, 53, 490–497.
- [6] Fukuda H, Kondo A, Noda H. *J. Biosci. Bioeng.* 2001, 92, 405–416.
- [7] Enweremadu CC, Mbarawa MM. *Renew. Sustain. Energy Rev.* 2009, 13, 2205–2224.
- [8] Leung DYC, Wu X, Leung MKH. *Appl. Energy* 2010, 87, 1083–1095.
- [9] Tur E, Onal-Ulusoy B, Akdogan E, Mutlu M. *J. Appl. Polym. Sci.* 2012, 123, 3402–3411.
- [10] Santacesaria E, Tesser R, Di Serio M, Guida M, Gaetano D, Garcia Agreda A. *Ind. Eng. Chem. Res.* 2007, 46, 5113–5121.
- [11] Cintas P, Mantegna S, Gaudino EC, Cravotto G. *Ultrason. Sonochem.* 2010, 17, 985–989.
- [12] Mazubert A, Poux M, Aubin J. *Chem. Eng. J.* 2013, 233, 201–223.
- [13] Hamzah AA, Hasan N, Takriff MS, Kamarudin SK, Abdullah J, Tan IM, Sern WK. *Chem. Eng. Res. Des.* 2012, 90, 1038–1044.



Alex Mazubert is a PhD student (graduation in November 2014) at the Laboratory of Chemical Engineering (LGC) (Institut National Polytechnique, Toulouse University, Toulouse, France) and a chemical engineer (ENSIACET, 2011). His studies focus on process intensification applied to transformation of fatty compounds.

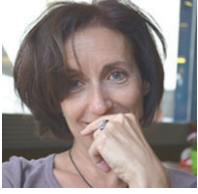


Joelle Aubin is a permanent scientific researcher at CNRS (French National Centre for Scientific Research) and works at the chemical engineering research centre (LGC), University of Toulouse, France. She holds an honours degree in chemical engineering from the University of Sydney, a Master's degree in process and environmental engineering from the Institut National Polytechnique (INPT, Toulouse, France) and a PhD from both the University of Sydney and INPT, obtained under a joint-supervision program. She is currently the leader of the research group Contactors, Mixing and Microstructured Technology within the Department of Science and Technology

for Process Intensification. Through her research she aims at developing innovative strategies for process improvement by controlling segregation and the hydrodynamics; significant emphasis is given to the specificities of equipment design, as well as the analysis and characterization of the flow and mixing occurring in the system.



Sébastien Elgue is a research engineer at the Institut National Polytechnique (INPT), Toulouse University, France. He holds his Engineer, Master's and PhD degrees in process and environmental engineering from INPT. He has worked as a technology manager in the field of process intensification, first in industry (Alfa Laval – ART Team) and currently at the Laboratory of Chemical Engineering (LGC – Toulouse France). His research interests include the development and the characterization of innovative PI technologies as well as new methodologies to support this development. Sébastien Elgue was involved in the creation of MEPI, a piloting and demonstration facility located in Toulouse, to strengthen the implementation of PI in industry and the development of Green Process Engineering. He is currently the technical manager at MEPI.



Martine Poux is a chemical engineer (ENSC Toulouse, 1985). She obtained her PhD (1989) and the accreditation to supervise research (HDR) in 1997; she holds a position as research engineer (Institut National Polytechnique, Toulouse University, Toulouse, France) at the Laboratory of Chemical Engineering (LGC). She has carried out research, in particular, in the fields of microwave processes, reactor hydrodynamics and new intensified technologies for green chemical processes. She is the co-chairman of the International Congress on Green Process Engineering lecture series (2007, 2009, 2011, 2014). Her research work was awarded five times at regional and national innovation competitions. Martine Poux has been a member of the Operating Committee of the French Society of Chemical Engineering (SFGP) since 1995. At an international level, she acted as the French secretariat office of the European Federation of Chemical Engineering. She is the general coordinator of the next European Congress on Chemical Engineering to be held in Nice in September 2015.

## Graphical abstract

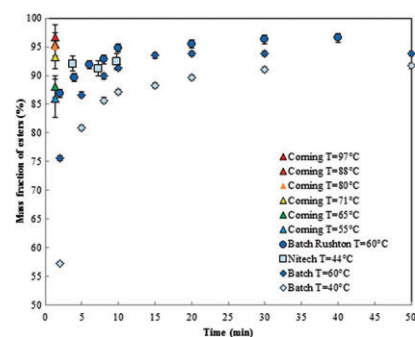
Alex Mazubert, Joelle Aubin, Sébastien Elgue and Martine Poux  
**Intensification of waste cooking oil transformation by transesterification and esterification reactions in oscillatory baffled and microstructured reactors for biodiesel production**

DOI 10.1515/gps-2014-0057

Green Process Synth 2014; x: xxx–xxx

**Original article:** The two biodiesel production reactions, transesterification and esterification, are realized with faster kinetics in two intensified technologies: microstructured and oscillatory baffled reactors.

**Keywords:** biodiesel; microstructured reactor; oscillatory baffled reactor; process intensification; waste cooking oil.





## Conclusion

The comparison of microstructured, oscillatory baffled and batch reactors has first shown the enhancement of transesterification and esterification reactions in the two intensified process technologies compared with the batch reactor. The two continuous innovative process technologies have a different range of operating conditions, especially in terms of temperature, making the direct comparison of the different experimental data complex, but still sufficient to orientate the rest of the research work. This experimental work highlights the excellent performance of the microstructured Corning® reactor, where conversions are attained in short residence times for the transesterification and esterification reactions with methanol with oil with 39% of FFA. However, oil with a high level of FFA (73%) used for esterification reaction caused fouling in the reactor. This was not the case in the glass oscillatory baffled Nitech® reactor, which also presents good performance, even at low temperature. An increase in the range of operating conditions for this reactor is required to achieve higher performances and this is possible by changing the reactor material (glass) for a more pressure-resistant material in order to increase pressure, increase boiling points of reactants and then increase the operating temperature.



# Chapter 3

Esterification with glycerol in  
microstructured, oscillatory baffled and  
microwave reactors

---



## Introduction

The esterification reaction of fatty acids with glycerol is detailed in the Part I, Section 1.3. The reaction scheme is recalled in **Fig. 1**. This reaction involves waste cooking oil without any pretreatment that contains high level of fatty acids and glycerol which is a co-product of the biodiesel formed during the transesterification reaction. The interest of such a reaction is to decrease the level of free fatty acids in the oil to carry out a base-catalyzed transesterification afterwards to obtain FAME. A more specific interest is the formation of monoglyceride, which is of interest for the formulations developed in the AGRIBTP project.

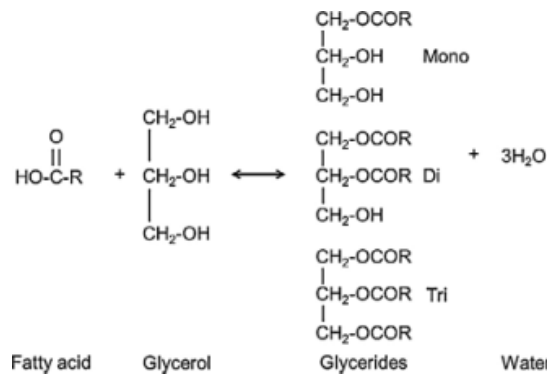


**Fig. 1.** Reaction scheme of the esterification of fatty acids with glycerol to glycerides and water.

The results found in the literature described in Part I, which are now summarized and completed in **Table 1**, indicate that temperatures up to 180°C are needed to reach conversions up to 95%. The increased temperature not only enhances kinetics, but it also decreases the viscosity of the reactive solution (see **Table 2** and **Fig. 2**), thereby increasing the Reynolds number and improving the contact between phases. The authors of the publications provided in **Table 1** use a system to remove the water to shift the equilibrium when operating pressure is low. Pressure is an important parameter because the presence of water influences the boiling point of the mixture, which has been measured experimentally at atmospheric pressure to be 120°C. Simulations have also been carried out to predict the boiling point of a binary mixture of glycerol/water 70/30 wt.% to be 112°C with Aspen and 122°C with ProPhyPlus (model SRK-MHV2-UNIFAC). A small excess of glycerol is chosen to minimize the viscosity of the reactive media and to reduce the recycle stream. Temperatures superior to 180°C are chosen to decrease the viscosity below 5 cP. The maximal temperature is 250 °C. Beyond this temperature glycerol decomposes.

**Table 1.** Operating conditions for direct esterification with glycerol used in literature. R is the molar ratio of glycerol to fatty acids, w is the mass fraction of catalyst to fatty acids, c is the conversion rate and t is the reaction time.

$R_{\text{Gly/FFA}}$	catalyst	$w_{\text{cata/FFA}}$	T (°C)	P (bar)	X (%)	t (h)	Reference
3	NaOH	0.1	180	Fill with N <sub>2</sub>	70-90	6	[1]
1.04	Zn	0.2	180-230	N/A	95	0.8	[2]
2	HSO <sub>3</sub> SBA-15	1-5	140-160	0.68	90	5	[3]
1	Fe-Zn	7	200	N/A	95	1	[4]
1.4	SO <sub>4</sub> <sup>2-</sup> /ZrO <sub>2</sub> -Al <sub>2</sub> O <sub>3</sub>	0.3	200	0.05	98.4	4	[5]
0.33	Lipozyme <sup>TM</sup>	-	40	0.07	65	23	[6]

**Table 2.** Data for temperature from 0 to 100 °C obtained in the work of Dorsey[7], and based on the parameterization of the work of Cheng [8] for temperatures from 100 to 190°C.

T (°C)	0	10	20	30	40	50	60	70
$\mu$ (cP)	12070	3900	1412	612	284	142	81.3	50.6
T (°C)	80	90	100	110	120	130	140	190
$\mu$ (cP)	31.9	21.3	14.8	10.8	8.2	6.3	5.1	2.4

The opposite reaction, the hydrolysis reaction or fat-splitting reaction, has also been studied. This reaction is of interest when one wants to produce fatty acids, which are also of interest in the AGRIBTP project. The literature data from Part I highlights that high temperatures (>250°C) and pressures (>50 bar) are needed to perform this reaction, like the Colgate-Emery process described in [9].

The objective of this chapter is to investigate the feasibility and performance of the microstructured, oscillatory baffled and microwave reactors for conducting the esterification reaction with glycerol and the hydrolysis reaction.

## 1. Material and methods

### 1.1. Products

Waste cooking oil was collected, filtrated at 400  $\mu\text{m}$  and supplied by the company Coreva Technologies (Auch, France). Two WCOs are studied with content of fatty acids of 39% and 73%.

These two different oils are the same as those used in the previous chapter for esterification with methanol in the microwave (Chapter 1, Part II), microstructured and oscillatory baffled reactors (Part II, Chapter 2). The pure oils (0% water, 0% solid wastes) have been characterized and the

profiles of the carbon chains are as follows: palmitic C16:0 (13.1%), stearic C18:0 (3.7%), oleic C18:1 (54.3%), linoleic C 18:2 (24.6%), arachidic C20:0 (4.3%) for the oil with **39%** FFA; caprylic C 8:0 (7.3%), capric C 10:0 (4.6%), lauric C 12:0 (2.7%), myristic C 14:0 ( 1.4%), palmitic C 16:0 ( 19.4%), palmitoleic C 16:1 ( 3.3%), stearic C 18:0 ( 3.9%), oleic C 18:1 ( 40.3%), linoleic C18:2 ( 11.3%) and alpha-linoleic C18:3 (0.53%) for the oil with **73%** FFA. Sulfuric acid (96%), cyclohexane (analytical grade) and ethanol (absolute, 99.9 %) were supplied by VWR, France. Glycerol (BioXtra,>99%), phenolphthalein, KOH-ethanol solution (1M or 0.1 M) and Scandium triflate fixed on polymer beads (ScTf<sub>3</sub>) were supplied by Sigma-Aldrich, France. Methyl imidazole (MI) was supplied by Alfa Aesar. N-méthyl-N-trimethylsilyl-heptafluorobutyramide (MSHFBA) was supplied by Marcherey-Nagel.

## 1.2. Experimental systems

The conventionally heated reactor consists of a 1 L jacketed vessel, a cooling system to avoid methanol vaporization, a mercury thermometer and a mechanical stirring unit. The agitation speed is fixed at 300 rpm. The esterification with glycerol reaction is carried out at 90°C. Methanol and the sulfuric acid catalyst are preheated in the reactor. The oil is also preheated in a thermal bath. The effect of agitation has been studied by varying the agitation system. The reaction performance using a 70 mm diameter three-bladed curved paddle is compared with that obtained in the same vessel stirred with a 40 mm diameter 6-bladed Rushton and three baffles to prevent the formation of a vortex. Indeed, in such two-phase systems, stirring has an effect on the dispersion of methanol in the oil. The smaller the droplets of one phase in another are, the higher the mass transfer is, implying faster kinetics.

The three innovative process technologies that are tested are the same as those used in the previous chapters (Part II, chapters 1 and 2):

- the microstructured reactor is the Corning® Advanced Flow™ glass reactor;
- the continuous oscillatory baffled reactor (COBR), NiTech® technologies;
- the microwave reactor is a CEM® Discover SP

In the previous chapter, a 100 mL round flask vessel was used in the microwave reactor. In this chapter, a reactor vessel of 10 mL has also been used (See **Fig. 2**). This setup is advantageous as the vessel is closed, thereby allowing operation under pressure and the possibility to attain temperatures higher than 120°C before the boiling point is reached. Secondly, the small volume of the reactor allows the use of small amounts solid catalyst (ScTf<sub>3</sub>), which is expensive. The agitation in this system is ensured by a magnetic stirrer rotating at 300 rpm.

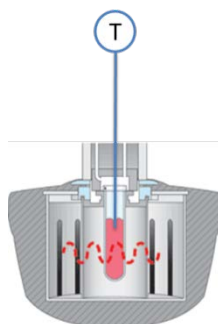


**Fig. 2.** CEM microwave reactor in its closed configuration with a 10 mL tube.

Due to high viscosity of glycerol, a heating plate is used to preheat the glycerol in order to decrease its viscosity and facilitate pumping in the Corning® and Nitech® setups. An insulated tube is used from the pumps to the Nitech® reactor to maintain the temperature attained with the thermostatic bath. Molar ratios of glycerol to fatty acid ranging from 0.85 to 29.4 have been used. Due to technical constraints, the maximum attainable temperature is 80°C, 60°C and 190°C respectively for the Corning®, Nitech® and microwave reactors.

The method for characterizing the obtained products is given in the Part II, Chapter 1, Section 2.3. GC analysis is used to determine monoglyceride selectivity. Titrations are used to determine the conversion of fatty acids.

## 2. Results and Discussion

### 2.1. Esterification with glycerol in the batch reactor

Esterification with glycerol was firstly performed in the batch reactor using the three-bladed curved paddle at a rotational speed of 300 rpm and at 90°C. Interestingly the reaction did not occur, with no conversion of fatty acids whatsoever. With the Rushton turbine at 700 rpm and baffles and at higher temperature, 113°C, higher conversions are obtained, but still insufficient. The results are represented in Fig. 3 for two molar ratios of glycerol to fatty acids and a molar ratio of catalyst to fatty acids of 0.22. It can be seen that after 3 h of reaction time, the conversions are still increasing and the thermodynamic equilibrium is still not reached. Indeed, at 113°C, the chemical kinetics still limits the progress of the reaction.

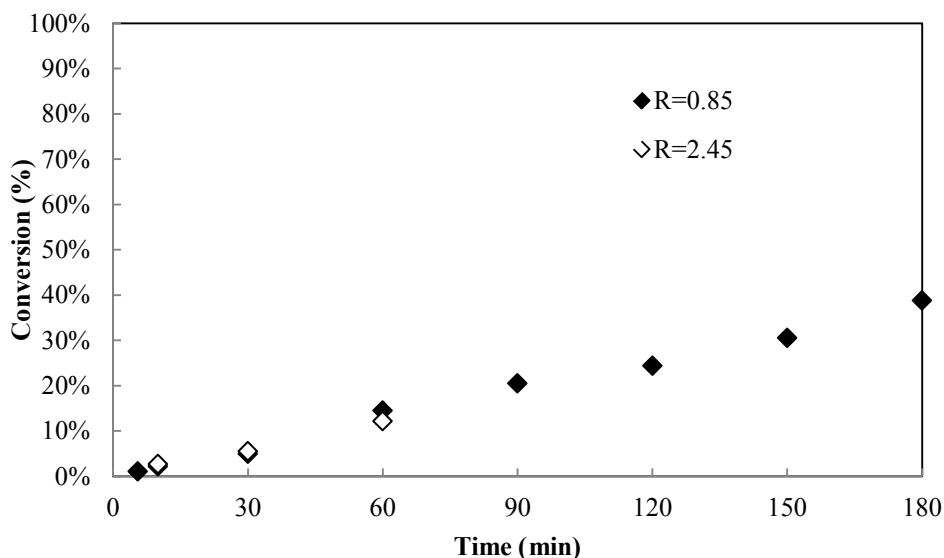


Fig. 3. Conversion of fatty acids as a function of time for two different molar ratios of glycerol to fatty acids. Molar ratio of sulfuric acid to fatty acids  $x$  is equal to 0.22.



## 2.2. Esterification with glycerol in the microstructured and oscillatory baffled reactors

The performance of the esterification reaction with glycerol has also been tested in the Corning® and the Nitech® reactors (see description in Part II, Chapter 2, section 2.2.). The reactants are pure glycerol and oil with 39% of free fatty acids. This level has been chosen due to the blockage issues encountered when using higher fatty acid level oil in the Corning® reactor. Moreover, collected waste cooking oils generally have a maximum amount of free fatty acids of 45% and the ultimate objective is to directly transform this type of oil without pretreatment, as for example by increasing the level of fatty acids through an extraction with methanol, a step mastered by the company Coreva Technologies.

The operating conditions, including estimations of net and oscillatory Reynolds numbers, and the conversions obtained in the two reactors are given in the **Table 3**. Definitions of net and oscillatory Reynolds number are given below and are used more in details in Part III:

$$\text{Net Reynolds number: } Re_{net} = \frac{\rho v D}{\mu} \quad \text{Eq. 2.2-1}$$

$$\text{Oscillatory Reynolds number: } Re_o = \frac{2\pi f x_0 \rho D}{\mu} \quad \text{Eq. 2.2-2}$$

Clearly the conversions are low, being less than 10%. Two effects can be given. Firstly, the presence of glycerol increases the viscosity of the mixture, thereby decreasing the Reynolds number under the range of Reynolds number obtained for transesterification and esterification with methanol reactions (See **Table 4**). The viscosities used to calculate Reynolds numbers have been estimated from data using triolein and oleic acid as model fluids [10], [11]. To obtain an approximate range of Reynolds numbers, the viscosity of a binary mixture is simply estimated to be equal to:  $\mu = w_1\mu_1 + w_2\mu_2$ , where  $w_i$  is the mass fraction of the compound  $i$ . The second effect is the nature of the reactants or intermediary products depends on the reaction in question. Concerning the transesterification reaction, diacylglycerides are formed as intermediates; these act as emulsifiers and thereby facilitate the dispersion of the polar phase in the oil. Concerning the esterification with methanol, it should be pointed out that methanol is far less viscous than glycerol, thereby making it possible to operate with excess methanol without an increase in viscosity and decrease in Reynolds numbers.

**Table 3.** Operating conditions and conversions obtained in the Corning® and Nitech® reactors. Estimation of net and oscillatory Reynolds numbers are given.

Reactor	T (°C)	Residence time (min)	Total flow rate (kg/h)	Re net (-)	Re o (-)	X (%)
Corning®	84.8	2	3.6	43	-	4.3
	80.4	3	2.3	28	-	9.0
Nitech®	62.0	20	4.3	24	70	5.9

**Table 4.** Comparison of Reynolds numbers for esterification reaction with glycerol. Comparison with experimental conditions for transesterification and esterification reactions.

Reaction	Corning®	Nitech®	
	Re net	Re net	Re o
Esterification with glycerol	25-50	25	70
Transesterification	40-90	10-15	100-140
Esterification	50-150	180-470	750-1000

To overcome the effect of the high viscosity of glycerol, the temperature of the medium can be increased to decrease viscosity (see **Table 2**). Due to the thermal resistance of the Corning® and Nitech® setups, the maximum operating temperature was fixed at 120°C. With the thermostat set point set to 110°C, the temperature in the Corning® and Nitech® reactors is around 80°C and 60°C. Increasing the temperature in Nitech® would have been possible by insulating the reactor, but only up to a certain limit, since the production of water by the reaction leads to boiling points of around 120°C. Moreover, depressurizations generated by oscillations can reduce this boiling point. Ideally, a system to increase pressure is needed, however the maximum permitted pressure in the glass Nitech® reactor is only 5 bar. Therefore, an increase in temperature in the Nitech® reactor is only possible by using more resistant material than glass, e.g. stainless steel (existing Nitech® DN22<sup>1</sup>, see **Fig. 4**). Nevertheless, tests at higher temperatures are possible in the microwave reactor.



**Fig. 4.** DN22 pilot-scale Nitech® reactor.

### 2.3. Esterification with glycerol in the microwave reactor

The potential existence of non-thermal effects occurring in microwave reactors have been discussed in the previous chapter and it was concluded that such effects do not exist for homogenous catalyzed esterification reaction. Nevertheless, the microwave reactor can still provide fast heating and allow high temperatures to be reached in the closed 10 mL vessel. Heterogeneous catalysis has shown interesting results in the literature data [2], [3], [4], [5], [6] for the esterification reaction with glycerol in **Table 1**. An example of heterogeneous catalysis coupled with microwave irradiation has been found for the esterification reaction with methanol with the use of scandium triflate [12]. In this work, in

<sup>1</sup> <https://www.youtube.com/watch?v=Vk5mIr90mpY>

addition to the tests using sulfuric acid catalyst in the microwave reactor, scandium triflate catalyst supported on polymer beads has also been tested. Both oils with 39% and 73% FFA have been used.

### 2.3.1. Homogenous catalysis: sulfuric acid

The reaction performance using the homogenous catalyst and microwave irradiation are presented in **Table 5**. Oil with 73% of FFA has been used as feedstock and the homogenous catalyst is sulfuric acid. The magnetic agitation speed is set to 300 rpm. Temperature is limited to 180°C due to the degradation of products in presence of acids and excessively high temperatures. The best results are obtained with a glycerol to fatty acids molar ratio of 1.85 and a molar ratio of catalyst to fatty acid of 0.077. An increase temperature has a positive effect on conversions, with 20.5% and 36.9% of conversion obtained respectively at 90°C and 140°C. These conversions are still relatively low, but significantly higher than those obtained in the microstructured and oscillatory baffled reactor and this is due to the possibility to reach higher temperatures in the microwave reactor.

### 2.3.2. Heterogeneous catalysis: Scandium triflate

**Table 6** and **Fig. 5** summarize the results obtained using heterogeneous catalysis and microwaves. The reaction has been carried out using oil containing 73% of FFA and the solid catalyst, scandium triflate, is fixed on polymer beads. The amount of catalyst is expressed in terms of the mass fraction of catalyst (scandium triflate and polymer beads) related to fatty acids (w) since the molar quantity of catalyst fixed on a polymer bead is not known.

**Table 5.** Experimental data obtained for esterification with glycerol reaction. Conversions (X) are calculated with their confidence interval I at different temperatures (T) and residence times (t). Two sets of parameters, molar ratio of glycerol to fatty acids (R) and molar ratio of catalyst to fatty acids (x) have been tested.

<b>T (°C)</b>	90	90	90	140	190
<b>R (-)</b>	15.1	1.85	1.85	1.85	1.85
<b>x (-)</b>	0.179	0.077	0.077	0.077	0.077
<b>t (min)</b>	50	2	50	50	50
<b>X (%)</b>	0	0	20.5	36.9	Degradation (black deposit)
<b>I (%)</b>	-	-	18.0	13.8	-

**Table 6.** Experimental data for the esterification reaction with glycerol. Conversions (X) are calculated with their confidence interval I at different temperatures (T) and residence times (t). Two sets of parameters, glycerol to fatty acids molar ratio (R) and mass fraction of catalyst to fatty acid (w), have been tested.

<b>T (°C)</b>	90	90	140	190	190	190	190	190	190	
<b>R (-)</b>	1.85	15.4	1.85	1.85	15.4	15.4	15.4	15.4	15.4	
<b>w (%)</b>	0.04	0.10	0.04	0.04	0.04	0.04	0.04	0.04	0.04	
<b>t (min)</b>	50	50	50	50	2	5	15	30	50	<b>I (%)</b>
<b>X (%)</b>	0	25.9	57.4	72.9	31.6	63.8	77.1	83.8	98.8	12.3

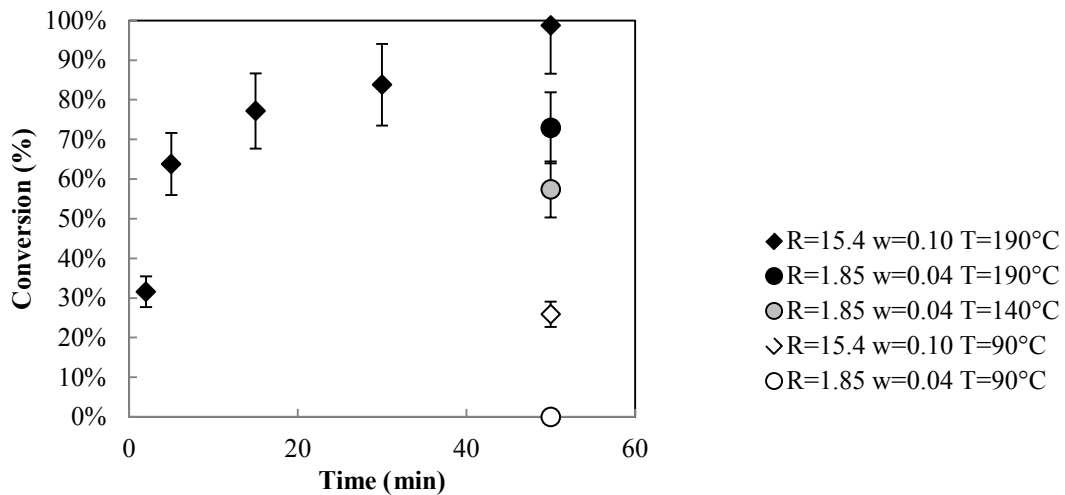


**Fig. 5.** Esterification with glycerol under heterogeneous catalysis (scandium triflate): study of the conversion as a function of residence time. Two different sets of parameters R and w have been tested.

**Table 7** and **Fig. 6** show the conversions and acid values for the esterification with glycerol using the heterogeneous scandium triflate catalyst and microwaves ( $T=190^{\circ}\text{C}$ ) as a function of time. A comparison with the literature data by [2] has been made. In their work, a batch reactor at  $220^{\circ}\text{C}$  was used with a solid catalyst Zn (0.3 %wt). Their oil feedstock contains 30% of FFA. The results obtained in this work are relatively close to those of [2], but lower acidity is obtained faster with scandium triflate and the oil containing more fatty acids (73%).

Heterogeneous catalysis offers higher conversions than those obtained with homogenous catalysis. At  $90^{\circ}\text{C}$  for the same molar ratio of reactants, a 25.9% conversion is obtained with  $\text{ScTf}_3$  whereas 0% conversion is obtained with sulfuric acid. At  $140^{\circ}\text{C}$ , the conversion is clearly higher with  $\text{ScTf}_3$ , being 57.4% compared with 36.9% with sulfuric acid. Indeed, in this case the molar ratios of reactants are not the same; the conversions are higher with a low molar ratio between the reactants for homogenous catalysis whereas the opposite effect is observed for  $\text{ScTf}_3$  as conversions are higher with a high molar ratio between the reactants.

**Table 7.** Comparison of results obtained in esterification with glycerol using scandium triflate as a catalyst at  $190^{\circ}\text{C}$  under microwave irradiation and a study by [2] made with zinc as a catalyst at  $220^{\circ}\text{C}$  using conventional heating.

t (min)	0	2	5	15	28	30	50	58
X (%)	-	31.6	63.8	77.1	-	83.8	98.8	-
Acid value (mg KOH/ g d'huile)	-	94.3	49.9	31.5	-	22.3	1.7	-
Acid value literature[2]	62	-	-	-	10	-	-	9

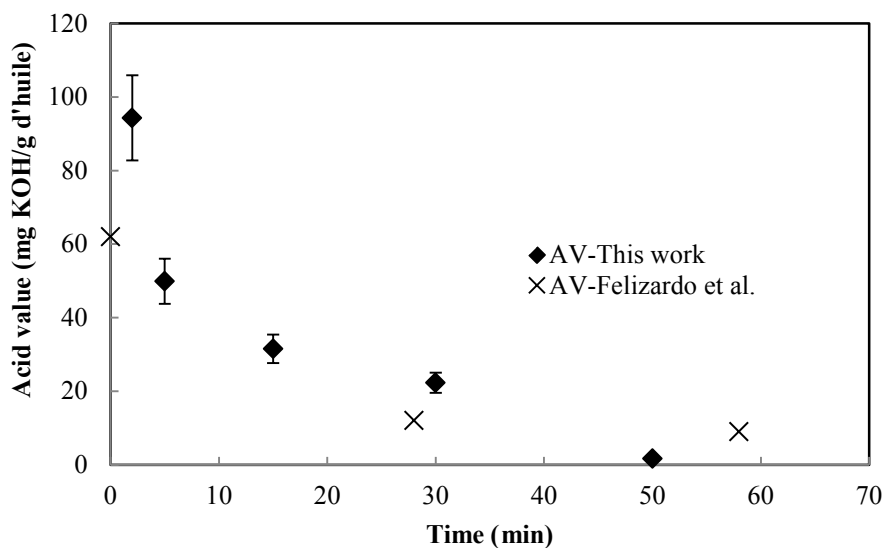


**Fig. 6.** Direct esterification with glycerol in microwave batch reactor. The acid values (AV) obtained in this work (dark diamonds) are compared to the work of Felizardo et al. [2].

**Table 8** and **Fig. 7** present the esterification reaction performance using an oil containing 39% of FFA as feedstock for the reaction in the 100 mL vessel at atmospheric pressure and 120°C. The reaction under the same conditions has also been performed in the 10 mL vessel reactor and the results are similar, with a 18.5% conversion obtained in a reactor volume of 100 mL and a 21.3% conversion obtained in a reactor volume of 10 mL. The increase of volume has no significant effect on conversions. The 71.7% conversion using the 39% FFA oil are inferior to the 98.8% conversion obtained with the oil containing 73% of FFA at 190°C (98.8%). The initial level of FFA of the oil has an effect on conversions, as the other part of oil is composed of products of the reaction, shifting equilibrium in the opposite direction. After 50 min, the conversion equals 18.5% for  $R=2.45$  and  $w=0.08\%$  and seems to have reached the equilibrium. This result is similar to the result obtained in the batch reactor with sulfuric acid at 113°C, where the conversion is 12.2% after 60 min for  $R=2.45$ .

**Table 8.** Esterification with glycerol with 39% FFA oil at atmospheric pressure in the 100 mL vessel or in the closed reactor at 10 mL.

<b>T (°C)</b>	120	120	120	120	120	120	120	190
<b>R (-)</b>	2.45	2.45	2.45	2.45	2.45	2.45	2.45	29.4
<b>w (%)</b>	0.08	0.08	0.08	0.08	0.08	0.08	0.08	0.18
<b>t (min)</b>	2	5	10	15	30	50	50	50
<b>X (%)</b>	11.4	13.8	16.0	17.5	17.4	18.5	21.3	71.7
<b>A (%)</b>	34.5	33.6	32.8	32.2	32.2	31.8	30.7	11.0
<b>V<sub>reactor</sub> (mL)</b>	100	100	100	100	100	100	10	10

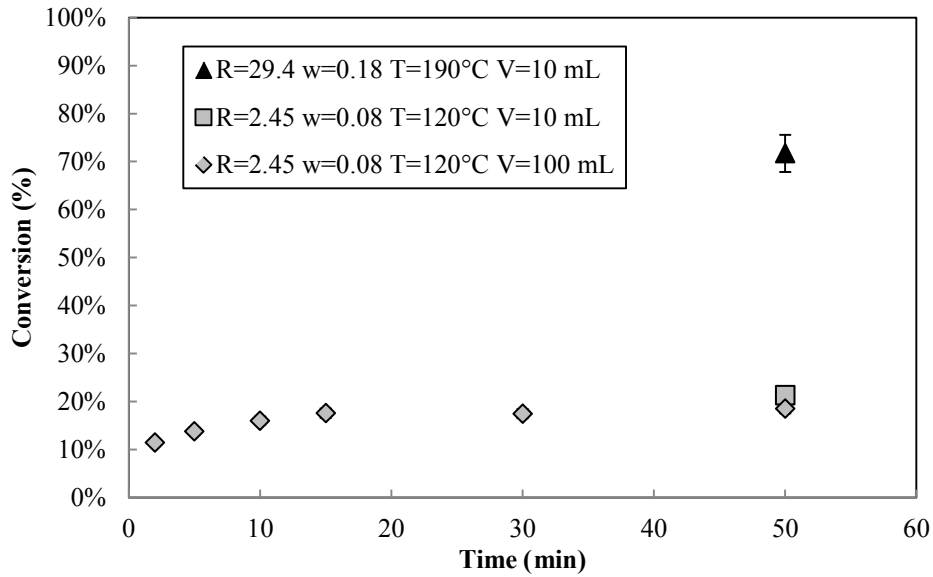
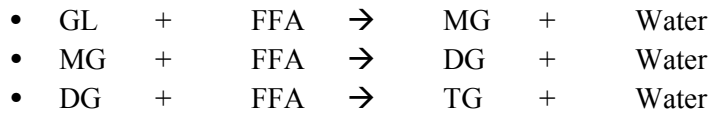


Fig. 7. Heterogeneous catalyzed esterification with glycerol reaction with 39% FFA oil.

The composition of a sample taken from the reaction at 190°C after 50 minutes has been determined by GC analysis. Selectivities obtained are given in **Table 9**. The selectivities related to fatty acids have been calculated considering consecutive reactions as following [3]:



$$S_{j/i} = \frac{|v_i|}{|v_j|} \frac{n_{j,f} - n_{j,0}}{n_{i,0} - n_{i,f}}$$

$$S_{MG/FFA} = \frac{n_{MG,f} - n_{MG,i}}{n_{FFA,i} - n_{FFA,f}}$$

$$S_{DG/FFA} = \frac{n_{DG,f} - n_{DG,i}}{n_{FFA,i} - n_{FFA,f}}$$

The selectivity in monoglycerides is significantly higher than that of diglycerides and no triglycerides have been formed. It is higher than the selectivity obtained in the work of Kotwal et al. [4], where the selectivity in monoglycerides at 95% conversion is 53.6% at 200°C. This is an interesting result since monoglycerides are the products of interest.

**Table 9.** Evolution of the compositions of oil after esterification with glycerol at 190°C with oil with 39% of FFA after 50 min.

%mol	Initial oil	End of the reaction	Selectivity related to FFA (%)
FA	73.0	24.5	-
MG	2.6	38.2	73.4
DG	10.3	23.2	26.6
TG	14.1	14.1	0

## 2.4. Hydrolysis reaction

Results obtained for the hydrolysis reaction are summarized in **Table 10**. Higher temperatures (250°C) and higher pressures (50 bar) are required to achieve high conversions for this reaction [9]. Moreover, other physical treatments exist to separate fatty acids from oil. In addition, the interest of fatty acids has decreased with the progress of the project in the development of formulations for building and public works. Consequently, the study of this reaction in a single intensified reactor was no longer pursued and work was focused on the transesterification, esterification with methanol and esterification with methanol reactions only.

**Table 10.** Increase of acidity of the oil (Ac) during the hydrolysis reaction in the different reactors with corresponding operating conditions (T: temperature, P: pressure, A: oscillation amplitude, f: oscillation frequency, R: molar ratio of water to oil, w: mass fraction of catalyst to oil, t: time).

	<b>Batch</b>	<b>Corning</b>	<b>OBR</b>	<b>Microwaves</b>				
<b>Catalyst</b>	H <sub>2</sub> SO <sub>4</sub>	H <sub>2</sub> SO <sub>4</sub>	H <sub>2</sub> SO <sub>4</sub>	H <sub>2</sub> SO <sub>4</sub>			TPAB	Triton
<b>P (bar)</b>	1	8.2	3.2	1				
<b>T (°C)</b>	90	118	51	100	140	140	140	140
<b>A (mm)</b>			22					
<b>f (Hz)</b>			0.7					
<b>R (water : oil)</b>	30	30	30	30	30	30	30	30
<b>w (%)</b>	5	5	5	5	5	5	5	5
<b>t (min)</b>	60	1.1	21.0	60	120	240	240	240
<b>Ac<sub>initial</sub> (%)</b>	2	0.4	2	2	39.0	39.0	39	39
<b>Ac<sub>final</sub> (%)</b>	2	4.0	3.9	2	49.0	49.2	39	39

## Conclusion

This chapter has shown that high temperatures are needed for esterification reaction with glycerol even in intensified process equipment, which confirms the results in the literature obtained in conventional reactors. The results show that the microstructured and oscillatory baffled reactors operating at mild temperatures (80 and 60°C) did not provide good reaction conversion; the highest conversion being only 9% (Corning® reactor with a residence time of 3 min). This result is nevertheless higher than the zero conversion obtained in the batch reactor at 90°C, showing the potential of such technologies. This confirms the results obtained in Chapter 1, where the microstructured and oscillatory baffled reactors showed better performance than the batch reactor for the transesterification and esterification reactions, due to higher mixing and higher capacity to generate emulsions with small droplets. However, the range of tested temperatures was limited in these equipment, thereby leading to low conversions. The tests carried out in the microwave reactor at higher temperature confirm this need of higher temperatures, as demonstrated in the literature results. In addition, these tests show the non-negligible influence of the initial amount of fatty acid in the oil and of the nature of the catalyst on the conversion. With a solid catalyst, scandium triflate immobilized on polymer beads, good conversion and satisfying selectivity in monoglycerides have been attained with the esterification reaction with glycerol. Finally, the hydrolysis reaction requires a higher range of temperature and pressure even with the use of intensified technologies. Due to the limited interest of this reaction for the AGRIBTP, the study of hydrolysis reaction was not further pursued.

## References

- [1] R. B. R. Choudhury, "The preparation and purification of monoglycerides. II. Direct esterification of fatty acids with glycerol," *J. Am. Oil Chem. Soc.*, vol. 39, no. 8, pp. 345–347, 1962.
- [2] P. Felizardo, J. Machado, D. Vergueiro, M. J. Correia, J. P. Gomes, and J. M. Bordado, "Study on the glycerolysis reaction of high free fatty acid oils for use as biodiesel feedstock," *Fuel Process. Technol.*, vol. 92, pp. 1225–1229, 2011.
- [3] L. Hermida, A. Z. Abdullah, and A. R. Mohamed, "Synthesis of monoglyceride through glycerol esterification with lauric acid over propyl sulfonic acid post-synthesis functionalized SBA-15 mesoporous catalyst," *Chem. Eng. J.*, vol. 174, no. 2–3, pp. 668–676, Nov. 2011.
- [4] M. Kotwal, S. S. Deshpande, and D. Srinivas, "Esterification of fatty acids with glycerol over Fe-Zn double-metal cyanide catalyst," *Catal. Commun.*, vol. 12, pp. 1302–1306, 2011.
- [5] Y. Wang, S. Ma, L. Wang, S. Tang, W. W. Riley, and M. J. T. Reaney, "Solid superacid catalyzed glycerol esterification of free fatty acids in waste cooking oil for biodiesel production," *Eur. J. Lipid Sci. Technol.*, vol. 114, no. 3, pp. 315–324, Mar. 2012.
- [6] S. M. Kim and J. S. Rhee, "Production of medium-chain glycerides by immobilized lipase in a solvent-free system," *J. Am. Oil Chem. Soc.*, vol. 68, pp. 499–501, 1991.
- [7] N. E. Dorsey, "Properties of Ordinary Water-Substance," *Reinhold*, 1940.
- [8] N.-S. Cheng, "Formula for the Viscosity of a Glycerol–Water Mixture," *Ind. Eng. Chem. Res.*, vol. 47, no. 9, pp. 3285–3288, May 2008.
- [9] H. L. Barnebey and A. C. Brown, "Continuous fat splitting plants using the Colgate-Emery process," *J. Am. Oil Chem. Soc.*, vol. 25, no. 3, pp. 95–99, 1948.
- [10] F. H. Rhodes and C. B. Barbour, "The viscosities of mixtures of sulfuric acid and water," *Ind. Eng. Chem.*, vol. 15, no. 8, pp. 850–852, 1923.
- [11] D. Valeri and A. J. Meirelles, "Viscosities of fatty acids, triglycerides, and their binary mixtures," *J. Am. Oil Chem. Soc.*, vol. 74, no. 10, pp. 1221–1226, 1997.
- [12] A. M. Socha and J. K. Sello, "Efficient conversion of triacylglycerols and fatty acids to biodiesel in a microwave reactor using metal triflate catalysts," *Org. Biomol. Chem.*, vol. 8, no. 20, p. 4753, 2010.





## Conclusions of Part II

Part II has investigated the performance of three intensified process technologies – microstructured, oscillatory baffled and microwave reactors – for FAME producing reactions: transesterification, esterification with methanol and esterification with glycerol reactions. Chapter 1 and Chapter 2 focus on the transesterification and esterification reactions. In Chapter 1, these reactions have been carried out in a microwave reactor. Chapter 2 investigated intensification of these reactions in a microstructured Corning® reactor and an oscillatory baffled Nitech® reactor. Finally, in Chapter 3, same experimental setups have been used to study the performance of the esterification with glycerol reaction.

Chapter 1 has shown the non-effect of microwave irradiation on reaction rates, which is an important result. This, in addition to the difficulty of transposing the batch microwave process to a scaled-up continuous one for a production of around 100 kg/h, has orientated us to focus on commercially developed continuous intensified technologies. Finally, Chapter 3 showed the limitations of the different intensified technologies for the esterification with glycerol reactions in terms of temperatures and pressures. The microwave reactor is indeed a well-adapted tool to rapidly confirm the literature results, i.e. that higher operating temperatures and conversions can be obtained rapidly and the use of a solid catalyst improves conversion.

In Chapter 2, the experimental comparison of the microstructured and oscillatory baffled reactors shows not only the feasibility of the continuous process for the different FAME reactions, but also the enhancement of reactions with conversions reached in shorter residence times compared with that required by a conventional batch reactor. Both intensified reactors have a different range of possible operating conditions. The microstructured reactor is able to work under pressure and thereby reach higher temperatures before the reactants reach their boiling points. The glass oscillatory baffled reactor is limited to temperature inferior to 45°C and pressure inferior to 5 bars but regardless of this, it still provides good conversions for the transesterification and esterification reactions. The study of esterification with glycerol, which is a slower reaction, has highlighted the limitations of the glass oscillatory baffled reactor due to the impossibility to work under pressure and higher temperatures. Since this reaction is one of the priorities of the AGRIBTP project, the final process technology should be able to perform this reaction. Indeed, the work presented in Chapter 3 shows that this reaction is possible, but at higher temperatures.

The most promising reactors for industrial purpose are however the microstructured reactor and the continuous oscillatory baffled reactor as these apparatus have higher processing capacity. The choice then between these two reactor types is not a straightforward task. Ultimately, oscillatory baffled reactors may be preferred for several reasons; there are no risks of tube clogging when high-level FFA oils are used and a wider range of operating conditions is potentially possible. Indeed, oscillatory baffled reactors can be manufactured in stainless steel, offering a higher resistance to pressure and the possibility to operate at higher temperatures because the boiling points of the reactants are increased. This technology is not available at the LGC; however, an international collaboration was set up between LGC Toulouse (France) and TNO Delft (Netherlands) to test this reactor with the esterification of fatty acids with glycerol, the main limiting reaction.

In addition, the comprehension of reaction enhancement in oscillatory baffled reactors justifies the development of new tools for its characterization, as well as studies oriented to improve reactor geometry and operating conditions. This is the subject of the next part, which focuses on the characterization and improvement of the intensified technology of oscillatory baffled reactors through

numerical simulations conducted at LGC Toulouse and experimental development in TNO Delft.



# Part III

Characterization and improvement of  
oscillatory baffled reactor technology

---



## Introduction

At the end of Part II, oscillatory baffled reactor has been considered as the most suitable technology. Chapter 1 shows microwave reactors did not enhance particularly reaction using homogenous catalysts. Chapter 2 shows oscillatory baffled and microstructured reactors perform a given conversion for transesterification and esterification reactions with shorter residence times. These two reactors are suitable for these reactions, however the oscillatory baffled reactor has been preferred to microstructured reactor as the latter has been blocked for oil with high level of free fatty acids. Finally, chapter 3 shows the limitation of the two intensified technologies to perform esterification reaction with glycerol due to a temperature limitation. Higher temperature is required, and modifications of the experimental setup of the oscillatory baffled reactor have to be made to increase conversions, and consequently increase the flexibility and multi-reaction capacity of the reactor.

This is the objective of this Part III which focuses on the characterization and possible improvements of oscillatory baffled reactors. Part III is divided in two chapters. The first one is treating of the experimental tests carried out on the oscillatory baffled reactor working at higher temperatures. In the second chapter, a study of hydrodynamics in the oscillatory baffled reactor has been realized, including numerical simulations and instantaneous velocities measurements, for a better understanding of the mixing and liquid-liquid dispersion in such a reactor technology.





# Chapter 1

Improvement of the robustness of  
oscillatory baffled reactor applied to  
viscous reactants

---



## Preamble

At the end of Part II, good results have been obtained for transesterification and esterification (with methanol) reactions, with high mass fraction of methyl esters and conversions obtained in shorter residence times than in batch reactor in microstructured and oscillatory baffled reactors. The microstructured Corning® reactor shows excellent performance, high pressure drop (5-15 bar depending on the flow rate) allows to increase temperature, keeping the more volatile reactant in the liquid state and increasing reaction rates. The glass Nitech® oscillatory baffled reactor shows good results, however oscillations generates local zones of low pressure leading to unwanted evaporation of reactants. To remain in the liquid state, temperature has been constrained to 40° C for transesterification and esterification reactions, as increase of pressure is limited by the resistance of the glass reactor (5 bar). Concerning esterification with glycerol reaction, high thermal losses lead to a temperature in the glass Nitech® oscillatory baffled reactor of only 60°C and 80°C in the Corning® reactor, leading to conversions of only 4.3% in the glass Nitech® oscillatory baffled reactor in 20 min and 9% in the Corning® microstructured reactor in 3 min (see Part II, Chapter 3). Tests at higher temperature have been carried out with sulfuric acid as a catalyst in the batch reactor, leading to a 39% conversion in 3 h at 113°C, and in the microwave reactor, leading to a 37% conversion in 50 min at 140°. With a solid heterogeneous catalyst, scandium triflate, higher conversions (> 98%) have been obtained at 190°C in 50 min.

The reaction appears to be possible at higher temperatures. The objective is then to transpose the good results obtained at higher temperatures in a technology intensifying mixing in order to get a better contact between the two phases. An improvement of the previous oscillatory baffled reactor setup appeared possible if a more pressure-resistant material is used, as stainless steel, with a good insulation for an effective heating. Showing the improvement of the setup is then possible on this esterification with glycerol reaction, reaction with low conversions in the two types of reactors working at low temperatures. Indeed, the main limitation of this reaction is the high viscosity of glycerol, decreasing with temperature increase and then leading to low Reynolds numbers. Achieve an experimental setup with the oscillatory baffled technology able to work under pressure and high temperature should improve the flexibility of reactors and extend its use to more reactions, especially reactions involving viscous reactants.

After some investigations to find a welcome laboratory, enterprise or company, an agreement has been found with the department of Process Intensification at TNO, Netherlands, localized in Delft, to build an international collaboration between them and INP Toulouse. This independent research organization, with more than 3500 employees, have projects in collaboration with companies in a wide range of expertise domains (health, industrial innovation, defense, energy, transport, building...) [1]. Their interest in this collaboration is the building of the experimental setup of such a reactor, and ours is to test the oscillatory baffled reactor setup able to work at higher pressure and temperature.

This work is the synthesis of the 3 months of international mobility (April-July 2014) and has been supported by INP Toulouse for international mobility funding, as well as the Réseau Franco-Néerlandais, who provided EOLEs scholarship. This Chapter 1 is in progress of submission (submission in December 2014), untitled "Performance comparison of a continuous oscillatory baffled reactor and a Helix reactor for the esterification of fatty acids using waste cooking oil and glycerol", written with the collaboration of M. Crockatt and M. Roelands from TNO, and submitted at the Chemical Engineering & Technology journal.



## Performance comparison of a continuous oscillatory baffled reactor and a Helix reactor for the esterification of fatty acids using waste cooking oil and glycerol

### 1. Introduction

Much recent research has focused on developing bio-sourced products that are renewable and sustainable to substitute fuels, solvents or formulations of mineral origin. The most common raw materials studied is virgin or food-grade oil, which are mainly used to produce biofuels that are constituted of fatty acids methyl esters. One drawback associated with this additional demand of food-grade oils for biofuel production is that it can lead to deforestation and desertification [2]. To avoid this competition, non-edible oils, such as jatropha or castor oil, have been also studied but these do still need very large plantation areas [3]. Waste cooking oils are consequently of particular interest as a renewable raw material for several reasons: they are two to three times cheaper than virgin oils [4], and their re-use and the transformation of WCO, instead of discarding it into sewers, significantly decreases water treatment costs [5].

WCO can be transformed into biofuels by base-catalyzed transesterification reactions, but these oils contain a proportion (between 3% and 45%) of free fatty acids, which must first be transformed by an acid-catalyzed esterification reaction to avoid the undesirable saponification reaction that may occur in the presence of an alkali catalyst. The reactant for the esterification of fatty acids is often methanol, which produces fatty acid methyl esters, or glycerol, a co-product of the transesterification reaction, which produces mono, di and triglycerides. Following the latter reaction, the oil is considered to be *regenerated* since its quantity of fatty acids has been decreased and the base-catalyzed transesterification is then possible [6]. The production of monoglycerides via the esterification reaction is also interesting since these compounds have various applications in cosmetics, pharmaceutical formulations and drug delivery systems [7]. The reaction scheme of esterification of fatty acids reaction with glycerol is given in **Fig. 1**.

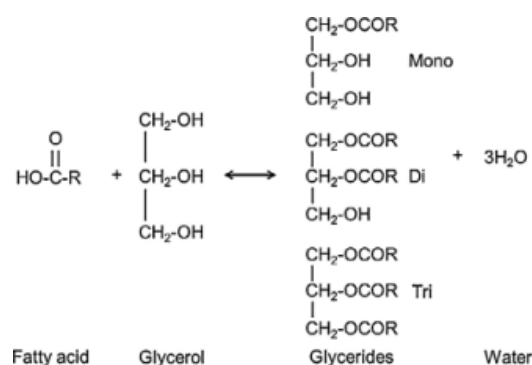


**Fig. 1.** Reaction scheme of the esterification of fatty acids with glycerol to glycerides and water.

Due to the high viscosity of glycerol at room temperature, operating temperatures greater than 130°C are typically needed for glycerol esterification in order to decrease the viscosity and then enhance the contact between immiscible the fatty acids and glycerol. This reaction has been performed a few times previously and the literature results are summarized in **Table 1**. Solid acid catalysts, including zinc (Zn), sulfonic acid fixed on ordered mesoporous silica (HSO<sub>3</sub>SBA-15), double metal cyanide Fe-Zn and solid superacid SO<sub>4</sub><sup>2-</sup>/ZrO<sub>2</sub>-Al<sub>2</sub>O<sub>3</sub> have been used and high conversions have been attained in several hours. In some cases, systems with nitrogen supply are used to remove water, which is product of the reaction, and to shift equilibrium. Selectivities obtained are between 42 and 70%.

Kotwal et al. [8] show the increase of selectivity in monoglycerides with an increase of molar ratio of glycerol to fatty acids, and a decrease of the residence time. The range of temperature studied is 140-230°C.

**Table 1.** Operating conditions for direct esterification with glycerol used in literature. R is the molar ratio of glycerol to fatty acids, w is the mass fraction of catalyst to fatty acids, c is the conversion rate and t is the reaction time.

$R_{\text{Gly/FFA}}$	Catalyst	$w_{\text{cata/FFA}}$ (%)	T (°C)	P (bar)	c (%)	$S_{\text{MG/FFA}}$ (%)	t (h)	Reference
3	NaOH	0.1	180	Fill with N <sub>2</sub>	70-90	42	6	[9]
1.04	Zn	0.2	180-230	N/A	95	N/A	0.8	[10]
2	HSO <sub>3</sub> SBA-15	1-5	140-160	0.68	90	70	5	[7]
1	Fe-Zn	7	200	N/A	95	70	1	[8]
1.4	SO <sub>4</sub> <sup>2-</sup> /ZrO <sub>2</sub> -Al <sub>2</sub> O <sub>3</sub>	0.3	200	0.05	98.4	59	4	[11]

The objective of this work is to compare two different oscillatory flow reactors on a reaction which has a thermodynamic equilibrium and kinetically limited by mass transfer, the esterification reaction of fatty acids with glycerol. Sulfuric acid (H<sub>2</sub>SO<sub>4</sub>) and dodecylbenzene sulfonic acid (DBSA) catalysis have been tested; the latter having shown good performance for the esterification reaction [12] since water is encapsulated in micelles and thereby shifts the equilibrium in the direction of monoglycerides formation. The reactor types studied are the continuous metallic oscillatory baffled reactor (OBR) and the pulsed Helix reactor. The OBR provides sufficiently long residence times, good mixing performance [13] and can easily generate liquid-liquid dispersions [14]. The Helix reactor provides radial mixing in laminar flow conditions, which is ensured by formation of Dean vortices. It also presents a near plug-flow behavior, high heat transfer rates and the absence of internals to ensure mixing limit the fouling or clogging issues. The reaction performance has been compared for different molar ratios of glycerol to fatty acids, operating temperatures, residence times and using two different acid catalysts.

The OBR is compared to a Helix reactor for this mass-transfer limited reaction. The comparison has been made at different molar ratio of glycerol to fatty acids, temperatures, residence times and using two different acid catalysts.

## 2. Materials and methods

### 2.1. Continuous oscillatory baffled reactor (OBR)

The OBR is made of stainless steel, with a 24 mm diameter, composed of two tubes of 1.5 m each connected by a bend. The opening diameter of periodically spaced baffles is 12 mm. The OBR has a total of 80 baffles, and is represented in **Fig. 2**. It has been operated in the horizontal position under pressure in order to attain temperatures up to 150°C. The wide the range of applications of this reactor, usually more specific to polymerization or crystallization operations, to reactions involving viscous reactants, as high temperatures decrease the viscosity of glycerol which could limit the mass transfer in the reactor. In the literature, such a metallic version of OBR has been studied under

atmospheric pressure conditions only [15]. Metallic OBRs are commercially available ([www.nitechsolutions.co.uk](http://www.nitechsolutions.co.uk)).

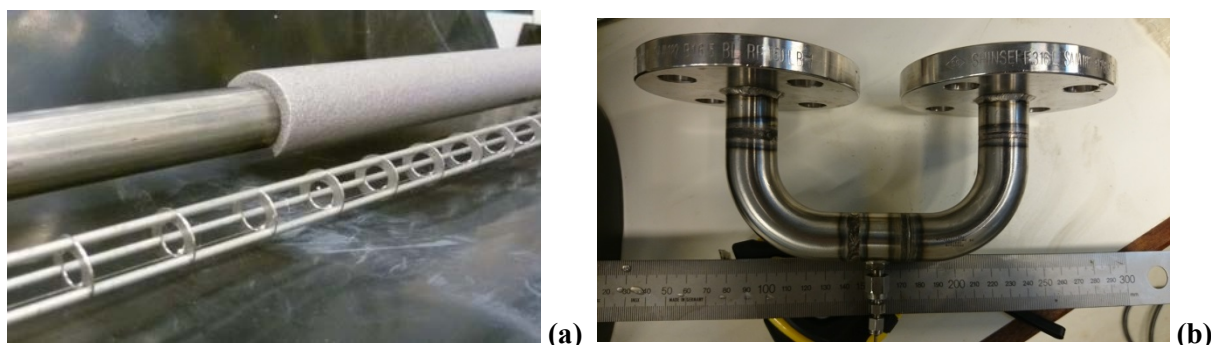


**Fig. 2.** (a) 24 mm diameter OBR with single orifice baffles. Three threads maintain the baffles together. (b) A bend without baffles is used to connect the two tubes of 1.5 m.

## 2.2. Pulsed Helix reactor

The 16 mm diameter Helix reactor of 6 m length, coiled 92 times, is represented in **Fig. 3**. It has been operated with the same operating conditions than the OBR.

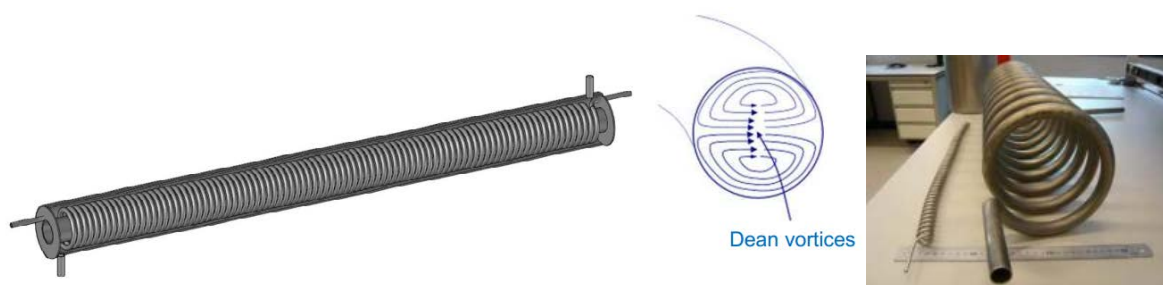


**Fig. 3.** 16 mm diameter Helix reactor. The total length of this coil is 6 m. Mixing is ensured by the formation of Dean vortices.

## 2.3. Experimental rig

The oscillatory motion of the flow occurs in the two compared reactors: a continuous oscillatory baffled reactor (OBR) and a Helix reactor. Both reactors have been insulated with Rockwool to prevent thermal losses. The associated experimental setup to generate an oscillating flow is described in **Fig. 4**. A system including a pulsation dampener filled with nitrogen and a backpressure regulator is used to increase minimal pressure in the reactor. This pressure is necessary to keep compounds in the liquid state. Indeed, the apparition of water during reaction decreases the boiling point of the mixture. Moreover, the oscillation of pressure implies sub-atmospheric pressure, thereby reducing the boiling point of the reactive mixture. A heat exchanger cools the mixture at the after reactor to avoid re-vaporization at the outlet of the backpressure regulator. The maximum temperature used in this work is 150°C, and the maximum pressure admitted is 10 bar. The pump generating the oscillations is a LDELEWA pump oscillating from 0.1 to 10 Hz. Amplitudes and corresponding displaced volumes are given in **Table 2**. The maximum value of oscillations, regarding resistance of the setup to strokes, corresponds to amplitude (A) of 6.5 mm and a frequency (f) of 1.4 Hz.

Net flow range for the OBR and Helix reactor is from 1.7-3.8 L/h, corresponding to net Reynolds numbers of 7-15. In the OBR, for  $A = 88$  mm and  $f = 1$  Hz, the oscillatory flow rate is 900

L/h corresponding to oscillatory Reynolds numbers of 3000. For  $A = 59$  mm and  $f = 1$  Hz, the oscillatory flow rate is 600 L/h corresponding to oscillatory Reynolds number of 2000, and finally, for  $A = 96$  mm and  $f = 1.4$  Hz, the oscillatory flow rate is 1370 L/h and oscillatory Reynolds number is 3000. In the Helix, for  $A = 298$  mm and  $f = 1$  Hz the oscillatory flow rate is 1350 L/h corresponding to oscillatory Reynolds numbers of 5100. For  $A = 198$  mm and  $f = 1$  Hz, the oscillatory flow rate is 900 L/h corresponding to oscillatory Reynolds number of 3400, and finally, for  $A = 298$  mm and  $f = 1.4$  Hz, oscillatory flow rate is 1890 L/h and oscillatory Reynolds number is 7100.

$$\text{Net Reynolds number: } Re_{net} = \frac{\rho v_{net} D}{\mu} \quad \text{Eq. 2.3-1}$$

$$\text{Oscillatory Reynolds number: } Re_o = \frac{2\pi f x_o \rho D}{\mu} \quad \text{Eq. 2.3-2}$$

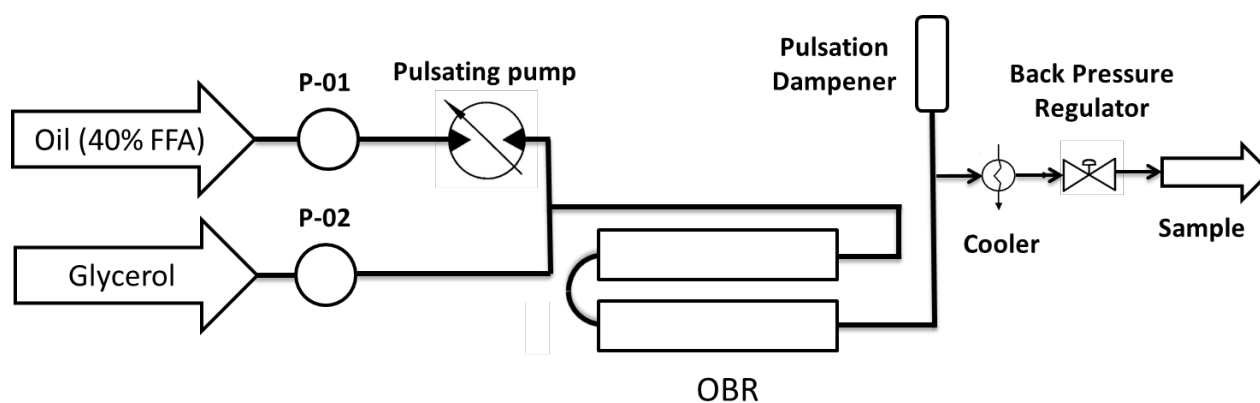


Fig. 4. Experimental setup of the oscillatory baffled reactor generating oscillations, work under pressure and reach temperatures up to 160°C.

Table 2. Amplitude of oscillations and corresponding displaced volume in each reactor. The diameter of the plunger is 92 mm. The oscillatory flow rates are calculated for a frequency of 1 Hz.

<b>Displaced volume (mL)</b>	6.6	13.3	19.9	26.6	33.2	39.9	46.5	53.2	59.8	66.5	199.4
<b>Oscillatory flow rates (L/h)</b>	150	300	450	600	750	900	1050	1200	1350	1500	4510
<b>Amplitude LEWA pump (mm)</b>	1	2	3	4	5	6	7	8	9	10	30
<b>Amplitude OBR (mm)</b>	15	29	44	59	73	88	103	118	132	147	441
<b>Amplitude Helix (mm)</b>	33	66	99	132	165	198	231	264	298	331	992

Two additional runs have been carried out in a conventionally heated and mechanically stirred reactor at 110°C, and in a commercially available Nitech® reactor, with a 15 mm diameter. The description of these two setups is described in our previous work [16].

## 2.2. Products

Waste cooking oil was collected, filtrated at 400  $\mu$  m and then supplied by the company Coreva Technologies (Auch, France). Oil with a 40% level of fatty acids is used in the metallic oscillatory baffled reactor (OBR). It has been characterized (0% water, 0% solid wastes). The profile of the carbon chains is: myristic C14:0 (0.1%), palmitic C16:0 (8.4%), palmitoleic C16:1 (0.1%), stearic C18:0 (3.9%), oleic C18:1 (31.9%), linoleic C18:2 (54.8%), arachidic C20:0 (0.3%), gadoleic C20:1 (0.2%), behenic C22:0 (0.4%). Oil with 40% level of fatty acids is used in the Helix reactor. It has been characterized (0% water, 0% solid wastes). The profile of the carbon chains is: palmitic C16:0 (4.3%), stearic C18:0 (2.4%), oleic C18:1 (87.1%), linoleic C18:2 (6.2%). Cyclohexane



(analytical grade) and was supplied by VWR, France. Sulfuric acid (96%), glycerol (BioXtra, >99%), ethanol (absolute, 99.9%) and dodecylbenzenesulfonic acid (DBSA) were supplied by Fisher, Belgium. Phenolphthalein and KOH-ethanol solution (0.1M) were supplied by Sigma-Aldrich, France. Methylimidazole (MI) was supplied by Alfa Aesar. N-méthyl-N-triméthylsilyl-heptafluorobutyramide (MSHFBA) was supplied by Marcherey-Nagel.

### 2.3. Characterization

The composition of oil produced from the esterification with glycerol reaction was characterized by gas chromatography (GC) using a Perkin Elmer Instrument based on the EN-14103 method. The chromatograph is equipped with a flame ionization detector (FID). The column used was Restek (CP-Sil 8 Rtx-5: 5% diphenyl, 95% dimethylpolysiloxane) 15 m x 0.32 mm x 0.25  $\mu\text{m}$ . The injection is "on-column" because the di- and triglycerides are not vaporized in the injector and are injected as liquids in the column. One internal standard (heptadecane) and six reference materials (triolein, monoolein, diolein, triolein, oleic acid, methyl oleate) supplied by Sigma-Aldrich were used for the GC calibration. The samples are diluted in cyclohexane. The operating conditions used for the oven were 55°C for 30 seconds, 45°C/min to 80°C, 10°C/min to 360°C and hold for 11 min. The carrier gas was helium at a constant pressure at the top of the column of 15 psi. The hydrogen flow was kept at 45 mL/min and the air flow was kept at 450 mL/min. The hydroxylated compounds (fatty acids, mono-, di- and triglycerides) are silylated by a mixture of N-méthyl-N-triméthylsilyl-heptafluorobutyramide (MSHFBA) and methylimidazole (MI). This reaction increases the volatility and the stability of injected hydroxylated compounds to enhance their detection. Composition of samples is determined with the internal standard method, mass fractions of mono-, di-, triglycerides are determined, then selectivities in monoglycerides are deduced.

The fatty acid level is determined by titration with a 0.1 N KOH-ethanol solution with phenolphthalein as colored indicator, based on the ISO 660 norm. The sample (about 1 mL) is diluted in ethanol (about 30 mL). The percentage of acidity  $A_c$  is given by the relationship:  $A_c = (V_{eq} \cdot M_{C18} \cdot C_{KOH}) / m_{oil}$ , where  $V_{eq}$  is the volume at the equivalence point,  $M_{C18}$  the molar mass of fatty acids,  $C_{KOH}$  the concentration of the KOH-ethanol solution and  $m_{oil}$  is the mass of oil of the sample. The percent conversion is given by the relationship:  $X = (A_{c_{initial}} - A_{c_{final}}) / A_{c_{initial}}$ .

## 3. Results and discussion

### 3.1. Repeatability study

In each reactor, the esterification reaction with glycerol was performed three times using the same operating conditions: a molar ratio of glycerol to fatty acids of 6, a molar fraction of catalyst to fatty acids of 0.11, a residence time of 22 min, temperature fixed at 150°C, and oscillation amplitude and frequency equal to 6 mm and 1 Hz, respectively. The results are given in **Table 3**. Reaction conversion and selectivities varies very little between experiments in each reactor and the standard deviations are small. The experiments are therefore considered repeatable, considering the intervals of confidence given for conversions and selectivities in OBR and Helix reactor.

**Table 3.** Conversion for the esterification reaction repeated 3 times with identical operating conditions ( $R = 6 (\pm 0.6)$ ,  $x = 0.1 (\pm 0.02)$ ,  $t = 22$  min ( $\pm 0.6$ ),  $T = 150^\circ\text{C}$ ,  $f = 1$  Hz,  $A = 6$  mm) in each reactor.

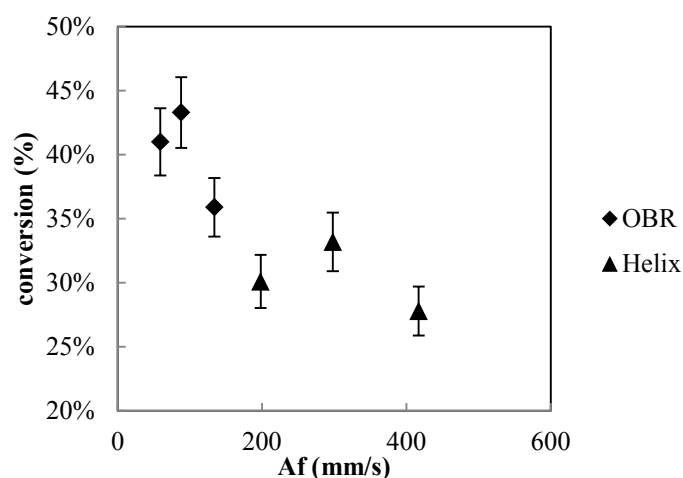
OBR						Helix reactor						
R (-)	x (%)	t (min)	c (%)	$S_{\text{MG/FFA}}$ (%)	$S_{\text{DG/FFA}}$ (%)	R (-)	x (%)	t (min)	c (%)	$S_{\text{MG/FFA}}$ (%)	$S_{\text{DG/FFA}}$ (%)	
6.7	0.081	21.7	41.0	87	13	6.7	0.111	21.7	31.5	84	16	
5.9	0.119	22.8	43.3	88	12	5.9	0.119	22.8	30.1	82	18	
5.6	0.105	22.6	43.8	84	16	5.6	0.116	22.6	33.2	89	12	
<b>Average (%)</b>	6.1	0.102	22.4	42.7	86	14	6.1	0.115	22.4	31.6	85	15
<b>Standard deviation (%)</b>	0.6	0.019	0.6	1.5	2.1		0.6	0.004	0.6	1.6	3.7	

### 3.2. Influence of oscillatory conditions

The effect of oscillatory conditions has been investigated by testing three values of the amplitude and two values of the frequency, thereby changing the amplitude-frequency product ( $Af$ ). The results obtained for both reactors are given in **Table 4** and **Fig. 5**. The best conversion in each reactor is obtained with an amplitude of 88 mm and a frequency of 1 Hz for the OBR and with an amplitude of 298 mm and a frequency of 1 Hz for the Helix reactor; these conditions have therefore been kept for the following experiments. The selectivities of monoglycerides are in the same range, between 80 and 90%.

**Table 4.** Influence of conditions of oscillations at  $150^\circ\text{C}$ , with a molar ratio of  $5.5 (\pm 0.5)$ , a residence time of  $22.5$  min ( $\pm 1$  min).

Reactor	R products	x (mol cata/mol FFA)	T ( $^\circ\text{C}$ )	t (min)	A (mm)	f (Hz)	$Af$ (mm/s)	c (%)	$S_{\text{MG/FFA}}$ (%)
OBR	5.9	0.12	150	22.8	59	1	59	41.0	91
OBR	5.6	0.12	150	22.6	88	1	88	43.3	85
OBR	5.4	0.10	150	22.0	96	1.4	134	35.9	82
Helix	5.9	0.12	150	22.8	198	1	198	30.1	82
Helix	5.6	0.12	150	22.6	298	1	298	33.2	89
Helix	5.4	0.10	150	22.0	298	1.4	417	27.8	90


**Fig. 5.** Influence of amplitude-frequency product on the conversion of fatty acids in the OBR and in the Helix reactor.

### 3.3. Influence of the molar ratio and temperature on the reaction catalyzed with sulfuric acid in the OBR

The effects of the glycerol to fatty acids molar ratio,  $R$ , and of temperature on the esterification reaction catalyzed with sulfuric acid in the OBR have been investigated and the results are summarized in **Table 5** and represented on the **Fig. 6** synthesizing the results of section 3.3, 3.4, 3.5 and 3.6. An increase in the molar ratio at a fixed temperature and residence times ( $22 \text{ min} \pm 2 \text{ min}$ ) in presence of sulfuric acid leads to an increase in reaction conversion. At  $130^\circ\text{C}$ , conversion increases from 5.4% to 23.2% when the molar ratio increases from 1.5 to 14.2. At  $150^\circ\text{C}$ , conversion increases from 43.3% to 50.2% when the molar ratio increases from 5.6 to 13.4. The increase in the molar ratio at a fixed temperature seems to shift the reaction equilibrium slightly, but not sufficiently to reach high conversions. By increasing the temperature, the thermodynamic equilibrium of the reaction is more easily reached. Increasing the temperature up to about  $150^\circ\text{C}$  enhances reaction conversion, however with further increase in temperature the conversion remains constant around 47%. The reaction is therefore not limited by reaction kinetics but by the thermodynamic equilibrium. Good selectivities are obtained at  $150^\circ\text{C}$ , in the range of 85-88%. A slight increase of the selectivity is obtained with an increase of the molar ratio. A slight decrease of the selectivity is obtained if temperature is increased from  $150$  to  $160^\circ\text{C}$ . The selectivities associated to conversions inferior to 20% have not been calculated due to too high uncertainties.

**Table 5.** Reaction conversion for esterification with glycerol reaction at different temperatures and molar ratio of glycerol to fatty acid in the OBR.

R (-)	X (mol cata/ mol FFA)	T ( $^\circ\text{C}$ )	t (min)	A (mm)	f (Hz)	c (%)	S <sub>MG/FFA</sub> (%)
5.4	0.22	100	22.0	6	1	9.9	/
1.5	0.06	130	23.7	6	1	5.4	/
2.5	0.10	130	22.4	6	1	13.7	/
14.2	0.10	130	22.4	6	1	23.2	91
5.6	0.12	150	22.6	6	1	43.3	85
6.7	0.11	150	21.7	6	1	43.8	88
8.9	0.10	150	21.5	6	1	46.6	88
13.4	0.09	150	24	6	1	50.2	88
8.7	0.11	160	21.4	6	1	47.6	85

### 3.4. Influence of residence time

In order to determine if the reaction is complete at the outlet of the reactor, the total flow rate has been decreased such that residence time is increased by a factor 2, i.e. from  $22 \text{ min} (\pm 2 \text{ min})$  to  $48 \text{ min} (\pm 1 \text{ min})$ . Reaction conversions are given in **Table 5** and represented on the **Fig. 6** synthesizing the results of section 3.3, 3.4, 3.5 and 3.6. It can be seen that conversion remains constant after an increase of residence time, indicating the thermodynamic equilibrium is reached. The selectivity of monoglycerides slightly decreases, from 88% to 81% in the OBR and from 92% to 78% in the Helix reactor, with the increase of the residence time, which is in agreement with the results previously found in literature [8].

**Table 6.** Conversion for esterification with glycerol reaction at different residence times in the OBR and Helix reactor.

Reactor	Catalyst	R (-)	x (mol cata/ mol FFA)	T (°C)	t (min)	A (mm)	f (Hz)	c (%)	S <sub>MG/FFA</sub> (%)
OBR	H <sub>2</sub> SO <sub>4</sub>	6.7	0.11	150	21.7	6	1	43.8	88
OBR	H <sub>2</sub> SO <sub>4</sub>	7.0	0.05	150	48.5	6	1	43.8	81
Helix	H <sub>2</sub> SO <sub>4</sub>	13.4	0.11	150	22	6	1	37.1	92
Helix	H <sub>2</sub> SO <sub>4</sub>	9.3	0.06	150	47	6	1	36.1	78

### 3.5. Influence of molar ratio R and temperature on the glycerol esterification catalyzed with DBSA

The previous reaction results obtained using the sulfuric acid catalyst show that the reaction is limited by thermodynamics, due to the increasing presence of reaction products forming in the reactive mixture. The DBSA catalyst also acts as a surfactant and generates the formation of reverse micelles, which encapsulate water (reaction product) and thereby should shift the reaction towards the formation of mono, di and triglycerides [12]. **Table 7** shows the conversions obtained using the DBSA catalyst in both reactor types. These results can be found **Fig. 6**. Compared with the previous results obtained with the sulfuric acid catalyst, reaction conversion is increased from 43.8% to 72.9% in the OBR and from 31.6% to 87% in the Helix reactor. The physico-chemical properties of the catalyst are therefore extremely important for the reaction performance. It is interesting to note that higher conversion is achieved in the Helix reactor using DBSA compared with the OBR; this is the opposite of what was observed with sulfuric acid catalyst. Lower selectivities are obtained with this catalyst, from 88% to 67% for the OBR, and from 84% to 66% for the Helix reactor.

**Table 7.** Results obtained for esterification with glycerol with DBSA in the two reactors.

Reactor	Catalyst	R (-)	x (mol cata/ mol FFA)	T (°C)	t (min)	A (mm)	f (Hz)	c (%)	S <sub>MG/FFA</sub> (%)
OBR	DBSA	7.8	0.06	150	23.4	6	1	72.9	67
OBR	H <sub>2</sub> SO <sub>4</sub>	6.7	0.11	150	21.7	6	1	43.8	88
Helix	DBSA	7.8	0.06	150	22	9	1	87.0	66
Helix	H <sub>2</sub> SO <sub>4</sub>	6.7	0.11	150	21.7	9	1	30.1	84

### 3.6. Influence of the reactor technology

The results obtained involving the two reactors, OBR and Helix reactor, are summarized in **Table 8** and **Fig. 6**. They are also compared with the results obtained in a glass Nitech® reactor and a conventionally stirred and heated batch reactor. For same range of conditions, i.e. at a temperature of 100°C for the OBR and 110°C for the batch reactor, the conversions are greater in the OBR by a factor of two. This higher performance in oscillatory baffled reactor was obtained at lower temperature, as the Nitech® reactor at 60°C gives similar conversions to the batch reactor at 110°C. The evolution of conversion as a function of the molar ratio at fixed temperature shows the same trends for both the OBR and Helix reactors, i.e. conversion increases with increasing molar ratio. However, higher conversion is obtained in the OBR (43.8-50.2%) compared with the Helix reactor (31.6-37.1%). A two-pass run in the OBR was also tested. This consists in collecting the product at the outlet, separating the two phases, then re-injecting the oleic phase as a reactant. This operating mode allows significantly higher conversion to be achieved, increasing from 50.2% for a single pass to 86.6% for

two passes. Although it requires two additional steps – decantation and reaction, a continuous process is still possible if the oleic phase is withdrawn at the top of the decanter. High selectivities have been obtained in OBR and Helix reactor, between 80 and 90% if catalyzed with sulfuric acid and 66% if catalyzed with DBSA, for an initial level of FFA of 40%. This is higher than selectivities obtained in the literature which were between 42 and 70%, but which were obtained with only fatty acids as starting material.

**Table 8.** Conversion and selectivity for esterification with glycerol with different in the OBR and Helix reactors.

Reactor	Catalyst	R (-)	x (mol cata/ mol FFA)	T (°C)	t (min)	A (mm)	f (Hz)	c (%)	S <sub>MG/FFA</sub> (%)
OBR	H <sub>2</sub> SO <sub>4</sub>	5.4	0.22	100	22.0	6	1	9.9	-
OBR	H <sub>2</sub> SO <sub>4</sub>	5.6	0.12	150	22.6	6	1	43.3	85
OBR	H <sub>2</sub> SO <sub>4</sub>	6.7	0.11	150	21.7	6	1	43.8	88
OBR	H <sub>2</sub> SO <sub>4</sub>	8.9	0.10	150	21.5	6	1	46.6	88
OBR	H <sub>2</sub> SO <sub>4</sub>	13.4	0.11	150	24	6	1	50.2	88
OBR	DBSA	7.8	0.06	150	23.4	6	1	72.9	67
OBR + intermediary decantation	H <sub>2</sub> SO <sub>4</sub>	12.8	0.09	150	23.7 1 <sup>st</sup> pass 29.8 2 <sup>nd</sup> pass	6	1	1 <sup>st</sup> pass: 50.2 2 <sup>nd</sup> pass: 75.3 Overall: 86.6	1 <sup>st</sup> pass: 87 Overall: 53
Helix	H <sub>2</sub> SO <sub>4</sub>	6.7	0.11	150	21.7	9	1	30.1	84
Helix	H <sub>2</sub> SO <sub>4</sub>	9.3	0.06	150	47	9	1	36.1	78
Helix	H <sub>2</sub> SO <sub>4</sub>	13.4	0.11	150	22	9	1	37.1	92
Helix	DBSA	7.8	0.06	150	22	9	1	87.0	66
Batch	H <sub>2</sub> SO <sub>4</sub>	2.85	0.22	110	30	/	/	5.5	/
<b>Nitech</b>	H <sub>2</sub> SO <sub>4</sub>	2.85	0.22	60	20	16.5	1.05	5.9	/

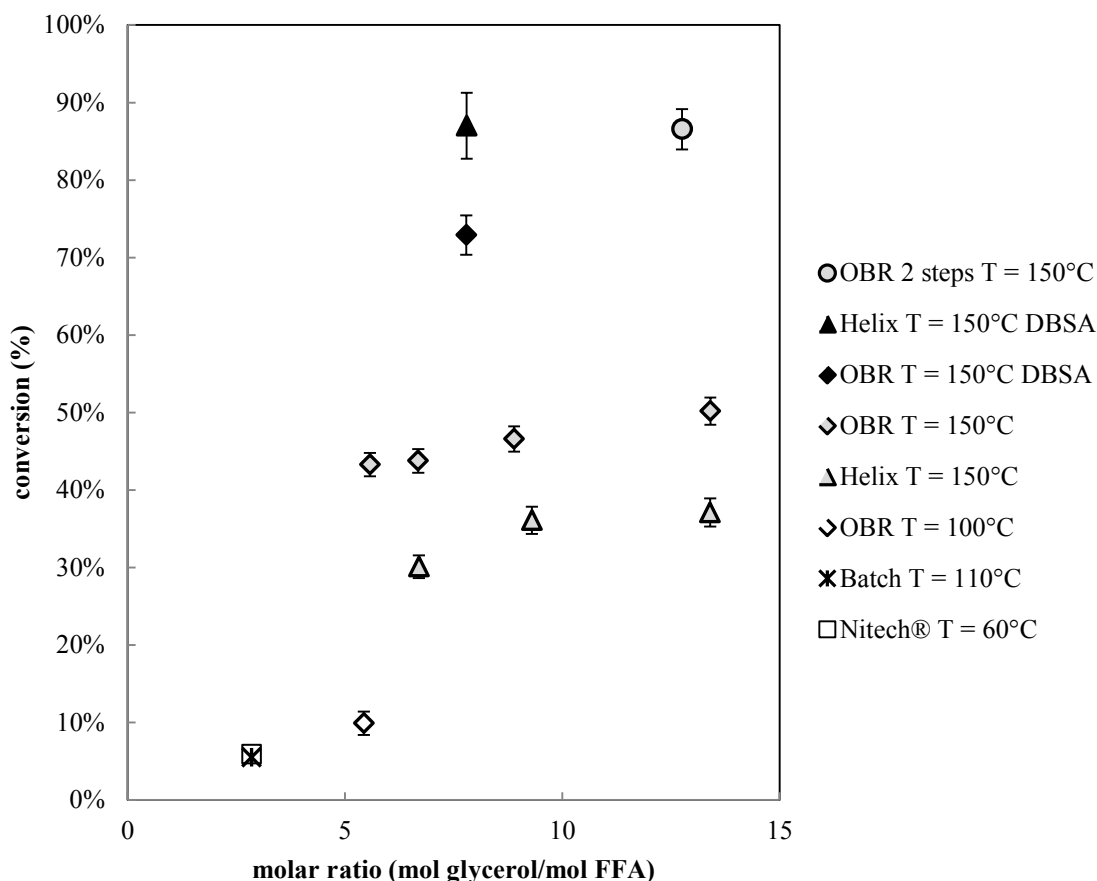


**Fig. 6.** Molar ratio of glycerol to fatty acids influence on conversions of esterification reaction with glycerol. Triangles represent the results obtained in the Helix reactor, diamonds represent the results obtained in the OBR, the circle represents the OBR with 2 steps, the square represents the results obtained in the Nitech® reactor, the cross represents the results obtained in the conventional batch reactor. Empty symbols corresponds to mild temperature (60-100°C), grey symbols corresponds to T = 150 °C and full symbols corresponds to results obtained with DBSA.

#### 4. Conclusions

The use of oscillatory flow under pressure and at high temperatures in the OBR and Helix reactor allows typically viscous reactants used in esterification of fatty acids present in WCO with glycerol to be handled in better conditions, and allows significantly higher reaction conversion to be achieved than in reactors operated at lower temperature. This pilot-scale reactor has a range of net flow rates of 1.7-3.8 L/h. The range of temperature, 130-160°C, and residence time, 20-50 min, is inferior to these used in literature, 140-230°C and 1-6h, but nevertheless sufficient to not be limited by kinetics. Indeed, the glycerol esterification reaction has a thermodynamic equilibrium, which can be shifted by increasing the molar ratio of reactants, however this increases conversion and selectivities only slightly (from 43% to 50% conversion and from 85% to 88% of selectivity for an increase in the molar ratio from 5.6 to 13.4). It has been shown that this thermodynamic limit is achieved since an increase in residence time by a factor of two at 160°C does not increase conversion, and even reduce slightly the selectivity of monoglycerides. The thermodynamic equilibrium can also be shifted by removal of one of the products. DBSA is a catalyst with surfactant properties, which enable water to be encapsulated, thereby shifting the reaction equilibrium and promoting product formation. Using DBSA as a catalyst has resulted in significant increases in conversion compared with sulfuric acid

catalyst, going from 47.6% to 72.9% in the OBR and from 36.1% to 87.0% in the Helix reactor, but selectivities are reduced by 10%. Another solution to increase reaction conversion is to carry out an intermediary decantation step, whereby the water phase is removed. This enables the overall conversion to reach 86.6% but this decreases the selectivities, and for selectivities to reach 87% after the 1st step, but only an overall selectivity of 53%. Reaction conversion is typically higher in the OBR than in the Helix reactor. This may be explained by the generation of smaller droplets and higher interfacial area due to high shear rates induced by the baffles. The higher conversion obtained in the Helix reactor with DBSA catalyst compared with that obtained in the OBR is difficult to explain but might be linked to the stability of micelles at the liquid-liquid interface. For both reactors, selectivities in monoglycerides are between 80 and 90% with sulfuric acid, which are superior to the selectivities obtained in the literature data (max. 70%), and equals to 66-67% with DBSA. This is a promising result for a monoglyceride production objective, but the starting material is oil containing 40% of free fatty acids, which leads to a small fraction of monoglycerides even with complete conversions. Higher production of monoglycerides may be obtained using only fatty acids as a reactant. As a general conclusion, this work has shown that for the glycerol esterification reaction both the OBR and oscillatory Helix reactor allow significantly higher conversions to be achieved compared with that obtained in conventional batch reactors or the commercially available Nitech® glass reactor at lower temperatures. This flexibility of operating at higher temperatures and pressures widens the range of applications of the oscillatory flow reactors, with or without baffles, to reactions involving viscous and immiscible reactants.

### **Acknowledgments**

This work is the result of an international collaboration between INP Toulouse and TNO Delft, who has provided the experimental facilities and technical support. The authors acknowledge INP Toulouse for international mobility funding, as well as the Réseau Franco-Néerlandais, who provided EOLE scholarship to A.M. This work is also part of the AGRIBTP project on bio-products for building and public works that is funded by the European Union, région Midi-Pyrénées and the French Government.

## References

- [1] “www.tno.nl.” [Online]. Available: www.tno.nl.
- [2] J. O. Metzger, “Fats and oils as renewable feedstock for chemistry,” *Eur. J. Lipid Sci. Technol.*, vol. 111, no. 9, pp. 865–876, Sep. 2009.
- [3] M. M. Gui, K. T. Lee, and S. Bhatia, “Feasibility of edible oil vs. non-edible oil vs. waste edible oil as biodiesel feedstock,” *Energy*, vol. 33, no. 11, pp. 1646–1653, Nov. 2008.
- [4] Y. Zhang, M. . Dubé, D. . McLean, and M. Kates, “Biodiesel production from waste cooking oil: 2. Economic assessment and sensitivity analysis,” *Bioresour. Technol.*, vol. 90, no. 3, pp. 229–240, Dec. 2003.
- [5] A. Banerjee and R. Chakraborty, “Parametric sensitivity in transesterification of waste cooking oil for biodiesel production—A review,” *Resour. Conserv. Recycl.*, vol. 53, no. 9, pp. 490–497, Jul. 2009.
- [6] A. Mazubert, M. Poux, and J. Aubin, “Intensified processes for FAME production from waste cooking oil: A technological review,” *Chem. Eng. J.*, vol. 233, pp. 201–223, Nov. 2013.
- [7] L. Hermida, A. Z. Abdullah, and A. R. Mohamed, “Synthesis of monoglyceride through glycerol esterification with lauric acid over propyl sulfonic acid post-synthesis functionalized SBA-15 mesoporous catalyst,” *Chem. Eng. J.*, vol. 174, no. 2–3, pp. 668–676, Nov. 2011.
- [8] M. Kotwal, S. S. Deshpande, and D. Srinivas, “Esterification of fatty acids with glycerol over Fe–Zn double-metal cyanide catalyst,” *Catal. Commun.*, vol. 12, no. 14, pp. 1302–1306, Aug. 2011.
- [9] R. B. R. Choudhury, “The preparation and purification of monoglycerides. II. Direct esterification of fatty acids with glycerol,” *J. Am. Oil Chem. Soc.*, vol. 39, no. 8, pp. 345–347, 1962.
- [10] P. Felizardo, J. Machado, D. Vergueiro, M. J. N. Correia, J. P. Gomes, and J. M. Bordado, “Study on the glycerolysis reaction of high free fatty acid oils for use as biodiesel feedstock,” *Fuel Process. Technol.*, vol. 92, no. 6, pp. 1225–1229, Jun. 2011.
- [11] Y. Wang, S. Ma, L. Wang, S. Tang, W. W. Riley, and M. J. T. Reaney, “Solid superacid catalyzed glycerol esterification of free fatty acids in waste cooking oil for biodiesel production,” *Eur. J. Lipid Sci. Technol.*, vol. 114, no. 3, pp. 315–324, Mar. 2012.
- [12] L. Gang, L. Xinzong, and W. Eli, “Solvent-free esterification catalyzed by surfactant-combined catalysts at room temperature,” *New J. Chem.*, vol. 31, no. 3, p. 348, 2007.
- [13] A. P. Harvey, M. R. Mackley, and P. Stonestreet, “Operation and Optimization of an Oscillatory Flow Continuous Reactor,” *Ind. Eng. Chem. Res.*, vol. 40, no. 23, pp. 5371–5377, Nov. 2001.
- [14] E. Lobry, T. Lasuye, C. Gourdon, and C. Xuereb, “Liquid–liquid dispersion in a continuous oscillatory baffled reactor – Application to suspension polymerization,” *Chem. Eng. J.*, vol. 259, pp. 505–518, Jan. 2015.
- [15] M. Y. Koh, T. I. Mohd. Ghazi, and A. Idris, “Synthesis of palm based biolubricant in an oscillatory flow reactor (OFR),” *Ind. Crops Prod.*, vol. 52, pp. 567–574, Jan. 2014.
- [16] A. Mazubert, J. Aubin, S. Elgue, and M. Poux, “Intensification of waste cooking oil transformation by transesterification and esterification reactions in oscillatory baffled and microstructured reactors for biodiesel production,” *Green Process. Synth.*, 2014.



# Chapter 2

## Characterization of oscillatory baffled reactor

---

**Contents**

1. Introduction .....	124
2. State of the art.....	124
2.1. Key design parameters .....	125
2.1.1. Diameter of the tube .....	125
2.1.2. Baffle design.....	126
2.1.3. Net Reynolds number .....	127
2.1.4. Oscillatory Reynolds number .....	128
2.1.5. Velocity ratio .....	128
2.1.6. Strouhal number .....	128
2.1.7. Nusselt number .....	129
2.2. Performance characterization .....	129
2.2.1. Pressure drop .....	129
2.2.2. Heat transfer .....	130
2.2.3. Two phase flow .....	130
2.2.4. Instantaneous velocities.....	131
2.2.5. Axial dispersion coefficient.....	132
2.3. Conclusions of the state of the art .....	136
3. Experimental measure of velocity vectors by PIV (Particle Image Velocimetry) .....	137
3.1. Material and methods .....	137
3.2. Results .....	139
3.2.1. Velocity fields .....	139
3.2.2. Eddy formation.....	144
3.2.3. Strain rate .....	149
3.3. Conclusion.....	150
4. Numerical simulations using Computational Fluid Dynamics (CFD) .....	152
4.1. Material and methods .....	152
4.1.1. Geometry and Mesh .....	152
4.1.2. Numerical methods.....	154
4.2. Validation of the method .....	157
4.2.1. Influence of the size of the mesh .....	157
4.2.2. Influence of number of particles.....	161
4.2.3. Length of the tube and parameters for particle injection.....	161
4.2.4. Comparison of the velocity fields obtained by CFD and by PIV .....	163
4.3. Results .....	165
4.3.1. Velocity fields .....	165

4.3.2. Axial dispersion coefficient.....	168
4.3.3. Fluid strain rate.....	171
4.3.4. Distance separating of pairs of initially adjacent particles.....	173
4.4. Conclusions.....	174
5. Sizing of an industrial scale OBR.....	176
6. Conclusions.....	179
References.....	180
Conclusions of Part III.....	185

## 1. Introduction

In the previous chapter (Part III, Chapter 1) it was demonstrated that problems associated with the generation of localized low pressure zones in the continuous oscillatory baffled reactor, such as reactant boiling and the dampening of oscillations, may be overcome by using a more resistant stainless steel reactor, which allows higher operating pressure and temperature. Indeed, this has shown to provide higher reaction conversions than those possible in the initial glass reactor. Nevertheless, the underlying hydrodynamic phenomena occurring in these reactors are still not entirely understood. This chapter focuses on the characterization of the mixing and flow in the oscillatory baffled reactor. To carry out this investigation, the state of the art on flow on continuous oscillatory baffled reactors has been reviewed. CFD simulations have then been carried out to develop indicators to characterize the hydrodynamic performance of the reactor, to determine the best process conditions and then to improve the baffle design. Finally, a short experimental campaign using Particle Image Velocimetry has been conducted to measure velocity fields and corroborate the results obtained in simulation.

## 2. State of the art

Continuous oscillatory baffled reactors (OBR) are tubular reactors equipped with periodically spaced baffles and operate with an oscillating flow rate. Typical tube diameters range from 12 to 800 mm and can be placed horizontally or vertically bend connections (see **Fig 2-1**). Reactants flow through the reactor with a net flow like in a conventional plug flow reactor, but an oscillatory flow is also superimposed to this net flow. The combination of the periodically spaced baffles and the periodic oscillating flow causes unsteadiness in the laminar flow. The mixing in the reactor is then due to vortex shedding when the oscillating flow rate is in the direction of the net flow and when the flow is reversed, where the liquid passes around the vortices and flows near the walls in opposite direction (see **Fig. 2-2**). Unlike streamline laminar flow, mixing is greatly enhanced in OBRs since radial and axial velocities are generated.

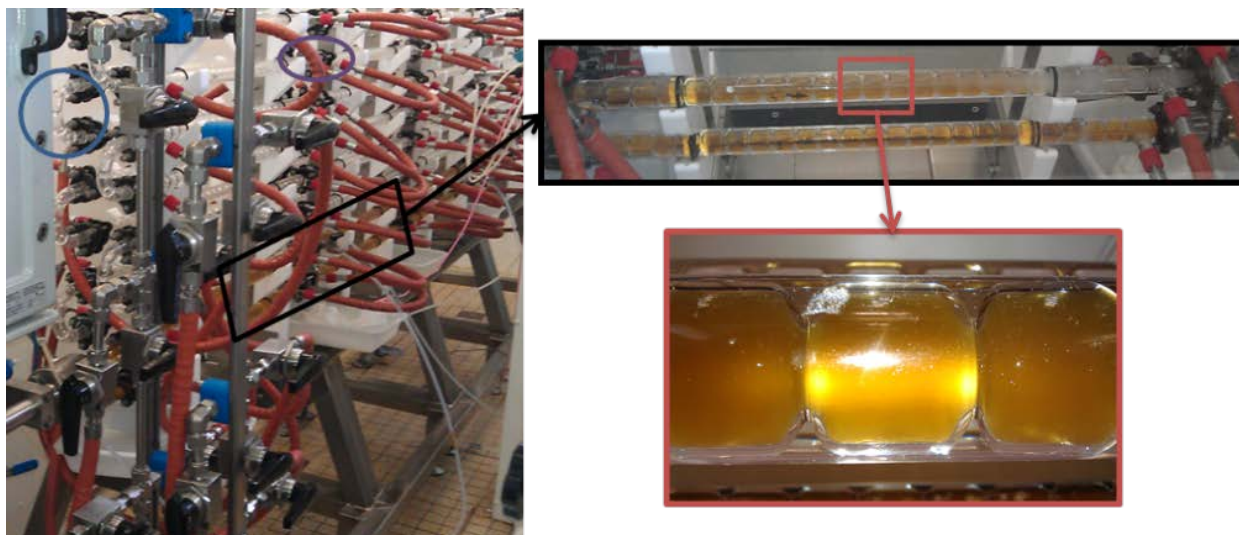


**Fig. 2-1.** Nitech® reactor previously tested in the Part II, Chapter 2. The blue circle shows a bend connection with baffles, and the purple circle shows the position of a straight connection. A tube is composed of periodically-spaced baffles (dark and red frames).

The OBR technology is inspired from pulsed columns created for liquid-liquid extraction. The first patent for pulsed columns was published by Van Dijk in 1935 and describes a vertical column equipped with an oscillating perforated sieve plate or with immobile internals. Later it was shown that solvent extraction could be enhanced by the oscillation of flow in a sieve plate column [1] or with the use of disc and doughnut internals [2]. At the end of the 80's, the concept of using pulsed columns as

horizontal tubular reactors was investigated [3]–[5]. The oscillatory baffled reactors can be placed in any position, horizontal or vertical depending on the application. In the 90's, studies confirmed the capacity of both baffle designs to perform good mixing [6]. This reactor technology has been studied for a wide range of applications, such as crystallization [7], polymerization [8], biodiesel production [9], bioprocesses [10], and has proven to give good results in terms of mixing, heat transfer, cooling rate, mass transfer, reaction, suspension of particles and axial dispersion [11]. Today the OBR technology is protected by several patents on the oscillatory motion (WO 0 60412, WO 057 661), baffles (sharp edged or helical stripe or strake) (US 4832500), reactor design (EP 107 6597), heterogeneous catalysis applications (US 5439991) or online separation (GB0706908).

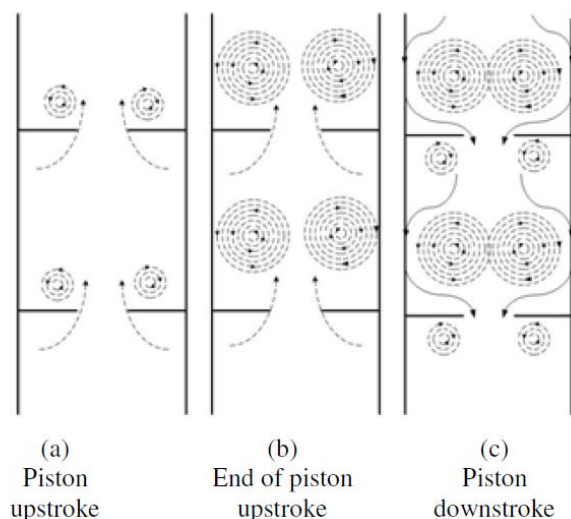


Fig. 2-2. Eddies shedding in baffled column [12]

To characterize oscillatory flow reactors, key design parameters are presented, with the corresponding recommendations from literature. The influence of these parameters has been studied on hydrodynamics. This state of the art is the basis of the development of characterization tools.

## 2.1. Key design parameters

### 2.1.1. Diameter of the tube

The choice of the diameter of the tube is often dependent of the targeted production rate [13]. From **Table 2-1**, it can be seen that with tube diameters in the range of 24-50 mm, it is possible to reach flow rates in the range of 7-100 L/h, which corresponds to net Reynolds numbers (see **Eq. 2.1.3-1**) up to 3000. These flow rates are suitable for industrial production in fine and specialty chemicals, pharmaceutical industries. In comparison, the 15 mm diameter Nitech® reactor (used in Part II, Chapter 2 and Chapter 3) is able to reach flow rates from 2.4 to 6 L/h, which corresponds to net Reynolds numbers (see **Eq. 2.1.3-1**) from 60 to 140 for a fluid with the same density and viscosity as water.

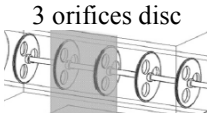
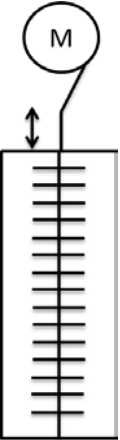
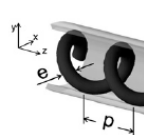
**Table 2-1.** Range of experimental conditions used for experiments on OBR. The net flow rate is  $F_{\text{net}}$ , the net Reynolds number is  $Re_{\text{net}}$ , the amplitude and frequency of oscillations are  $A$  and  $f$  and the diameter is  $D$ .

$F_{\text{net}}$ (L/h)	$Re_{\text{net}}$ (-)	$A$ (mm)	$f$ (Hz)	$D$ (mm)	Reference
10	40-130	5-25	0.2-5	39.6	[14]
7.2	0-3000	0-8	0.1-20	24	
7.2	0-2000	0-25	0.05-10	54	[15]
43.2	0-3000	0-60	0.01-10	150	
30-114	250-1000	0-15	0-3	40	[16]

### 2.1.2. Baffle design

The most common baffle design is an equally-spaced and sharp-edged single orifice baffle. For this baffle type, the spacing between baffles ( $L/D$ ) is typically fixed at 1.5 [17] and the baffle opening ratio (which equals to the ratio of the opening section out of the section of the tube :  $D_0^2/D^2$ ) is generally in the range of 0.2-0.4 [18], but is usually set at 0.25, which corresponds to  $D_0 = 0.5D$  [19]. Baffle thickness,  $e$ , is generally fixed at  $e/D = 1/25$  [15]. Other baffle designs have also been studied in the literature and are summarized in **Table 2-2**. Perforated plates have been employed to deal with an increase in the column diameter [14], [15]. They show similar axial dispersion with those of single orifice baffles for a same diameter [15]. Baffles with three orifices have also been studied in a horizontal column, leading to the formation and the propagation of three bidirectional eddies [20]. Finally, a study has been conducted using two immiscible liquids (oil and methanol) in a reciprocating plate column with perforated baffles to correlate droplet size with oscillatory conditions [21]. More recently, helicoidally-shaped baffle designs has been studied [18], [22]. These are easy to insert in columns and a plug flow behavior maintained for a wider range of oscillatory conditions. For this type of baffle, geometric parameters are similar as those used with single orifice baffles as the pitch to diameter ratio is fixed at 1.5 and the diameter the helical coil is 1.2 mm, which corresponds to an opening section ratio of 23%. These geometric parameters are used in the work of Solano et al. [22] and have shown good performance in terms of plug-flow behavior [18].

**Table 2-2.** Description of experimental set-ups using different baffle designs. V/H indicates if the column is in the horizontal (H) or vertical (V) position.

	V/H	Design	D (mm)	e (mm)	L/D (-)	Reference
<b>Single or multiperforated plates</b>	V	Single orifice plate and multi-orifice plate (37 x 12 mm)	24, 54 and 150 mm	1, 2 and 6	1.5	[15]
	H	 <p>3 orifices disc 3 orifices of 17mm diameter Total diameter: 60 mm</p>		3.25	0.875	[20]
	V	Perforated plates 39 orifices of 3 mm of diameter	39.6 mm	-	0.63 1.26 2.53	[14]
	V	Reciprocating plate column (the reactor is static, the multi-orifice baffles oscillate) 	Reactor diameter : 25.4 mm Plate diameter : 25 mm Orifice diameter : 6 mm	1	1	[21]
<b>Helicoid</b>	V or H	Helicoid e = 1.2 mm p = 7.5 mm 	5 mm	1.2	1.5	[22]

### 2.1.3. Net Reynolds number

The net Reynolds number is a dimensionless number, which compares inertial and viscous effects, is defined as following:

$$\text{Net Reynolds number: } Re_{net} = \frac{\rho v D}{\mu} \quad \text{Eq. 2.1.3-1}$$

where  $\rho$  and  $\mu$  the density and viscosity of the fluid,  $v$  the net velocity and  $D$  the diameter of the tube.

In OBRs, the recommended minimum value of the net Reynolds number to achieve convection is 50 [13].

#### 2.1.4. Oscillatory Reynolds number

The definition of the Reynolds number that is specific to OBRs is the oscillatory Reynolds number, which is defined as:

$$\text{Oscillatory Reynolds number: } Re_o = \frac{2\pi Af\rho D}{\mu} \quad \text{Eq. 2.1.4-2}$$

where A and f the amplitude and frequency of oscillations.

In this definition, the characteristic velocity is usually taken as the maximal velocity of oscillations since the velocity varies with time:

$$v = A\omega\sin(\omega t) \quad \text{Eq. 2.1.4-3}$$

$$v_{max} = A\omega = 2\pi Af \quad \text{Eq. 2.1.4-4}$$

Alternatively, the velocity  $u_p$  at the smallest section of tube at the baffle can be considered [23].

$$u_p = \pi Af \frac{A_{piston}}{A_{pipe}} \quad \text{Eq. 2.1.4-5}$$

The most commonly used definition in literature uses  $v_{max}$ ; this does not take into account the higher velocities around baffles or the presence of baffles in the calculations of net or oscillatory Reynolds numbers.

The recommended minimum oscillatory Reynolds number to achieve convection is 100 [13]. For  $Re_o < 250$ , the flow is essentially 2D axisymmetric and mixing intensity is low, for  $Re_o > 250$ , flow becomes 3D and mixing becomes more intense, finally for  $Re_o > 2000$ , flow is fully turbulent [24].

#### 2.1.5. Velocity ratio

The velocity ratio, which is also used as a design parameter, is defined as following:

$$\psi = Re_o/Re_{net}$$

This ratio should be greater than one for the oscillatory flow to be dominant and for the full effect of the vortex cycle [24]. The minimum velocity ratio required for the system to operate with a plug-flow behavior is 1.8-2, and the typically recommended range is between 2 and 6 [13], [24].

#### 2.1.6. Strouhal number

Physically, the Strouhal number compares the local flow velocity with the average flow velocity. It is used to measure the frequency of oscillatory phenomena, which depend on Reynolds number. A well-known example of such oscillatory patterns is the periodic vortex shedding behind a blunt body subjected to a steady flow.

Generally, the Strouhal number is defined as [25]:

$$Str = \frac{f_s d}{u_o} \quad \text{Eq. 2.1.5-1}$$



where  $f_s$ ,  $d$  and  $u_0$  are the frequency of the observed phenomena, the characteristic dimension of the system and the free stream velocity, respectively.

For an application to flows in oscillatory baffled reactors, the frequency of the vortex shedding is replaced by oscillatory frequency [23]. This is justified by the fact that two vortices are generated per cycle (one during the co-current oscillation, and the second during the counter-current oscillation), leading to in reality  $f_s = 2f$  [23]. The velocity term is equal to  $\omega x_0$  like for the definition of the oscillatory Reynolds number. The characteristic dimension is defined as the orifice diameter  $D_0$ .

$$Str = \frac{D_0}{\pi x_0} \quad \text{Eq. 2.1.2-2}$$

The last form of the relation used in most of publications is:

$$Str = \frac{D}{4\pi x_0} \quad \text{Eq. 2.1.2-3}$$

This is different from the previous definition as  $f_s$  is directly replaced by  $f$ , and the diameter of the baffle, which generally equals to  $D_0 = D/2$  is used as the characteristic dimension.

As it was mentioned for the Reynolds numbers, the Strouhal number is not time-dependent, whereas the flow velocity in OBRs is time-periodic and the formation of vortices is time-dependent. The vortices are generated when the velocity of the flow increases, then disappear when velocity decreases. Other vortices shed when velocity is negative (when the flow is in the opposite direction). However, the hypothesis of a quasi-steady flow is taken to justify the use of dimensionless numbers that are constant with time [26].

The effect of the modified Strouhal number is then a dimensionless tool for characterizing the formation of vortices, analogously to the vortex shedding after a cylinder in steady flow. Nevertheless, it is difficult to study  $Str$  and  $Re_0$  separately because the former contains the amplitude of oscillations, and the latter amplitude and frequency of oscillations [24].

### 2.1.7. Nusselt number

The Nusselt number is used to characterize heat transfer and corresponds to the ratio of convective heat transfer to conductive heat transfer.

$$Nu = \frac{hL}{k} \quad \text{Eq. 2.1.3-1}$$

where  $h$  the convective heat transfer coefficient,  $L$  the characteristic length and  $k$  the thermal conductivity.

## 2.2. Performance characterization

The main effects of these key design parameters on hydrodynamics pressure drop, heat transfer, droplet size of liquid-liquid dispersions, axial to radial velocity ratio and axial dispersion coefficient are detailed in this section.

### 2.2.1. Pressure drop

In the previously tested glass reactor in Part II, maximum pressure is 5 bar, and in Part III, Chapter 2, maximum pressure is 10 bar. As an increase of oscillations leads to an increase of the pressure drop in the reactor, the prediction of pressure drop in a given system is important to

determine geometric parameters as length or diameter for a fixed set of oscillatory conditions. This pressure has to be monitored experimentally to protect the reactor and to ensure that the maximum supported pressure is not exceeded. Jealous et al. [27] proposed a quasi-steady state model for determining pressure drop from power dissipation in pulsed columns:

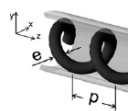
$$\Delta P = \frac{n\rho(2\pi Af)^2(1/S^2-1)}{2C_0^2} \quad \text{Eq. 2.2.1-1}$$

where  $n$  is the total number of baffles,  $S$  is the fractional open area and  $C_0$  is the standard orifice coefficient, usually taken as 0.6.

### 2.2.2. Heat transfer

The dimensionless Nusselt number is used to characterize heat transfer. The Nusselt number is higher in presence of oscillations for a same net Reynolds number. The higher the oscillating Reynolds number, the better the heat transfer; it increases by a factor 4 compared with a smooth tube for  $Re_{net} = 600$  and a factor 5 for  $Re_{net} = 800$  [19]. In the helicoidally-shaped baffled oscillatory column, a similar result is obtained: the Nusselt number is four times higher than that in a straight tube, however the Strouhal number has no effect on the Nusselt number [22]. The literature results are summarized in **Table 2-3**.

**Table 2-3.** Summary of literature studies on heat transfer in oscillatory baffles reactors.

Correlations	V/H	Design	Diameter	Technique	Reference
Effect of Af, net and oscillatory Reynolds numbers on the Nusselt number	H	Single orifice (7 mm)	12 mm	Experimental	[19]
Effect of frequency and oscillatory Reynolds number on the Nusselt number.	H	Helicoid $e = 1.2$ mm $p = 7.5$ mm 	5 mm	CFD	[22]

### 2.2.3. Two phase flow

Studies on two phase flow in OBRs are of interest because the reactions performed in the current project involve immiscible reactants and products. Previous studies have found that the OBRs is capable of generating a range of droplet diameters varying from 0 to 2000  $\mu\text{m}$  for the silicon oil/water emulsion [16]. In [16], the Sauter diameter  $d_{32}$  has been directly correlated with the oscillation amplitude and frequency. The results via the correlations in given in **Table 2-4** show that frequency has a greater influence on drop size in vertical columns, whereas it is the amplitude that has a greater influence in horizontal column. In the reciprocating plate column, non-reactive and reactive oil in methanol emulsions (with or without catalyst) have been studied. Sauter diameters are superior in the presence of a catalyst than those in the non-reactive emulsions or at the beginning of the reaction. This is due to the generation of mono and diglycerides during the reaction which play the role of surfactants. The Sauter diameter is correlated with power consumption, showing the drop diameter increases with the ratio of power consumption weighted by the mass of the emulsion, and interfacial area is correlated to amplitude ( $A$ ), frequency ( $f$ ) and superficial velocity ( $u_{net}$ ) [21]:

$$a = 3.3 (Af)^{0.74} u_{\text{net}}^{-1.20}$$

Eq. 2.2.3-1

Table 2-4. Previous work on the characterization of two-phase flow in OBRs. Af is the product of amplitude and frequency of oscillations.

Correlations	V/H	Design	Diameter	Emulsion	Reference
$d_{32} = x_0^{-0.76} f^{0.85}$	H	Simple orifice	40 mm	Silicon oil/Water	[16]
$d_{32} = x_0^{-0.89} f^{-0.53}$	V		40 mm		
$d_{32}$ as a function of height of column and Af and as a function of power consumption.	V	Reciprocating plate column	25.4 mm	Oil droplets dispersed in methanol	[21]
Interfacial area as a function of Af and velocity u					

#### 2.2.4. Instantaneous velocities

Experimental results found in the literature data focus on the measurement of radial and axial velocities and the observation of eddies. The velocities are either calculated by CFD (Computational Fluid Dynamics) simulation or measured experimentally by PIV (Particle Image Velocimetry). The interest of obtaining velocity measurements is to understand flow mechanisms, and be able to maintain mixing conditions and velocities in the reactor when diameter of the column is increased for scale-up, changing parameters as amplitude and frequency of the oscillations. A summary of the results obtained by different studies is given in Table 2-5.

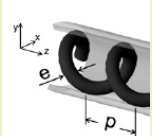
Mixing is observed qualitatively by CFD with formation of eddies, which increase radial mixing. Radial mixing is also promoted by increasing the oscillatory Reynolds number [22]. The generated radial flow is quantified by the axial to radial velocity ratio. It is calculated by taking the ratio of the mean values of the radial and axial velocity vectors taken on a plane [28]. Axial and radial velocities in OBRs have been calculated via CFD using laminar models in most of the cases, which have been validated with PIV [26], [28], [29], or advanced turbulence models, such as the Implicit Large Eddy Simulation (ILES) or Large Eddy Simulation (LES), which have been validated by PIV measurements [20], [28]. It is possible to change the velocity ratio by varying the oscillating amplitude or frequency [12]. It is recommended that this ratio be between 2 and 2.5 for good mixing, and less than 3.5 [30] such that the radial flow dominates and to limit axial dispersion. This velocity ratio has also been shown to decrease with an increase in oscillatory Reynolds number [31]. This ratio is between 1 and 3 for oscillatory Reynolds numbers superior to 100, which is in agreement with the previous recommended range. In addition, it has been shown that the individual axial and radial velocities are different depending on the instantaneous flow rate due to the time dependency of the sinusoidal velocity, which is proportional to oscillation frequency. For a scale-up interest, with the same operating conditions, the axial to radial velocity ratio increases when diameter increases from 50 to 100 mm, whereas it remains the same when diameter passes from 100 to 200 mm [30].

Another study has been carried out in order to characterize the symmetrical nature of the velocity field [32]. Using numerical simulations and PIV experiments two flow mechanisms are deduced. Firstly, for Strouhal numbers less than 0.1, when  $Re_o = 200$  the flow passes essentially through the center of the tube, which wobbles and rotates, due to a shear (Kelvin-Helmholtz) instability, and small eddies are generated near baffles. At Strouhal numbers greater than 0.5, the flow pattern consists of pairs of toroidal eddies that start from a baffle and end at the middle of a cell. They collide with other pairs of eddies that are generated by the opposite baffle during the return of the flow rate. This collision implies the rupture of the flow symmetry if the oscillatory Reynolds number is greater than 225. An increasing size of eddies as a function of Strouhal number has also been

observed [33]. However, for different Strouhal numbers at the same net and oscillatory Reynolds numbers, it is difficult to find any difference in eddy size or shape [22].

It is interesting to point out that in our previous work [34] a decrease in conversion was observed for  $Str > 0.1$  and for same range of Reynolds number ( $Str = 0.16$ ,  $A = 7.5$  mm,  $f = 1.4$  Hz), which contradicts the previous results given by [32]. Indeed, the Strouhal number is inversely proportional to amplitude, but there is a minimum amplitude for the generation of vortices, which is estimated at about a quarter of the space between baffles ( $h$ ) [35]. The amplitude for the Strouhal number leading to low conversion equals to 7.5 mm, which is near the value of this minimum as it corresponds to  $0.29h$ .

**Table 2-5.** Summary of previous works that measure or simulate velocity fields in a oscillatory flow column. Parameters observed are axial to radial velocity ratio, qualitative visualization, effect of the Strouhal and oscillatory Reynolds numbers, amplitude, frequency. For CFD techniques, the models used are given.

Study	V/H	Design	Diameter	Technique	Reference
Qualitative observation of radial mixing Effect of Str at high $Re_o$	H	Helix $e = 1.2$ mm $p = 7.5$ mm 	$d = 5$ mm	CFD: Laminar	[22]
Axial and radial velocity profiles	H	3 orifices (diameters of 17 mm) plates	$D = 60$ mm	PIV LDV (Laser Doppler Velocimetry) CFD : ILES (Implicit Large Eddy Simulation)	[20]
Effect of diameter on average mean velocity and on axial to radial velocity ratio	V	Single orifice plate ( $D_o = 23$ mm)	50 mm Baffle spacing 75 mm	PIV CFD : LES (Large Eddy Simulation)	[28]
Effect of amplitude or frequency on the axial to radial velocity ratio	V	Single orifice plate $d = 75$ mm	$d = 145$ mm	CFD : Laminar	[12]
Effect of reactor diameter on the axial to radial velocity ratio	V	Single orifice plate $(D_o/D)^2$ $= 0.22$	50, 100 et 200 mm	CFD : Laminar	[30]
Effect of the $Re_o$ on the axial to radial velocity ratio		Single orifice plate		CFD : Laminar	[31]
Effect of position and $Re_o$ on the strain rate	V	Single orifice plate	50 mm	PIV	[26]
First 3D CFD simulation Validation with PIV	V		50 mm 23 mm orifice	PIV CFD : LES	[29]
Effect of $Re_o$ on the symmetry of flow patterns	V	Single orifice plate	50 mm	CFD: Laminar PIV	[32]
Effect of Str on the eddy length	V	Single orifice plate	145 mm	CFD: Laminar	[33]

### 2.2.5. Axial dispersion coefficient

The axial dispersion model is mathematically described by Levenspiel [36] :

$$\frac{\partial C}{\partial t} = D_{ax} \frac{\partial^2 C}{\partial x^2} \quad \text{Eq. 2.2.5-1}$$

$$\frac{\partial C}{\partial \theta} = \left( \frac{D_{ax}}{uL} \right) \frac{\partial^2 C}{\partial z^2} - \frac{\partial C}{\partial z} \quad \text{Eq. 2.2.5-2}$$

with  $z = (ut + x)/L$  and  $\theta = tu/L$ . ( $D_{ax}/uL$ ) is a dimensionless vessel dispersion number.

A more well-known version of this dimensionless number is the reciprocal, which is the Peclet number and represents the ratio of the convective transport to diffusive transport, as defined by the following [37]:

$$Pe = \frac{uL}{D_{ax}} \quad \text{Eq. 2.2.5-3}$$

In order to consider plug flow behavior in the reactor, the Peclet number (Pe) has to be greater than 100. The coefficient of axial dispersion ( $D_{ax}$ ) is a characteristic of the geometry of a reactor. This coefficient can be used to predict reaction yields or selectivities in a particular reactor geometry. This coefficient is obtained from the variance of the residence time distribution. Another possible interpretation of the residence time distribution is the tanks-in-series model [36], where the number of tanks in series  $N$  can be considered as proportional to the Peclet number. The reactor has a plug-flow behavior for  $N > 10$  [18].

The studies that deal with the calculation of the axial dispersion coefficient and the effect of operating parameters are summarized in **Table 2-6**.

**Table 2-6.** Summary of literature results that determine the coefficient of axial dispersion. V or H indicates if the studied columns are vertical or horizontal. The techniques used to calculate these coefficients are residence time distribution RTD or with computational fluid dynamics (CFD) with the distribution of a tracer.

Correlations	V/H	Design	D (mm)	Technique	Axial coefficient (m <sup>2</sup> /s)	Ref.
Effect of $Re_o$ , $Re_{net}$ , viscosity and Pe on the axial dispersion coefficient	V	Pulsed sieve plate column 39x3 mm	39.6	RTD	$1 \times 10^{-5} - 9 \times 10^{-4}$	[14]
Effect of $Re_o$ , Str, $Re_{net}$ on the axial dispersion coefficient. Comparison of single orifice plate to perforated plate (D = 150 mm)	V	Single orifice plate	24 54 150	RTD	$10^{-4} - 10^{-2}$	[15]
Correlation of the axial dispersion coefficient to A, f and u.	V	Single orifice	40	RTD	$9 \times 10^{-4}$ $1.5 \times 10^{-3}$	[16]
	H	Baffles 1x18 mm	40	RTD		
Effect of viscosity on the axial dispersion coefficient	H	Single orifice of 11.5 mm opening	25	CFD	$1.2 \times 10^{-3} - 9.6 \times 10^{-3}$	[31]

Several studies have investigated the influence of Reynolds number on this coefficient by calculating the axial dispersion coefficient  $D_{ax}$  using the residence time distribution obtained experimentally [14], [15] or with numerical simulations [31].

The different cases studied by Palma et al. [14] are detailed in **Table 2-2**. For a net velocity of 2.67 mm/s and a reactor length of 2.4 m, the axial dispersion coefficient ( $D_{ax}$ ) has been calculated for different baffle spacings ( $h$ ), oscillatory amplitude ( $A$ ) and frequency ( $f$ ). To complete these results, the Peclet ( $Pe$ ) and oscillatory Reynolds ( $Re_o$ ) numbers have been calculated from the published axial dispersion coefficient and from oscillatory conditions in **Table 2-7**. It can be seen that the Peclet number decreases with increasing oscillatory Reynolds number. Furthermore, the Peclet number is greater than 100 only for low values of oscillation amplitude and frequency (i.e. 5 mm and 1 Hz) for a baffle spacing of 25 mm. According to the authors, the inverse Peclet number increases linearly with the product of  $Af$  divided by the velocity. It quantifies the observed decrease of Peclet number with the increase of oscillatory Reynolds number which is proportional to  $Af$ .

**Table 2-7.** Calculations of Peclet numbers ( $Pe$ ) from the axial dispersion coefficients determined in [14].

D (mm)	A (mm)	f (Hz)	$D_{ax}$ (m <sup>2</sup> /s)	$Re_o$ (-)	Pe (-)	Reference
25	5	1	6.00E-05	1200	107	[14]
25	25	1	2.20E-04	6100	29	
25	5	3.5	7.00E-05	4300	92	
25	25	3.5	5.20E-04	21400	12	
50	5	1	8.00E-05	1200	80	
50	25	1	1.50E-04	6100	43	
50	5	3.5	1.40E-04	4300	46	
50	25	3.5	3.80E-04	21400	17	
100	5	1	1.00E-04	1200	64	
100	25	1	1.00E-04	6100	64	
100	5	3.5	1.00E-04	4300	64	
100	25	3.5	3.20E-04	21400	20	

Smith and Mackley [15] determined the axial dispersion coefficient ( $D_{ax}$ ) for different oscillatory Reynolds numbers and different tube diameters. For a net Reynolds number of 107, the Peclet numbers have been determined from the axial dispersion coefficient found in their work, as given in **Table 2-8**. The mean characteristic velocity has been deduced from the net Reynolds number. Again, it can be seen that an increase of oscillatory Reynolds number increases the axial dispersion coefficient, which means it decreases Peclet numbers, except at low oscillatory Reynolds numbers (40 to 200) where the Peclet number increases. This value of the oscillatory Reynolds number can be found in a study of the symmetry of the flow patterns in OBRs [32], where it is shown that dissymmetry appears in the flow at  $Re_o > 225$ , caused by the collision of the eddies generated in the forward flow and those generated during the return flow rate.

The axial dispersion has also been characterized with the tanks-in-series model in oscillatory baffled reactors [38][39], showing the presence of a maximum value for the value of the number of tanks-in-series with the increase of the oscillatory Reynolds number around 100, which is in agreement with the evolution observed by Smith and Mackley [15]. This maximum is at a higher oscillatory Reynolds number if the net Reynolds number increases.

It should also be pointed out that in **Table 2-8** the Peclet numbers are relatively low, being always less than 35. In this work, it was also shown that an increase of the net Reynolds number (from 56 to 430), increases the axial dispersion coefficient. Finally, a multi-orifice plate is used for

comparison with the single orifice baffle of the same diameter (150 mm) and this leading to a decrease in the axial dispersion coefficient.

**Table 8.** Calculations of Peclet numbers (Pe) from the axial dispersion coefficients determined in [14]

D (mm)	v (m/s)	L (m)	D <sub>ax</sub> (m <sup>2</sup> /s)	Re <sub>o</sub> (-)	Pe (-)
24	4.5E-03	1	4E-04	40	11
24	4.5E-03	1	2E-04	200	30
24	4.5E-03	1	3E-04	1000	15
24	4.5E-03	1	3E-03	4000	1
54	2.0E-03	2	4E-04	10	10
54	2.0E-03	2	4E-04	40	10
54	2.0E-03	2	1E-04	200	40
54	2.0E-03	2	7E-04	1000	6
54	2.0E-03	2	2E-03	4000	2
150	7.1E-04	4.5	1E-04	200	32
150	7.1E-04	4.5	2E-04	1000	16
150	7.1E-04	4.5	4E-03	4000	1

In the work of Smith and Mackley [15], the axial dispersion coefficient remains constant with the position of the sample probe (L), as it equals to 1.08 cm<sup>2</sup>/s for a distance of 870 mm and 1.09 cm<sup>2</sup>/s for a distance of 2616 mm [14], but it has an effect on the Peclet number (Pe = uL/D) as these values have been calculated from these axial dispersion coefficients and correspond to Peclet numbers of 22 and 66. The Peclet number is then increasing with L. The effect of viscosity on the axial dispersion coefficient has also been studied [14]. It is difficult to conclude as the axial dispersion coefficient decreases for D = 24 and 54 mm, but increases for D = 150 mm. The effect of viscosity should directly impact the oscillatory Reynolds numbers by decreasing it if viscosity increases, which should, if we consider the evolution of the axial dispersion coefficient with oscillatory Reynolds number of the **Table 2-7**, decrease axial dispersion coefficient for oscillatory Reynolds number superior to 200, or increase it for oscillatory Reynolds number inferior to 200. This is confirmed by the work of Manninen et al. [31], with an increase of the axial dispersion coefficient with the increase of the viscosity (or the decrease of the oscillatory Reynolds number), which corresponds to the decrease of the axial dispersion coefficient for oscillatory Reynolds number between 40 and 200.

Correlations have been determined to calculate the axial dispersion coefficient as a function of the net and oscillatory Reynolds numbers and the Strouhal number [15]:

$$D_{ax} = 7.0 \times 10^{-7} Re_{net}^{0.8} + 7.5 \times 10^{-7} Re_o e^{-0.4 Str} + (3.0 \times 10^{-12} Re_{net}^{1.6}) / (7.0 \times 10^{-7} Re_{net}^{0.8} + 7.5 \times 10^{-7} Re_o^{-0.4 Str}) \quad \text{Eq. 2.2.5-4}$$

The axial dispersion coefficient has been correlated to amplitude, frequency and net velocity for horizontal and vertical columns, and Peclet number has been correlated to net and oscillatory Reynolds numbers [16]:

$$\text{Vertical column:} \quad D_{ax} = 0.072(Af)^{0.6} u^{0.4} \quad \text{Eq. 2.2.5-5}$$

$$\text{Horizontal column:} \quad D_{ax} = 0.0658(Af)^{0.66} u^{0.34} \quad \text{Eq. 2.2.5-6}$$

$$Pe = 462 (\pm 13.67\%) Re_o/Re_{net}^{-0.60(\pm 6.44\%)} \quad (R^2 = 0.798) \quad \text{Eq. 2.2.5-7}$$

These correlations confirm the obtained trends for the evolution of the axial dispersion coefficient with the axial dispersion coefficient and have been obtained empirically. It is nevertheless difficult to find a relationship between the correlations obtained in the work of Smith and Mackley [15] and in the work of Pereira [16], but the trend is similar, showing an increase of the axial dispersion coefficient (or decrease of the Peclet number) with the increase of the oscillatory Reynolds number.

### 2.3. Conclusions of the state of the art

The studies found in literature have focused on the characterization of droplet size of liquid-liquid dispersion, the calculation of the axial to radial velocity ratio and calculations of axial dispersion coefficient, by studying the influence of key design parameters, such as the presented dimensionless numbers, the amplitude and frequency of oscillations, as well as geometric parameters (tube diameter, baffle spacing, opening and design). Additional calculations have been made to determine the Peclet numbers associated with the axial dispersion coefficients determined in literature and these show the plug-flow behavior of oscillatory baffled reactors strongly depends on the oscillatory parameters.

The pressure drop is determined by the correlation provided by Jealous and Johnson [27]. It is a key parameter for the design of the final reactor for the choice of geometric parameters, such as reactor length and diameter. Heat transfer and the quality of liquid-liquid dispersion are ensured by an increase of the oscillatory conditions, i.e. the oscillatory Reynolds number. On the other hand, this oscillatory Reynolds number should be limited to a certain range for mixing considerations, as the axial dispersion coefficient increase with an increase of the oscillatory Reynolds number for  $Re_o > 200$ . The Peclet number has to be sufficiently high for the reactor to have a plug flow behavior. This Peclet number depends on the characteristic length of the reactor, and so it has to be related to a characteristic residence time. The mixing in the reactor can also be characterized by the axial to radial velocity ratio, with a recommended range between 2 and 3.5 to stay in the plug flow conditions. Some connections between the presented results have been made, for example the generation of axisymmetric eddies for oscillatory Reynolds numbers less than 200 [32], that promote radial mixing, which is in good agreement with the decrease of axial dispersion coefficient calculated for the same range of oscillatory Reynolds numbers [14]. Moreover, the effect of viscosity can be connected to the discussion on the effect of oscillatory Reynolds number as an increase in viscosity decreases the net or oscillatory Reynolds numbers. The effect of Strouhal number is difficult to identify since no specific effect has been attributed to a change in this number, except for the size of the eddies [33]. This state of the art has highlighted the recommendations for the choice of the conditions of oscillations, flow rates and geometric parameters, showing the potential of numerical simulations and particle image velocimetry for the characterization of the flow in the OBRs. The understanding of the flow characteristics in such reactors could be improved by the determination of range of oscillatory Reynolds number and Strouhal number leading to the generation of eddies, the determination of axial dispersion coefficient for short residence times and then correlation of the Peclet number with reactor length in order to estimate minimum residence time with plug flow behavior. It also appears that a study of baffle geometry could be of interest, using the presented means of characterization, as the determination of axial dispersion coefficient and proposing new ones.



### 3. Experimental measure of velocity vectors by PIV (Particle Image Velocimetry)

Particle Image Velocimetry (PIV) is a non-intrusive experimental technique used to measure instantaneous flow fields. An experimental setup has been constructed to use this technique to measure the flow fields in an oscillatory flow reactor, which is the glass Nitech® reactor in this study. The objective of this part of the work is to investigate the effect of the oscillatory Reynolds number on the flow patterns.

#### 3.1. Material and methods

PIV measurements have been carried out in a Nitech® glass tube with a length  $L = 70$  cm and diameter  $D = 15$  mm.

The effect of the oscillatory Reynolds number is studied by increasing the viscosity of the fluid. For this, a binary mixture of glycerol and water at different glycerol compositions is used: 0%, 24.7%, 41.3 % and 54.6 w t.% of glycerol, which corresponds to viscosities of 0.001, 0.002, 0.0052 and 0.0112 Pa.s, respectively. The net flow rate is fixed at 8.9 L/h. The corresponding oscillatory Reynolds numbers are 1890, 980, 410 and 200 and the corresponding net Reynolds numbers are 211, 110, 46 and 22. Secondly, the effect of the oscillatory amplitude is studied at constant viscosity (0.0112 Pa.s). The oscillatory amplitude is set from 5 mm to 25 mm and the frequency is fixed at 1 Hz, which corresponds to oscillatory Reynolds numbers ranging from 49 to 244. The Nitech® glass tube is immersed in a rectangular tank made of Plexiglas and two 70 cm long quartz windows. **Fig. 3-1** shows the PIV-experimental setup and the simplified process flow diagram is represented in **Fig. 3-2**. The pump is fed by a stirred tank containing the fluid mixed with 20 -50  $\mu\text{m}$  rhodamine-doped melamine seeding particles that is pumped in the Nitech® tube. The oscillations are superimposed onto the net flow. The PIV measurements were taken using a double pulsed Litron Lasers Nano S PIV Nd:YAG laser (continuum) at a frequency of 14 Hz and a wavelength of 532 nm (green). A high resolution (1600x1200 pixels) camera (Imager Pro X 2M LaVision) was used to record the consecutive images of the flow on a vertical plane along the tube.

The laser sheet is projected onto a mirror positioned at 45° under the tube in order to create a vertical measurement plane, as shown in **Fig. 3-2(a)**. The illuminated area covers 61 mm x 16.5 mm, which corresponds to three cells of the Nitech® tube. A flowmeter, a pressure transducer and a PT100 are connected to the line to collect mass flow rate, pressure and temperature with the commercial software DasyLab9. The image pairs are acquired at 14 Hz, with a time delay between image pairs of 2656, 1328, 885, 664, 531  $\mu\text{s}$  for amplitudes of 5, 10, 15, 20 and 25 mm, respectively. These images are processed using a commercial software DaVis® v.8.1. The instantaneous velocity fields are calculated using a cross-correlation between image frames in a multipass mode with decreasing window size from 64x64 px<sup>2</sup> to 32x32 px<sup>2</sup> (1.55 mm<sup>2</sup>), both windows sizes having 50% overlap.

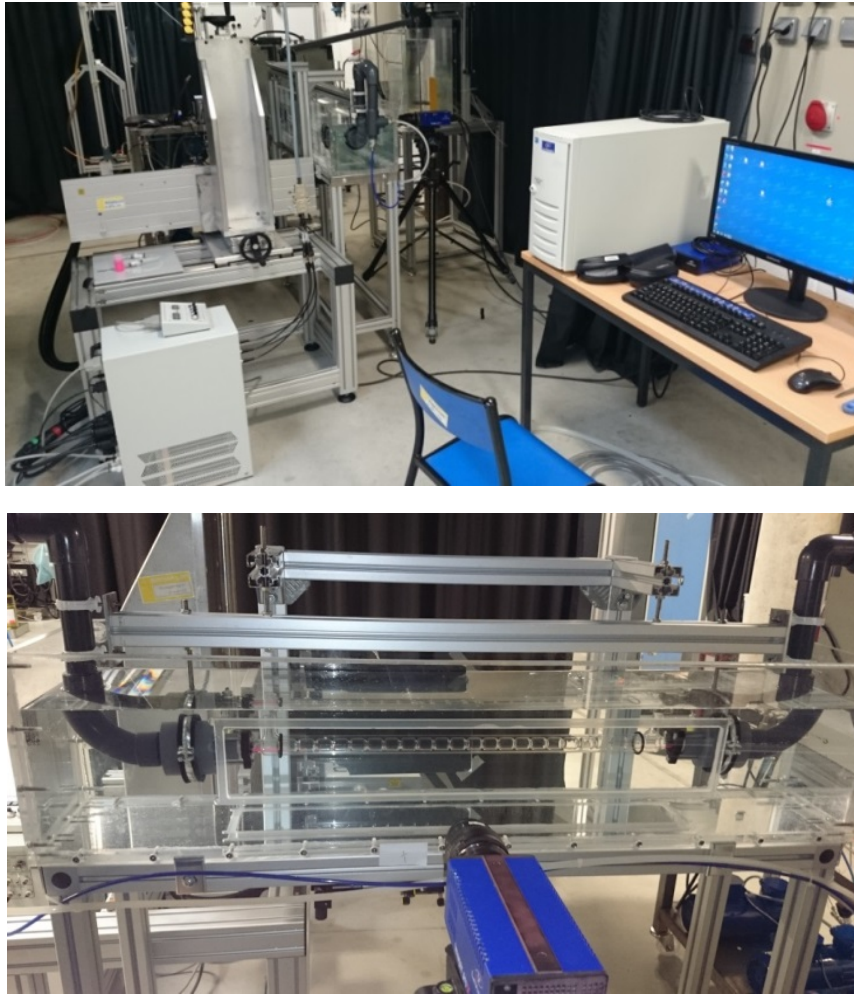


Fig. 3-1. The experimental setup used to perform Particle Image Velocimetry (PIV) measurements.

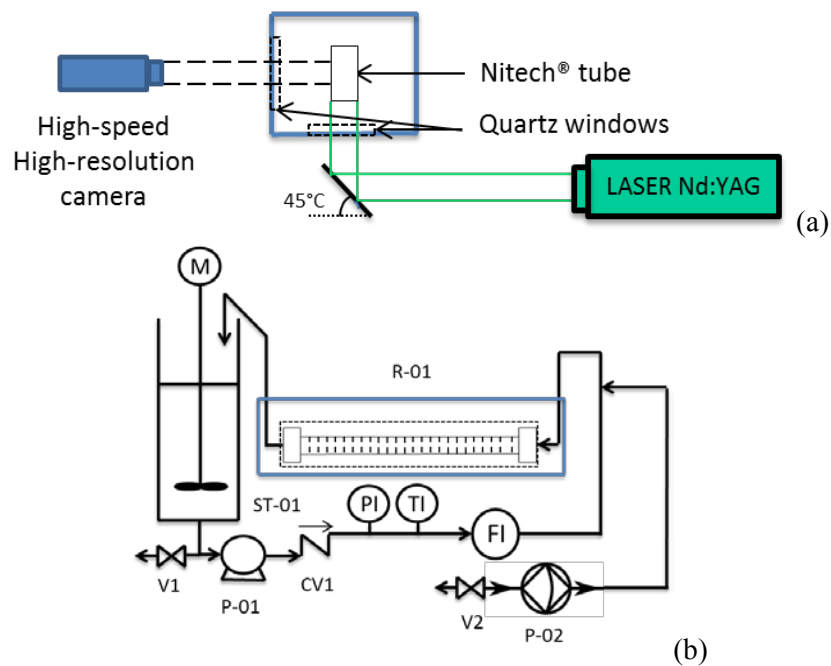
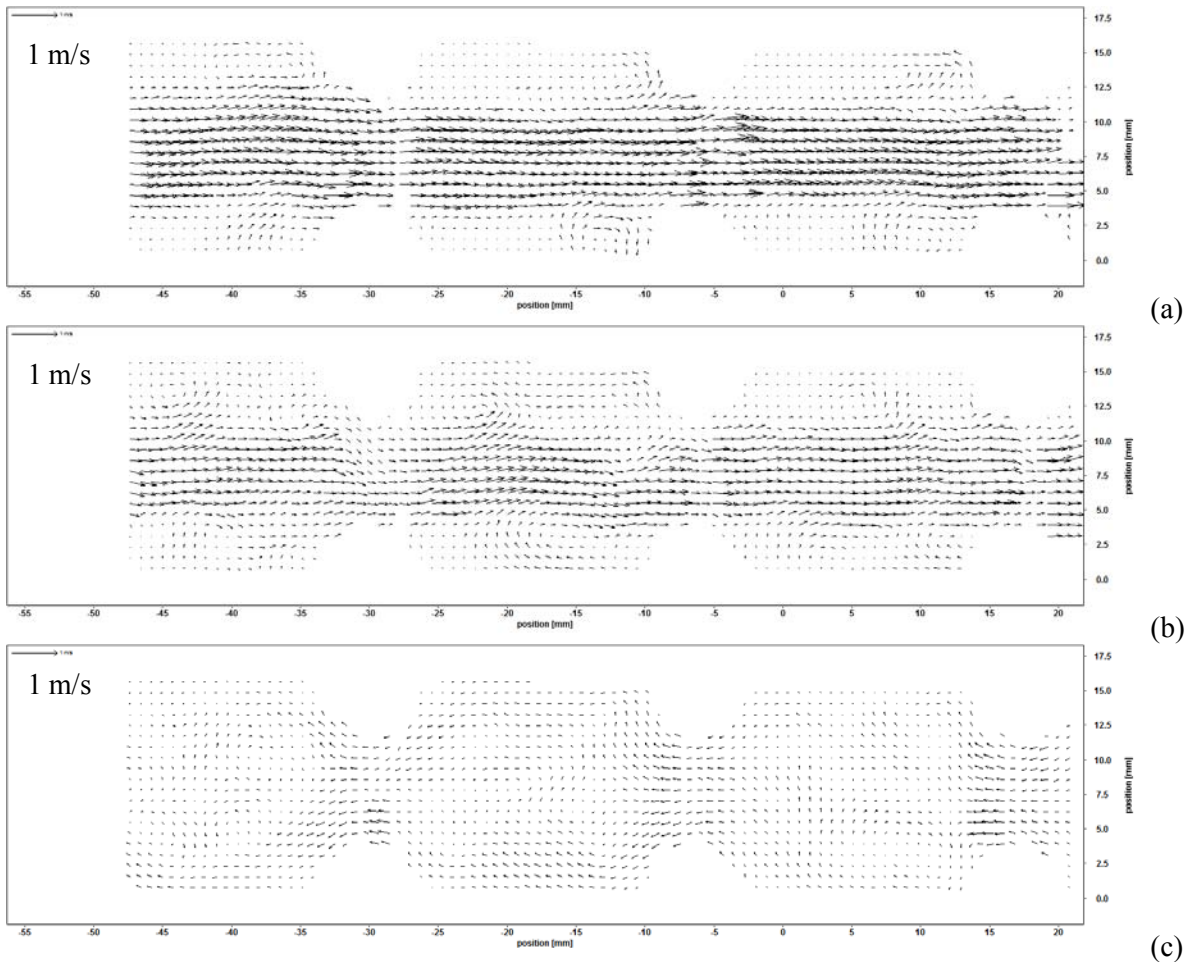


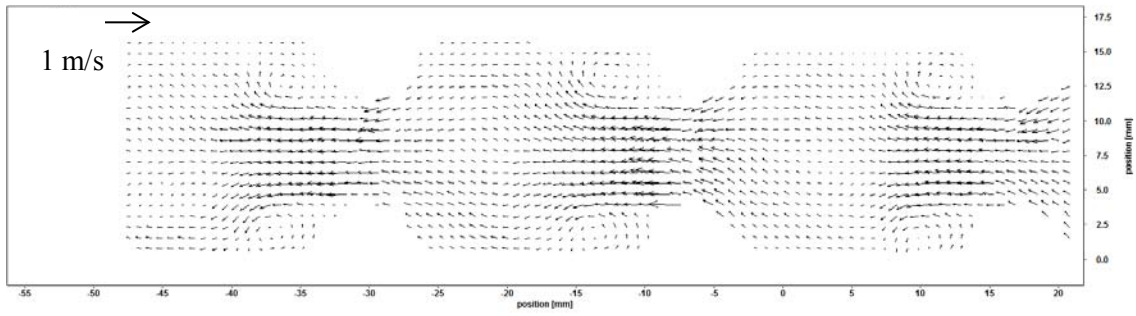
Fig. 3-2. Schematic diagram of the experimental setup containing The Nitech® tube R-01. Cross-sectional view (a). Front view (b). ST-01 is the stirred tank, V1 and V2 are valves, P-01 and P-02 are gear pumps, CV1 is a check valve. PI is the pressure transducer, TI is the PT100 and FI is the mass flow rate.

## 3.2. Results

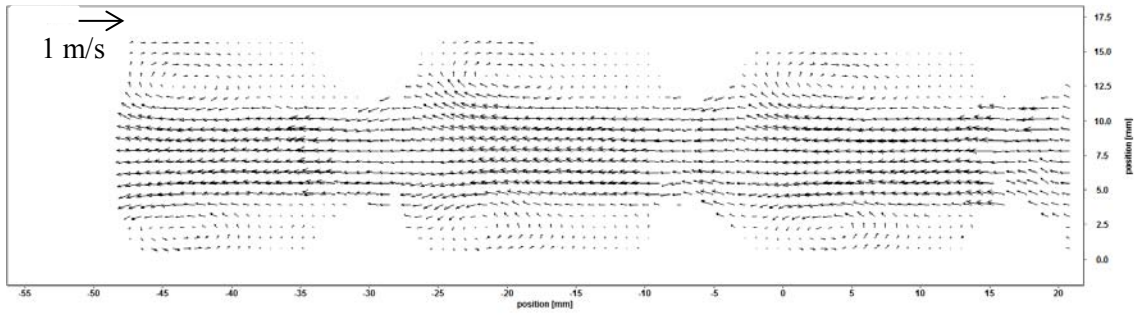
### 3.2.1. Velocity fields

The velocity fields as a function of time are represented in **Fig. 3-3**. At  $t/T = 0$  the positive velocity is at its maximum value; the velocity fields at other selected times are represented in **Fig. 3-3** (k). No eddies are formed during the deceleration of the flow between  $t/T = 0.14$  and  $t/T = 0.29$  (**Fig. 3-3** (b) and (c)) in the direct flow (velocity  $> 0$ ). The eddies, in the reverse flow (velocity  $< 0$ ) are generated at  $t/T = 0.36$  (**Fig. 3-3** (d)), and propagate in the cell (i.e. the distance between two baffles) (**Fig. 3-3** (e) and (f)) until the flow velocity has reached its maximum value. No eddies are formed when the flow decelerates between  $t/T = 0.64$  and  $t/T = 0.71$  (**Fig. 3-3** (g) and (h)). New eddies are formed at the other side of the baffle when the flow changes direction (velocity  $> 0$ ) at  $t/T = 0.86$  (**Fig. 3-3** (i)), and these propagate in the cell between  $t/T = 0.93$  and  $t/T = 0$  (**Fig. 3-3** (j) and (a)). The instantaneous flow patterns in the different cells of each image are quasi-identical.

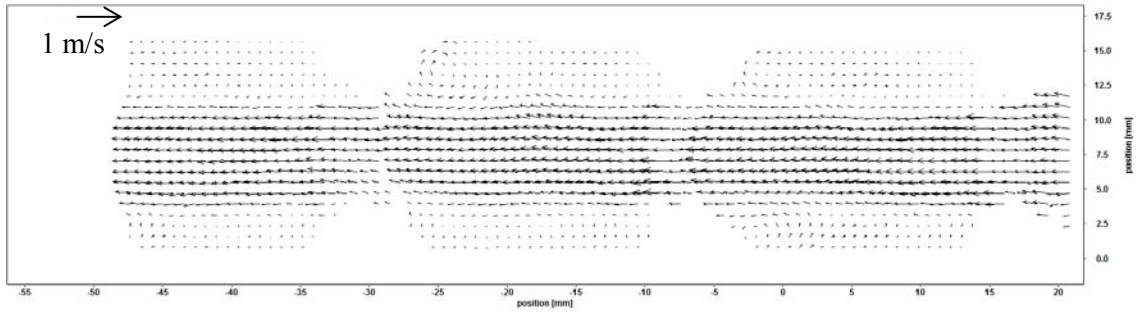




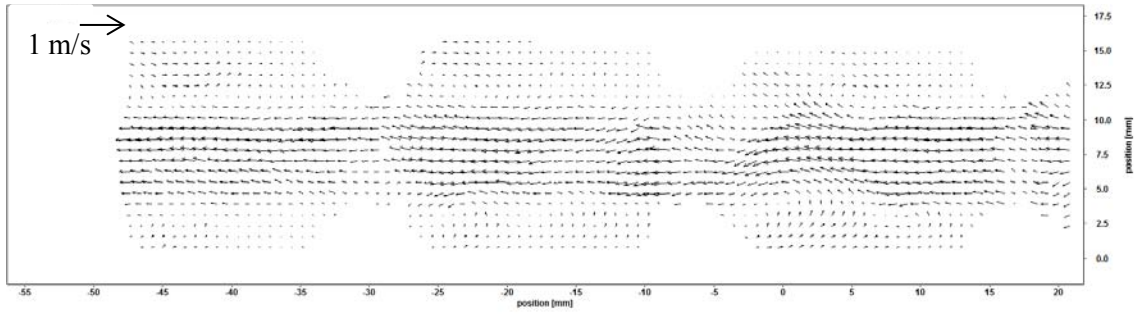
(d)



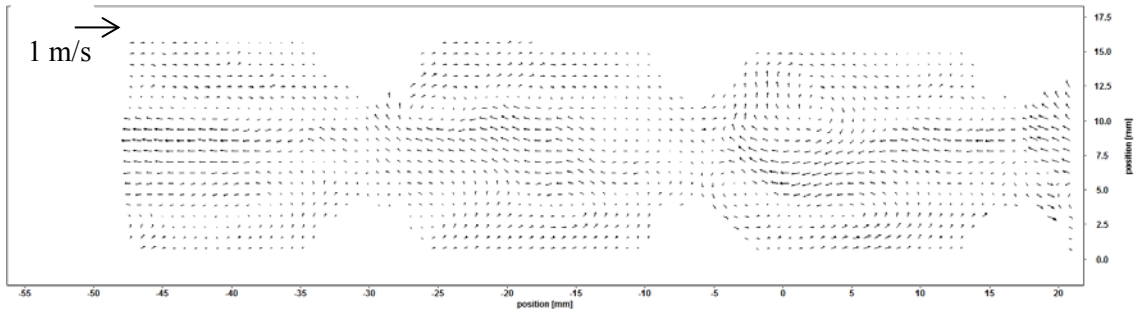
(e)



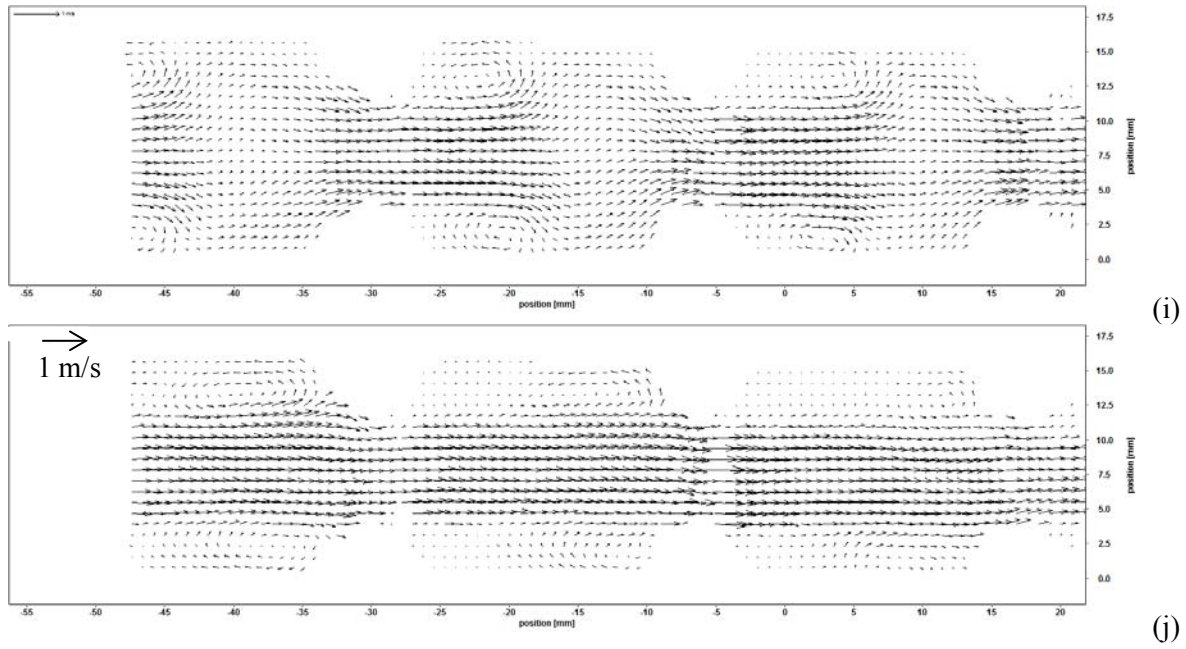
(f)



(g)



(h)



**Formation and propagation of eddies**

(k)

**Fig. 3-3.** Velocity fields obtained by PIV measurement at  $t/T = 0$  (a), 0.14 (b), 0.29 (c), 0.36 (d), 0.43 (e), 0.5 (f), 0.64 (g), 0.71 (h), 0.86 (i), 0.93 (j) at  $Re_o = 200$  ( $\mu = 0.0112$  Pa.s,  $A = 20$  mm,  $f = 1$  Hz). The different  $t/T$  are represented by blue squares on (k) which represents the normalized velocity as a function of the time normalized by the period. The green squares shows the time where eddies are formed and propagates.

**Fig. 3-4** represents the velocity fields obtained by PIV measurements for different oscillatory Reynolds numbers (1890, 980, 410, 200) obtained with an increase in the viscosity and with frequency conditions  $A = 20$  mm and  $f = 1$  Hz. The time frame is  $t/T = 0.86$ , which corresponds to the formation of eddies in the positive flow. The flow patterns are similar for the four  $Re_o$ , with the formation of eddies in a similar position. However, it can be seen that the lengths of the velocity vectors in eddies formed at  $Re_o = 200$  (**Fig. 3-4** (d)) are smaller than those obtained for higher  $Re_o$ . The repeatability of flow patterns is acceptable for  $Re_o$  in the range of 200-980 but is imperfect for  $Re_o = 1890$ . Moreover, in this case, the flow patterns are not axisymmetrical.

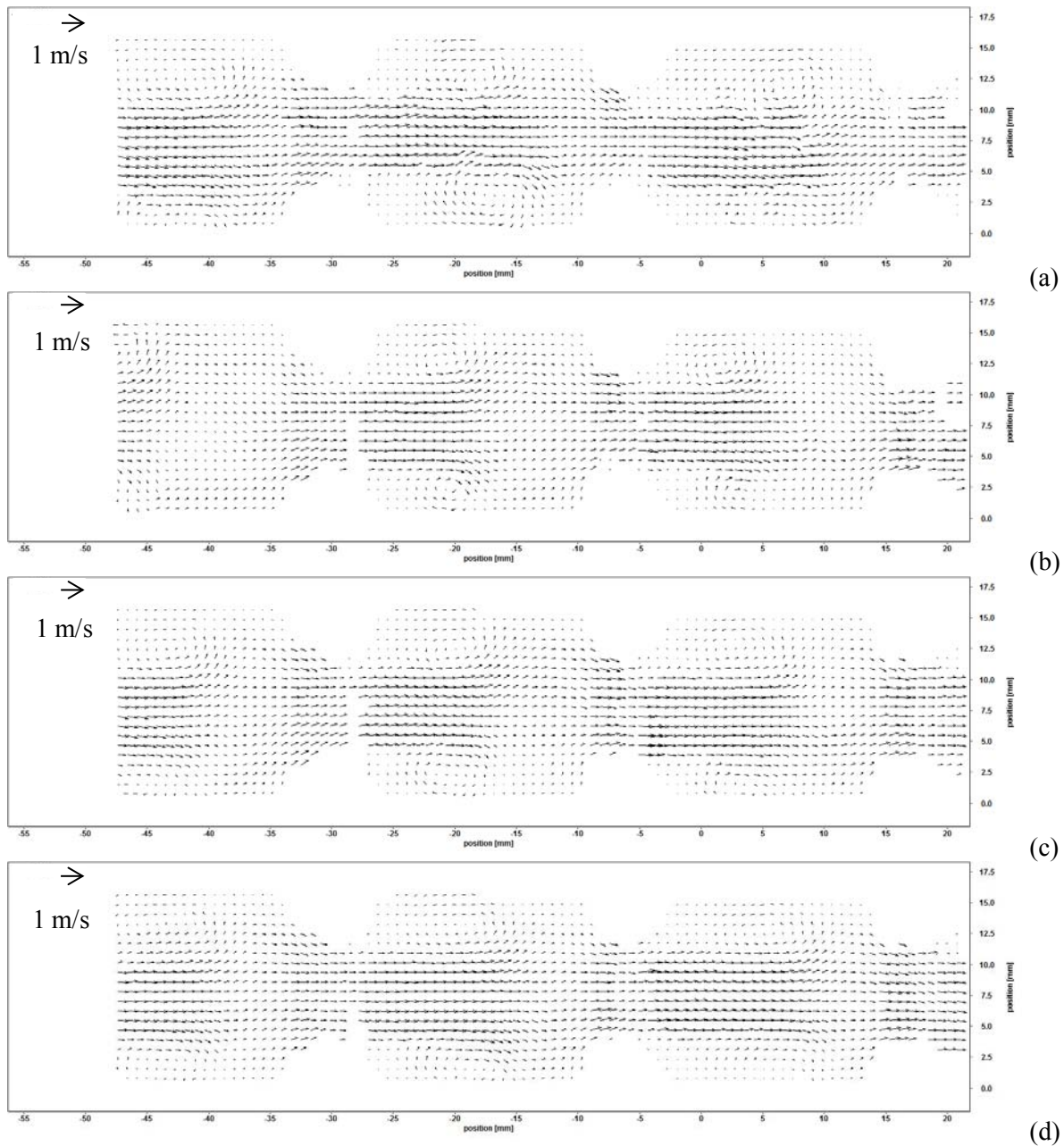


Fig. 3-4. Velocity field obtained by PIV measurement at  $t/T = 0.86$  at  $Re_o = 1890$  (a), 980 (b), 410 (c) and 200 (d) ( $A = 20$  mm,  $f = 1$  Hz).

Fig. 3-5 represents the phase-averaged normalized axial velocities at  $t/T = 0.86$  and  $X = -23$  mm for different oscillatory Reynolds numbers (1890, 980, 410 and 200) induced by different viscosities. The difference between the profiles obtained at different  $Re_o$  are in the range of the root-mean-square velocity which is around 50% between  $Y/D = 0.8$  and  $Y/D = 1$ . Nevertheless, the absolute value of the negative axial velocities increases with an increase of the oscillatory Reynolds number.

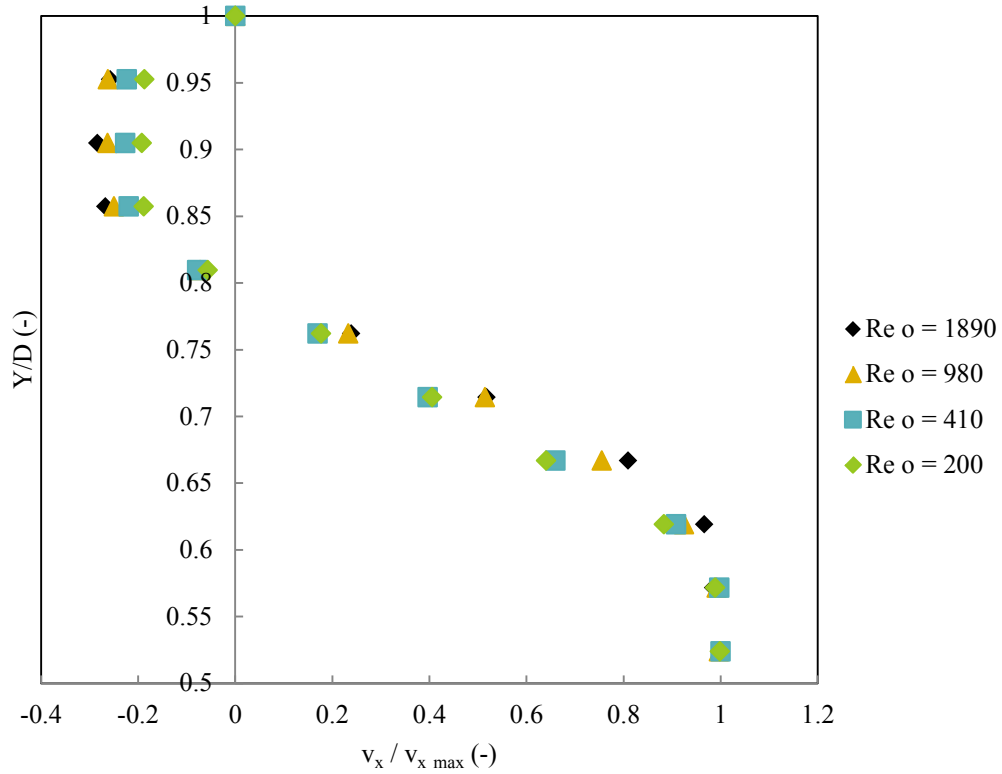


Fig. 3-5. Profile of the phase-averaged axial velocity at  $X = -23$  mm obtained by PIV measurement at  $t/T = 0.86$  and at different  $Re_o$ .

Fig. 3-6 shows the influence of the oscillatory amplitude on the velocity profiles at  $X = -23$  mm. The negative normalized axial velocities, representative of the velocities of eddies are between -0.25 and -0.15 at these amplitudes. The standard deviations of the phase-averaged calculation are in the same range of the values of the negative axial velocities, so there are no noticeable differences with an increase of the amplitude. The axial velocity profiles are superimposed in the center of the tube since the increase of the amplitude is directly proportional to the increase of the velocity and the flow is laminar.

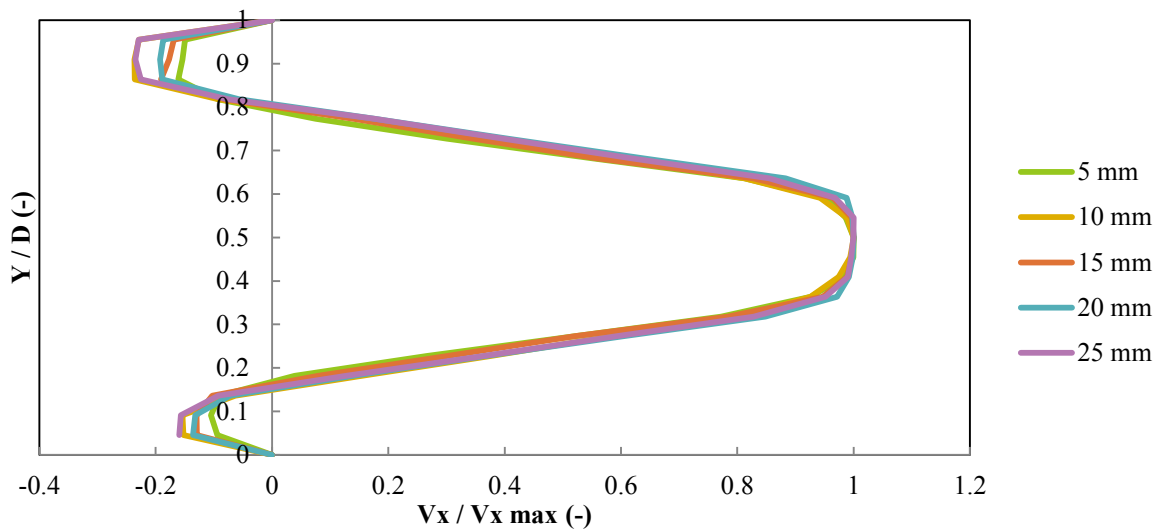


Fig. 3-6. Velocity profile at  $X = -23$  mm for  $\mu = 0.0112$  Pa.s and  $f = 1$  Hz for different amplitudes.

### 3.2.2. Eddy formation

The **Fig. 3-7** represents the axial velocity field for  $A = 20$  mm at different  $t/T$  (0.86, 0.93 and 1). The negative axial velocities are represented in blue and correspond to the presence of a recirculation eddy. The length of eddies increases as the velocity approaches its maximum value (**Fig. 3-7 (d)**). They are formed near baffles, at the beginning of a cell (space between two baffles), and then propagate to the end of the cell up to the next baffle. **Fig. 3-8** represents the axial velocity fields for amplitudes of 5, 10, 15, 20 and 25 mm at  $t/T = 0.86$  and for  $\mu = 0.00112$  Pa.s. The negative axial velocities show the presence of only the half of eddies, as the velocities in eddies have also a positive part, but presence of flow fields can help to see the rest of the eddy.

These observations are confirmed by the vorticities. **Fig. 3-9** represents the vorticity and the velocity fields for  $t/T = 0.86, 0.93$  and 1 for  $\mu = 0.00112$  Pa.s and for different amplitudes at  $t/T = 0.86$  and for  $\mu = 0.00112$  Pa.s in **Fig. 3-10**. Vorticity is calculated by the following equation:

$$-Rot(z) = E_{xy} - E_{yx} = \left( \frac{\partial v_x}{\partial y} - \frac{\partial v_y}{\partial x} \right) \quad \text{Eq. 3.2.2-1}$$

Where  $v_x$  is the axial component of the velocity and  $v_y$  is the radial component of the velocity.

It is visible in **Fig. 3-9** that eddies grow at  $t/T = 0.86$  and propagate at  $t/T = 0.93$  and  $t/T = 1$ . From **Fig. 3-10**, it can be seen that the width of these eddies is imposed by the width of the baffle, which equals to  $D - D_0$  and is not dependent of the amplitude of oscillations (or Strouhal number).



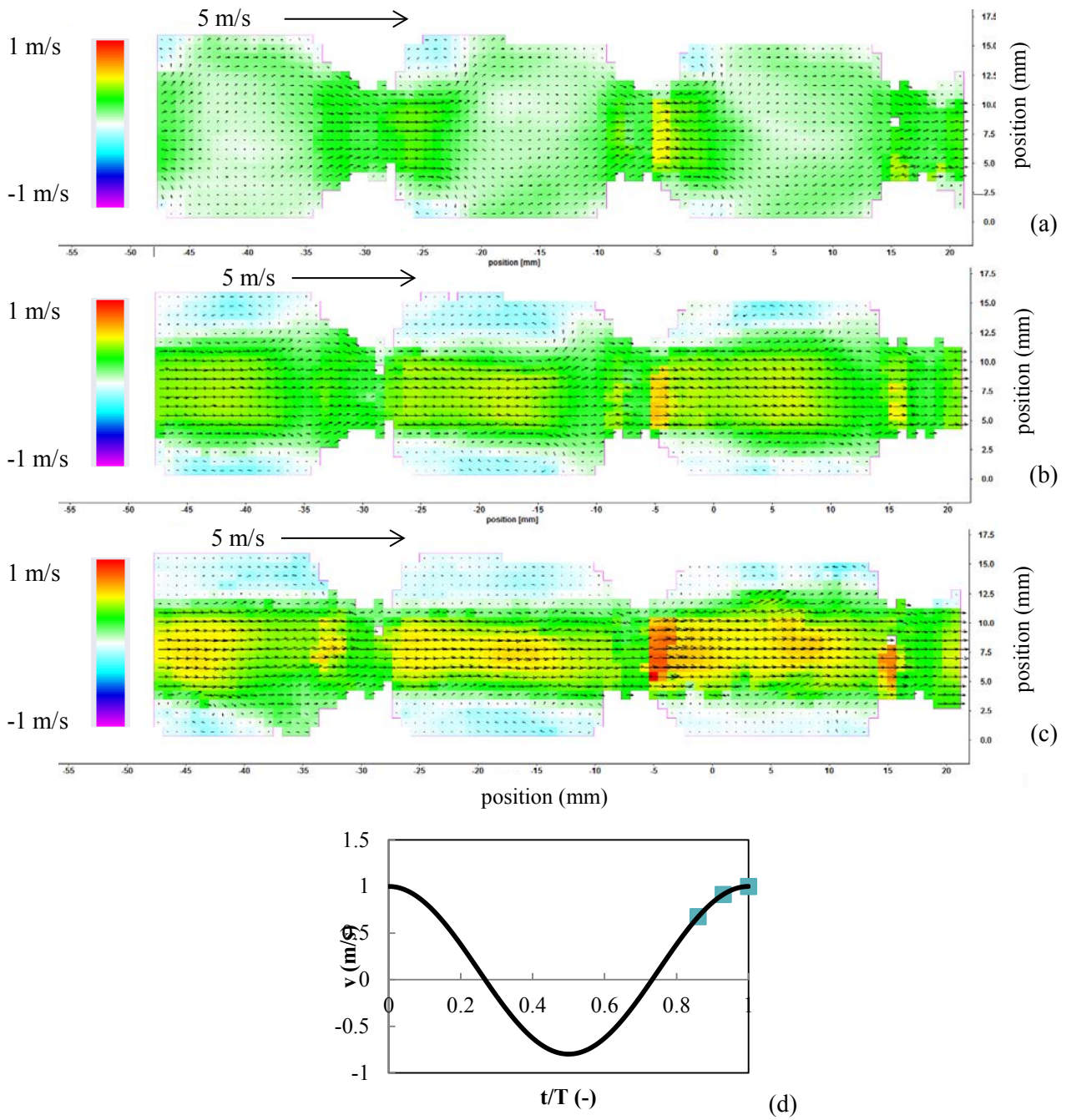


Fig. 3-7. Axial velocity field for  $t/T = 0.86$  (a),  $0.93$  (b) and  $1$  (c) at  $A = 20$  mm and  $f = 1$  Hz obtained by PIV measurements. Blue zones represent negative axial velocities. The positions of the different  $t/T$  on the velocity cycle are given in (d).

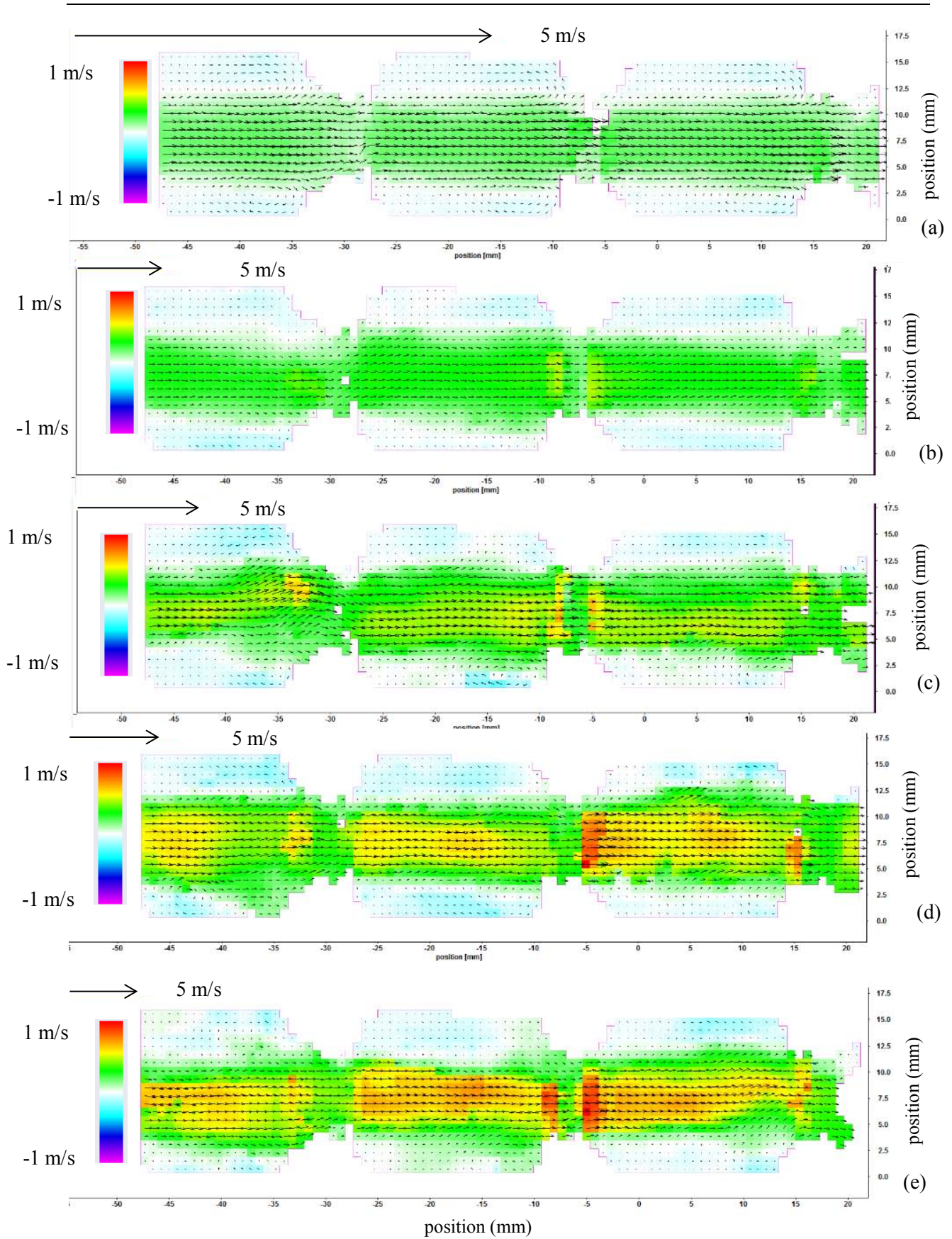
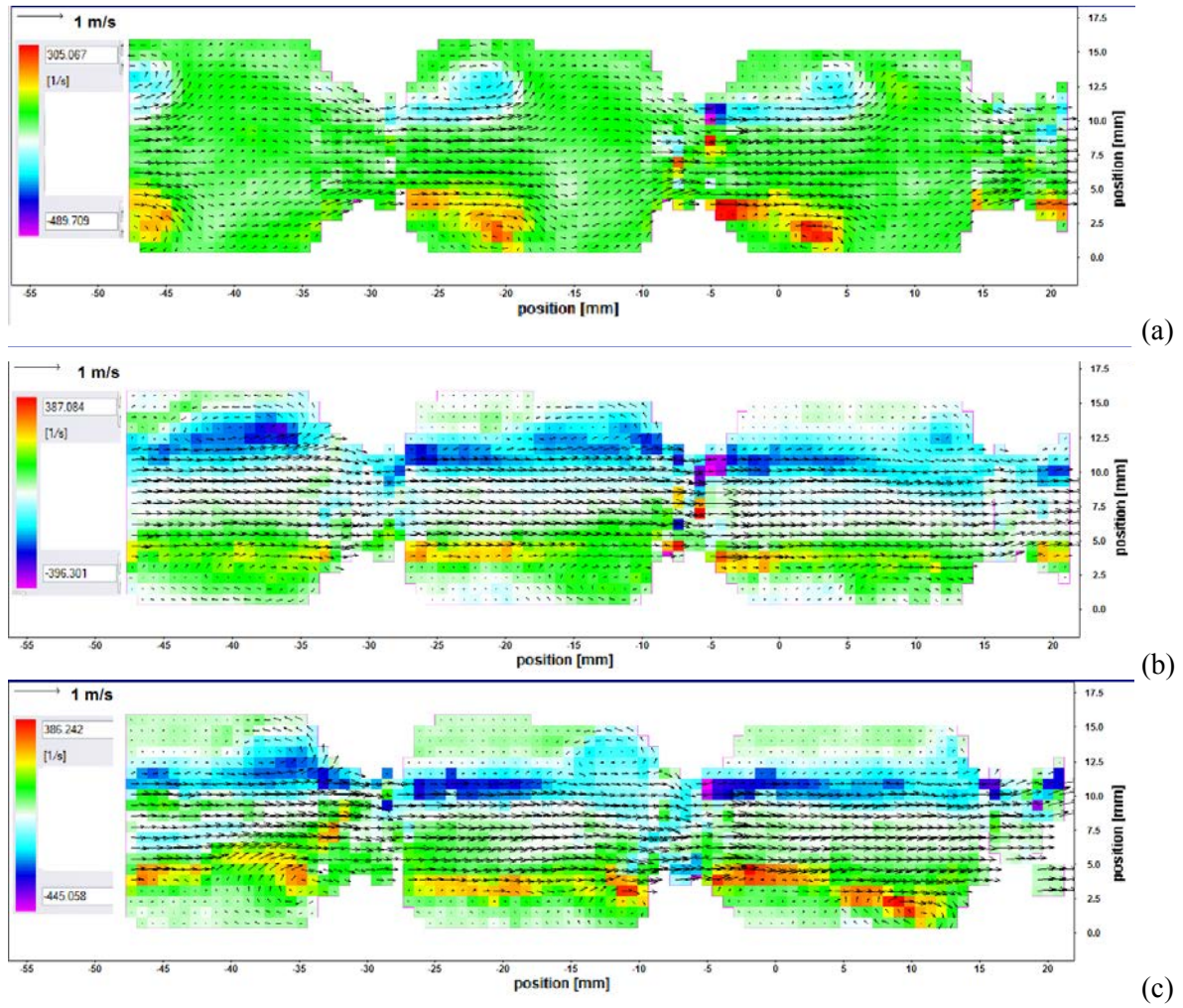
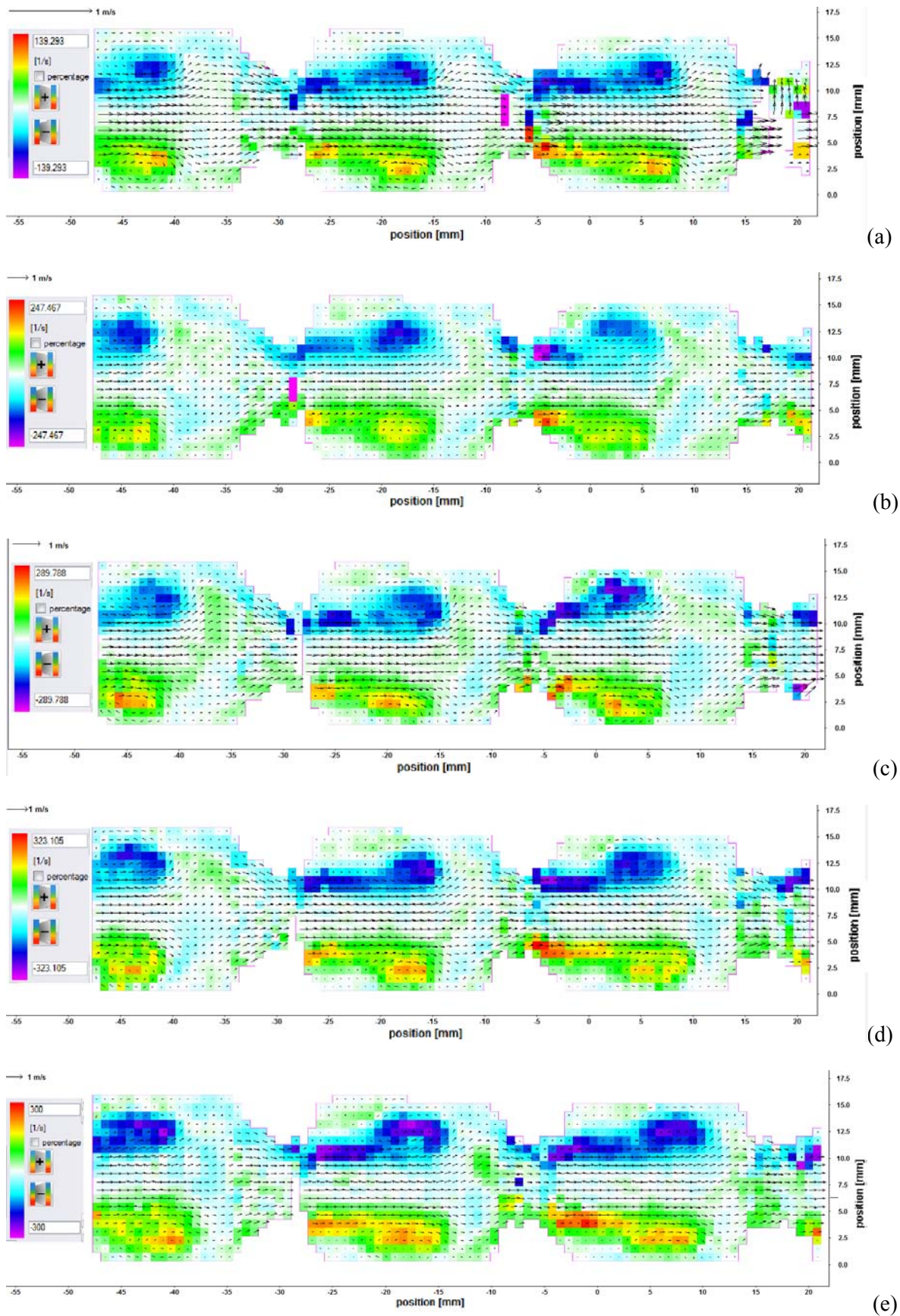


Fig. 3-8. Axial velocity field for  $A = 5$  (a), 10 (b), 15 (c), 20 (d), 25 (e) mm at  $t/T = 1$  and  $f = 1$  Hz obtained by PIV measurements. Blue zones represent negative axial velocities.



**Fig.3-9.** Vorticities and velocity fields for  $A = 20$  mm and  $f = 1$  Hz at (a)  $t/T = 0.86$ , (b)  $t/T = 0.93$  and (c)  $t/T = 1$  obtained by PIV measurements.



**Fig. 3-10.** Vorticities and velocity fields for  $A = 5$  (a), 10 (b), 15 (c), 20 (d), 25 (e) mm at  $t/T = 0.86$  and  $f = 1$  Hz obtained by PIV measurements.

### 3.2.3. Strain rate

**Fig. 3-11** represents the axial strain rate  $\varepsilon_{xx}$  calculated and displayed with the Davis software (**Eq. 3.2.3-1**). The maximum shear strain rate is obtained in the orifice of the baffles. Maximum values are 106, 203, 341, 405 and 587 s<sup>-1</sup> for A = 5, 10, 15, 20 and 25 mm.

$$\varepsilon_{xx} = \frac{\partial v_x}{\partial x}$$

**Eq. 3.2.3-1**

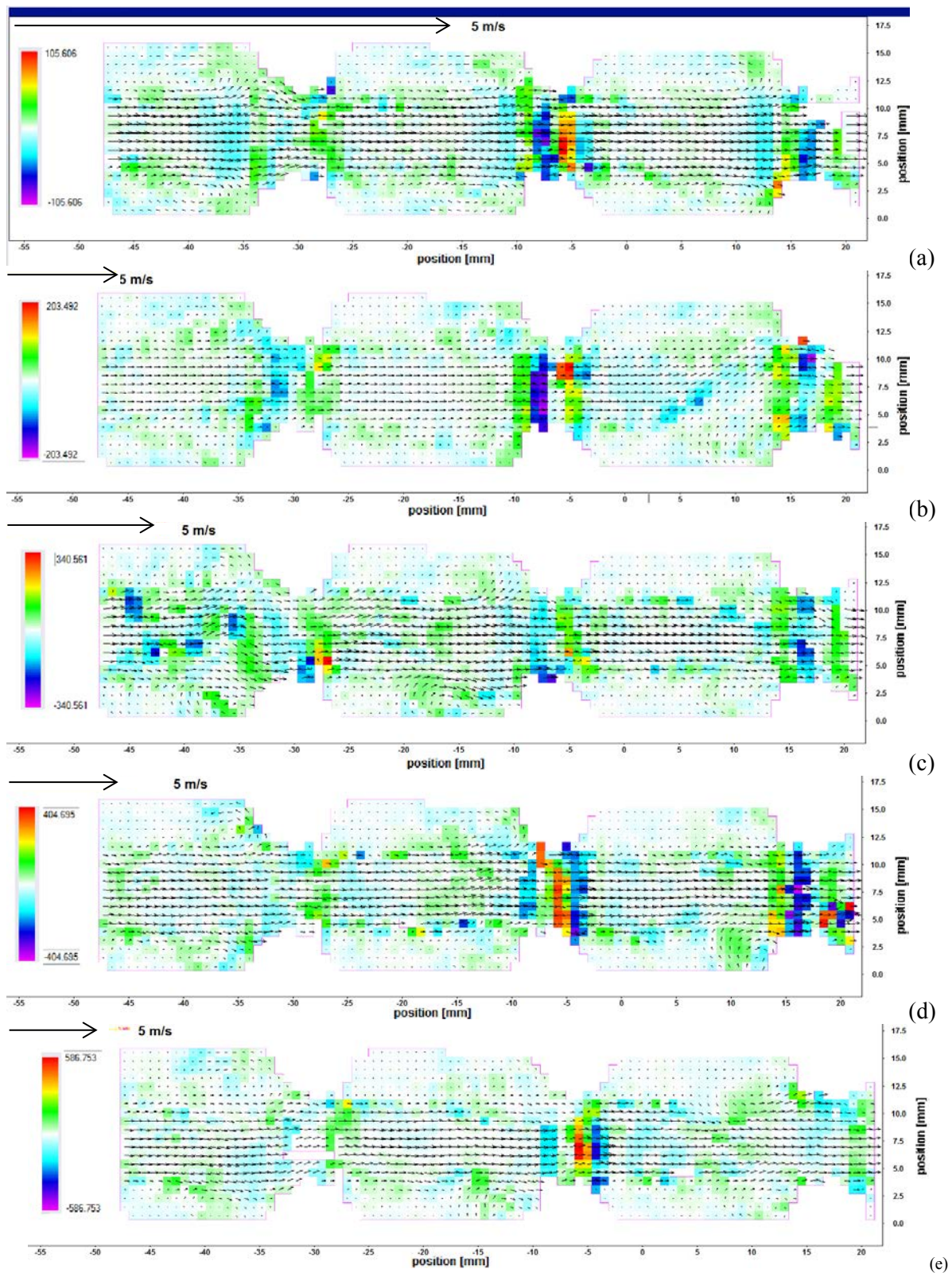


Fig. 3-11. Axial strain rate at  $A = 5$  (a), 10 (b), 15 (c), 20 (d), 25 (e) mm at  $t/T = 1$  and  $f = 1$  Hz obtained by PIV measurements. Maximum values of the axial strain rates are 106, 341, 405 and 587  $s^{-1}$ .

### 3.3. Conclusion

The PIV measurements allow the visualization of the velocity flows in the Nitech® glass reactor. Although the flow patterns in oscillatory flow reactors have been mainly described in

literature, they have been described in this paragraph with additional information, including axial velocities, vorticities and shear strain rates. The analysis has focused on the generation of eddies, which are responsible of the radial mixing in the reactor that is known to enhance the plug-flow behavior of the reactor. The size of eddies is time-dependent as they are formed during the increase of velocity (near its maximum value) in the forward semi-cycle, or during the decrease of velocity (near its minimum value) in the backward semi-cycle and they propagate in the whole cell, from one baffle to another. The similarity of normalized profiles of axial velocities as a function of  $Y$  at different viscosities and at different oscillatory amplitudes shows the existence of a laminar flow. Moreover, it has been observed through the calculation of axial velocities and the vorticities that the size and shape of the eddies are independent of the amplitude for the range of  $Re_0$  of 50-250. The width of eddies corresponds to the distance  $D-D_0$  in this range of  $Re_0$ . The strain rates have been calculated and increase linearly with the amplitude.

Further improvements could be obtained for this setup by synchronizing image acquisition with oscillation frequency to be perfectly in the same phase for different acquisitions. The frequency controller should also be replaced by a digital frequency controller, which is much more sensitive. This experimental setup has the advantage of being highly flexible, as it is possible to adapt it to other reactor designs with different baffle geometries.

In addition to this short experimental study, numerical simulations have been carried out to compare different baffle designs, and study the influence of the oscillatory conditions and net flow rate on different indicators of the mixing or the capacity to generate a liquid-liquid dispersion.

#### 4. Numerical simulations using Computational Fluid Dynamics (CFD)

The objective of the work described in this section is to use Computational Fluid Dynamics (CFD) simulations to evaluate mixing quality and liquid-liquid dispersion generation capacity of a given reactor geometry. To do this residence time distributions, position of initially adjacent particles and strain rates are calculated. The performance of different baffle designs and operating conditions are compared and the design(s) that are best adapted for the reactions of transformation of waste cooking oil are then identified. The PIV data of Section 3 have been used to validate the results of the numerical simulations presented in this section.

##### 4.1. Material and methods

This section details the definition of the geometry, the mesh and the methods used in the general purpose CFD software, *ANSYS CFX v.14.5.7*, as well as the data processing carried out with *Matlab*.

##### 4.1.1. Geometry and Mesh

Five OBR geometries with different baffle designs were generated with *Design Modeler*. The different baffle designs studied are shown in **Fig. 4-1** and the geometrical characteristics are given in **Table 4-1**. All the geometries correspond to a tube diameter of 15 mm. The single orifice baffles (B) are similar to the Nitech® reactor design previously used in the Part II; the discs and baffles (DB) consist of alternating discs and single orifice baffles (also called disc and doughnuts); spring 1 (S1) is a single helix ribbon; spring 2 (S2) is a single helix ribbon that changes turning direction every period; the double spring (DS) consists of two helix ribbons (like a strand of DNA).

**Table 4-1.** Characteristics of the different baffle designs.

<b>Baffle design</b>	<b>B</b>	<b>DB</b>	<b>S1</b>	<b>S2</b>	<b>DS</b>
Distance between 2 baffles or pitch of spring (mm)	26	26	26	26	26
Change of spring turning direction (mm)	-	-	No change	Every 52 mm (2 cells)	No change
Distance between baffle and disc or distance between two springs (mm)	-	13	-	-	13
Tube diameter (mm)	15	15	15	15	15
Orifice or opening diameter (mm)	8	8	7.5	7.5	7.5
Length of first and last cell (mm)	25	25	25	25	25
Baffle thickness (mm)	2	2	1	1	1



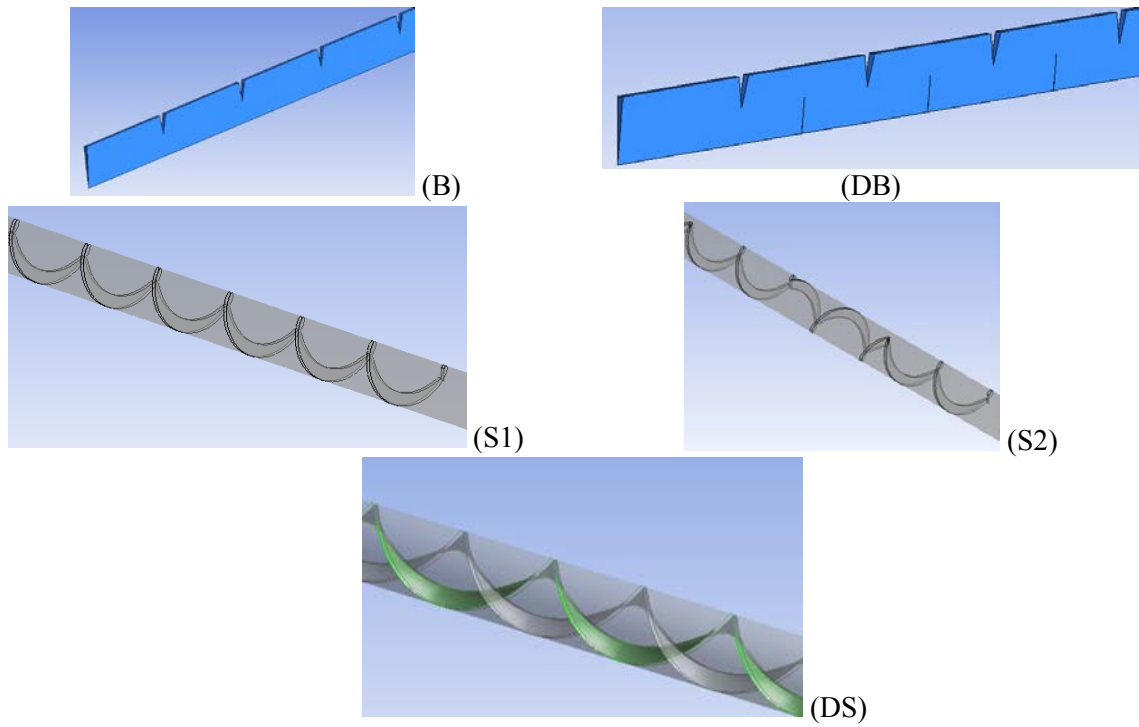


**Fig. 4-1.** Different baffle geometries used in the 15 mm diameter tube (a): single orifice baffles (B), discs and baffles (DB), spring baffle (S1), spring baffle with two senses (S2) and double spring (DS).

The mesh for geometries B and DB contain approximately 20 000 elements (40 000 nodes). The mesh for geometries S1, S2 and DS contain 900 000 elements (290 000 nodes). The meshes are shown in **Fig 4-2**.

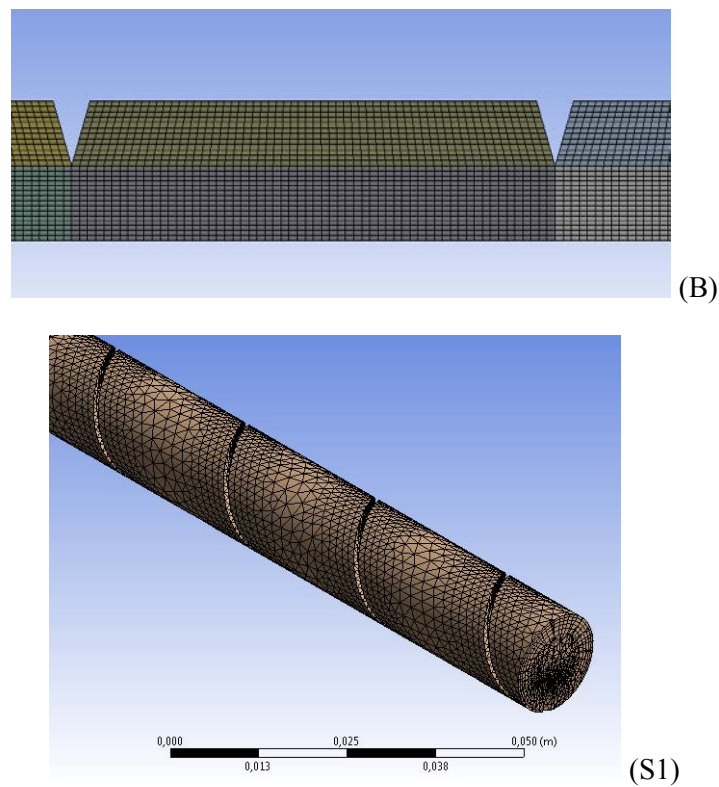


**Fig. 4-2.** The mesh used for geometries B (similar to the mesh of DB) and S1 (similar to the mesh of S2 and DS).

### 4.1.2. Numerical methods

The numerical simulations of the flow in the OBR geometries was performed using *ANSYS CFX v.14.5.7*. This is a commercial CFD package which solves the Navier-Stokes equations using a finite volume method via a coupled solver. These equations are the continuity equation (**Eq. 4.1.2-1**) and momentum equation (**Eq. 4.1.2-2**):

$$\frac{\partial}{\partial x_j} [\rho u_j] = 0 \quad \text{Eq. 4.1.2-1}$$

$$\frac{\partial}{\partial t} (\rho u_i) + \frac{\partial}{\partial x_j} (\rho u_i u_j + P \delta_{ij} - \tau_{ij}) = 0 \quad \text{Eq. 4.1.2-2}$$

where  $u_i$  is the velocity component (m/s),  $\rho$  is the density (kg/m<sup>3</sup>),  $P$  is the pressure (Pa), the viscous stress  $\tau_{ij}$  equals to:

$$\tau_{ij} = 2\mu S_{ij} \quad \text{Eq. 4.1.2-3}$$

where the viscous strain rate is defined by:

$$S_{ij} = \frac{1}{2} \left( \frac{\partial u_i}{\partial x_j} + \frac{\partial u_j}{\partial x_i} \right) \quad \text{Eq. 4.1.2-4}$$

The solver uses a second order upwind biased discretization. Simulations were considered converged when the normalized residuals for the velocities and pressure are below  $1 \times 10^{-4}$ . The velocity fields in the OBR are first solved to provide an initial condition. These calculations were then restarted in transient mode to calculate the particle trajectories within the flow field, which are used to characterize the axial dispersion, the strain rate and the axial and difference of position of initially adjacent particles.

#### 4.1.2.1. Flow computation

The fluid considered in these simulations is a model Newtonian fluid with density,  $\rho = 921.7 \text{ kg/m}^3$  and dynamic viscosity,  $\mu = 0.035 \text{ Pa}\cdot\text{s}$ . This corresponds to the properties of a mixture of oil and methanol at 25°C and a molar ratio of methanol to oil of 6. The model used to describe this fluid is laminar, since the low viscosity of the liquid implies low Reynolds numbers. The simulation is transient due to the time dependence of the oscillatory flow. The velocity in the reactor is given by the equation:

$$v = v_{net} + 2\pi f x_0 \cos(2\pi f t) \quad \text{Eq. 4.1.2.1-1}$$

The boundary condition at the OBR inlet is described by a laminar velocity profile at  $t = 0$  with the equation:

$$v(t = 0) = v_{initial} = 2v \left( 1 - \left( \frac{r}{R} \right)^2 \right) \quad \text{Eq. 4.1.2.1-2}$$

where  $r$  is the radial position  $r = (Y^2 + Z^2)^{1/2}$  and  $R$  is the radius of the reactor (7.5 mm).

#### 4.1.2.2. Particle tracking

Small particles, having the same density of the fluid, are followed using a Lagrangian particle tracking method. Their diameter is set at  $1 \times 10^{-6} \text{ m}$  and they are initially located at the same  $X$ -position

( $X_0$ ) along the  $Y$ -axis. The number of particles has been fixed at 2484 for 2D geometries and 4968 for 3D geometries. With this method, there is no interaction between particles, their Stokes number is so small that they follow the flow faithfully and molecular diffusion is not taken into account. The movement of the particles in the flow is determined by integrating the vector equation of motion for each particle and the kinematic equation to determine its position:

$$m_p \frac{d\vec{v}}{dt} = F_D \quad \text{and} \quad \frac{d\vec{x}}{dt} = \vec{v}(x) \quad \text{Eq. 4.1.2.2-1}$$

where  $m_p$  is the mass of the particle and  $F_D$  is the drag force, calculated using the Schiller Naumann drag law. This equation of motion is integrated with a fourth-order Runge-Kutta scheme with adaptive step size. Information available on these particles is: the position on the  $X$ ,  $Y$  and  $Z$ -axis, travel time ( $t$ ), the local fluid strain rate (FSR) and the three velocity components ( $v$ ).

The effect of the variation of the oscillatory Reynolds number has been investigated over the range 26 to 66, by varying the amplitude from 5 mm to 25 mm and frequency from 0.635 Hz to 1.606 Hz, at a fixed net velocity fixed to  $1.405 \times 10^{-2}$  m/s, which corresponds to a flow rate of 8.9 L/h and a net Reynolds number of 6. This corresponds to the flow rate obtained in the Nitech® reactor in Part II, Chapter 2. The effect of the net Reynolds number has been also investigated over the range 3.7 to 9.3 by varying the net velocity from 9.435 mm/s to 23.58 mm/s. The information collected for particles at each time step is used to determine quantitative indicators that characterize mixing or liquid-liquid dispersion.

#### *Distance separating initially adjacent particles*

The  $X$ - and  $Y$ -distances separating initially adjacent particles are followed as a function of time. This is used to quantify mixing: fluid elements experiencing high separation in the  $Y$ -direction are in zones of good radial mixing, whereas fluid elements with very little separation experience poorly radial mixing. Small separation distances in the  $X$ -direction highlight near plug-flow behavior, whereas large separation distances suggest a wide residence time distribution.

Calculations are performed for pairs of adjacent particles. The time evolution of the distance separating the pair of particles is determined at every time step for 50 s. The principle of the calculations is given for one pair of particles in **Fig. 4-3**.

At time  $t$ ,  $\Delta X = X(\text{particle A}) - X(\text{particle B})$

$\Delta X(t)$  is integrated for each pair of particles ( $I_c$ ):

$$I_c = \frac{1}{t_n} \sum_{i=0}^{t_n} \frac{\Delta X_{i+1} + \Delta X_i}{2} (t_{i+1} - t_i) \quad \text{Eq. 4.1.2.2-2}$$

The average value of  $I_c$  is calculated ( $I_m$ ):

$$I_m = \frac{1}{n_{\text{particles}}} \sum_{i=0}^n I_c(i) \quad \text{Eq. 4.1.2.2-3}$$

and the standard deviation  $\sigma$ :

$$\sigma(I) = \sqrt{\frac{1}{n_{\text{particles}}} \sum_{i=0}^n I_c(i)^2 - I_m^2} \quad \text{Eq. 4.1.2.2-4}$$

An analogous calculation is made for the radial separation (with  $R = (Y^2 + Z^2)^{1/2}$ ).

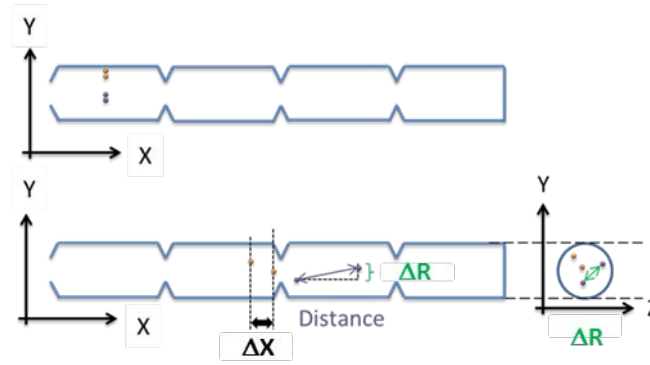


**Fig. 4-3.** Principle of the calculations on the time evolution of the distance separating initially adjacent particles. After a given time, the axial distance  $\Delta X$ , and the radial distance  $\Delta R$  separating each pair of particles are calculated.

### *Residence time distribution*

The RTD for the fluid flowing through the various OBR geometries was calculated by determining the particle trajectories and by recording the particle residence times from 248 mm after the inlet to 166 mm before the outlet of the OBR geometry. The residence time distribution can then be calculated by the following equation [40]:

$$E(t) = \frac{\Delta N_w}{N_w} \frac{1}{\Delta t} \quad \text{Eq. 4.1.2.2-5}$$

where  $\Delta N_w$  is the number of particles that have a residence time in the reactor between time  $t$  and  $t + \Delta t$  each weighted by their initial velocity normalized by the maximum velocity in the tube, and  $N_w$  is the total number of particles released in the reactor. From  $E(t)$ , the first and second moments are the mean residence time  $t_m$  and the variance  $\sigma^2$ . The reactor Péclet number  $Pe$  is given by the following equation, valid for open-open vessel:

$$\frac{\sigma^2}{t_m^2} = \frac{2}{Pe} + \frac{8}{Pe^2} \quad \text{Eq. 4.1.2.2-6}$$

The Péclet number is defined as:

$$Pe = \frac{uL}{D_{ax}} \quad \text{Eq. 4.1.2.2-7}$$

where  $L$  is the length of the tube and  $D_{ax}$  is the axial dispersion coefficient. The principle of the determination of Péclet number and axial dispersion coefficient is illustrated in **Fig. 4-4**. The characteristic length  $L$  corresponds to the distance between the plane where the particles are released (at  $X = X_0$ ) and the plane where the residence times of particles are recorded (at  $X = X_{detection}$ ).

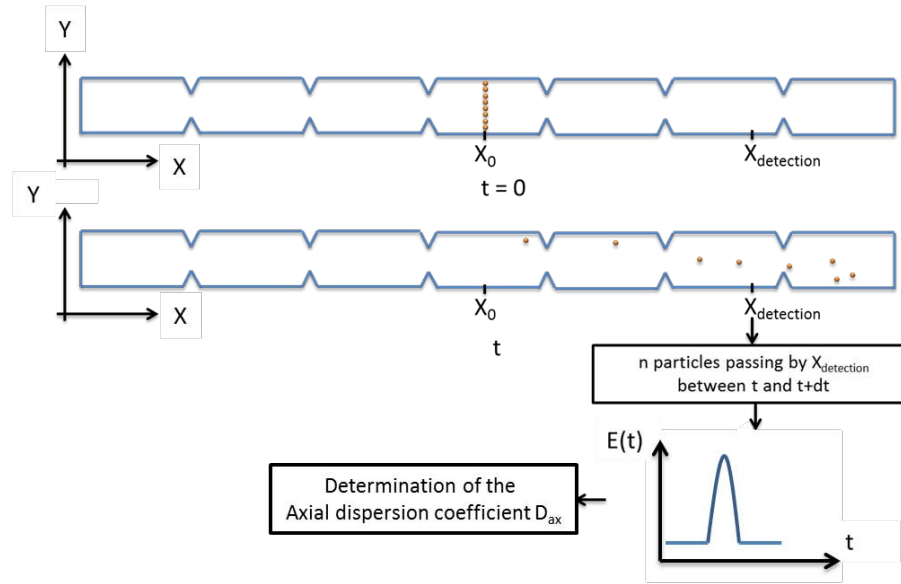


**Fig. 4-4.** Particles, distributed on the  $Y$ -axis, are released at the position  $X_0$ . The number of particles passing the  $X_{\text{detection}}$  between a time  $t$  and  $t + dt$  are counted. This leads to the residence time distribution function  $E(t)$ , from which the axial dispersion coefficient  $D$  is determined.

### Shear strain rate history

The shear strain rate tensor is given by

$$S_{ij} = \frac{1}{2} \left( \frac{\partial u_i}{\partial x_j} + \frac{\partial u_j}{\partial x_i} \right) \quad \text{Eq. 4.1.2.2-8}$$

which gives the following equation, for an incompressible fluid, for the magnitude of the strain rate

$$SSR = \left[ \left( \frac{\partial u_x}{\partial y} + \frac{\partial u_y}{\partial x} \right)^2 + \left( \frac{\partial u_x}{\partial z} + \frac{\partial u_z}{\partial x} \right)^2 + \left( \frac{\partial u_y}{\partial z} + \frac{\partial u_z}{\partial y} \right)^2 \right]^{1/2}$$

$$\text{Eq. 4.1.2.2-9}$$

This provides an indication of the capacity of the flow in each geometry to provide sufficient shear rates for drop breakup, which is important for liquid-liquid dispersion and emulsion applications. At every time step, the strain rate magnitude is recorded for each particle. The maximum strain rate and the mean strain rate for each particle over time are then calculated. Finally, the average strain rate experienced by the ensemble of particles is determined.

## 4.2. Validation of the method

The parameters fixed for the mesh, the particle tracking and the geometry are justified in this paragraph to show they do not impact the results obtained by the numerical methods. Secondly, the velocity fields obtained by PIV measurements have been compared with the velocity fields obtained by CFD.

### 4.2.1. Influence of the size of the mesh

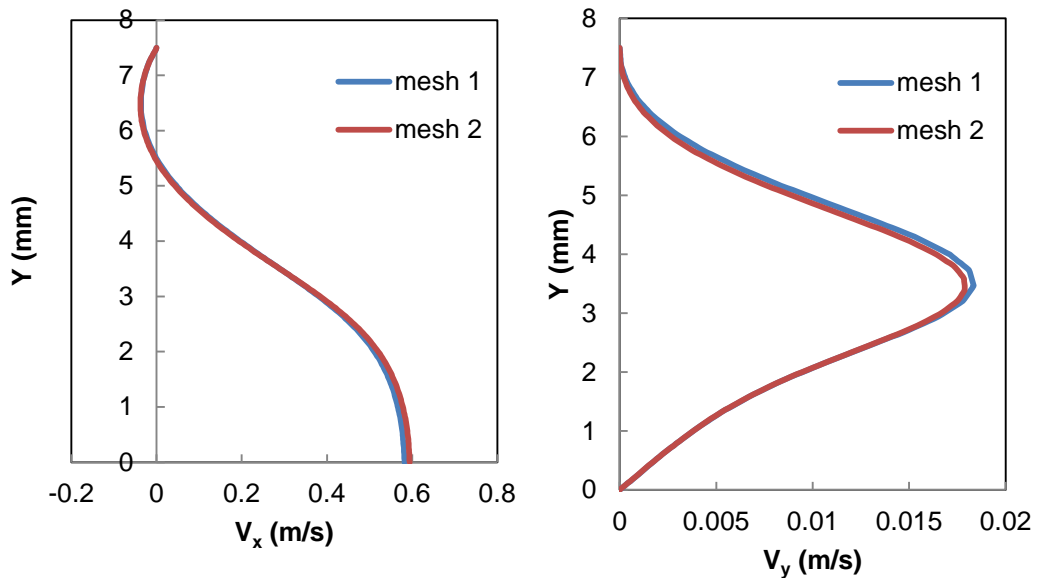
Due to the geometrical symmetry, the B and DB geometries have been simulated in 2D using a thin wedge with symmetry boundary conditions on the front and back faces. This hypothesis is justified since a symmetrical flow pattern has been verified for oscillatory Reynolds numbers less than 255 [32], which is the case in our simulations ( $Re_o < 66$ ).

The mesh has to be sufficiently fine for the results to be independent of the size of the mesh. Three mesh sizes have been tested (see **Table 4-2** and **Fig. 4-5**) for the two-dimensional geometry, which concerns tubes with single orifice baffles or with disc and baffles. The oscillatory conditions are fixed at  $A = 16.5$  mm and  $f = 1.05$  Hz.

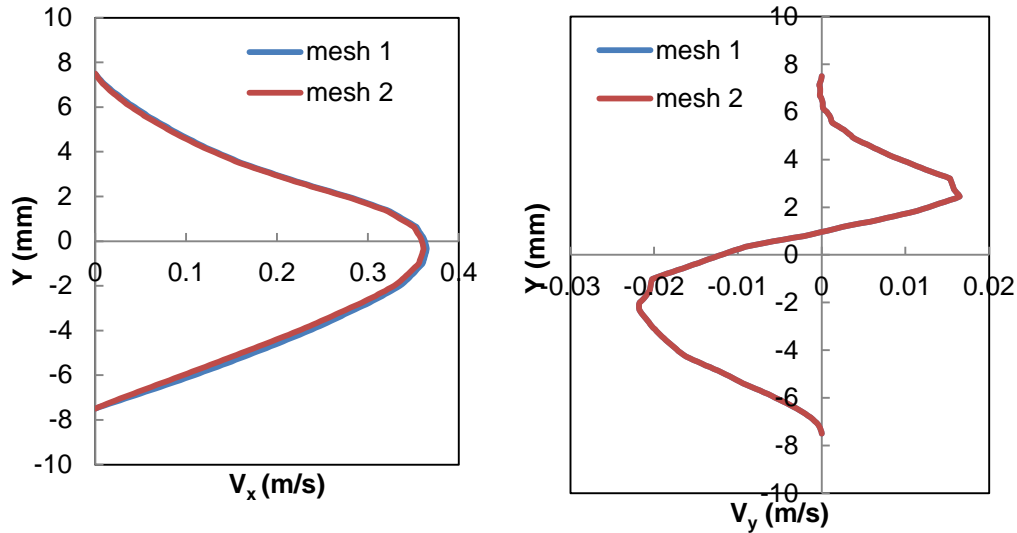
The axial and radial velocity profiles  $V_x$  and  $V_y$  at  $X = 58$  mm in geometries B and S1 are given in **Fig. 4-5**. The relative difference is 2.0 % between the maximum axial velocities and 2.6% between the maximum radial velocities in B and the relative difference is 0.9% between the maximum axial velocities and is 0% between the maximum radial velocities. The CFD solution is independent of mesh for the two-dimensional and to the three-dimensional geometries.

**Table 4-2.** Characteristics of the different tested meshes The different meshes used for the two-dimensional geometries are named 2D. Two lengths have been used corresponding to 10 or 20 baffles, named 1L or 2L. The meshes used for the three-dimensional geometries are named 3D.

2D			
Geometry			
Mesh	Nodes	Elements	$n_{\text{baffles}}$
1-2D-1L	39919	19440	10
2-2D-1L	70505	34560	10
3-2D-1L	109731	54000	10
1-2D-2L	73159	35640	20
2-2D-2L	129225	63360	20
3D			
geometry			
Mesh	Nodes	Elements	$n_{\text{baffles}}$
1-3D	289502	902049	20
2-3D	495306	1578932	20



(B)



(S1)

Fig. 4-5. Axial and radial velocity profiles as a function of  $Y$  at  $X = 58$  mm for  $A = 16.5$  mm and  $f = 1$  Hz in (B) and (S1) obtained with mesh 1 and mesh 2.

Table 4-3 shows the influence of the size of the mesh on the axial dispersion coefficient, the mean residence time and the fraction of particles reaching  $X_{detection}$ . The calculation of axial dispersion coefficient shows good reproducibility and the independence of the size of the mesh on the results. For  $A=16.5$  mm,  $f = 1.05$  Hz, two meshes for the reactor with single orifice baffles with 20 cells have been tested and the relative difference between mesh 1 and mesh 2 of the axial dispersion coefficient, the mean residence time and the fraction of particles reaching  $X_{detection}$  is less than 6%. For three-dimensional meshes, the difference the two mesh sizes tested is low, with a relative difference less than 1.1%.

Table 4-3. Influence of the size of the mesh on axial dispersion coefficient  $D_{ax}$ , mean residence time ( $t_m$ ) and fraction of particles that have passed " $X_{detection}$ ".

Baffle design	$n_{baffles}$	$X_{detection}$	$X_0$	$D_{ax}$ ( $m^2/s$ )	$t_m$ (s)	Fraction	mesh
B	20	404	248	2.05E-03	5.8	98.40%	1-2D-2L
		404	248	2.17E-03	5.4	98.80%	2-2D-2L
	<b>Relative difference (%)</b>				<b>5.9</b>	<b>6.0</b>	<b>0.4</b>
S1	20	404	248	1.29E-03	6.1	98.2	1-3D
		404	248	1.28E-03	6.2	98.3	2-3D
	<b>Relative difference (%)</b>				<b>0.8</b>	<b>1.1</b>	<b>0.1</b>

The calculation of difference of the distance separating initially adjacent particles is not affected by a decrease of the refinement of the mesh. Results of the influence of the size of the mesh are given in Table 4-4. Different meshes have been tested, leading to relative differences less than 5.1% between the mesh 1 and 2 in all the cases. Therefore mesh 1 is considered as being sufficiently fine.

**Table 4-4.** Influence of the size of the mesh for calculations of difference of position of initially adjacent particles.  $\Delta X$  and  $\Delta R$  are the mean difference of particle position on the  $X$ -axis and on the  $YZ$  plan. Std is the associated standard deviation representing the distribution of this difference over particles. Oscillatory conditions are fixed at  $A = 16.5$  mm and  $f = 1$  Hz.

Baffle design	$n_{baffles}$	$\Delta X$ (mm)	Std $\Delta X$ (mm)	$\Delta R$ (mm)	Std $\Delta R$ (mm)	mesh
B	10	43.3	27.4	1.6	0.62	1-2D-1L
	10	42.7	26	1.62	0.64	2-2D-1L
	10	42.7	26.8	1.6	0.64	3-2D-1L
<b>Relative difference mesh 1-mesh 2 (%)</b>		<b>1.4%</b>	<b>5.1%</b>	<b>1.3%</b>	<b>3.2%</b>	
<b>Relative difference mesh 2 - mesh 3 (%)</b>		<b>0.0%</b>	<b>3.1%</b>	<b>1.2%</b>	<b>0.0%</b>	
B	20	67.6	36.5	1.87	0.55	1-2D-2L
	20	65.3	37.7	1.8	0.55	2-2D-2L
<b>Relative difference (%)</b>		<b>3.4%</b>	<b>3.3%</b>	<b>3.7%</b>	<b>0.0%</b>	
S1	20	49.2	26.3	1.92	0.41	1-3D
	20	49.5	26.4	1.93	0.43	2-3D
<b>Relative difference (%)</b>		<b>0.6%</b>	<b>0.4%</b>	<b>0.5%</b>	<b>2.4%</b>	

The influence of the size of the mesh for the calculation of the particle strain rate is presented in **Table 4-5**. The results are the same for the three tested meshes, with a maximum relative difference below 0.4%.

**Table 4-5.** Influence of the size of the mesh for calculations of average and maximum fluid strain rates (FSR) with their corresponding standard deviations. Oscillatory conditions are fixed at  $A = 16.5$  mm and  $f = 1$  Hz.

Baffle design	B			S1		
	$n_{baffles}$	10	10	10	20	20
mesh	1-2D-1L	2-2D-1L	3-2D-1L	1-3D	2-3D	
<b>Ave. FSR (<math>s^{-1}</math>)</b>	44.5	44.4	44.5	43.2	43.2	
<b>Rel. diff. to mesh n-1 (%)</b>	-	0.3	0.2	-	0.1	
<b>std FSR (<math>s^{-1}</math>)</b>	6.5	6.7	6.5	2.4	2.4	
<b>Rel. diff. to mesh n-1 (%)</b>	-	2.6	0.1	2.4	1.2	
<b>ave max FSR (<math>s^{-1}</math>)</b>	286.5	286.2	286.3	243.1	242.2	
<b>Rel. diff. to mesh n-1 (%)</b>	-	0.1	0.0	-	0.4	
<b>std max FSR (<math>s^{-1}</math>)</b>	48.9	49.8	49.5	41.2	41.3	
<b>Rel. diff. to mesh n-1 (%)</b>	-	1.8	0.7	-	0.2	

The presented results are independent of the mesh size. The mesh 1-2D for geometries B and S1 has been used for the rest of the study. The mesh 1-2D used for geometry B has also been used for geometry DB. The mesh 1-3D used for geometry S1 has also been used for geometry S2 and DS.



#### 4.2.2. Influence of number of particles

**Table 4-6** shows the influence of the number of particles released at  $X_0$  on the statistics concerning the axial dispersion coefficient, difference of position of initially adjacent particles, and strain rate history in the single orifice baffle (B) geometry with  $A = 16.5$  mm,  $f = 1.05$  Hz,  $X_0 = 0.248$  mm and  $X_{detection} = 404$  mm. It can be seen from **Table 4-6** that the results obtained on the distance separating initially adjacent particles, the residence time distribution and the fluid shear strain rates converge for a total of 2484 particles. As a result, 2484 particles were used for all other simulations.

**Table 4-6.** Influence of the number of particles on the difference of position of initially adjacent particles on  $X$  ( $\Delta X$ ) and  $R$  ( $\Delta R$ ), the axial dispersion coefficient  $D_{ax}$ , the mean residence time  $t_m$ , the fraction of particles which has reached  $X_{detection}$  and the time-averaged and maximum fluid strain rate with their associated standard values.

No. particles	150	2484	4968	Rel. diff. 150-2484 particles (%)	Rel. diff. 2484-4968 particles (%)
$\Delta X$ (mm)	75.1	67.6	66.3	10.0	1.9
std $\Delta X$ (mm)	33.0	36.5	37.0	10.6	1.4
$\Delta R$ (mm)	2.1	1.9	1.9	9.5	0.0
std $\Delta R$ (mm)	0.64	0.55	0.54	14.1	1.8
$D_{ax}$ (m <sup>2</sup> /s)	2.03E-3	2.05E-3	2.11E-3	1.0	2.9
$t_m$ (s)	6.2	5.8	5.7	7.3	0.9
Frac (%)	98.7	98.4	98.2	0.3	0.2
ave FSR (s <sup>-1</sup> )	44.2	44.2	43.4	0.0	1.8
std FSR (s <sup>-1</sup> )	5.4	6.3	6.1	16.7	3.2
ave max FSR (s <sup>-1</sup> )	299.3	296.2	296.2	1.0	0.0
std max FSR (s <sup>-1</sup> )	39.6	42.7	44.7	7.8	4.7

#### 4.2.3. Length of the tube and parameters for particle injection

The oscillatory motion of the flow in the reactor implies that the axial positions, where the particles are released ( $X_0$ ) and where residence time is measured ( $X_{detection}$ ), have to be carefully chosen. Indeed if the  $X_0$  and  $X_{detection}$  are too close to the tube inlet and outlet, respectively, the particles can leave the computational domain due to the oscillating flow, but cannot re-enter. To avoid this, the tube has to be sufficiently long and  $X_0$  and  $X_{detection}$  must be at a sufficient distance from the inlet and outlet, respectively. Furthermore, the simulation time must be long enough to allow a maximum number of particles to flow from  $X_0$  to  $X_{detection}$ . It was found that 98% of the particles released at  $X_0$  reached  $X_{detection}$  within 50 s so the simulation time was set to 50 s.

To determine the necessary reactor length and the positions of  $X_0$  and  $X_{detection}$ , calculations have been carried out for the single orifice baffle geometry with an amplitude of 16.5 mm, a frequency of 1.05 Hz and a net velocity of  $1.405 \times 10^{-2}$  m/s. **Fig. 4-6** and **Table 4-7** show the fraction of particles measured at  $X_{detection}$  and the axial dispersion coefficient for different reactor lengths and different positions of  $X_0$  and  $X_{detection}$ . The first reactor length is 310 mm, corresponding to 10 baffles. It can be seen that fraction of particles measured at  $X_{detection}$  is not greater than 95%. Indeed, it was observed that some particles leave the computational domain via the inlet and outlet, but do not re-enter the domain, which is physically incorrect. When the reactor length is increased to 570 mm, which corresponds to 20 baffles, the fraction of particles detected at  $X_{detection}$  is greater than 98% for five of the seven cases tested, as it can be seen in **Fig. 4-6**. The criterion for the choice of the length is a fraction of particles

greater than 98% and a maximum distance between  $X_0$  and  $X_{detection}$  (minimize  $X_0$  and maximize  $X_{detection}$ ). Based on this criteria, the reactor length was set to 570 mm and the positions  $X_0 = 248$  mm and  $X_{detection} = 404$  mm for all of the following simulations. The fraction of particles also has a major role in the accuracy of the calculated axial dispersion coefficient as it can be seen in **Fig. 4-7**, indeed the value of the axial dispersion coefficient increases by a factor of two if the fraction of particles increases from 92-95% to 98%. The uncertainty of the axial dispersion coefficient has been estimated at 8%.

**Table 4-7.** Influence of  $X_0$ ,  $X_{detection}$  and  $L$  on the fraction of particles that have passed the  $X_{detection}$  position.

10 baffles:  $L = 310$  mm:

$X_0$ (mm)	$X_{detection}$ (mm)	$X_{detection}/L$ (-)	Fraction (-)	$D_{ax}$ (m/s)
64	125	0.40	94.5%	8.5E-04
64	175	0.56	93.2%	9.6E-04
64	225	0.73	92.5%	1.0E-03

20 baffles:  $L = 570$  mm:

$X_0$ (mm)	$X_{detection}$ (mm)	$X_{detection}/L$ (-)	Fraction (-)	$D_{ax}$ (m/s)
169	322	0.56	98.1%	2.0E-03
169	375	0.66	97.62%	1.9E-03
248	352	0.62	98.9%	2.1E-03
<b>248</b>	<b>404</b>	<b>0.71</b>	<b>98.4%</b>	<b>2.0E-03</b>
272	375	0.66	98.9%	2.4E-03
272	425	0.75	98.4%	2.2E-03
272	475	0.83	97.8%	2.2E-03
<b>Average</b>				2.11E-03
<b>Standard deviation (%)</b>				8%

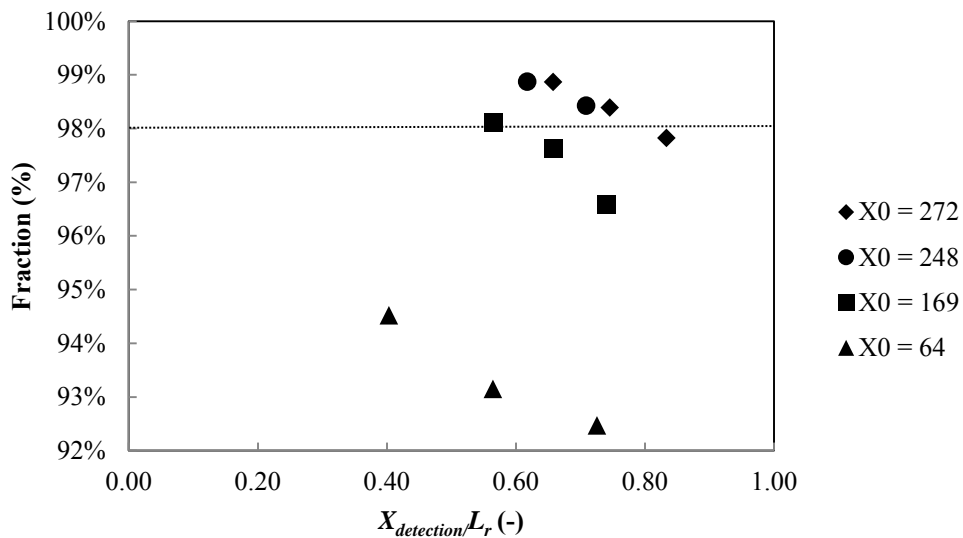


**Fig. 4-6.** Influence of  $X_0$ ,  $X_{detection}$  on the fraction of particles which has passed the  $X_{detection}$  position.

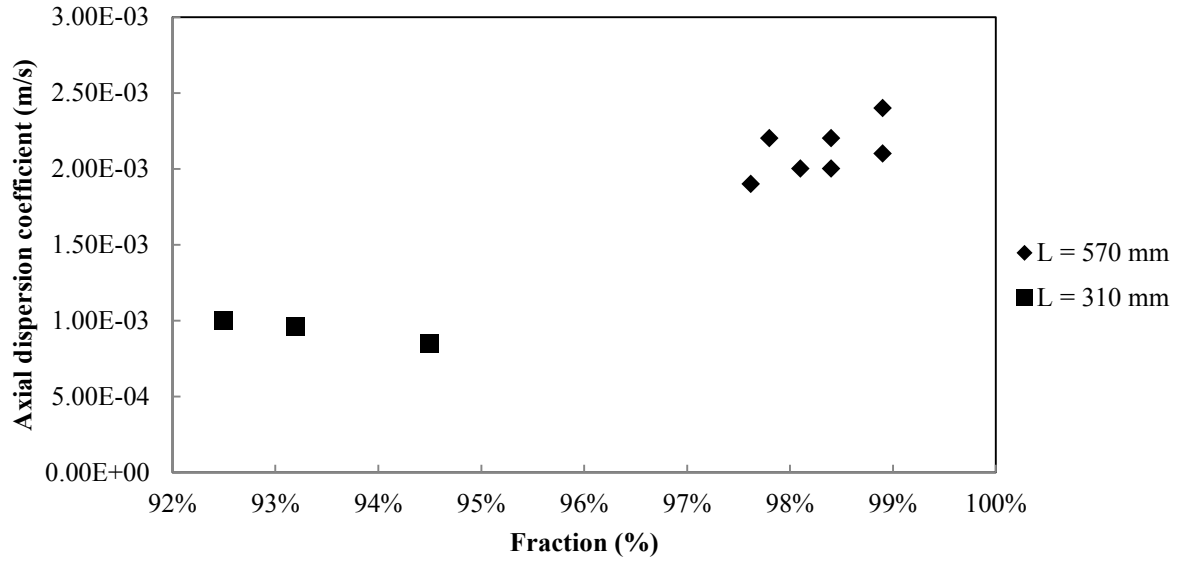
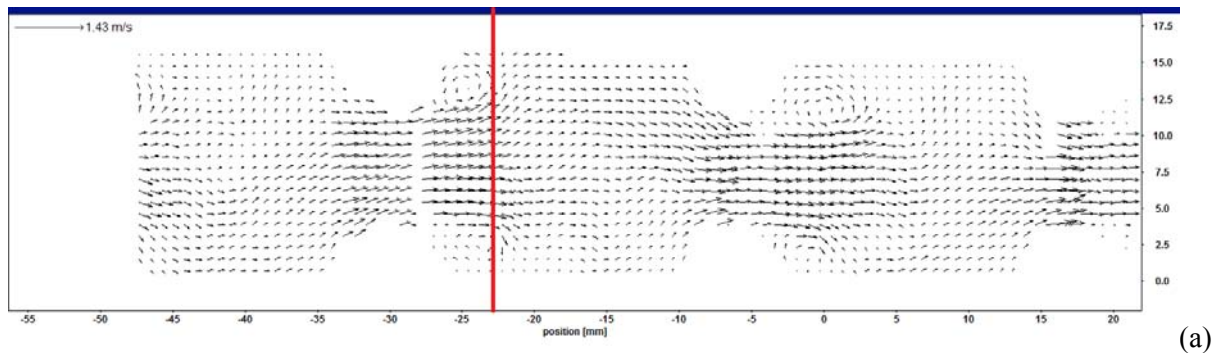


Fig. 4-7. Influence of the fraction of particles on the axial dispersion coefficient.

#### 4.2.4. Comparison of the velocity fields obtained by CFD and by PIV

Fig. 4-8 shows the velocity fields obtained at  $t/T = 0.86$  by PIV (a) and by CFD (b), which corresponds to the apparition of the vortices near baffles for a positive displacement of the flow. The velocities obtained by PIV measurements are compared with those obtained in simulation for the same conditions. In both cases, a toroidal recirculating eddy is formed near a baffle, which is represented in two-dimension by two eddies.



(a)

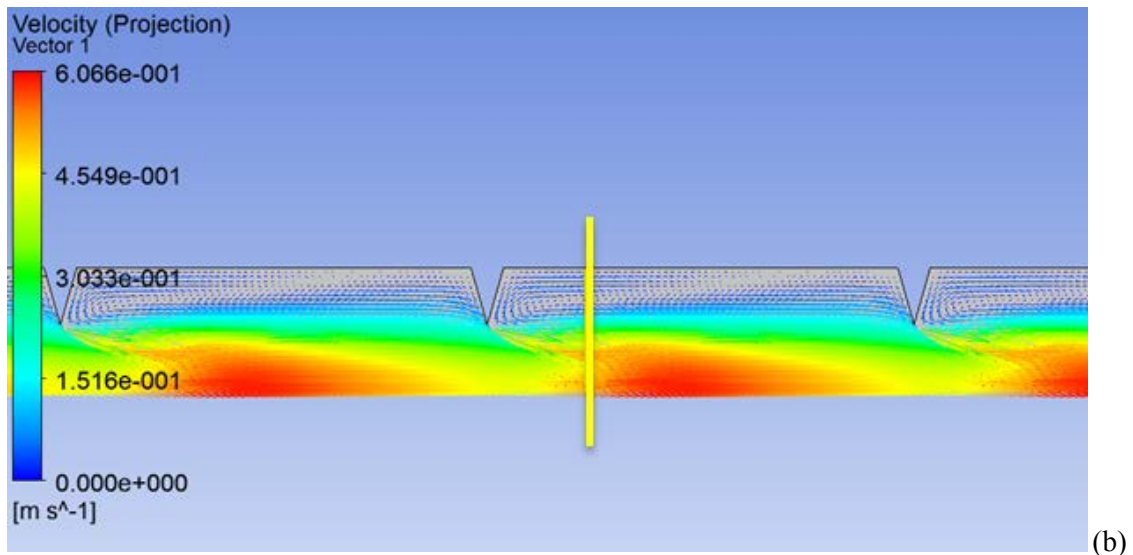


**Fig. 4-8.** Velocity fields obtained by PIV measurements (a) and simulations (b) for  $A = 20$  mm and  $f = 1$  Hz at  $t/T = 0.86$ . The  $X$  plane for data extraction has been fixed at 6 mm after the center of the baffle.

In **Fig. 4-9** the phase-averaged axial velocities at  $X = -23$  mm (i.e. 6 mm after the baffle) and  $X = -20$  mm (i.e. 3 mm after the baffle) measured with PIV at  $Re_o = 200$  are compared with the axial velocities obtained in CFD ( $Re_o = 200$ ) at an  $X$  position 6 mm after the baffle. The obtained profiles are not perfectly confounded to the profile obtained by PFD. This can be explained by the experimental error of the velocity measurement near walls (for  $Y/D$  between 0.8 and 1) due to optical distortions. Secondly, the shape and size of the eddies are slightly different as the geometries of the Nitech® tube and the simulated geometry B are not perfectly identical, therefore it implies the size and force of recirculation eddies are not strictly identical.

Consequently, despite these slight discrepancies, the estimation of the velocity fields and associated quantities using a laminar flow simulation is adequate for the purpose of reactor design considered here.

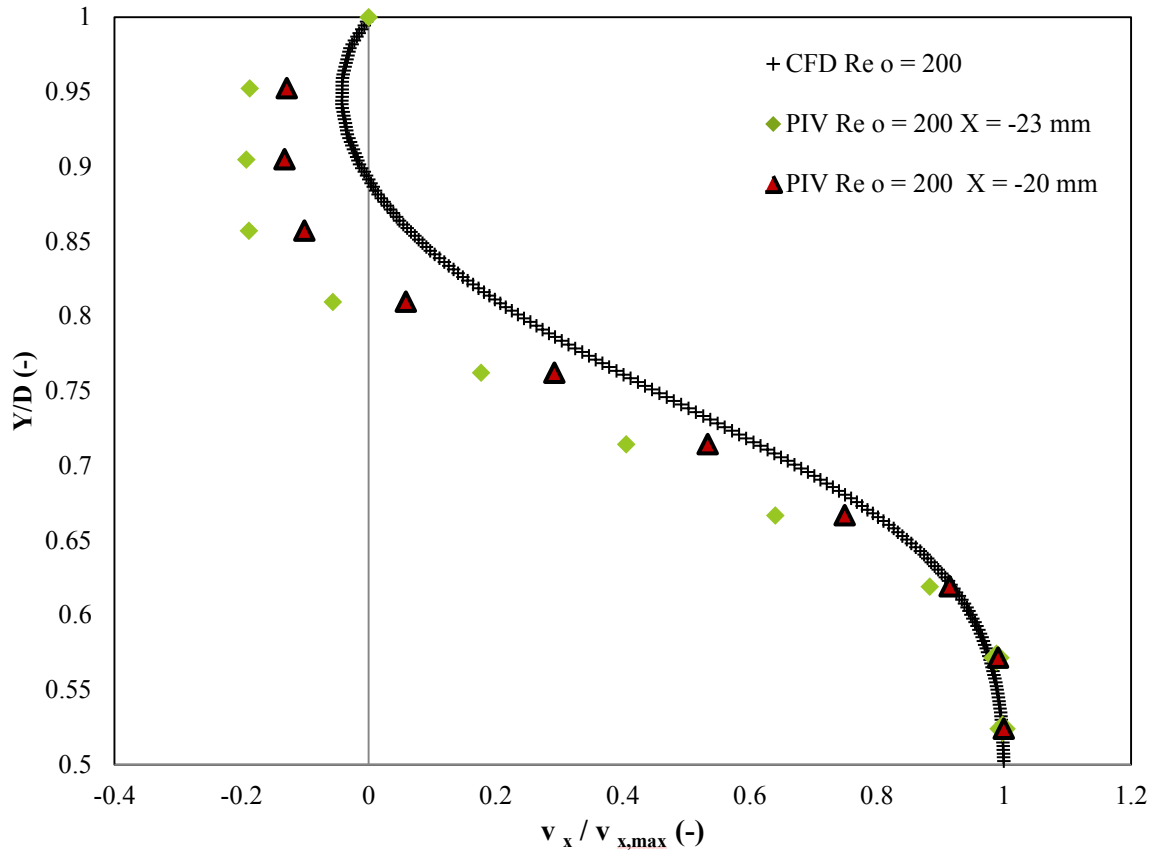


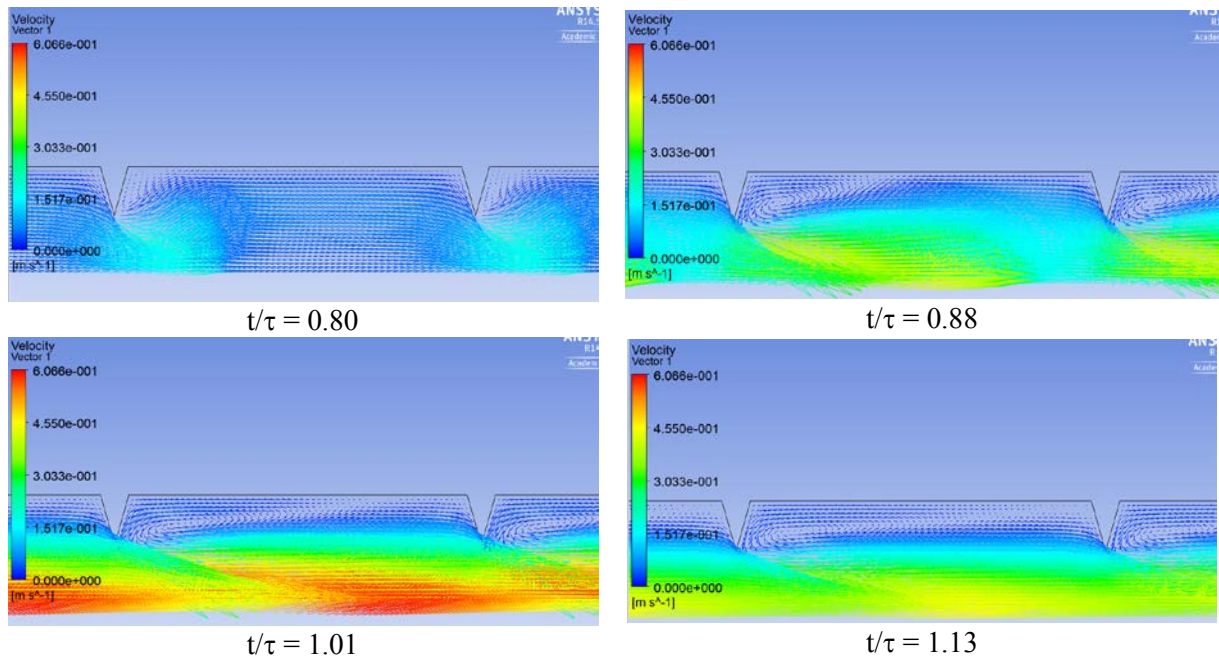
**Fig. 4-9.** Velocity profile at  $X = -23$  mm for  $A = 20$  mm and  $f = 1$  Hz at different oscillatory Reynolds numbers. The CFD velocity profile at  $Re_o = 200$  is compared with those obtained in PIV at  $Re_o = 200$ . The error bars represent the phase-averaged fluctuations.

### 4.3. Results

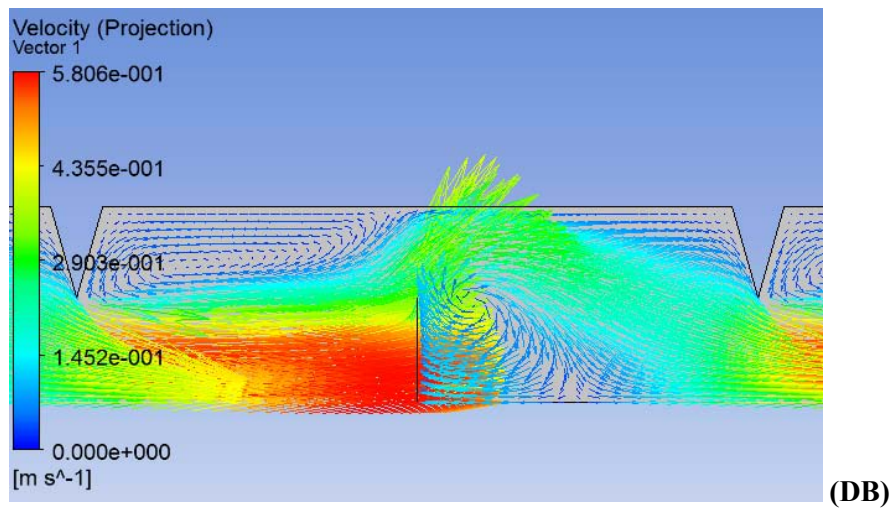
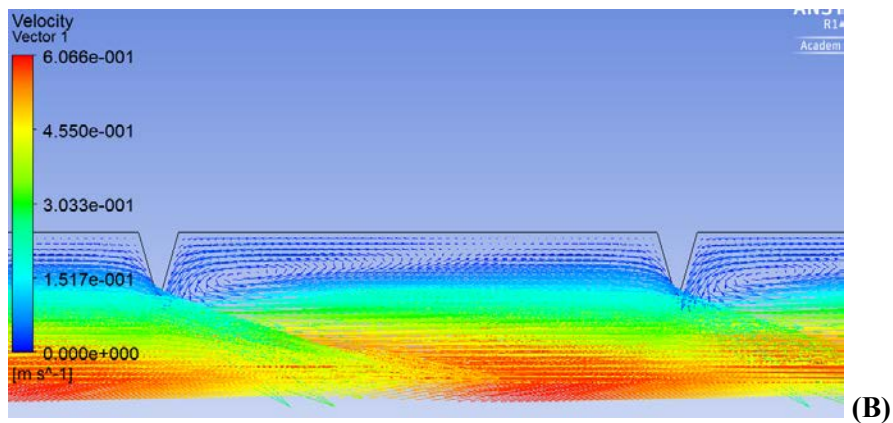
#### 4.3.1. Velocity fields

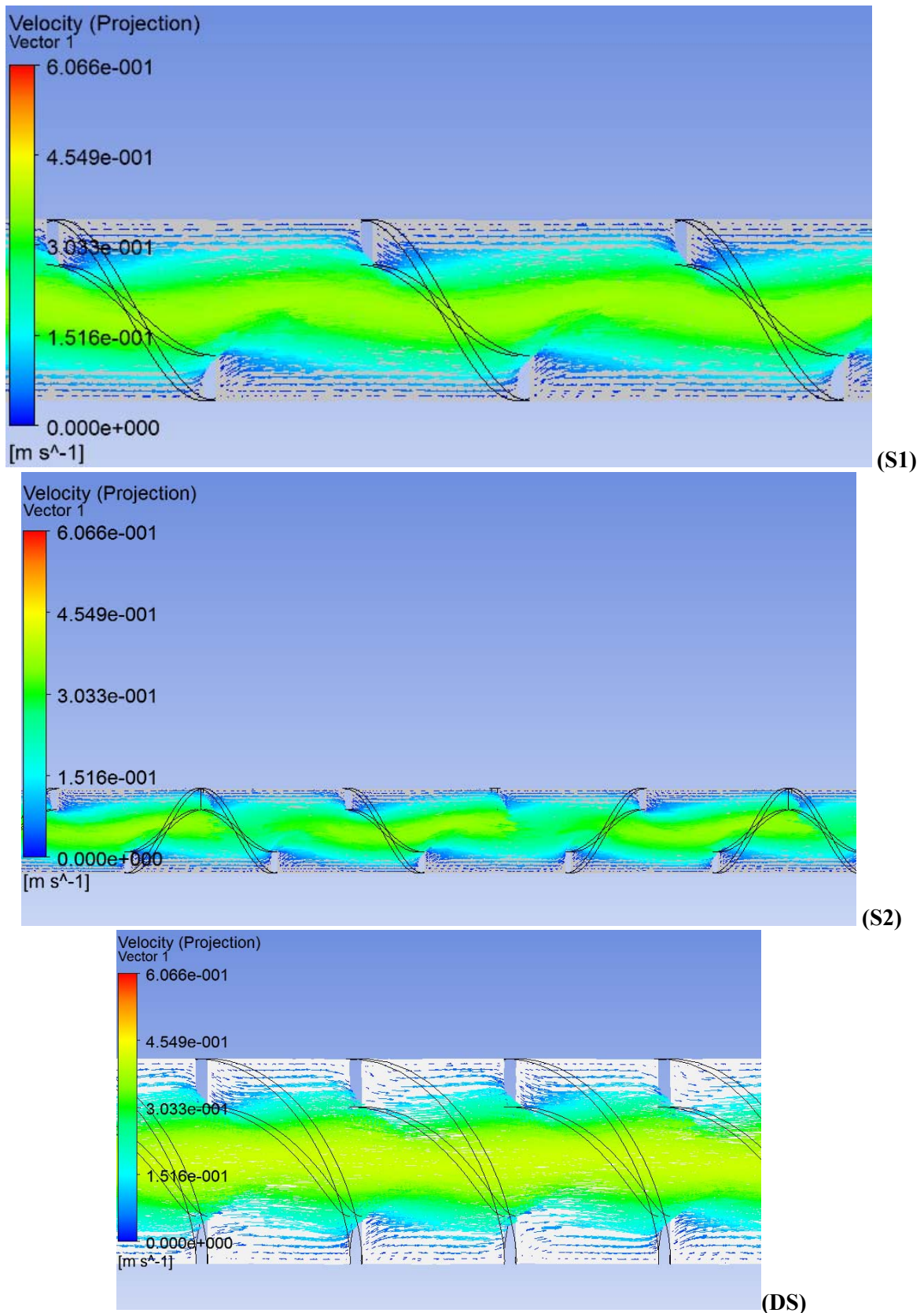
**Fig. 4-10** shows the time-dependence of the velocity fields. The first observations of flow patterns show a potential high axial dispersion with acceleration of fluid near baffles and a relatively slow recirculation near baffles.

The **Fig. 4-11** shows the flow patterns at  $t/\tau = 1.01$  obtained in the different geometries. In geometry B (**Fig. 4-11 (a)**), the flow patterns show an acceleration of fluid near the baffles and a relatively slow recirculation near baffles resulting in high velocities along the axis of the tube. The acceleration of fluid at the centre of the tube is limited in geometry DB (**Fig. 4-11 (b)**) due to the presence of discs. In comparison with geometry B, an additional recirculation eddy exists in geometry DB near the disc. For geometry S1 (**Fig. 4-11 (c)**), the gradient of velocities is smaller as the velocity at the center of the tube (0.4 m/s) compared with the velocity at the center of the tube obtained in geometry B (0.6 m/s). Recirculation areas are not present near baffles and dead zones are visible near walls. The double spring geometry DS (**Fig. 4-11 (e)**) increases the presence of dead zones and the velocity at the centre of the tube is slight higher than in geometry S1 (0.45 m/s).



**Fig. 4-10.** Velocity vectors obtained with baffles with single orifice (B) for different times for  $Re_o = 43$  ( $A = 16.5$  mm and  $f = 1.05$  Hz) and  $Re_n = 6$  ( $v_{net} = 1.405$  cm/s).

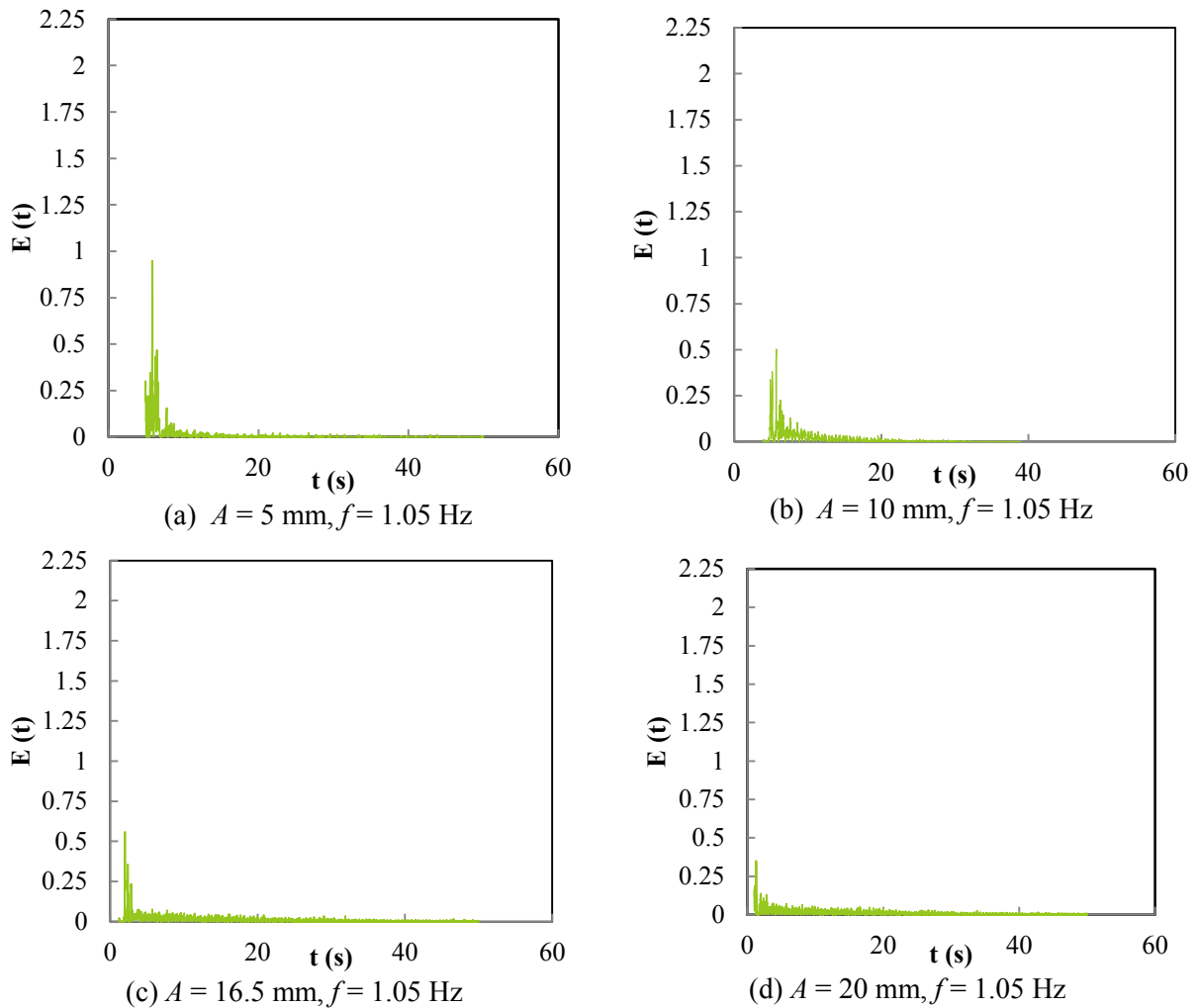




**Fig. 4-11.** Velocity vectors obtained in the different baffle geometries: (B), (DB), (S1), (S2) and (DS) geometries at  $t/\tau = 1.01$  for  $Re_o = 43$  ( $A = 16.5$  mm and  $f = 1.05$  Hz) and  $Re_n = 6$  ( $v_{net} = 1.405$  cm/s).

### 4.3.2. Axial dispersion coefficient

The residence time distribution for different oscillatory amplitudes and frequencies obtained in geometry B are given in **Fig. 4-12**. The residence time distribution  $E(t)$  of an ideal plug-flow reactor is an infinitely high peak with zero width. The dispersion model represents the non-ideality of the reactor. It involves an axial dispersion coefficient  $D_{ax}$  which is calculated from the residence time distribution, which has a width and a finite height, as represented in **Fig. 4-12**. It can be seen that the maximum value of the residence time distribution  $E(t)$  decrease with an increase of the amplitude and of the frequency. The highest peak is obtained for  $A = 16.5$  mm and  $f = 0.635$  Hz (**Fig. 4-12** (f)). The residence time distribution obtained for  $A = 20$  mm and  $A = 25$  mm ( $f = 1$  Hz) (**Fig. 4-12** (d) (e)) and obtained for  $f = 1.273$  Hz and  $f = 1.606$  Hz ( $A = 16.5$  mm) (**Fig. 4-12** (g) (h)) have a very low maximum.





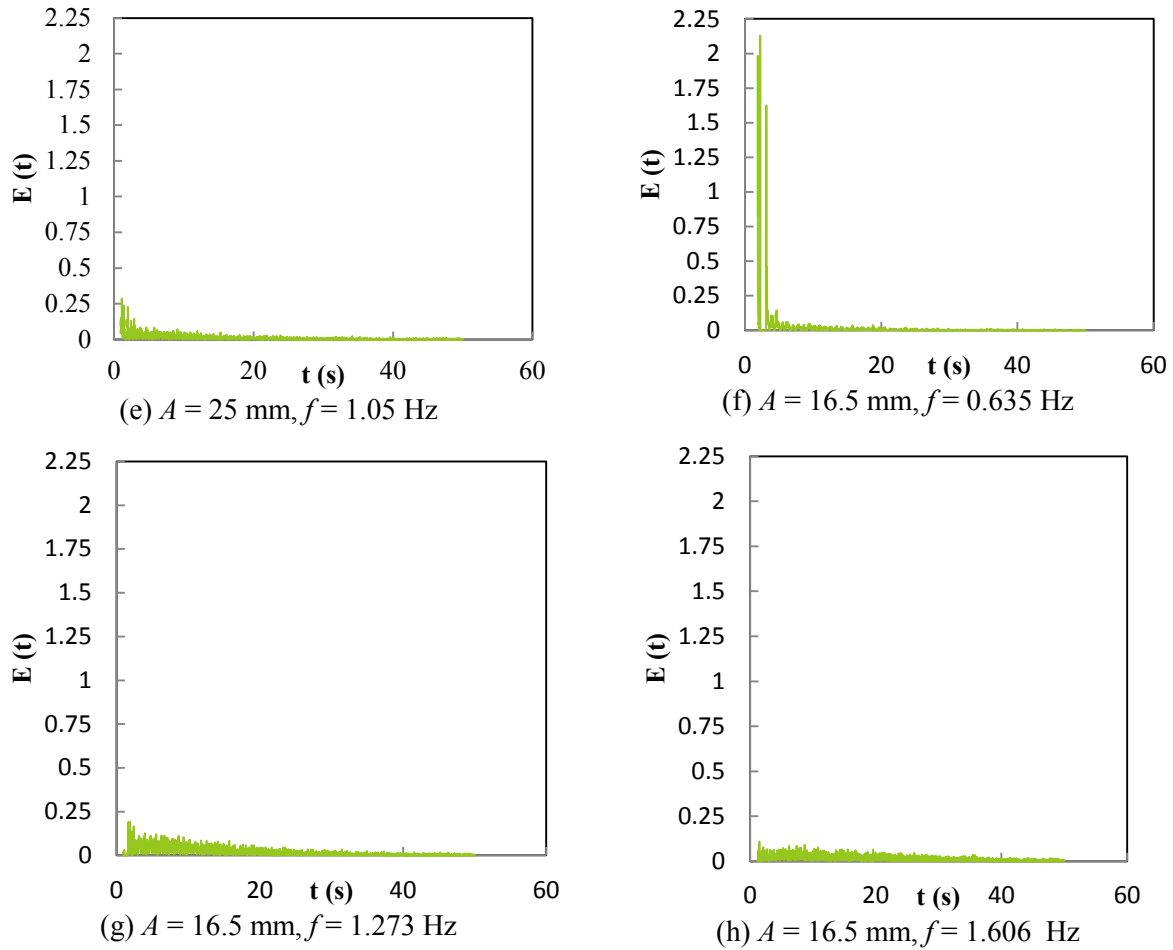


Fig. 4-12. Residence time distribution  $E(t)$  obtained for geometry B for different oscillatory amplitudes and frequencies.

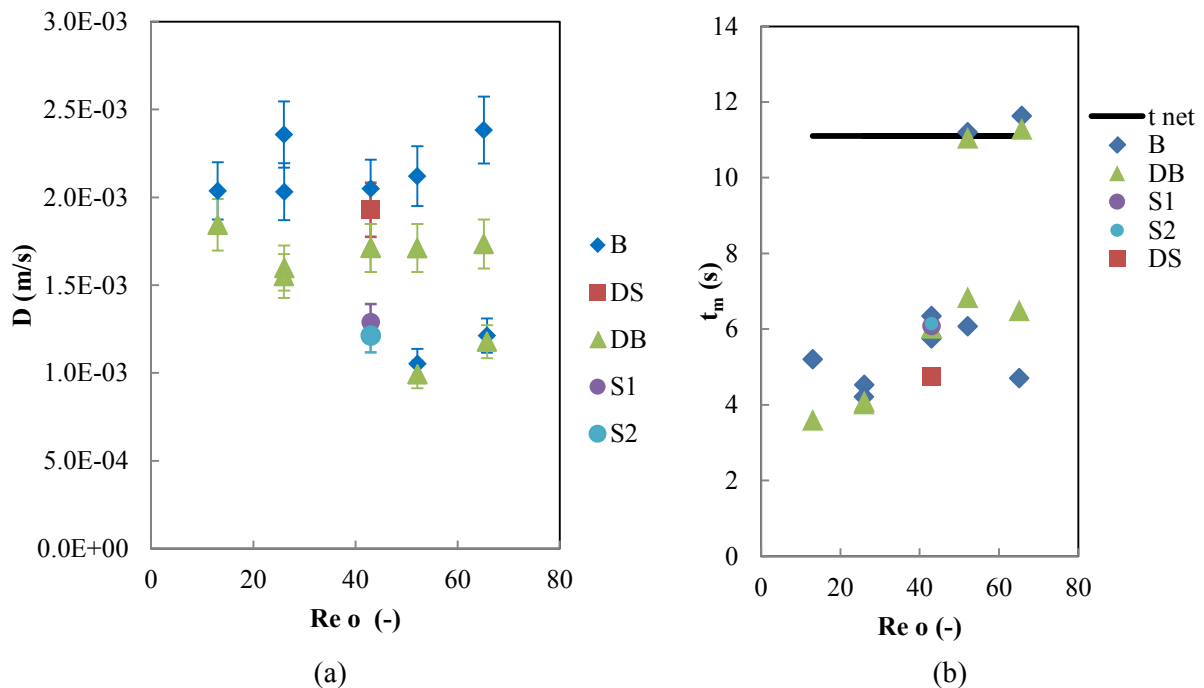
The axial dispersion coefficients and the mean residence times at different oscillatory Reynolds numbers are presented in Fig. 4-13. It can be seen that axial dispersion coefficients are approximately constant with an increase of the oscillatory Reynolds number in the studied range. For higher oscillating frequencies (1.273 Hz and 1.606 Hz) in geometries B and DB, lower values of the axial dispersion coefficient are obtained, but the shape of the RTD curves for these frequencies (Fig. 4-12 (g) and (h)) are very different to those obtained in plug-flow reactors. The associated Péclet numbers are also very low (between 1.1 and 2.2), being less than 10, which is the minimum value for the validity of the axial dispersion model [36]. Nevertheless, the trends show that to limit axial dispersion the best geometry is the spring S2 ( $D_{ax} = 1.21 \times 10^{-3} \text{ m}^2/\text{s}$ ), followed by S1 ( $D_{ax} = 1.29 \times 10^{-3} \text{ m}^2/\text{s}$ ), and then DB ( $D_{ax} = 1.71 \times 10^{-3} \text{ m}^2/\text{s}$ ), DS ( $D_{ax} = 1.93 \times 10^{-3} \text{ m}^2/\text{s}$ ) and B ( $D_{ax} = 2.05 \times 10^{-3} \text{ m}^2/\text{s}$ ). Fig. 4-13(b) shows that in general the calculated mean residence times are significantly lower than the theoretical average residence time (or space time), which implies the presence of stagnant backwaters and reduced effective reactor volume [36]. The lowest residence time is obtained in the DS geometry, and the presence of dead zones is clearly visible in Fig. 4-11 (DS).

Table 4-8 presents the effect of the net Reynolds number on the axial dispersion coefficient. For the single orifice baffle geometry, with  $A = 16.5 \text{ mm}$  and  $f = 1.05 \text{ Hz}$ , the Péclet number clearly decreases with an increase of the net Reynolds number. In addition, Fig. 4-14 (a) shows that the Péclet number increases with the length of reactor, due to a constant axial dispersion coefficient, which remains constant with an increase of the length (difference between  $X_0$  and  $X_{detection}$ ). The plug-flow behavior is then obtained by increasing the reactor length, which corresponds to an increase of the

residence time. For example in geometry B,  $Pe = 30$  for a length of 5.0 m, which corresponds to a residence time of 5.9 m in with  $v_n = 1.405$  cm/s. If one supposes that the axial dispersion coefficient remains constant with an increase of the length for any baffle design, then in S2, the  $Pe = 30$  for a length of 2.6 m, which corresponds to a residence time of 3.5 min. A decrease of the axial dispersion coefficient is then directly proportional to a decrease of the necessary residence time to achieve plug-flow behavior. Moreover, **Fig. 4-12(b)** shows the effect of  $L$  on the mean residence time. The increase of the length of the reactor decreases the difference between the mean residence time calculated from residence time distribution and residence time calculated from the ratio of volume and flow rate.

**Table 4-8.** Effect of the net Reynolds number on the axial dispersion coefficient and the mean residence time. The geometry is the single baffle orifice (B). The oscillatory conditions are  $A = 16.5$  mm and  $f = 1.05$  Hz.

Flow rate (L/h)	$v_n$ (cm/s)	$Re_n$	$D_{ax}$ (m <sup>2</sup> /s)	$t_m$ (s)	$t_{net}$ (s)	Frac. (%)	$Pe$ (-)
6.0	0.943	3.7	1.21E-3	7.7	16.5	96.0	1.2
8.9	1.405	5.5	2.01E-3	6.3	11.1	98.4	1.1
12.0	1.886	7.5	3.05E-3	3.8	8.3	99.1	1.0
15.0	2.358	9.3	4.30E-3	2.4	6.6	99.6	0.9



**Fig. 4-13.** Effect of Reynolds number on the axial dispersion coefficient (a) and on the mean residence time (b).

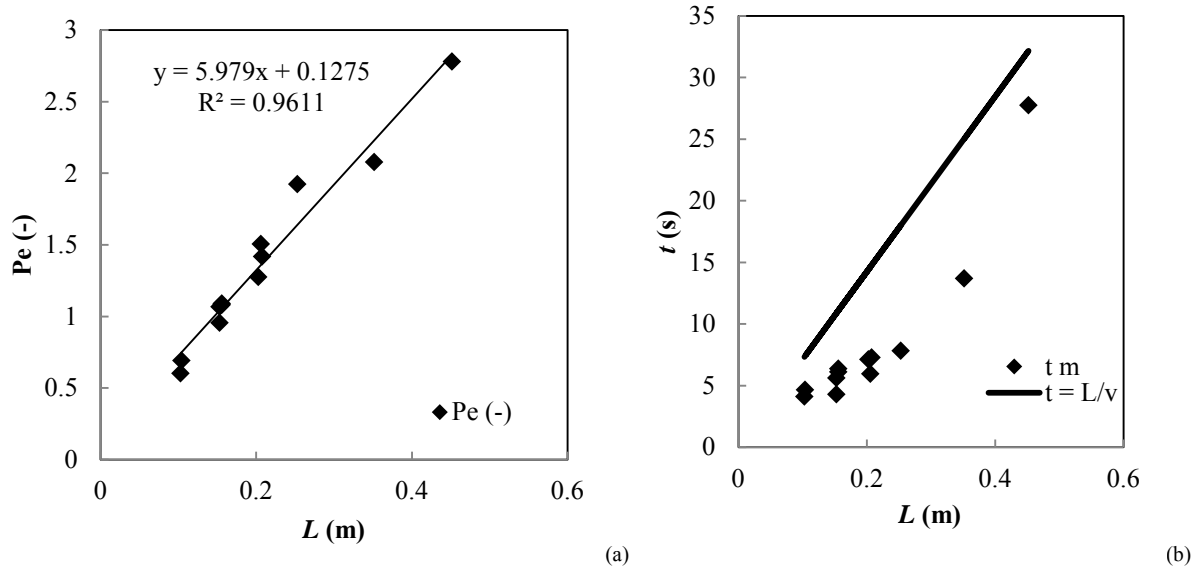


**Fig. 4-14.** Effect of the length of the reactor on the Péclet number (a) and the mean residence time ( $t_m$ ) (b). The geometry is the single baffle orifice (B). The oscillatory conditions are  $A = 16.5$  mm and  $f = 1.05$  Hz. The residence time  $t$  is calculated with the ratio of the length  $L$  and the net velocity  $v$ .

### 4.3.3. Fluid strain rate

A particle experiences different shear strain rates during its time in the reactor. The calculations give the time-averaged strain rate and also the maximum strain rate, see **Fig. 4-15**. Differences exist between particles depending on their initial position on the  $Y$ -axis. An averaged value is calculated and this justifies the use of standard deviations to quantify the differences of the particle strain rates among all the particles.

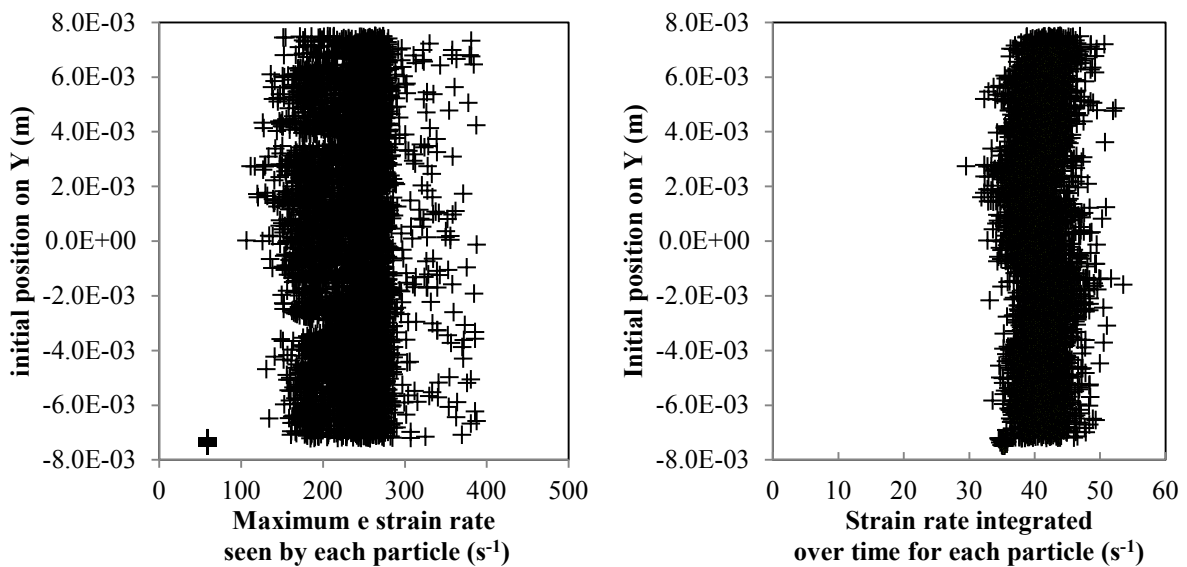


**Fig 4-15.** S2 geometry with  $A = 16.5$  mm and  $f = 1.05$  Hz : (a) Maximum strain rate experienced by each particle and (b) time-averaged strain rate experienced by each particle as a function of the initial radial position.

The **Fig. 4-16** shows the influence of the oscillatory Reynolds number and the baffle design on the maximum and time-averaged strain rate. The error bars indicate the standard deviation of the strain rate experienced by the ensemble of particles at each operating condition. The geometry leading to the

highest maximum particle strain rates is DB ( $FSR_{max,m} = 340 \text{ s}^{-1}$ ). Following this is geometry B ( $FSR_{max,m} = 296 \text{ s}^{-1}$ ), and finally DS, which is in the same range of values ( $FSR_{max,m} = 255 \text{ s}^{-1}$ ), S1 ( $FSR_{max,m} = 243 \text{ s}^{-1}$ ) and S2 ( $FSR_{max,m} = 231 \text{ s}^{-1}$ ). The highest time-averaged value of the particle strain rate is obtained in DB ( $FSR_m = 57 \text{ s}^{-1}$ ), then secondly in DS ( $FSR_m = 51 \text{ s}^{-1}$ ). The higher number of obstacles encountered by the particles in geometries DB and DS may be the cause of this higher value. Finally, the shear rates experienced in geometries B ( $FSR_m = 44 \text{ s}^{-1}$ ), S1 ( $FSR_m = 43 \text{ s}^{-1}$ ) and S2 ( $FSR_m = 41 \text{ s}^{-1}$ ) are in the same range, but the standard deviation is lower in the spring baffle designs, i.e. there are smaller differences of strain rate experienced by the particles for the spring designs. **Table 4-9** shows the influence of the net Reynolds number on the strain rates. The shear strain rates, maximum or time-averaged decrease slightly with a decrease of the net Reynolds number, which is the same evolution as the effect of the oscillatory Reynolds number.

These values are in the same range of those obtained by PIV measurements (106, 203, 341, 405 and  $587 \text{ s}^{-1}$  for  $A = 5, 10, 15, 20$  and  $25 \text{ mm}$ ) in section 3.2.3. The maximum strain rates are slightly lower than the PIV measurements due to the fact that they are averaged over all the particles, which is not the case in the PIV measurements which shows zones of high shear strain rates. A fraction only of the particles flow through these zones.

**Table 4-11.** Results obtained for particle strain rates in the different reactor geometries.

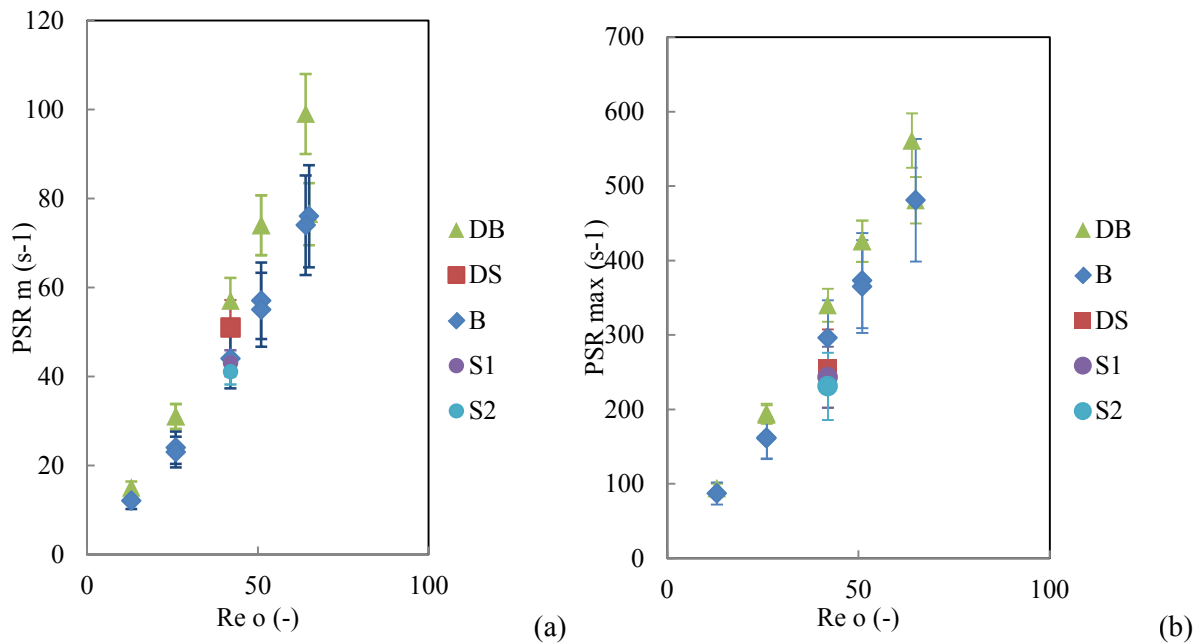


**Fig. 4-16.** The particle strain rates, average (a) and maximum (b), calculated in the different geometries for different amplitude-frequency products  $Af$ . The error bars represent the standard deviations.

**Table 4-9.** Effect of the net Reynolds number on the fluid strain rate. The geometry is the single baffle orifice (B). The oscillatory conditions are  $A = 16.5 \text{ mm}$  and  $f = 1.05 \text{ Hz}$ . %err represent the ratio of Std FSR and FSR.

Flow rate (L/h)	$v_n$ (cm/s)	$Re_n$	$FSR_m$ ( $\text{s}^{-1}$ )	Std. FSR ( $\text{s}^{-1}$ )	%err	$FSR_{max,m}$ ( $\text{s}^{-1}$ )	Std. $FSR_{max}$ ( $\text{s}^{-1}$ )	%err
6	0.943	3.7	43.5	6.1	13.9	291.0	39.0	13.4
8.9	1.405	5.5	44.0	6.0	14.3	296.0	43.0	14.4
12	1.886	7.5	43.2	7.6	17.5	299.0	54.7	18.3
15	2.358	9.3	44.8	6.4	14.3	305.0	58.3	19.1

#### 4.3.4. Distance separating of pairs of initially adjacent particles

**Fig. 4-17** shows how pairs of initially adjacent particles separate in the flow as a function of their initial position. An adequate geometry ideally should promote a high separation of particle pairs in the radial direction ( $R$ ) (radial mixing), whereas particle separation should be minimized in the axial direction ( $X$ ), such that a plug-flow behavior is achieved. The results obtained in all the baffle geometries are given in the **Fig. 4-18**. The standard deviations of the ensemble of particle pairs are indicated by the error bars.  $\Delta R$  is enhanced in DS by a factor two compared with S1, S2, B and DB.  $\Delta R$  is in the same range for B and DB, but standard deviations for DB are typically less than that for B, which means that the differences in flow experience among the particle pairs positioned on the  $Y$ -axis are less significant. Similar  $\Delta R$  is achieved in S1 and S2, which is slightly higher than that produced in B and DB.  $\Delta X$  is similar for both B and DB geometries. As for  $\Delta R$ , the standard deviation is smaller for DB geometry.  $\Delta X$  is reduced by 18% in DS and 27% in S1 and 31% in S2. This follows the same trend that has been observed for the axial dispersion coefficient, where the lowest values of the coefficient  $D_{ax}$  were obtained with S2 and then S1. **Table 4-10** shows the influence of the net flow rate on the distance separating the initially adjacent particles.  $\Delta X$  decreases by a factor of two with an increase of the net flow rate from 6 to 15 L/h, which corresponds to an increase of the net Reynolds number from 3.7 to 9.3.

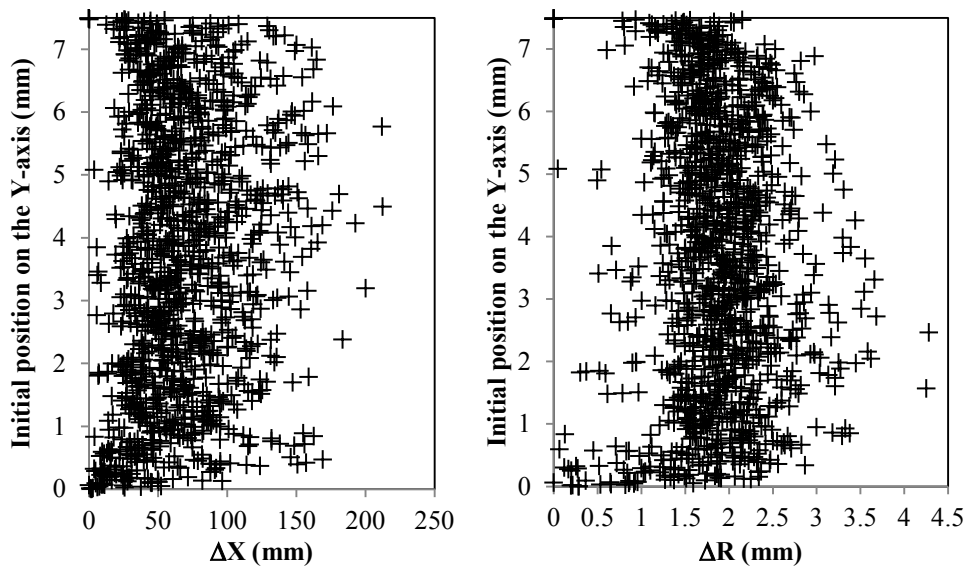


**Fig. 4-17.** Axial (a) and radial (b) separation distances of particles pairs as a function of their initial position on the  $Y$ -axis, for a baffle with single orifice (B), with an amplitude of 16.5 mm and a frequency of 1.05 Hz.

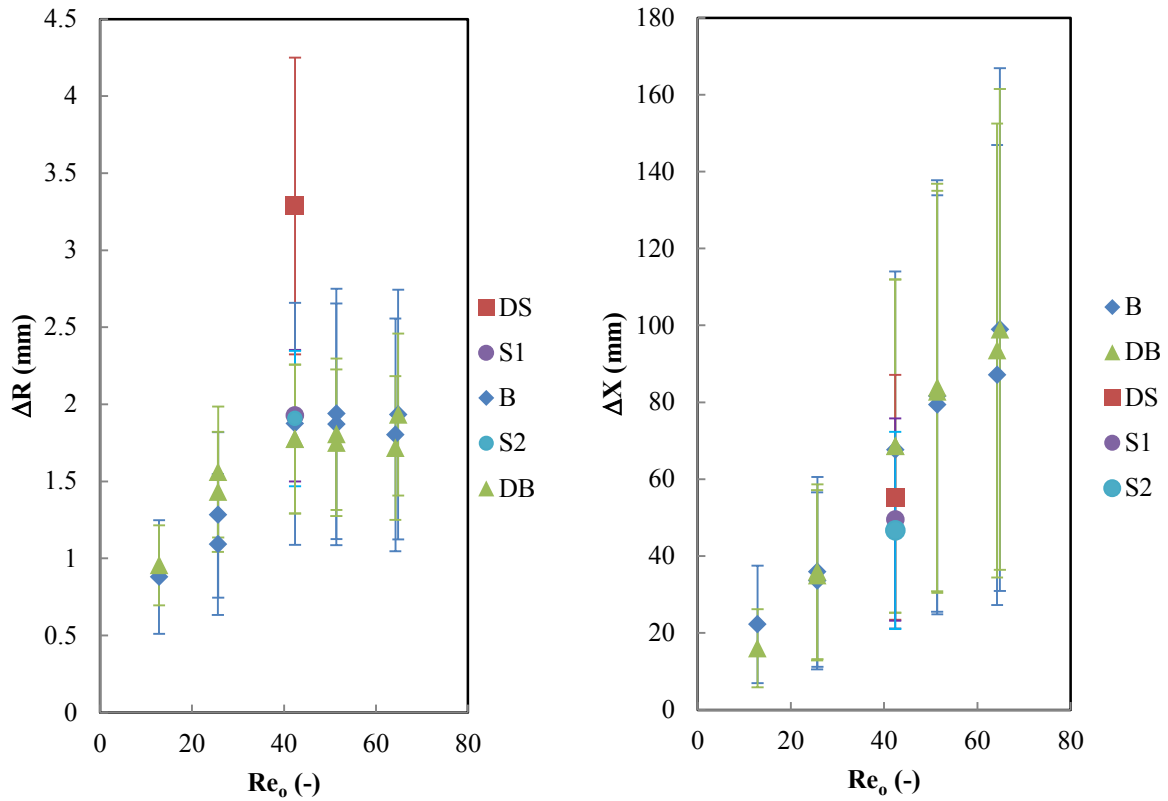


**Fig. 4-18.** (a) Radial and (b) axial separation distances of initially adjacent particles for different geometries and varying  $Re_o$ . The error bars represent the standard deviations.

**Table 4-10.** Effect of the net Reynolds number on the axial and radial distances separating of initially adjacent particles. The geometry is the single baffle orifice (B). The oscillatory conditions are  $A = 16.5$  mm and  $f = 1.05$  Hz. %err represent the ratio of  $\Delta X$  (or  $\Delta R$ ) and Std  $\Delta X$  (or Std  $\Delta R$ ).

Flow rate (L/h)	$v_n$ (cm/s)	$Re_n$	$\Delta X$ (mm)	Std. $\Delta X$ (mm)	%error	$\Delta R$ (mm)	Std. $\Delta R$ (mm)	%error
6	0.943	3.7	74.0	39.8	53.8	1.9	0.5	27.3
8.9	1.405	5.5	67.6	36.5	54.0	1.9	0.6	29.5
12	1.886	7.5	57.0	35.9	63.0	1.7	0.6	36.3
15	2.358	9.3	48.0	32.2	67.1	1.5	0.6	36.8

#### 4.4. Conclusions

In this section, CFD has been used to simulate the flow in oscillatory flow reactors equipped with various baffle designs and operating under different flow conditions. Different indicators, including residence time distribution, fluid strain rate and difference of position of initially adjacent particles have been calculated for each geometry in order to compare its performance for mixing and liquid-liquid dispersion.

It has been shown that the axial dispersion coefficient for each geometry remains constant with a change of oscillatory Reynolds numbers for  $Re_o$  between 10 and 65. However, the axial dispersion coefficient has to be minimized in order to obtain the highest Péclet number possible and be as close as possible to plug flow behavior. Without this, the inhomogeneity of the concentration

profile could lead to unwanted secondary reactions. The lowest axial dispersion coefficient was obtained in the spring geometries, (S1) and (S2), having values equal to  $1.3 \times 10^{-3} \text{ m}^2/\text{s}$  and  $1.2 \times 10^{-3} \text{ m}^2/\text{s}$ , respectively. The disc and baffles (DB) gives a lower axial dispersion coefficient than the single orifice baffles geometry (B). The same trend is obtained for the distances separating initially adjacent particle pairs after a certain flow time: the lowest axial separation distance is obtained for the S2 geometry. However, the same results are obtained for disc and baffles (DB) and single orifice baffles (B) geometries. The effect of the oscillatory Reynolds number is visible in geometries DB and B and this effect is linear. The distance separating initially adjacent particles in the radial direction,  $\Delta R$ , shows a higher value for the double spring (DS) geometry. For the other geometries,  $\Delta R$  stays in the same range but standard deviations are lower in the spring geometries than those obtained in disc and baffles geometry (DB), which is lower than that obtained with single orifice baffles (B). The S2 geometry is the design that would minimize the separating distance in the axial (X) direction, which implies better plug flow in the oscillatory flow reactor.

Concerning the capacity to generate liquid-liquid dispersions, the strain rates have been studied as an indicator on the capacity of a given geometry to shear the fluid. It can be seen that an increase of the oscillatory Reynolds numbers increases both the average and maximum strain rate seen by the particle. This trend was already observed for liquid-liquid dispersions studied in the literature [41], [42]. This study allows us to identify the geometry that is *a priori* the most suitable to generate high shear strain rates and then be more likely to generate small size liquid-liquid dispersions. The disc and baffle geometry (DB) shows the highest values of particle strain rates. The double spring geometry (DS) shows a maximum strain rate that is less than that obtained with the single orifice baffle (B) and the disc and baffle (DB) geometries, but the average strain rate is between the one obtained in (DB) and (B) geometries. Even though the maximum values of the strain rate in the spring baffle designs (S1) and (S2) are less than that obtained in (B), the average value of the strain rate is close to these of (B).

The most suitable geometry, for a purely dispersive purpose would be the disc and baffle (DB) geometry, however, the esterification with glycerol reactions considered in this project are accompanied by secondary reactions (formation of diglycerides or triglycerides), which can be limited by a plug-flow behavior. This suggests that the spring baffle design (S2), would be a good choice for this type of reaction. In this case, since the axial dispersion coefficient is the same with an increase of the oscillatory Reynolds number, the loss of dispersion capacity can be compensated by an increase of the oscillatory conditions.

## 5. Sizing of an industrial scale OBR

One of the objectives of the AGRIBTP project is to develop an industrial tool for the transformation of waste cooking oil at an industrial scale. For this, a scaled-up design of the continuous OBR technology is put forth that allows a total flow rate ( $F$ ) of 100 kg/h and a residence time ( $t$ ) of 20 min. This residence time is indeed sufficient for the transesterification, esterification with methanol and esterification with glycerol reactions. To reach such flow rates, geometric parameters such as diameter, baffle spacing and reactor length, as well as oscillatory and net Reynolds numbers, pressure drop and Peclet number estimations have been made on the basis of the methodology given by Stonestreet and Harvey [13].

The suggested reactor technology and the suggested baffle design is the same as that used experimentally in Part III, Chapter 1, which corresponds to the metallic OBR. The oscillatory conditions are to be kept at  $A = 88$  mm and  $f = 1$  Hz, which corresponds to an oscillatory Reynolds number of 2875. The tube diameter is the key parameter. The length ( $L$ ) is calculated from  $D$ ,  $t$  and  $F$ :

$$L = \frac{Ft}{\pi\left(\frac{D}{2}\right)^2}$$

The baffle spacing ( $h$ ) is set at  $1.5D$ . The number of baffles depends on this spacing ( $h$ ) and the reactor length ( $L$ ). The opening of the baffle  $D_0$  is set at  $0.5D$ . According to Smith and Mackley [43], the axial dispersion coefficient  $D_{ax}$  for orifice baffles is the same for a tube diameter of 24, 54 and 150 mm and its value is between  $1 \times 10^{-3}$  and  $2 \times 10^{-3}$  m<sup>2</sup>/s at  $Re_o = 2000-3000$ . In the numerical simulation, the axial dispersion coefficient has been estimated at  $2 \times 10^{-3}$  m<sup>2</sup>/s for the geometry B corresponding to the OBR. Consequently, for the following calculations,  $D_{ax}$  has been set at  $2 \times 10^{-3}$  m<sup>2</sup>/s. The Peclet number associated with the different reactor lengths and velocities have been calculated. All these calculations are represented in **Table 5-1** for different reactor diameters.

In this analysis, only pressure drop has been considered; this is slightly different to power dissipation, which was employed in Stonestreet and Harvey's [13] methodology. In their work [13], the recommended range of the velocity ratio ( $Re_{net}/Re_o$ ) is between 2 and 6 in order to achieve plug-flow conditions. Since the oscillatory conditions from the Part III, Chapter 1 have been conserved here ( $Re_o = 2875$ ), this velocity ratio is in a significantly higher range ( $> 20$ ). Moreover, the plug-flow behavior is characterized in this work by the Peclet number instead of the number of tanks-in-series ( $Pe = uL/D_{ax}$ ), which was used by Stonestreet and Harvey [13].



**Table 5-1.** Geometric parameters for the building of the oscillatory baffled reactor at the production scale. The chosen parameters are written in bold.

D (mm)	$v_{net}$ (m/s)	$Re_{net}$ (-)	L (m)	$Re_o$ (-)	Velocity ratio	H (mm)	N (-)	$\Delta P$ (bar)	Pe (-)	V (L)
64	8.63E-03	120	10.4	2875	24.0	96	107.9	6.3	45	0.283
66	8.12E-03	116	9.7	2875	24.8	99	98.4	5.7	40	0.301
68	7.65E-03	113	9.2	2875	25.5	102	90.0	5.2	35	0.320
70	<b>7.22E-03</b>	<b>109</b>	<b>8.7</b>	<b>2875</b>	<b>26.3</b>	<b>105</b>	<b>82.5</b>	<b>4.8</b>	<b>31</b>	<b>0.339</b>
72	6.82E-03	106	8.2	2875	27.0	108	75.8	4.4	28	0.358
74	6.46E-03	104	7.8	2875	27.8	111	69.8	4.0	25	0.378
76	6.12E-03	101	7.3	2875	28.5	114	64.5	3.7	22	0.399
78	5.81E-03	98	7.0	2875	29.3	117	59.6	3.5	20	0.420
80	5.53E-03	96	6.6	2875	30.0	120	55.3	3.2	18	0.442
82	5.26E-03	93	6.3	2875	30.8	123	51.3	3.0	17	0.465
84	5.01E-03	91	6.0	2875	31.5	126	47.7	2.8	15	0.488

The criteria for the choice of the diameter are:  $\Delta P < 5$  because a minimum overpressure of 3 bars is required, flexibility of operating conditions (oscillatory amplitude and frequency, net flow) and  $Pe > 30$  to have correct plug-flow conditions.

According data in **Table 5-1**, the suggested geometry for a production of 100 kg/h and a residence time of 20 min is:

$D = 70$  mm,  $L = 8.7$  m,  $h = 105$  mm,  $D_0 = 35$  mm,  $N = 82$  baffles,  $\Delta P = 4.8$  bar,  $Pe = 31$  if  $D = 2 \times 10^{-3}$  m<sup>2</sup>/s.

Elbows could also be used for a more compact design, which would consist of for example 6 tubes of 1.45 m or 3 tubes of 2.9.

Simulations carried out in the section 4 have shown that the baffle design S2 provides the lowest axial dispersion coefficient ( $D_{ax} = 1.2 \times 10^{-3}$  m<sup>2</sup>/s). In laminar conditions, it has been shown that the baffle design S2 provides lower axial dispersion than the baffle design used in the OBR, based on the results obtained with numerical simulations. For the same geometric parameters, if  $D_{ax} = 1.2 \times 10^{-3}$  m<sup>2</sup>/s with S2, the Peclet number equals 52. It can therefore be assumed that lower axial dispersion will be obtained at  $Re_o = 2875$ .

To use this reactor for the esterification reaction with glycerol, a system is needed to increase the pressure (3 bars) in order to reach higher temperatures (150 °C). The simplified process flow diagram presented in **Fig. 5-1** is similar to that obtained in Part III, Chapter 1. The pulse dampener has to be carefully selected. A pulse dampener tested during the experiments on the OBR at TNO has been damaged because its Viton membrane was worn due to oscillations and chemicals. The alternative of using a vessel filled with nitrogen is a good solution to dampen the oscillations, but a system to control the gas-liquid interface is required.

A solution to the mediocre conversions (73% with DBSA, 50% with sulfuric acid) obtained for the esterification reaction with glycerol is first to use of a higher level of free fatty acids in the initial oil to have a final product with a higher concentration in monoglycerides with DBSA as a catalyst. The second solution is the use of an intermediary decantation with sulfuric acid as a catalyst,

since decantation is too long with DBSA. This solution has been tested in Part III, Chapter 1, and leads to a 86% conversion and a 53% selectivity in monoglycerides. However, the residence time was too long, which is a cause of the decrease of the selectivity. The intermediary decantation should occur after 10 min only (i.e. half of the residence time). The glycerol and water layer has to be removed. An evaporation step can be used to remove water from the glycerol phase and then it can be recycled in the main reactor.

An industrial scale oscillatory baffled reactor with a feed flow of 100 kg/h has been sized based on experimental work carried out on a pilot-scale 24 mm diameter metallic OBR and on CFD simulations. The residence time is set to 20 min, which is sufficient to perform the transesterification and esterification with methanol and esterification with glycerol reactions. The added-value of the new baffle design S2, which has shown good performance in terms of plug-flow behaviour in the CFD simulations, still has to be validated with an experimental rig in order to determine residence time distribution. This type of reactor is highly flexible as the oscillatory conditions, temperature, residence time and the net flow rate can be modulated for the need of the different reactions.

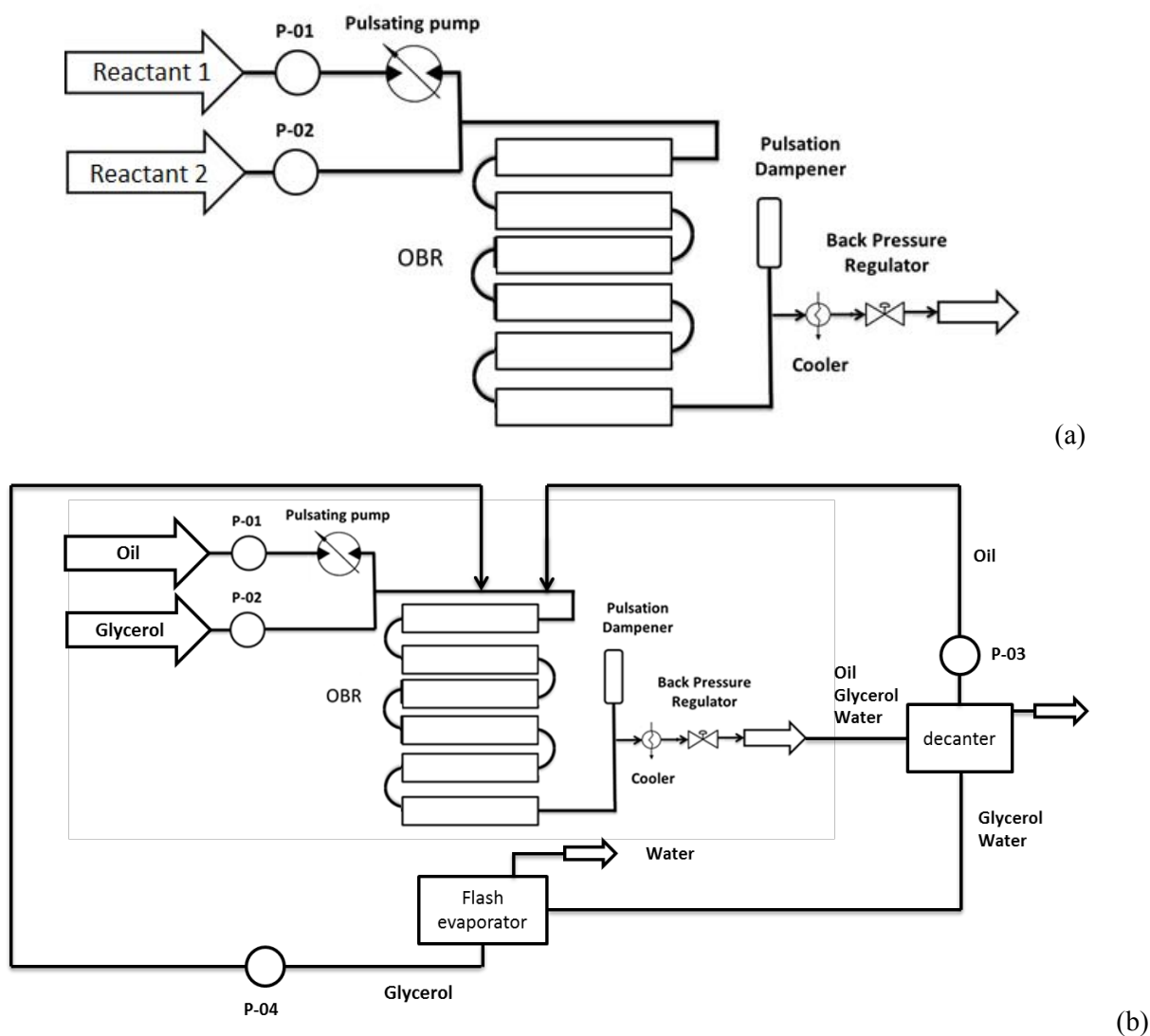


**Fig. 5-1.** Simplified Process Flow Diagram of the process associated with the suggested scaled-up reactor (a). Suggested separation module used to remove water for the esterification reaction with glycerol (b).

## 6. Conclusions

This chapter has firstly presented the state of the art of the recommended geometrical parameters, such as tube diameter, baffle design, baffle spacing, reactor length to diameter ration, net and oscillatory Reynolds numbers, to use with oscillatory baffled reactors. In addition, the current knowledge on flow and mixing, residence time distribution, heat transfer, pressure drop and liquid-liquid dispersions in OBRs has been summarized. It is highlighted that the axial dispersion coefficient is independent of the diameter of the tube for constant oscillatory Reynolds number and it also remains constant with increasing reactor length. Peclet numbers have been determined from the literature data, showing that the Peclet number is proportional to the reactor length. Higher Peclet numbers are thus obtained with higher residence times.

This chapter also presents PIV measurements performed in a glass Nitech® reactor that are used to analyze velocity fields, eddy formation and shear strain rates. It has been shown that eddies are formed and then propagate at the maximum and minimum of the velocity of the oscillating flow cycle. The size of the eddies is independent of the oscillatory amplitude at  $Re_o = 200$ . Moreover, shear strain rates have been calculated and increase linearly with the oscillatory amplitude.

In addition to the experimental measurements, CFD simulations have been used as a complementary tool to characterize the mixing in the OBR. Although velocity fluctuations in the flow have been observed due to the formation of eddies, the laminar flow simulations are accurate enough for the reactor design purposes required by this work. For this, virtual particles have been released in the fluid and calculations have been made from the particle information to develop mathematical indicators of mixing, through the determination of the axial dispersion coefficients and the distance separating two initially adjacent particles. The shear strain rate history of particles has also been calculated, which are in good agreement with the range of shear strain rates calculated by PIV measurements. The effects of oscillatory Reynolds number on the flow and the performance of new baffle designs have been evaluated using these indicators. In particular, it has been shown that the axial dispersion coefficient is independent of the oscillatory Reynolds number for the studied range ( $Re_o = 20-60$ ). The axial dispersion coefficient is also independent of the reactor length, which means that the Péclet number increases with the reactor length, which confirms the observations made from the literature studies. To reach a Péclet numbers greater than 30, a residence time of at least 6 min is required. The lowest axial dispersion was obtained in the S2 geometry. The shear strain rates generated with S2 are a bit lower than those in the other baffle designs but, if necessary, these could be increased by increasing the oscillatory flow rate and consequently the oscillatory Reynolds number.

To meet the design objective of a reactor providing a total flow rate capacity of 100 kg/h and a residence time of 20 min, a reactor sizing methodology has been presented and dimensions of an industrial scale OBR reactor have been put forth:  $D = 70$  mm,  $L = 8.7$  m,  $h = 105$  mm,  $D_o = 35$  mm,  $N = 82$  baffles,  $\Delta P = 4.0$  bar,  $Pe = 42$  if  $D = 2 \times 10^{-3}$  m<sup>2</sup>/s. The performance OBR may be improved by a change in baffle design; indeed the CFD simulations demonstrated a decrease in axial dispersion with the use of S2 baffle design and leads to an increased Peclet number of 52. Nevertheless, a specific experimental study using the S2 design would be required to confirm this hypothesis. A decrease in the axial dispersion would indeed be beneficial for the esterification with glycerol reaction since a limited axial dispersion (high Péclet number) implies a plug-flow behavior, which limits the concentration gradients in the reactor and thus secondary reactions. Another means to improve the esterification reaction with glycerol would be to shift the thermodynamic equilibrium by using a separation module to remove water from the reactive mixture.

---

**References**

- [1] G. A. Sehmel and A. L. Babb, "Holdup Studies in a Pulsed Sieve-Plate Solvent Extraction Column," *Ind. Eng. Chem. Process Des. Dev.*, vol. 2, no. 1, pp. 38–42, 1963.
- [2] G. Angelov, E. Journe, A. Line, and C. Gourdon, "Simulation of the flow patterns in a disc and doughnut column," *The Chemical Engineering Journal*, vol. 45, pp. 87–97, 1990.
- [3] A. W. Dickens, M. R. Mackley, and H. R. Williams, "Experimental residence time distribution measurements for unsteady flow in baffled tubes," *Chemical Engineering Science*, vol. 44, no. 7, pp. 1471–1479, 1989.
- [4] M. R. Mackley, G. M. Tweddle, and I. D. Wyatt, "Experimental heat transfer measurements for pulsatile flow in baffled tubes," *Chemical engineering science*, vol. 45, no. 5, pp. 1237–1242, 1990.
- [5] T. Howes and M. R. Mackley, "Experimental axial dispersion for oscillatory flow through a baffled tube," *Chemical Engineering Science*, vol. 45, no. 5, pp. 1349–1358, 1990.
- [6] M. R. Mackley and X. Ni, "Mixing and dispersion in a baffled tube for steady laminar and pulsatile flow," *Chemical Engineering Science*, vol. 46, no. 12, pp. 3139–3151, 1991.
- [7] X. Ni and A. Liao, "Effects of Cooling Rate and Solution Concentration on Solution Crystallization of L -Glutamic Acid in an Oscillatory Baffled Crystallizer," *Crystal Growth & Design*, vol. 8, no. 8, pp. 2875–2881, Aug. 2008.
- [8] X. Ni, J. C. Johnstone, K. C. Symes, B. D. Grey, and D. C. Bennett, "Suspension polymerization of acrylamide in an oscillatory baffled reactor: from drops to particles," *AIChE journal*, vol. 47, no. 8, pp. 1746–1757, 2001.
- [9] A. P. Harvey, M. R. Mackley, and T. Seliger, "Process intensification of biodiesel production using a continuous oscillatory flow reactor," *Journal of Chemical Technology & Biotechnology*, vol. 78, no. 2–3, pp. 338–341, Feb. 2003.
- [10] M. S. R. Abbott, A. P. Harvey, G. V. Perez, and M. K. Theodorou, "Biological processing in oscillatory baffled reactors: operation, advantages and potential," *Interface Focus*, vol. 3, no. 1, pp. 20120036–20120036, Dec. 2012.
- [11] E. Lobry, "Batch to continuous vinyl chloride suspension polymerization process: a feasibility study," Institut National Polytechnique de Toulouse, 2012.
- [12] W. K. Sern, M. S. Takri, S. Kartom, M. Z. Kamarudin, and N. Hasan, "Numerical simulation of fluid flow behaviour on scale up of oscillatory baffled column," *Journal of Engineering Science and Technology*, vol. 7, no. 1, pp. 119–130, 2012.
- [13] P. Stonestreet and A. P. Harvey, "A mixing-based design methodology for continuous oscillatory flow reactors," *Trans IChemE*, vol. 80, 2002.
- [14] M. Palma and R. Giudici, "Analysis of axial dispersion in an oscillatory-flow continuous reactor," *Chemical Engineering Journal*, vol. 94, pp. 189–198, 2003.
- [15] K. B. Smith and M. R. Mackley, "An experimental investigation into the scale-up of oscillatory flow mixing in baffled tubes," *Institution of Chemical Engineers*, pp. 1001–1011, 2006.
- [16] N. E. Pereira, "Characterisation of a continuous oscillatory baffled tubular reactor," Heriot-Watt University, Edinburgh, 2002.
- [17] C. R. Brunold, J. C. B. Hunns, M. R. Mackley, and J. W. Thompson, "Experimental observations on flow patterns and energy losses for oscillatory flow in ducts containing sharp edges," *Chemical Engineering Science*, vol. 44, no. 5, pp. 1227–1244, 1989.

- [18] A. N. Phan and A. P. Harvey, "Effect of geometrical parameters on fluid mixing in novel mesoscale oscillatory helical baffled designs," *Chemical Engineering Journal*, vol. 169, no. 1–3, pp. 339–347, May 2011.
- [19] M. R. Mackley and P. Stonestreet, "Heat transfer and associated energy dissipation for oscillatory flow in baffled tubes," *Chemical engineering science*, vol. 50, no. 14, pp. 2211–2224, 1995.
- [20] X. Nogueira, B. J. Taylor, H. Gomez, I. Colominas, and M. R. Mackley, "Experimental and computational modeling of oscillatory flow within a baffled tube containing periodic-tri-orifice baffle geometries," *Computers & Chemical Engineering*, vol. 49, pp. 1–17, 2013.
- [21] I. S. Stamenković, I. B. Banković-Ilić, P. B. Jovanić, V. B. Veljković, and D. U. Skala, "Hydrodynamics of a cocurrent upflow liquid–liquid reciprocating plate reactor for homogeneously base-catalyzed methanolysis of vegetable oils," *Fuel*, vol. 89, no. 12, pp. 3971–3984, Dec. 2010.
- [22] J. P. Solano, R. Herrero, S. Espín, A. N. Phan, and A. P. Harvey, "Numerical study of the flow pattern and heat transfer enhancement in oscillatory baffled reactors with helical coil inserts," *Chemical Engineering Research and Design*, vol. 90, no. 6, pp. 732–742, Jun. 2012.
- [23] X. Ni and P. Gough, "On the discussion of the dimensionless groups governing oscillatory flow in a baffled tube," *Chemical engineering science*, vol. 52, no. 18, pp. 3209–3212, 1997.
- [24] P. Stonestreet and J. Van der Veecken, "The effects of oscillatory flow and bulk components on residence time distribution in baffled tube reactors," *Trans IChemE*, vol. 77, 1999.
- [25] V. Strouhal, "Ueber eine besondere art der tonerregung," *Ann. Phys. Chem.*, vol. 5, pp. 216–251, 1878.
- [26] X. Ni, J. A. Cosgrove, A. D. Arnott, C. A. Greated, and R. H. Cumming, "On the measurement of strain rate in an oscillatory baffled column using particle image velocimetry," *Chemical engineering science*, vol. 55, no. 16, pp. 3195–3208, 2000.
- [27] A. E. Jealous and H. F. Johnson, "Power requirements for pulse generation in pulsed columns," *Industrial Engineering and Chemistry*, vol. 47, pp. 1159–1166, 1955.
- [28] X. Ni, H. Jian, and A. W. Fitch, "Evaluation of turbulent integral length scale in an oscillatory baffled column using large eddy simulation and digital particle image velocimetry," *Trans IChemE*, vol. 81, 2003.
- [29] X. Ni, H. Jian, and A. W. Fitch, "Computational fluid dynamic modelling of flow patterns in an oscillatory baffled column," *Chemical Engineering Science*, vol. 57, pp. 2849–2862, 2002.
- [30] H. Jian and X. Ni, "A Numerical Study on the Scale-Up Behaviour in Oscillatory Baffled Columns," *Chemical Engineering Research and Design*, vol. 83, no. 10, pp. 1163–1170, Oct. 2005.
- [31] M. Manninen, E. Gorshkova, K. Immonen, and X.-W. Ni, "Evaluation of axial dispersion and mixing performance in oscillatory baffled reactors using CFD," *Journal of Chemical Technology & Biotechnology*, vol. 88, no. 4, pp. 553–562, Apr. 2013.
- [32] M. Zheng, J. Li, M. R. Mackley, and J. Tao, "The development of asymmetry for oscillatory flow within a tube containing sharp edge periodic baffles," *Physics of Fluids*, vol. 19, no. 11, p. 114101, 2007.
- [33] A. A. Hamzah, N. Hasan, M. S. Takriff, S. K. Kamarudin, J. Abdullah, I. M. Tan, and W. K. Sern, "Effect of oscillation amplitude on velocity distributions in an oscillatory baffled column (OBC)," *Chemical Engineering Research and Design*, vol. 90, no. 8, pp. 1038–1044, Aug. 2012.

- 
- [34] A. Mazubert, J. Aubin, S. Elgue, and M. Poux, “Intensification of waste cooking oil transformation by transesterification and esterification reactions in oscillatory baffled and microstructured reactors for biodiesel production,” *Green Processing and Synthesis*, 2014.
- [35] P. Gough, X. Ni, and Symes, K. C., “Experimental Flow Visualisation in a Modified Pulsed Baffled Reactor,” *Journal of Chemical Technology & Biotechnology*, vol. 69, pp. 321–328, 1997.
- [36] O. Levenspiel, *Chemical reaction engineering*. New York: Wiley, 1999.
- [37] O. Potier, J.-P. Leclerc, and M.-N. Pons, “Influence of geometrical and operational parameters on the axial dispersion in an aerated channel reactor,” *Water Research*, vol. 39, no. 18, pp. 4454–4462, Nov. 2005.
- [38] A. N. Phan and A. Harvey, “Development and evaluation of novel designs of continuous mesoscale oscillatory baffled reactors,” *Chemical Engineering Journal*, vol. 159, no. 1–3, pp. 212–219, May 2010.
- [39] A. N. Phan, A. Harvey, and J. Lavender, “Characterisation of fluid mixing in novel designs of mesoscale oscillatory baffled reactors operating at low flow rates (0.3–0.6ml/min),” *Chemical Engineering and Processing: Process Intensification*, vol. 50, no. 3, pp. 254–263, Mar. 2011.
- [40] J. Aubin, L. Prat, C. Xuereb, and C. Gourdon, “Effect of microchannel aspect ratio on residence time distributions and the axial dispersion coefficient,” *Chemical Engineering and Processing: Process Intensification*, vol. 48, no. 1, pp. 554–559, Jan. 2009.
- [41] N. E. Pereira, “Characterisation of a continuous oscillatory baffled tubular reactor,” Heriot-Watt University, Edinburgh U.K., 2002.
- [42] E. Lobry, T. Lasuye, C. Gourdon, and C. Xuereb, “Liquid–liquid dispersion in a continuous oscillatory baffled reactor – Application to suspension polymerization,” *Chemical Engineering Journal*, vol. 259, pp. 505–518, Jan. 2015.
- [43] K. B. Smith and M. R. Mackley, “An Experimental Investigation into the Scale-up of Oscillatory Flow Mixing in Baffled Tubes,” *Chemical Engineering Research and Design*, vol. 84, no. 11, pp. 1001–1011, Nov. 2006.







### Conclusions of Part III

Part III has focused on the improvement of the operating conditions of the glass oscillatory baffled reactor tested in Part II. In Chapter 1 an experimental rig that includes a metallic oscillatory baffled reactor, which operates under pressure (3-10 bar) and at high temperatures (130-150°C) has been set up. Using this pilot-scale rig, 50% conversion and 88% selectivity in monoglycerides for the esterification reaction with glycerol was obtained using sulfuric acid catalyst at 150°C and a residence time of 22 min. This conversion was able to be increased to 86% with the use of an intermediary decantation step, however in detriment of selectivity in monoglycerides, which decreases to 53%. A 73% conversion and a 67% selectivity was obtained with the DBSA catalyst. The reactor has shown better performance than a coiled oscillatory flow reactor without baffles.

Chapter 2 has focused on the characterization of the OBR reactor using CFD simulations and PIV measurements. Via the development of different characterization indicators, the numerical and experimental results have enabled a better understanding of the flow occurring in this device, which has ultimately led to the design of new baffles, and in particular the S2 design. An industrial scale reactor, which has a total flow rate capacity of 100 kg/h, has then been sized with the following geometrical parameters:  $D = 70$  mm,  $L = 8.7$  m,  $h = 105$  mm,  $D_0 = 35$  mm,  $N = 82$  baffles,  $\Delta P = 4.0$  bar,  $Pe = 42$  if  $D = 2 \times 10^{-3}$  m<sup>2</sup>/s (OBR baffle design) or  $Pe = 52$  if  $D = 1.2 \times 10^{-3}$  m<sup>2</sup>/s (S2 baffle design).

Furthermore, it is expected that the proposed S2 geometry will increase the Peclet number for the same reactor parameters, thereby providing improved plug-flow behavior, which is needed to limit the secondary reactions (i.e. formation of di and triglycerides) during the esterification with glycerol reaction. The process associated to the reactor corresponds to the process developed and built in Chapter 1.

The mediocre conversions obtained with non-treated waste cooking oil with a level of fatty acids of 40% are mainly due to the thermodynamic equilibrium of the reaction and conversion levels should be increased by the use of oil with a higher level of fatty acids and using DBSA catalyst. If this is not possible, an intermediary decantation step can be used to remove water and glycerol from the reactive media and thereby shift this equilibrium. In this case, the use of sulfuric acid as a catalyst is required to facilitate this decantation.

Finally, the reactor presented in Part III offers a wider range of operating conditions with higher operating pressures (3-10 bar) and temperatures (150°C) than that possible in the glass Nitech® reactor. These characteristics also allow the possibility to handle reactions that involve viscous and immiscible reactants, such as the esterification with glycerol reaction, in a continuous and compact technology with a residence time of 20 minutes. An improved baffle design has been proposed to limit the axial dispersion in the reactor and then to limit concentration gradients, which are responsible for secondary reactions (as formation of di and triglycerides).



# CONCLUSION



The objective of this PhD thesis is to propose a continuous and intensified reactor to carry out transformation of waste cooking oils (WCO) into fatty acids methyl esters (FAME) and glycerol by transesterification, and into fatty acids by the hydrolysis. The high level of free fatty acids of WCO can be also reduced by esterification with methanol to produce FAME, or with glycerol to produce mono, di and triglycerides. The objective of production capacity is 100 kg/h.

These reactions are mass-transfer limited since the reactants and products of these reactions are immiscible. The first objective of the work was to identify the different reactor technologies that are suitable for these reactions, and then to compare them and to define the most adapted technology. Amongst microstructured, cavitation, microwave, oscillatory baffled and membrane reactors, static mixers and reactive distillation, three reactor types were selected: microwave, microstructured and oscillatory flow reactors. A commercially available version of each technology was experimentally tested: a CEM Discover single mode microwave reactor and two continuous flow reactors - a Corning® Advanced-Flow™ glass reactor and a glass NiTech® oscillatory baffled reactor. The three technologies have shown good results for transesterification, esterification with methanol and esterification with glycerol reactions. With the microwave reactor, results obtained were similar to a conventional reactor but with faster heating whatever the reaction. With the microstructured and oscillatory flow reactors, high conversions were obtained in shorter residence times compared with a conventionally heated and stirred reactor for transesterification and esterification with methanol reactions. The esterification reaction with glycerol required higher temperatures and longer residence times than those tested experimentally and low conversions were obtained in the tested NiTech®, which is limited to low temperature (< 45°C), and the tested Corning® reactor, which is limited in terms of residence time. Further investigations on this reaction were possible in the microwave reactor, which has provided high conversions using a heterogeneous catalyst  $\text{ScTf}_3$  at 190°C. Low conversions were still obtained for the hydrolysis reaction, even at high temperatures under microwave irradiation. The investigations on this reaction were not pursued due to the limited interest in this reaction within the project and further work focused on the esterification reaction with glycerol. Finally, the oscillatory baffled reactor and microstructured reactors have been preferred to microwave reactors because of the already existing transposition to the continuous mode and the possibility to reach flow rates of 1-15 kg/h, whereas the development of the microwave technology at flow rates of 100 kg/h is confronted with major challenges due to the limited penetration depth of the microwaves and the design of a specific microwave reactor for industrial purposes. The oscillatory baffled reactor was finally preferred to the Corning® reactor for two reasons. Firstly, even with similar reaction performances, the oscillatory baffled reactor was considered more robust and flexible as oil with high levels of free fatty acids easily clogged the Corning® reactor. Secondly, the flexibility in terms of flow rates of the oscillatory baffled reactors has been preferred, since mixing is ensured by a variable oscillatory flow rate, whereas it is ensured by the net flow rates in the Corning® reactor, but it is possible to modulate the residence time by the addition of Corning® plates.

At this point, the development of the oscillatory baffled reactor to extend its range of temperature is necessary to perform the esterification with glycerol reaction. This has been done in collaboration with TNO, in Delft, Netherlands. An experimental rig was setup to operate under pressure in order to increase the boiling points of reactants and reach higher operating temperatures. This also reduces the viscosity of reactants as glycerol and increases kinetics. With such a system, the reaction is not limited by kinetics but by the thermodynamic equilibrium. The conversion of 40 wt.% of fatty acids contained in the waste cooking oil by the esterification reaction with glycerol is 50.2% at 150°C with sulfuric acid as a catalyst, with a selectivity in monoglycerides of 88%. This conversion increases to 72.9% but with a selectivity in monoglycerides of 67% at 150°C with DBSA as a catalyst.

A two-step process, with an intermediary decantation to separate the water and glycerol from the oleic phase has been tested, leading to an overall conversion of 86.6% but an overall selectivity of 53%. It shows the thermodynamic equilibrium can be shifted by removing water from the reactive media, either by the formation of micelles with the use of a catalyst that has surfactant properties, or by decantation.

In parallel, a non-exhaustive state of the art has been made to understand the geometric parameters involved in the design of this type of technology and the existing means of characterization of the mixing in the reactor and its capacity to generate liquid-liquid emulsions in two-phase systems. To complete the knowledge of this reactor technology, an experimental rig has been built in the laboratory allowing the visualization and measurement of the flow patterns in the glass NiTech® reactor using Particle Image Velocimetry (PIV). The instantaneous flow fields have enabled the formation of the eddies and the zones of high shear strain rate to be observed and better understood. Computational Fluid Dynamics simulations using ANSYS-CFX have been performed in laminar conditions to understand flow mechanisms in oscillatory baffled reactors and to provide complementary information to that obtained by PIV. Based on the velocities fields provided by the numerical simulations, new indicators have been proposed to characterize the mixing and other quantities by injecting virtual particles in the oscillatory baffled reactor. This particle tracking technique has also been employed to study the residence time distribution and to calculate the difference of the axial and radial positions of the particles over time. The simulated fluid is single phase, but the strain rate history of particles has been calculated as it may play a role in the generation of liquid-liquid emulsions. It has been shown that the oscillatory Reynolds number has no influence on the axial dispersion coefficient (for  $Re_o = 20-60$ ). The shear strain rates increases linearly with the oscillatory amplitude and frequency. Several baffle geometries have been tested and a new spring baffle design (S2) has been considered as the most adapted baffle design to limit the axial dispersion and widen the range of conditions to have a plug-flow behavior. These simulations pointed out, with operating conditions similar to these used in the NiTech® glass reactor (8.9 L/h, 15 mm diameter), that a minimum residence time of 6 min with single orifice baffles is needed to reach Péclet numbers more than 30, which corresponds to an acceptable plug-flow behavior. This minimum residence time can be decreased to 3.5 min with a S2 design. The shear strain rates experienced by the particles are lower with this geometry, but this can be compensated by an increase of the oscillatory conditions.

On the basis of the knowledge on the oscillatory baffled reactor behavior, the data for the sizing of an oscillatory baffled reactor with a production capacity of 100kg/h and a residence time of 20 min have been proposed. In this industrial scale reactor, transesterification and esterification with methanol or with glycerol could be carried out.

The esterification with glycerol reaction can certainly be improved in two ways. The first is the use of waste cooking oil that contains a higher level of fatty acids. The second one is the addition of a system that removes the water from the system, since the intermediary decantation of the glycerol phase with sulfuric acid catalyst is fast. The process associated with the reactor is similar to that built for the pilot-scale reactor used at TNO, with the presence of a pulse dampener and a backpressure regulator to increase the pressure.

This PhD thesis allowed us to propose an intensified reactor by the achievement of several steps. Firstly, the feasibility of the targeted reactions has been proven at pilot scale. The range of the operating conditions has been improved with the set-up of an experimental rig, which has allowed higher operating pressures (3-10 bar) and temperatures (150°C). In parallel, a comparison of baffle designs has been carried out through CFD simulations to enhance mixing. Finally, an industrial scale

reactor with production capacity of 100 kg/h has been proposed with a classical oscillatory baffled reactor with single orifice baffles. The added value of the new spring baffle design, which has been determined by CFD simulations, is the increase of the Péclet number, which is yet to be validated experimentally with a pilot scale rig. This would lead to the proposition of a new reactor design.

This reactor is pluri-reactional as it can perform the transesterification, the esterification with methanol and the esterification with glycerol reactions. It can thereby handle viscous reactants as glycerol. This reactor technology is also compatible with solid catalysts as the oscillations prevent sedimentation of the solid suspensions. For the same reason, this type of reactor shows good performance in polymerization reactions. Other types of reactions can also be tested in such a flexible technology as other mass-transfer limited reactions, but also exothermic reactions, as heat transfers are improved with oscillations. The limit of this reactor is that it is not adapted for rapid selective reactions with reaction times inferior to 5 min as it implies low reactor lengths and low Péclet numbers, which results as a flow different of the ideal plug-flow reactor. This causes gradient of concentrations that can generate undesired secondary reactions and decrease selectivities.

More generally, this type of intensified reactor technology allows the reactions to be carried out in reduced reaction times, in more compact facilities, in the continuous mode to ensure an excellent reproducibility, good control of the product quality and improve process safety.

